PAVDAM – PROBABILISTIC AND VOLUMETRIC DESIGN OF ASPHALT MIXTURES

André de Fortier Smit

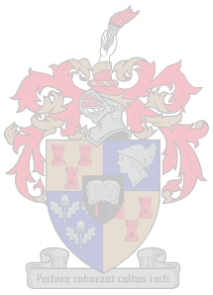

Dissertation presented for the degree of Doctor of Philosophy (Engineering) at the University of Stellenbosch

PROFESSOR K. J. Jenkins Ph.D
Promotor

December 2002

DECLARATION

I the undersigned hereby declare that the work contained in this dissertation is my own original work and that I have not previously in it's entirety or in part submitted it at any university for a degree.

André de Fortier Smit
24 November 2002

Abstract

The dissertation presents a design procedure for HMA mixes based on probabilistic and volumetric approaches, hereafter referred to as PAVDAM. Central to PAVDAM is the use of an analytical model for estimating the voids in the mineral aggregate (VMA) of asphalt mixes. Validation of the mix design procedure was done through accelerated pavement testing (APT) with the Model Mobile Load Simulator (MMLS3) at the National Center for Asphalt Technology (NCAT) test track in Opelika, Alabama. In addition, the semi-circular bending (SCB) test was evaluated to serve as an analysis tool to augment the proposed mix design procedure. Non-linear finite element analyses using a quasi-isotropic material model were done using the CAPA-3D finite element system developed at the Technical University of Delft in the Netherlands to better characterise the tensile strength properties of specimens tested with the SCB.

PAVDAM is partly based on performance related and analytical procedures such as the Stategic Highway Research Program (SHRP) Superpave and the Belgium Road Research Centre (BRRC) design method. The mix design system was developed based on gyratory compaction procedures. In this regard, the criteria relating gyratory compaction to design traffic as specified in Superpave are used. PAVDAM differs from other mix design methods in that a probabilistic approach is used to account for the variabilities associated with mixture components and properties during the manufacturing stage. It serves as a subset of the volumetric optimisation stage of the mix design process.

The development of an analytical model to estimate the VMA of an asphalt mix was the central theme of the dissertation. The analytical model developed is based on modified Aim and Toufar (MAT) packing models developed under SHRP research and used in the concrete industry. The MAT packing models are based on the theory

underlying the packing of monosized spheres and the combination of successive binary systems. These models were further refined for use in the asphalt industry. A probabilistic procedure based on the BRRC PRADO packing model is used to account for the influence of size ratio of the successive monosized binary systems. The result was a model that allows an estimation of the VMA of a mix from the gradation of the mix, the voids in the filler and the porosities of the individual aggregate fractions making up the mix. Research was undertaken to couple VMA estimates with gyratory compaction levels. This allowed estimates to be made of the optimum binder contents of mixes for different design traffic levels.

The VMA of a mix is difficult to estimate accurately since it is difficult to quantify the factors influencing VMA such as gradation, particle shape, angularity, texture and rugosity. Furthermore, the influence of binder content and compaction must be taken into account. The MAT packing model underestimates the VMA of mixes compared to measured values. For this reason it is necessary to calibrate the model to allow more accurate estimations. More sophisticated models are required to more accurately estimate the VMA of mixes. It is recommended that the development of these be explored further.

Asphaltic materials are inherently heterogeneous and there are a large number of factors that influence their volumetric properties. Because of this, Monte Carlo simulation techniques are used in PAVDAM to evaluate the combined effect of the variabilities of significant material properties. The dissertation expands on the different variabilities and the effects of variability on mixture volumetrics and mix design verification. The dissertation outlines the algorithms and procedures used in PAVDAM to estimate the binder content of a mix. In order to validate the PAVDAM model, analyses were done to determine the reliability of specific NCAT MMLS3 test section mixes in terms of densification in the field. A comparison of PAVDAM estimated and field binder contents allowed a ranking of the reliabilities of the different section mixes in terms of field densification at the design traffic level. This ranking compared favourably with that obtained from an analysis of actual densification trends monitored in the field under full-scale trafficking.

Initial FEM analyses of the SCB using linear elastic isotropic modelling allowed

the development of equations to characterise the tensile strength and modulus characteristics of specimens tested using the SCB. It was emphasized that these equations do not provide a realistic assessment of the strengths or moduli of asphaltic materials. The strengths and moduli of these materials are influenced by strain rates within the materials that cannot be assessed using a simple linear elastic approach. To address this, an alternative FEM analyses using CAPA-3D was undertaken. An approach was adopted to account for the influence of tensile and compressive strain rates on modulus. The analyses made use of a quasi-isotropic material model and it was shown to better characterise the tensile strengths of HMA materials using the SCB. The analyses also indicated that the tensile strengths determined using the equations initially developed based on a linear elastic approach result in strengths that are unrealistically high. It is recommended that further finite element research be done using non-linear material modelling to evaluate the very complex stress-strain conditions within an SCB specimen to better characterise fracture response. It is also recommended that the fatigue characterisation of HMA be explored based on strength tests using the SCB.

PAVDAM represents a rational approach to mix design, a shift from experimental empiricism towards scientific fundamentalism. PAVDAM can be used to define the spatial composition of asphalt mixes. The influence of mix component variability may be addressed and reliability assessments of candidate gradations are possible during volumetric optimisation. Furthermore, changes in the volumetric properties of asphalt mixes may be investigated. As such, PAVDAM is a mix design management tool and can only be effective when used as part of a system that closely monitors variability and systematically refines the underlying packing model.

Opsomming

Die verhandeling lewer 'n asfalt mengsel ontwerp metode gebaseer op statistiese en volumetriese metodes, genaamd PAVDAM. PAVDAM gebruik 'n analitise model om 'n skatting te maak van die ruimtes in die aggregaat (VMA) van asfalt mengsels. Stawing van die mengsel ontwerp metode is gedoen deur vesnelde plaveisel toetse met die Model Mobiele Las Simuleerder (MMLS3) op die National Center for Asphalt Technology (NCAT) se toetsbaan in Opelika, Alabama. Die Semi-Circular Bending (SCB) toets is ook geëvalueer om die voorgestelde ontwerp metode te analiseer. Nielineêre eindige element analise met gebruik van 'n kwasi-isotropiese materiaal model is gedoen met die CAPA-3D eindige element (FEM) stelsel ontwikkel deur die Tegniese Universitieit van Delft in Nederland om die treksterkte van monsters getoets met die SCB beter te karakteriseer.

PAVDAM is deels gebaseer op gedragsverwante en analitise prosedures soos die Strategic Highway Research Program (SHRP) Superpave en die Belgium Road Research Centre (BRRC) ontwerp metodes. Die mengsel ontwerp stelsel is ontwikkel gebaseer op girator verdigtingsmetodes. Die girator verdigtingskriteria soos voorgeskryf in Superpave is gebruik. PAVDAM verskil van ander mengsel ontwerp metodes omdat daar gebruik gemaak word van statistiese metodes om die veranderlikhede geassosieer met mengsel komponente en ontwerp prosedures gedurende die vervaardigingsfase. Dit dien as 'n komponent van die volumetriese optimeringsfase van 'n mengsel ontwerp proses.

Die sentrale tema van die verhandeling was die ontwikkeling van 'n analitisie model om 'n skatting te maak van die VMA van asfalt mengsels. Die analitise model wat ontwikkel is is gebaseer op gewysigde Aim and Toufar (MAT) pakkingsmodelle ontwikkel as deel van SHRP navorsing en wat gebruik word deur die betonindustrie. Die MAT pakkingsmodelle is gebaseer op die teorie van die pakking van eenvormige

groote sfere en die kombinasie van binêre sisteme. Die modelle is verder ontwikkel vir gebruik in die asfaltindustrie. 'n Statistiese prosedure gebaseer op die BRRC se PRADO pakkingsmodel is gebruik om die invloed van groote verhouding (size ratio) van opeenvolgende binêre sisteme in ag te neem. Die gevolg was 'n model wat gebruik kan word om 'n skatting te maak van die VMA van 'n mengsel vanaf die mengsel gradering, ruimtes in die vulstof en die porositeit van die individuele aggregaat fraksies wat die mengsel saamstel. Navorsing is gedoen om die VMA te koppel aan girator verdigtingsvlakke. Die gevolg is dat skattings gemaak kan word van die optimum bindstof inhoude van mengsels vir verskillende verkeer ontwerp vlakke.

Dit is moeilik om 'n akkurate skatting van die VMA van mengsels te maak omdat dit moelik is om faktore wat VMA beïnvloed te kwantifiseer, soos byvoorbeeld gradering, partikel vorm, hoekigheid en tekstuur. Die invloed van bindstof inhoud en verdigting moet ook in ag geneem word. Die MAT pakkings model onderskat die VMA van mengsels in vergeleke met gemete waardes. Daarom is dit noodsaaklik dat die model gekalibreer word om meer akkurate skattings van mengsel VMA te maak. 'n Meer gesofistikeerde model is nodig om meer akkuraat die VMA van mengsels te skat. Dit word voorgestel dat die ontwikkeling van hierdie modelle verder ondersoek word.

Asfalt materiaale is inherent heterogeen en daar is 'n groot aantal faktore wat die volumetriese einskappe van die mengsels beïnvloed. Om hierdie rede word gebruik gemaak van Monte Carlo simulasie in PAVDAM om die gekombineerde effek van veranderlikheid in ag te neem. Die verhandeling brei verder uit op verskillende veranderlikhede en die effek van veranderlikheid op die volumetriese einskappe van mengsels en die stawing van die model. Die algoritme en prosedures wat deur PAVDAM gebruik word om 'n skatting te maak van die optimum bindstof inhoud van 'n mengsel word in die verhandeling uiteengesit. Vir stawing van PAVDAM is analises gedoen om die betroubaarheid van NCAT MMLS3 toets seksies in terme van verdigting in die veld te bepaal. Vergelykings tussen PAVDAM geskatte en veld bindstof inhoude het gelei tot 'n rangorde van die betroubaarheid van die verskillende seksie mengsels in terme van verdigting in die veld onder die ontwerp vervoer. Hierdie rangorde het goed vergelyk met die wat gekry is van analise van die werklike verdigtingstendense soos in die veld gemonitor is onder volskaalse verkeer.

Voorlopige FEM analise van die SCB met gebruik van lineêr isotropiese modelering het gelei tot die ontwikkeling van vergelykings om die treksterke en styfheidseienskappe van monsters getoets met die SCB te skat. Dit word beklemtoon dat hierdie vergelykings nie 'n realistiese skatting van die treksterkte of styfhede van asfalt materiaale gee nie. Die treksterkte en styfhede van die materiaale word beïnvloed deur verplasingstempo's binne die materiaale wat nie deur lineêr elastiese benaderings bepaal kan word nie. Om dit aan te spreek is alternatiewe FEM analise gedoen deur gebruik te maak van CAPA-3D. 'n Benadering is gevolg om die invloed van trek en druk verplasingstempo's op styfheid in ag te neem. Die analise het gebruik gemaak van 'n kwasi-isotropiese materiaal model en dit het 'n beter karakterisering van die treksterkte van asfalt mengsels tot gevolg gehad. Dit word voorgestel dat verdere eindige element navorsing gedoen word met gebruik van nie-lineêre materiaal modellering om die breekgedrag van SCB monsters beter te kan karakteriseer. Dit word ook voorgestel dat die vermoeiings eienskappe van asfalt mengsels ondersoek word gebaseer op treksterketoetse met gebruik van die SCB.

PAVDAM is 'n rasionele benadering tot mengsel ontwerp, 'n paradigma skuif weg van empiriese metodes tot wetenskaplik fundamentele metodes. PAVDAM kan gebruik word om die ruimtelike samestelling van asfalt mengsels te definieer. Die invloed van veranderlikheid kan in ag geneem word en betroubaarheidsskattings van kandidaat mengsels is moontlik gedurende die volumetriese optimiseringsfase. Verder kan veranderings in die volumetriese eienskappe van mengsels ondersoek word. As sulks is PAVDAM 'n hulpmiddel vir die bestuur van mengsel ontwerp en kan net effektief wees wanneer dit gebruik word as deel van 'n stelsel wat die mengselveranderlikheid monitor en sistematies die onderliggende pakkings model verbeter.

For Jilly, Angie, James and Harry

Table of Contents

List of Tables

List of Figures

Acknowledgements

The dissertation was written over three continents between 1997 and 2002. Completion thereof would not have been possible without financial and moral support. I gratefully acknowledge the organisations and people that provided both in good measure.

The research undertaken as part of the dissertation was sponsored by the following organisations:

1. Institute for Transport Technology, University of Stellenbosch
2. South African Department of Transportation
3. Foundation for Research Development
4. South African Road Federation
5. South African National Road Agency Limited
6. Delft Technical University
7. Texas Department of Transportation
8. National Center for Asphalt Technology

Support, motivation, patience and encouragement were shown to me by -
My creator.

My teachers and examiners: Prof. Fred Hugo, Prof. Martin van de Ven, Prof. Kim Jenkins, Prof. André Molenaar, Dr. Louis Francken, Prof. Alex Visser and Dr. Jan van Vuuren.

My family and friends: Jillian, Angela, James, Harry, my mom Sheila, my brothers and sister, Charles and Evelyn Stride and the Meiring family.

My colleagues and peers: Ken Fults, Byron Kneifel, Mark Crawford, Dale Rand, Corey Schwarz, Richard Izzo, Gregory Cleveland, Roy Collins, Hercu du Preez, Joe Button, Arif Chowdhury, Terry Dossey, Thomas Ritter, Gerald Peterson, Colin Isaacs,

Louis Fredericks, Oom Dries Rossouw, William Douries, Gavin Williams, Carl Weston, Jeremy Jarvis, Jannie Grobler, Johan Muller, Pieter Poolman, Julian Wise, John Onraet, Mervyn Henderson, Riaan Burger, Phil Blankenship, Lubinda Walubita, Peter Njanga, Delysia Baard, Liezl Rabie, Prof. Ray Brown, Buzz Powell, Billy Wilson, Jennifer Brown, Tim Voller, Rosli Hainen, Jianjun Peng, Jagan Gudimettla, Brian Prowell, John Gardener, Allen Cooley, Cynthia Lynn, Carol Tapley and Vinnie Hester.

Thank you!

André de Fortier Smit
Stellenbosch, South Africa
22 November, 2002

List of symbols

Organisations

AI	:	Asphalt Institute
AAPT	:	Association of Asphalt Paving Technologists
ARRB	:	Australian Road Research Board
AASHTO	:	American Association of State Highway and Transportation Officials
ASTM	:	American Society for Testing and Materials
BRRC	:	Belgian Road Research Centre
COLTO	:	Committee of Land Transport Officials
CSIR	:	Council for Scientific and Industrial Research
CTR	:	Center for Transportation Research
FHWA	:	Federal Highway Administration
ITT	:	Institute for Transport Technology
LCPC	:	Laboratoires des Ponts et Chaussées
NAA	:	National Aggregates Association
NAPA	:	National Asphalt Pavement Association
NCAT	:	National Center for Asphalt Technology
NCHRP	:	National Cooperative Highway Research Program
NITRR	:	National Institute for Transport and Road Research
OECD	:	Organisation for Economic Co-Operation and Development
PAWC	:	Provincial Administration of the Western Cape
RILEM	:	Int. Union of Testing and Research Labs for Materials and Structures
SABITA	:	Southern African Bitumen and Tar Association
SHRP	:	Strategic Highway Research Program
TPA	:	Transvaal (now Gauteng) Provincial Administration
TRB	:	Transportation Research Board

TRL : Transport Research Laboratory
TTI : Texas Transportation Institute
TxDOT : Texas Department of Transportation

Materials and Tests

AC : Asphalt Concrete
ACV : Aggregate Crushing Value
BBR : Bending Beam Rheometer
BTB : Bitumen Treated Base
CIT : Confined Impact Test
DBM : Dense Bitumen Macadam
DCP : Dynamic Cone Penetrometer
DSR : Dynamic Shear Rheometer
DST : Dynamic Shear Test
FACT : Fines Aggregate Crushing Test
FI : Flakiness Index
FWD : Falling Weight Deflectometer
GPR : Ground Penetration Radar
GSP : Gyratory Shear Press
HMA : Hot Mix Asphalt
ITS : Indirect Tensile Strength Test
LAMBS : Large Aggregate Mix for Bases
LVDT : Linear Variable Differential Transducer
MATTA : MATerials Testing Apparatus
MDD : Multi-Depth Deflectometer
MDL : Maximum Density Line
MTS : Materials Testing System (Electro-hydraulic closed-loop)
NAT : Nottingham Asphalt Tester
PEN : Penetration value of bitumen
PG : Performance Grade

PI	:	Penetration Index
PRD	:	Percentage Refusal Density
R&B	:	Ring and Ball
ROC	:	Run Of Crusher
RTFOT	:	Rolling Thin Film Oven Test
SASW	:	Spectral Analysis of Surface Waves
SCB	:	Semi Circular Bending
SGC	:	Superpave Gyratory Compactor
SMA	:	Stone Mastic Asphalt
SPA	:	Seismic Pavement Analyser
SSD	:	Surface Saturated Dry
SST	:	Superpave Shear Tester
TSR	:	Tensile Strength Ratio
UCS	:	Unconfined Compressive Strength

Evaluation

AADE	:	Annual Average Daily E80
AAMAS	:	Aggregate Asphalt Mixtures Analysis System
ADHAT	:	Average Design High Air Temperature
APT	:	Accelerated Pavement Testing
ANOVA	:	ANalysis Of VAriance
ESAL	:	Equivalent Standard Axle Load
E80	:	Equivalent 80 kN axle
FEM	:	Finite Element Method
HDAP	:	Heavy Duty Asphalt Pavements
HVS	:	Heavy Vehicle Simulator
LCC	:	Life Cycle Cost
LTPP	:	Long Term Pavement Performance
MESA	:	Millions of Equivalent Standard Axles
MLS	:	Mobile Load Simulator
MMLS1	:	Model Mobile Load Simulator Mk. 1

MMLS3	:	Model Mobile Load Simulator Mk. 3
PMS	:	Pavement Management System
PRADO	:	Programs for Road Asphalt Design and Optimisation
PRS	:	Performance Related Specifications
PSI	:	Present Serviceability Index
SPDM	:	Shell Pavement Design Manual
SIM	:	Stress In Motion
VRSPTA	:	Vehicle Road Surface Pressure Transducer Array
WIM	:	Weigh In Motion
WMAPT	:	Weighted Mean Annual Pavement Temperature

Asphalt mix design

BRD	:	Bulk Relative Density
G_{mb}	:	Bulk relative density of mix
G_{mm}	:	Maximum theoretical density of the mix (Rice)
G_{sb}	:	Bulk relative density of aggregate blend
G_b	:	Bulk relative density of binder
M_b	:	Mass of binder
M_s	:	Mass of stone
N_{ini}	:	Superpave initial compaction level
N_{des}	:	Superpave design compaction level
N_{max}	:	Superpave maximum compaction level
N_{ref}	:	Refusal compaction level
P_b	:	Percent binder content by mass of the total mix
P_{ba}	:	Percent absorbed binder by mass of the total aggregate
P_{be}	:	Percent effective binder content by mass of the total mix
S_{bit}	:	Stiffness of the bitumen
S_{mix}	:	Stiffness of the mix
V_b	:	Volumetric binder content
V_a	:	Volume of air voids

V_{be}	:	Volume of effective binder
V_s	:	Volume of aggregate
V_{se}	:	Volume of effective aggregate
VIM	:	Voids In the Mix
VFA	:	Voids Filled with Asphalt (Same as VFB)
VFB	:	Voids Filled with Binder
VMA	:	Voids in the Mineral Aggregate

Other

AVG	:	Statistical average
COV	:	Coefficient Of Variation
FEM	:	Finite Element Method
MAT	:	Modified Aim and Toufar packing model
RSA	:	Republic of South Africa
STDEV	:	Standard deviation
TMH1	:	Technical Methods for Highways No. 1
TRH4	:	Technical Recommendations for Highways No. 4
TRH8	:	Technical Recommendations for Highways No. 8
TRH14	:	Technical Recommendations for Highways No. 14
UK	:	United Kingdom
USA	:	United States of America

Chapter 1

Introduction

This dissertation addresses the volumetric design of hot mix asphalt (HMA). A probabilistic approach is adopted to account for variabilities associated with the design of these mixes, particularly during the manufacturing stage. The chapter begins by outlining the elements and objectives of asphalt mix design and defines the focus of the dissertation. A motivation for the development of this new approach is then given. To define the theme of the dissertation, primary and secondary objectives are stated. Finally, a plan of development and brief overview of the contents of each chapter is given.

1.1 Elements and objectives of asphalt mix design

Francken, in commentary to a report on the spatial composition of asphalt mixes [Van de Ven et al., 1999] points out that mix design procedures must account for:

- Characteristics of the individual components (aggregates and bitumen).
- Interaction of the components in the mix.
- The manufacture of the mix.
- The transportation of the mix from plant to the field.

- The laying and compaction of the mix in the field.
- The short and long term evolution of the product in the field.

This is an extensive list and indicates the many variables influencing asphalt mix design. The steps to be taken in an integrated mix design method are illustrated in Figure 1.1 and may be summarised as follows:

1. Obtain information from the pavement design such as traffic loads, climate and function of the layer, which may influence the mix design process.
2. Characterise the raw materials to be used.
3. Define alternative formulations (candidate or trial gradations).
4. Preparation, conditioning and compaction of specimens.
5. Volumetric analysis of mixes.
6. Performance evaluation of mixes.
7. Quality verification.

The end result of this process is an asphalt mix with the desired quality, optimised in terms of gradation, binder content and performance. The focus of the dissertation will be on the volumetric analysis of asphalt mixes. The procedure developed as part of the dissertation differs from other conventional methodologies in that a probabilistic approach is included as part of the volumetric optimisation stage. Probabilistic approaches are usually used to assess reliability levels during performance optimisation or as part of quality control during implementation. The dissertation illustrates the benefits of assessing the reliability of asphalt mixes during the volumetric mix design phase. Hence a link is established between volumetric definition and probabilistic design.

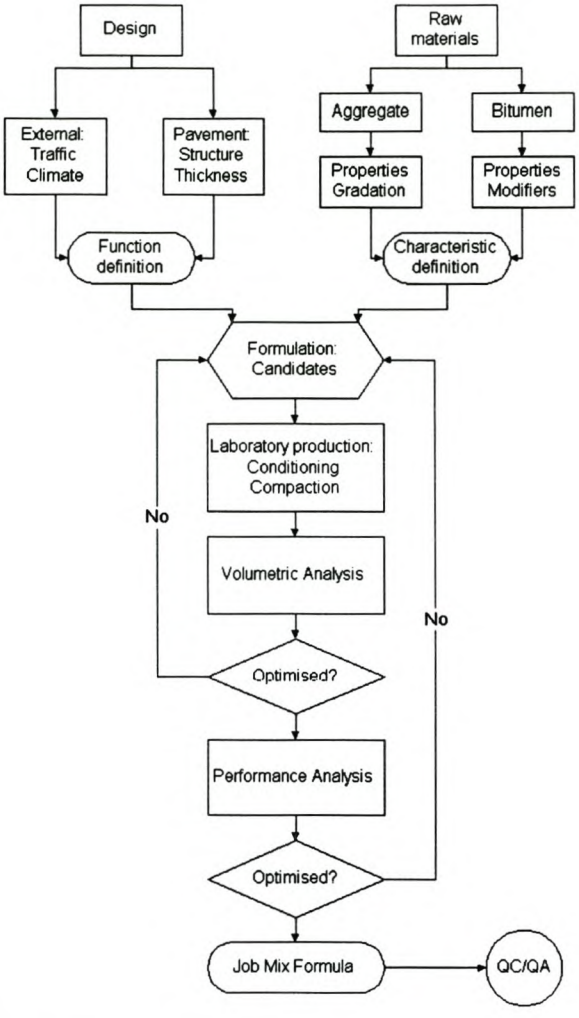

Figure 1.1: Integrated mix design method

The new approach includes packing models to estimate the voids in the mineral aggregate (VMA) of asphalt mixes based on the gradation and properties of the mix components. The use of packing models to estimate the VMA of asphalt mixes is controversial and the motivation for use of these models is given in the next section. Aspects of the performance evaluation of HMA are also addressed. The dissertation discusses the development of the semi-circular bending test (SCB) and accelerated pavement testing (APT) using the Model Mobile Load Simulator Mk.3 (MMLS3).

1.2 Motivation

Kandhal, upon reviewing a report on the conceptualisation of spatial composition for asphalt mixes [Van de Ven et al., 1999], pointed out that it is difficult to develop accurate and useful models to predict VMA in asphalt mixes because of the problems in quantifying many variables that affect the VMA in compacted mixes. Variables such as particle shape, angularity, surface texture and the effect of degradation during compaction in the laboratory are difficult to quantify. Furthermore, the amount of VMA in the mix depends on the laboratory compactive effort, which must also be accounted for. He concludes that after all these variables are included in the model(s) one can only get a rough estimate of VMA. He points out that one cannot rely on the estimate and the mix still has to be compacted to determine the actual VMA otherwise a mix may be rejected based on an estimated VMA. In his own words:

> "A VMA model may be useful if it is reasonably accurate, a wide variety of aggregates are available to the contractor, and the highway agency does not specify a narrow band of gradation. In a vast majority of cases, the contractor has access to only 2 or 3 aggregates (including both coarse and fine aggregates) and has an agency specified gradation band. It is much easier to try 2 or 3 gradations in actual trial mixes and determine the actual VMA. To use the VMA models the contractor has to conduct some additional aggregate tests. In lieu of that time he can go ahead and make 3 trial mixes and determine the actual VMA (he has to do it anyway to verify the "estimated" VMA). In my opinion, there is no pressing, practical need to develop the models for predicting VMA. There are other more pressing research needs that should be tackled first. To develop a good HMA mix design system and development of realistic VMA requirements for South Africa mixes is more important than predicting

VMA in mixes."

Kandhal expresses some valid concerns on the use of analytical models to estimate the VMA of mixes. The dissertation addresses most of these. In particular, attention is given to the accuracy of the prediction model and use is made of probabilistic approaches to address variabilities influencing mix design.

Two principal parameters in mix design are the voids in the mineral aggregate (VMA) and the voids in the mix (VIM). The VMA of a mix governs the amount of binder that can be added to the mix and the VIM may be used to regulate the compactibility of the mix to ensure stability and durability. The VMA of a mix is strongly influenced by the aggregate gradation. Determining the design aggregate structure of a mix is the first and usually most difficult step in the mix design process. Typically this is done using a trial and error procedure. Candidate gradations are mixed with binder and compacted. The volumetric properties are then evaluated to determine whether the candidate gradation satisfies specific criteria. If none of the candidate gradations satisfies the criteria, new candidates must be designed and the evaluation procedure repeated. This is a major disadvantage of the trial and error approach. Other disadvantages are:

- Candidate aggregate gradations are often chosen arbitrarily without regard for the resulting aggregate structure e.g. candidate gradations chosen to pass above, through or below the restricted zone, an approach adopted in the Superpave mix design method that will be discussed in more detail in the next chapter.

- Because only a limited number of candidate gradations can be evaluated, the best candidate is not necessarily the optimum gradation.

- No information can be gained with regards the spatial composition of the mix including filling or replacement (substitution) mechanisms in the aggregate and the structure of the voids within a compacted mix.

The motivation behind developing an analytical model for predicting the VMA of a compacted mix may be summarised as follows:

1. With the VMA known, the volumetric properties of the mix are defined.
2. The model will allow mix design without tedious evaluation of candidate gradations in the laboratory.
3. Optimum binder contents of asphalt mixes may be estimated without even compacting the mix.
4. The spatial composition of an asphalt mix may be better defined.
5. Interaction between the aggregate filler, fine and coarse fractions as well as filling or replacement mechanisms may be controlled.
6. The aggregate skeleton of an asphalt mix may be structured.
7. The reason for performance or failure of an asphalt mix may be better understood.
8. Economic decisions can be made without the risk of forfeiting the performance of the mix.

The main motivation for developing the analytical model, however, is that it represents a rational approach to mix design, a shift from experimental empiricism towards scientific fundamentalism. The fundamental packing mechanisms underlying asphalt mixtures determine the performance of the mix. An understanding of these mechanisms is essential in reaction to more performance-related or -based mix design specifications.

Like any other process, mix design must be managed to ensure quality. Models that allow the estimation of VMA in a mix allow a better understanding of the most

important aspect of an asphalt mix i.e. the gradation or aggregate structure. Management of a process entails systematic monitoring and evaluation. With time, VMA models will become more refined and more accurate, enabling optimisation of the mix design process. The influence of variability and changes in the aggregate structure, or binder and aggregate volumes on the volumetric properties may be predicted using these models. The spatial composition may be better defined. The intention therefore is not so much to cut down on laboratory tests required to characterise an asphalt mix, but rather to 1) augment the mix design information, 2) promote an understanding of the mechanisms influencing volumetric properties and 3) encourage the management thereof.

1.3 Research objectives

The primary objective of the study is the development of a probabilistic and volumetric design method for HMA towards a better understanding of the performance of asphalt mixes in the field. Pavement performance is a function of material properties, loads and environmental factors, with their specific variabilities as well. To achieve this the following secondary objectives were established:

1. Understand the different philosophies underlying the design of asphalt mixes.
2. Evaluate and develop accurate packing models to estimate the VMA of asphalt mixes.
3. Identify the variabilities of factors influencing the mix design process.
4. Develop procedures to account for the variabilities of these factors.
5. Combine the packing model and probabilistic procedures to address variability within a single model, the Probabilistic and Volumetric Design of Asphalt Mixes

or PAVDAM.

6. Demonstrate the use of PAVDAM.

7. Validate PAVDAM.

Included in the dissertation is a discussion on the development of the semi-circular bending (SCB) test. This test is proposed as a possible replacement to the indirect tensile test (ITS) for the performance evaluation and/or quality control of HMA. Finite element analyses were done to allow characterisation of tensile strength and moduli of materials tested using the SCB. Accelerated pavement testing using the MMLS3 was done on selected sections at the NCAT test track for the purpose of validating PAVDAM. PAVDAM was developed to serve as a subset of the volumetric optimisation stage forming part of a mix design and analysis system. The SCB test may be used as part of the performance optimisation stage of this system to further evaluate the performance charactersitics of mixes developed using PAVDAM, which focusses more on the volumetric design of HMA. Accelerated pavement testing using the MMLS3 may be used as a performance related tool for the further (high-level) evaluation of mix performance.

1.4 Organisation

The dissertation was structured to follow the development of PAVDAM. Figure 1.2 shows a flowchart of the research undertaken as part of the dissertation.

Chapter 1 is a literature review of specific aspects of asphalt mix design and analysis towards an understanding of philosophies underlying the mix design of HMA. The different volumetric parameters used in mix design are also reviewed with consideration given to the nature of minimum VMA and film thickness mix design approaches. The characterisation of filler and filler-binder systems is also addressed.

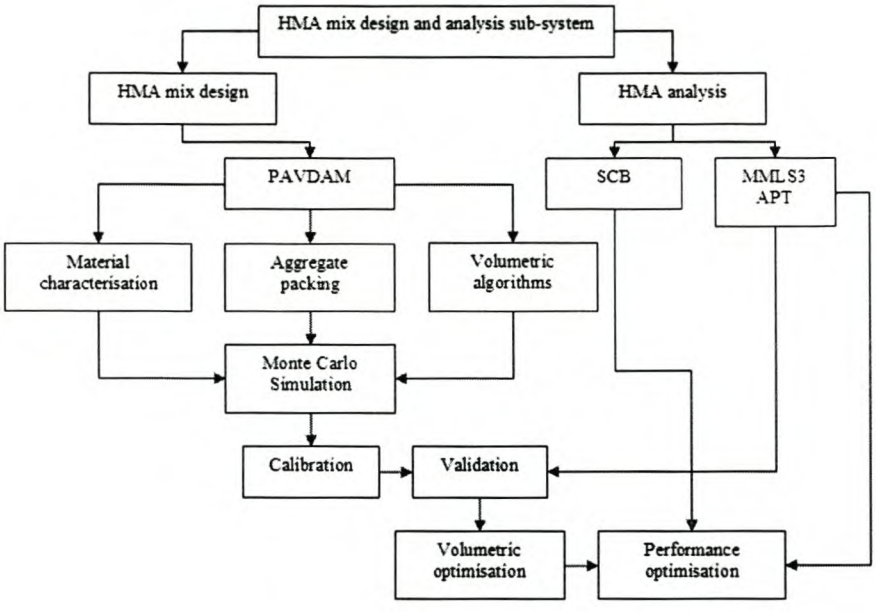

Figure 1.2: Flowchart of dissertation research

Chapter 3 is a review of different aggregate packing methods based on binary systems. A critical evaluation of these models is given towards identifying a suitable packing model for incorporation into PAVDAM. Application of the packing models is also discussed.

Chapter 4 introduces the concept of probability and reliability and recommends a strategy for implementation thereof in a mix design system. Factors influencing mix design are discussed and the variabilities of these are identified. The probabilistic approach based on Monte Carlo simulation, together with the analytical packing model form part of PAVDAM. The interaction between the two is outlined.

Chapter 5 discusses the use of PAVDAM, calibration and validation thereof. The full-scale and MMLS3 tests done at the NCAT test track are discussed towards validation of the model.

Chapter 6 discusses the development of the SCB and finite element analyses towards characterisation of the tensile strengths and moduli of materials tested using

the SCB. A comparison between ITS and SCB strength and fatigue test results is given.

Chapter 7 draws conclusions and makes recommendations.

1.5 References

M. F. C. van de Ven, K. J. Jenkins, and A. D. F. Smit. Conceptualisation of spatial composition. ITT Report 2-1999, Institute for Transport Technology, University of Stellenbosch, Stellenbosch, 1999.

Chapter 2

HMA mix design - An overview

This chapter presents a general overview of HMA mix design. Different mix design processes are defined and aspects to consider are presented. These aspects are divided into specific stages defining the mix design process:

1. Identifying external influences
2. Material characterisation
3. Mix gradation
4. Laboratory production and compaction
5. Volumetric optimisation
6. Performance optimisation
7. Performance prediction
8. Quality control and assurance

The chapter discusses each of these stages. This is followed by an overview of volumetric mix design approaches. Finally the important aspect of filler-binder interaction is addressed.

2.1 Introduction

Luminari [1997], in a state-of-the-art report to RILEM, defined asphalt mix design as:

> "... a series of procedures and/or tests followed or executed to select aggregate, aggregate gradation, binder types and content, additive/modifier type and contents to produce a bituminous mixture that satisfies specific requirements."

The challenge in formulating an optimum asphalt mix is achieving an acceptable balance between often opposing mix properties and taking account of environmental and economic considerations. Over the years, asphalt mix design methods have evolved from approaches based on recipes and empirical tests to approaches based on fundamental tests and *in situ* pavement performance prediction models. Mix design procedures may be divided into recipe, empirical, analytical, volumetric, performance related, and, performance based mix design categories. The dissertation introduces an extension to the volumetric mix design category i.e. probabilistic volumetric mix design. The following is a brief definition of each.

2.1.1 Mix design categories

Recipe

Recipe mix design specifications define numerous characteristics of the compacted mix including the grading, binder content, volumetric properties as well as compaction and mixing temperatures, compaction levels, etc. These specifications were and still are determined on the basis of (local) experience of traditional mixes of known composition in terms of established physical or mechanical performance over long time periods and under given traffic and weather conditions.

Empirical

The basic concept in empirical mix design methods (such as the Hubbard-Field, Hveem and Marshall mix design methods) is the selection of a binder content based on the optimisation of several variables that are not directly related to performance. Luminari [1997] states that the use of conventional empirical tests such as the Marshall for mix assessment and selection are based "solely on the comparability with the results of long and vast experience of such materials in road applications." Information obtained from these tests is therefore limited, which led to the development of more fundamental laboratory tests that could reproduce *in situ* conditions during the stages of mix preparation, construction and field operation.

Analytical

Analytical mix design models were originally devised to rationally proportion mix components on a volumetric basis. Starting from knowledge of the grading curve and certain materials characteristics, these models allow the prediction of voids in the mineral aggregate of a compacted mix. The suitable binder content is determined either by theoretical procedures (using the surface area of the aggregate) or experimentally (often empirically) by optimising volumetric characteristics. An important development in analytical mix design procedures has been the refinement of materials characterisation methods based on tests measuring the kind of performance that the component materials are expected to deliver.

Volumetric

Luminari [1997] points out that "...if the choice of design binder content and aggregate gradation is obtained by analysing the proportional volumes of air voids, binder

and aggregates for mixes that have been compacted using a test procedure that reproduces in the laboratory the *in situ* compaction process, then the mix design process can be defined as volumetric."

Performance related

The 1970's saw the development of performance related methods for characterising the intrinsic properties, that is, those independent of the test conditions, of mixes in relation to the stress/strain conditions induced by external forces. Fundamental tests were developed to measure material complex and resilient moduli, Poisson's ratio, as well as the laws governing the accumulation over time of fatigue damage, permanent deformation and crack growth. These methods of characterising materials were also introduced in the design of asphalt mixes to verify the mechanical behaviour of such materials once the optimum mix had been determined empirically or analytically. More recently, simulation tests have been developed that reproduce in the laboratory those processes involved in mix production and laying (such as the gyratory shear compactor) or during the pavement life (such as wheel tracking).

Performance based

The design of asphalt mixes is becoming increasingly characterised by a performance based approach that permits prediction of mix performance during the design life of the mix under traffic and environmental influences. Luminari [1997] cites that this design approach "...is not based on the criterion of obtaining the highest mechanical performance, but is otherwise conceived in such a way that the mix composition selected guarantees the minimum optimised level of the various performance characteristics required." The conversion of laboratory performance into field performance is achieved by means of shift factors calibrated on the basis of previous performance.

Probabilistic-Volumetric

The dissertation introduces the concept of volumetric-probabilistic mix design. In this approach, variabilities associated with the design of HMA are accounted for in the selection of an optimum binder content. In the dissertation elements of the analytical mix design procedure are incorporated in that a packing model is used to estimate the voids in the mineral aggregate of a mix based on its gradation and an appropriate binder content is selected by optimising volumetric characteristics.

2.1.2 External factors influencing HMA mix design

Luminari [1997] proposes that the first stage in a mix design process should be the preliminary analysis of the mix composition with the external stages of problem definition and material characterisation acting as inputs. External influences often define the function and purpose of the mix. Primary external influences to consider are listed:

Design traffic

Categorisation of anticipated effective volumes of traffic related to specific damage e.g. the number of high temperature axles causing rutting. Damage may be related to that caused by a standard axle i.e. 80 kN axle load (E80) or equivalent standard axle load (ESAL), usually raised to the fourth power. Design traffic is accounted for in mix design by relating its effect to laboratory compaction effort (number of blows, passes or gyrations). Besides load and equivalency, other traffic related factors to consider include tyre pressures, truck speeds, traffic wander, braking and shoving effects and fuel spillage.

Pavement structure

Material properties (stiffness, Poisson's ratio, thickness) of the sub-layers affect stress and strain response. Rut resistance becomes an issue when pavement layers are under compression. Likewise, fatigue resistance is more relevant when pavement layers are subjected to tensile forces. Besides performance, the effective compaction of HMA depends on the nature of the underlying support. Other factors to consider include: cracks from underlying cemented layers, construction tolerances, road geometry, drainage and materials availability.

Environment

Primary factors to consider are temperature and rainfall. The environment is often interrelated with the other factors i.e. temperature and design traffic, rainfall and mix permeability or the need for drainage layers.

2.1.3 Material characterisation

The preliminary analysis of the mix composition should permit the definition of alternative formulations (candidate or trial gradations) to optimise the choice of the initial gradings from the supplied fractions. Even at this level it is necessary to keep in mind the intended function of the layer as this will affect, amongst other things, the voids and consequently the optimum binder content to obtain a workable and durable mix. The material characterisation stage includes the selection of binder and aggregate (including gradation) based on the function of the mix.

HMA binders are selected based on external influences but also to directly influence the performance properties of the mix. Binders used in HMA may be characterised in terms of penetration, softening point, viscosity, bulk relative density, Fraass breaking point and stiffness determined using performance based testing.

Characterisation of aggregates includes definition of the gradation, engineering properties and quality or integrity. Gradations define the aggregate skeleton or structure with distinctions between dense, coarse, fine, continuous, gap or open graded mixes. Given the relevance of mix gradation it is discussed separately in the next section. Aggregate properties accounted for include angularity, flakiness (flat and elongated particles), clay content, shape, size, rugosity and absorption. Quality addresses the toughness, soundness, and presence of deleterious materials. Aggregates may be subdivided into stone, sand and filler components:

- Stone (+ 2.36 mm)

  Stones must be satisfactory in terms of angularity, gradation, particle shape, bulk relative density, static compressive strength, polishing and friction, and, resistance to abrasion.

- Sand (- 2.36 mm + 0.075 mm)

  The angularity of sands is an important property influencing both the stability and workability of the mix. The quantity of sand in a mix is particularly relevant. Superpave specifies the gradation of a mix by placing control points on the 2.36 mm sieve to control the amount of sand sized particles in the mix. The upper control point limits the amount of sand in the mix. The lower control point ensures adequate sand is contained in the mix to ensure a dense graded mixture. Sand equivalent or methylene blue tests are recommended to test the quality of sands.

- Filler (- 0.075 mm)

  The following properties of fillers are relevant: percentage passing the 0.075 mm sieve, Rigden voids (voids in dry compacted filler), stiffening effect measured using ring and ball apparatus, water number ("bitume getal") , bulk relative

density, water sensitivity, swelling potential, and, moisture content. Characterisation of fillers is further discussed in Section 2.3.1.

2.1.4 Mix gradation

The gradation of a mix defines its structure or skeleton. Mixes with stone skeletons have a high proportion of stone (at least 70 percent by mass of the total mix). Typically these mixes are open graded such as SMA or porous asphalt. Mixes with sand skeletons are most widely and often used in pavement engineering. These are typically continuously graded mixes, the mechanical properties of which depend on the optimum packing and internal friction of the sand particles. Mixes with filler skeletons have a high filler content (> 25 percent) and are used for specific purposes such as the German "Gietasfalt". The dissertation will focus on dense continuously graded HMA mixes.

The gradations of dense continuously graded mixes are often defined in terms of the following equation:

$$P = \left(\frac{d}{D}\right)^n \tag{2.1}$$

where

P = Percentage passing a sieve size of d, mm

D = Maximum aggregate size, mm

n = Gradation exponent

The Fuller gradation is Equation 2.1 with a gradation coefficient (n) of 0.5. It was shown by Nijboer [1943] that there is an optimum grading exponent for minimum VMA (maximum packing density). He studied aggregate gradations plotted on a log-log gradation chart with percentage passing plotted against sieve opening in microns. The gradation used in the study plotted as straight lines on the log-log

scale. Regardless of whether an angular crushed stone or rounded gravel was used, the gradation with minimum VMA plotted as a straight line with a slope of 0.45. Equation 2.1 is not always suitable for the design of mixes with large aggregates and in these cases it is often more practical to use the modified Cooper equation [Cooper et al., 1985] that allows control over the filler content of the mix:

$$P = \frac{(100 - F)(d^n - 0.075^n)}{(D^n - 0.075^n)} + F \tag{2.2}$$

where

P = Percentage passing a sieve size of d, mm

D = Maximum aggregate size, mm

F = Filler content (- 0.075 mm material)

n = Gradation exponent

In general, it is believed that gradings with an exponent of 0.45 may be too dense with insufficient void space to accommodate the binder for a durable mix. The solution generally adopted is to increase VMA by moving the gradation away from the maximum density curve. This may be accomplished by reducing the gradation exponent and, consequently, making the mix finer. This results in a higher binder content caused by the increased fines (increased surface area of the graded aggregates), which may increase susceptibility to permanent deformation. An increase in VMA may also be achieved by increasing the exponent and making the gradation coarser. This approach is generally adopted for base materials.

Restricted zone

In the Superpave mix design procedure, a restricted zone is specified. Gradation curves must not pass through this zone. Avoidance of the restricted zone moves the

grading of the material away from the maximum density curve to allow sufficient VMA to carry a high enough binder content for good workability.

Gradations that pass through the restricted zone have been called "humped gradations" because of their characteristic hump shape in this area. The Asphalt Institute [AI, 1995] claim that in most cases, a humped gradation indicates a mixture that contains too much fine sand in relation to total sand. This gradation may result in a mix that is tender under compaction during construction and offers reduced resistance to permanent deformation during its performance life. This phenomenon was documented by Goode and Lufsey [1962] when they reported on "problem mixtures" associated with the detrimental effect of gradation humps in the finer aggregate. Mixes that pass above the restricted zone will tend to be sandier and have a weaker aggregate structure than mixes that pass below the restricted zone. Coarser mixes may also be more permeable than finer mixes. The restricted zone encourages the development of gap graded mixes. Mixes that pass below the restricted zone are gap graded. The significance of the restricted zone has been questioned by asphalt technologists since often mixes passing through this zone are not overly tender at all.

2.1.5 Laboratory production and compaction

This stage includes the production of the specimens from the preparation to conditioning and compaction. Preparation of specimens in the laboratory allows stricter control of design variables including gradation, binder content and mixing and compaction temperatures. Properties of specimens prepared in the laboratory from materials sampled at the asphalt plant are subject to greater variation but may be more representative.

Laboratory conditioning

Conditioning includes heating and maintaining prepared uncompacted asphalt material at elevated temperatures for specific periods to simulate hardening (oxidation and volatile loss) and ageing of the mix during manufacturing and transportation and during the first year or two of service. Superpave [McGennis et al., 1994] recommends 4 hours at 135 °C. Austroads [1997] recommends 1 hour at 150 °C. The latter conditioning period is often more practical in production laboratories.

Laboratory compaction

The compaction method and procedure used to prepare specimens is critical since it serves to reproduce or relate in the laboratory, compaction in the field during construction and in service. Having said this, it is important to recognise, however, the physical and spatial differences between an asphalt mix compacted within a confined mould to that of a mix compacted in the field. Laboratory compaction techniques used include impact Marshall [AI, 1995] and Hugo [1970], gyratory, vibratory and roller compaction, the latter typically being used for the production of specimens for performance testing [SHRP, 1994; Harvey et al., 1994; Sousa et al., 1993]. A major drawback of impact compaction is that it does not produce specimens similar to road cores; not in terms of duplicating the densities of the cores but rather the performance properties of the asphalt mix, air void distribution and aggregate orientation. The French mix design method developed by Duriez [1950] in the 1930s consisted of compacting samples by simple compression that often crushed the aggregates because of the high stresses to which these were subjected. The French started using gyratory shear compactors in the late 1970s when a method was developed that proved to be discriminating in separating the behaviour of grading components in the evaluation of compactibility [Moutier, 1993]. This discriminating element was also one of the

reasons why gyratory compaction was selected for Superpave. The dissertation will focus primarily on the *gyratory* compaction of mixes for mix design, and in particular the Superpave gyratory compactor (SGC).

HMA mix design methods used around the world include procedures that relate laboratory compaction to design traffic level. The Asphalt Institute varied number of blows to be applied with the Marshall hammer [AI, 1995]. The new South African design guidelines [PMGHDP, 2000] include a unique procedure. Laboratory compaction is done using a modified Marshall hammer that measures specimen densification during compaction using displacement transducers. The measurement of specimen densification with each Marshall blow was first investigated as part of an undergraduate study of students at the University of Stellenbosch as reported by Smit et al. [1999]. The trend towards relating laboratory compaction effort and field design traffic is significant and supports the trend from empirical based towards performance based mix design procedures.

Superpave gyratory compaction

The SGC also measures specimen height during compaction. This allows an estimation of specimen density during compaction that may be related to field compaction. The SGC is able to compact laboratory mixtures to densities well in excess of those anticipated in the field after years of trafficking. The problem has been identifying the level at which the density would stabilise in the field, depending on the level of traffic and pavement temperature conditions, and then designing accordingly. Design levels of compaction are specified in the so called "N-design" table suggesting compaction efforts based on design traffic levels and average high air temperature. The N-design table was determined on the basis of limited laboratory compaction and in-place density data from different traffic levels in different climatic zones [Blankenship et al., 1994]. Post SHRP research was done to evaluate this table concluding that the N_{des}

gyratory compaction level may be too high, at least for lower traffic [Brown et al., 1996]. Furthermore, research has shown that the number of design gyrations required should be reduced and in cases of low traffic level by as much as 30 gyrations [Brown and Mallick, 1998]. More recent research under NCHRP Project 9-9 [NCHRP, 1999] supports this reduction and recommended consolidation of the N-design compaction matrix to exclude temperature levels and only four traffic levels. The recommended revision of the N-design table is shown in Table 2.1.

Table 2.1: NCHRP recommended consolidation of N-design table [NCHRP, 1999]

Design ESALs (million)	$\mathbf{N_{ini}}$	$\mathbf{N_{des}}$	$\mathbf{N_{max}}$
< 0.1	6	50	74
0.1 - 1	7	70	107
1 - 30	8	100	158
≥ 30	9	130	212

Superpave distinguishes between different compaction levels as shown in the table, defined as follows:

- N_{ini}. The initial compaction level used to assess the compactibility of the mixture and represents mix behaviour during breakdown rolling.
- N_{des}. The design compaction level anticipated after several years of in-service traffic and the anticipated compaction level at the end of the design period.
- N_{max}. The maximum compaction level at the end of the design period and set to safeguard against underestimating the design traffic.

NCHRP [1999] comments on the gyratory compaction of large stone HMA (37.5 nominal size). They point out that large stone mixes placed in the top 100 mm of the pavement structure should be designed using the suggested levels of N_{des} shown in Table 2.1. Research results from laboratory prepared specimens indicated that

the number of gyrations for mixes greater than 100 mm from the finished pavement surface may be reduced by approximately 28 percent to account for the reduced vertical pressure and lower temperatures at increased depths within the pavement structure. For mixes at depths greater than 200 mm from the finished pavement surface, the design number of gyrations may be reduced by a greater percentage. Therefore, for mixes that are placed below 100 mm in the pavement structure, the design number of gyrations may be reduced by one level from those shown in Table 2.1. When placed more than 200 mm into the pavement structure, the design gyrations may be reduced by two levels. However, if it is likely that these mixes will be open to traffic for any significant period of time (more than 2-3 days) prior to the construction of the overlying layer, the design number of gyrations for the mix should remain at the level used for the surface course mix.

Different agencies are also adopting variations of the N-design table to suit specific needs. An example is the Virginia Department of Transportation that recommends an N_{des} of 65 gyrations for specific mixes used on low volume roads and for base layers [Prowell and Haddock, 2002]. The Texas Department of Transportation are in the process of establishing Superpave design levels that correspond with their vast knowledge on the behaviour of typical Texas type mixes designed using the Texas gyratory compactor.

Compaction energy principles

Early research with the Superpave Gyratory Compactor (SGC) suggested that the number of gyrations versus compaction density relationship alone is insufficient to adequately define the relative resistance of different mixes to compaction, particularly when the compaction response curves of these mixes are not parallel [Hugo et al., 1996]. In such cases, the total energy that is used to achieve compaction may be a more appropriate measure of the resistance to compaction as the mix densifies.

This was confirmed at the international workshop on the use of the gyratory shear compactor where it was stated that even if two gyratory compaction curves are equal in terms of density against cycles, their shear characteristics could be significantly different [Horvli, 1996].

Recent research to evaluate the compactibility of mixes has used shear stress and power measurements [de Sombre et al., 1998; Butcher, 1997]. Research has identified shear stress characteristic stages during the compaction of gyratory specimen [Gauer, 1996; Butcher, 1997]. The first stage is where the shear resistance increases to a maximum followed by the second stage where the shear stress decreases to a point where constant shear stress occurs (third stage) and where a decrease in the height of the specimen is only achieved by a decrease in binder. Bahia et al. [1998] have introduced gyratory compaction energy indices as new measures to relate to construction and in-service performance of mixtures. They assume that since the major contributor to resistance to densification is the aggregates, the densification characteristics of mixtures are not highly dependent on the temperature. They claim that it is therefore possible to use the SGC results to relate field compaction at high temperatures as well as at ambient temperatures. They believe that the SGC data is under utilised in mixture design and point out that what appears to be missing in the current analysis of SGC data is the recognition that SGC densification curves represent behaviour of material under two different field conditions:

1. Compaction during construction (using rollers) at high temperatures with the objective of reducing air voids to an acceptable level with minimum effort.

2. Densification under traffic at ambient temperatures with the objective of maintaining air voids within acceptable levels for as many repetitions of traffic axles (design traffic) as possible.

The assumption that mainly the aggregates resists mix densification is obviously

mix specific. The approach suggested by Bahia et al. [1998] has not been validated. The approach may be justified in hotter climates but even then, gyratory compaction in the laboratory cannot account for environmental influences impacting the performance of in-service pavements.

Refusal density

Another important compaction concept is that of refusal compaction. This concept was introduced to assess the level of compaction that is ultimately achieved in the field after heavy trafficking. It is well known that HMA often looses stability and may become susceptible to shear failure when the VIM fall below the 3 percent level. Criteria are increasingly being specified to ensure that mixes do not densify beyond this limit, assessed by measuring VIM at refusal compaction. Refusal compaction may be defined as the effort required to densify HMA to its maximum density. For Superpave gyratory compaction, 300 gyrations are usually sufficient to achieve refusal compaction since increases in density with increased effort beyond this are often insignificant. Austroads [1997] specify that VIM must not be less than 2 percent after the application of 350 gyrations using the Australian gyratory compactor. Smith and Edwards [1996] recommend 2 minutes compaction with a (Kango) vibratory hammer to achieve refusal compaction.

2.1.6 Volumetric optimisation

This stage in the mix design process has to do with the volumetric analysis of the alternative (candidate) HMA mixtures and judgement based on specific criteria. A basic understanding of mass-volume relationships of compacted HMA is important from both a mixture design standpoint and from a field construction standpoint. Mix design is a volumetric process with the purpose of determining the optimum volume

of bitumen and aggregates required to produce a mixture with the desired properties. Measurements in the laboratory or field of the volume of aggregates and bitumen are, however, difficult and impractical. Therefore, to simplify the measurement problem, masses are used instead of volumes, and the relative density of the materials is used to convert from mass to volume.

The component diagram by McGennis et al. [1994] shown in Figure 2.1 is a simple example of a spatial model based on bulk volumetric properties. From this component diagram it is clear that when converting the total mass of aggregate to volume, the differences in densities of the coarse aggregate, fine aggregate and filler have to be taken into account. The effect of absorbed bitumen is also shown.

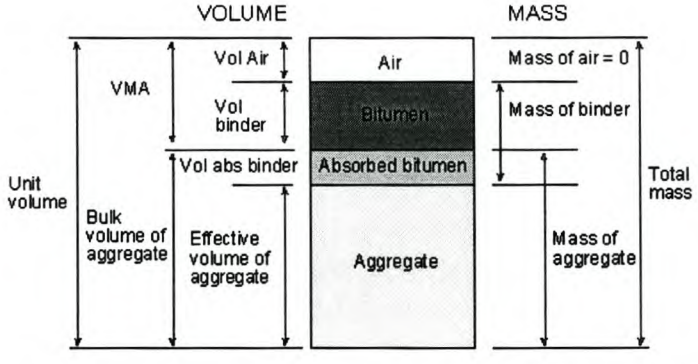

Figure 2.1: Component diagram of compacted mix [McGennis et al., 1994]

Volumetric parameters used to define the spatial composition of HMA include voids in the mineral aggregate (VMA), voids in the mix (VIM) and voids filled with binder (VFB). VIM consist of the small air spaces between the bitumen coated aggregate particles. Based on the spatial model illustrated in Figure 2.1, VMA are defined as the inter-granular voids between the aggregate particles in a compacted mix that includes VIM and the effective binder content (V_{be}), expressed as a percentage of the total volume. VFB are the percentage of the voids in the mineral aggregate that are

filled with bitumen, not including the absorbed bitumen. To calculate these parameters it is necessary to have data on the bulk relative density of the compacted mix (G_{mb}), the appropriate relative density values of the individual components of the mixture i.e. aggregate (G_{sb}) and binder (G_b), and the binder content (P_b).

Binder absorption

The accurate calculation of VIM, VMA and VFB is compounded by the partial absorption of bitumen into the aggregate. As part of the SHRP research, Curtis et al. [1993] investigated the fundamental properties of asphalt-aggregate interactions including adhesion and absorption. They conclude that absorption is a phenomenon that is not understood. They were able to model absorption according to the fundamental principles of fluid mechanics. They point out that binders with higher viscosities and aggregates with small pore diameters limit absorption. They found *no* evidence for selective absorption of binder in aggregate pores. Selective absorption has been postulated as being the reason for the phenomenological observation that when absorption occurs the binder remaining on the outside of the aggregate becomes hard and brittle i.e. the solvent part of the binder penetrates the pores but the polar part does not. Kandhal and Khatri [1991] recommend determining absorption by using Rice's test after ageing the mix at 135 °C for 4 hours. In their study absorption was found to follow a hyperbolic relationship with time and no significant difference in absorption was observed beyond four hours of ageing. The degree of absorption depends on the type of aggregate and binder.

Volumetric properties

The mix parameters VMA, VFB and VIM are not independent, but are related as follows:

$$\text{VIM} = (\text{VMA})\left(\frac{100 - \text{VFB}}{100}\right) \tag{2.3}$$

Moreover, for a given binder content:

$$\text{VFB} = \frac{P_b G_{sb}}{G_b}\left(\frac{100 - \text{VMA}}{\text{VMA}}\right) \tag{2.4}$$

The relationship between the volumetric properties VIM, VMA and VFB can also be charted using so called mix design charts. McRae [1956] illustrated the use of mix design charts as far back as 1956. Coree [1998] points out that in the process of mix design or production, it is frequently necessary to seek to change the magnitude of VIM, VMA or VFB, but it is not always clear what effect such a change might have on the other parameters nor whether that change may in itself compromise compliance in another direction. He emphasises that no such change in any one parameter should ever be contemplated without checking the effects on the other two. Mix design charts provide a means whereby the effect of changes may be monitored.

Figure 2.2 presents a linear plot that presents all three volumetric components of a mixture, and that is universal in application, i.e. it is independent of differing relative densities and can be used without modification for any mixture. The y-axis represents the VIM or V_a. The x-axis represents the percent effective binder volume (V_{be}) and is found by the difference between the VMA and VIM. The diagonal lines are lines of equal VMA. Since VMA = $V_a + V_{be}$, lines connecting equal values on the two axis are lines of VMA of those magnitudes. The lines radiating from the origin are lines of equal VFB (Superpave uses the abbreviation VFA shown on the chart for voids filled with asphalt). There is a further series of lines shown, sloping slightly left-to-right off the vertical. These are referred to as *trajectories*. Trajectory lines are constructed by joining any point on the plot (V_{be}, V_a) to the point (0, 100).

Coree [1998] points out that the volumetric chart has a number of uses:

1. Feasible region: Unrealistic, or unfair, volumetric specifications can be identified.

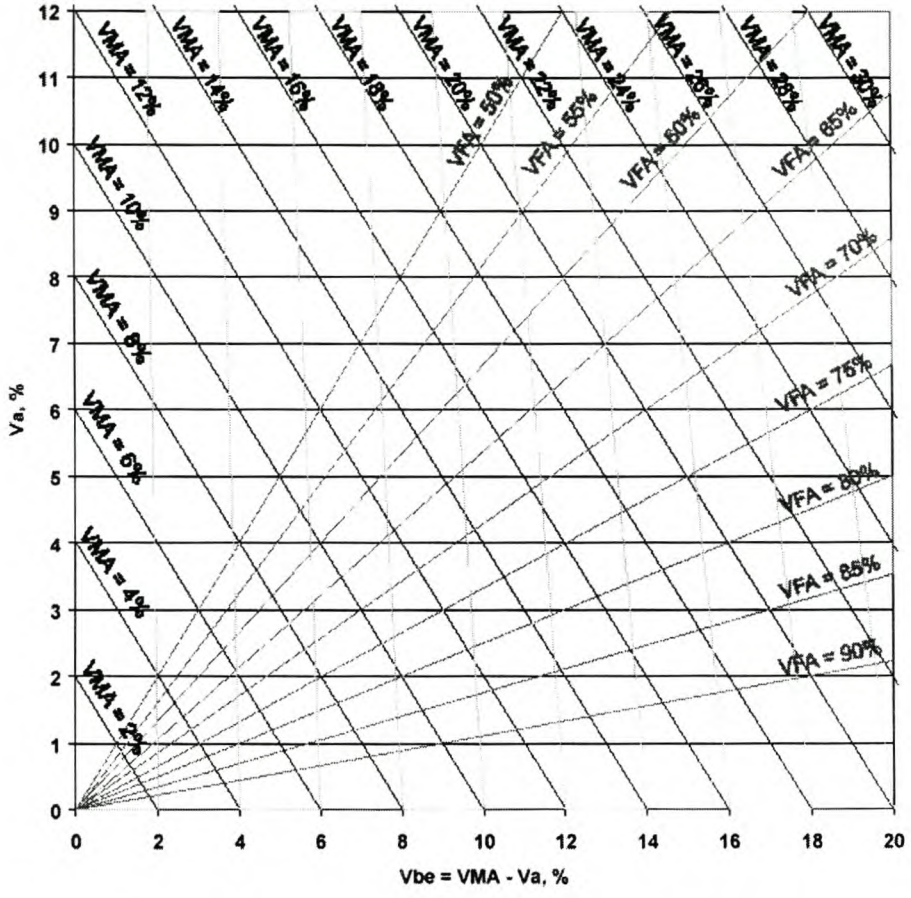

Figure 2.2: Universal volumetric chart [Coree, 1998]

2. Trajectory: The volumetric parameters (VIM, VMA and VFB) are dependent upon the degree of compaction. Thus the same mixture can exhibit different volumetric properties at different degrees of compaction. By following the trajectory line at a specific void content, the volumetric properties at other void contents (compaction levels) can be determined.

3. Quality control: The trajectory lines can also be used in a QC/QA monitoring function. All samples of the same mixture, at whatever level of compaction, should fall on the same trajectory line. If a sample plots significantly off its trajectory line, the implication is that something has changed in the mixture

itself (regardless of compaction).

The mix design chart illustrates the dynamic nature of an asphalt mix as the changes in the volumetric properties of a mix with compaction may be defined. Figure 2.3 shows the mix design chart with gyratory compaction data collected by the author for illustration purposes. The compaction data is from an asphalt base mix with a nominal maximum aggregate size of 19 mm. The mix was compacted at four different binder contents i.e. 4.5, 5.0, 5.5 and 6.0 percent. The trajectory lines indicating these binder contents are shown on the chart. At each of the binder contents, the volumetric properties of the mix are plotted at three compaction levels i.e. 50, 150 and 250 gyrations. Notice that the trajectory lines at each of the binder contents pass through the points at the different compaction levels as expected. The x-axis has been truncated to save space, but the parallel lines running top to bottom from left to right are lines of equal VMA. The lines running from bottom to top from left to right actually pass through the origin and are lines of equal VFB. The corresponding VMA and VFB values for the lines have been included using a slightly smaller font size.

Volumetric criteria

In the design process, volumetric criteria have been established to assist with the selection of optimum binder contents. These criteria are also used to judge the quality of HMA mixes as will be discussed in Section 2.1.9. Criteria are typically established for VIM, VMA and VFB and often film thickness to ensure workability (during construction) and performance (in-service). Superpave places certain restrictions on the compaction characteristics of a mix at the three compaction levels defined previously. These design criteria are established on the basis of compaction density as shown in Table 2.2.

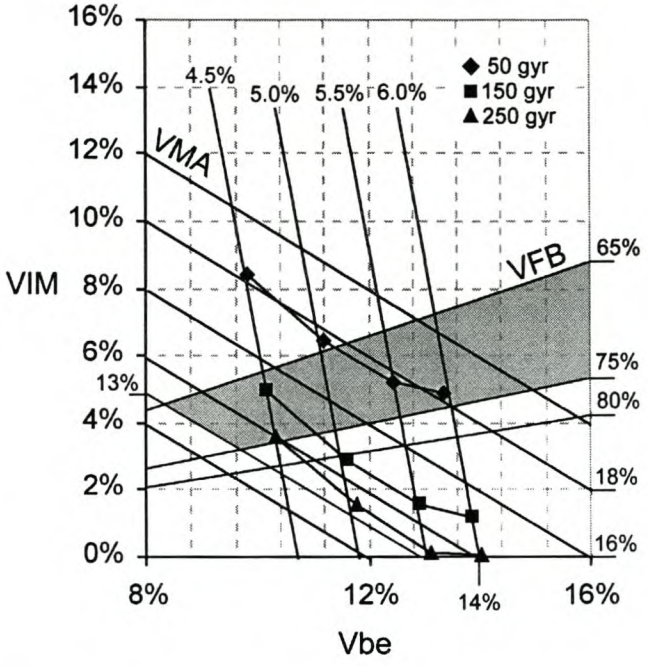

Figure 2.3: Mix design chart with real life compaction data

Moutier [1993] points out that the use of volumetric criteria in mix design is often disadvantageous in that, if certain criteria are restrictive, the design mix will quite often be difficult to obtain. Mix design criteria should therefore be chosen with consideration given to the interdependency between volumetric parameters. This may be illustrated with reference to the mix design chart in Figure 2.3. This particular mix was designed for a highly trafficked road used in the Western Cape, South Africa. The optimum binder content of the mix was selected as 4.7 percent based on the Marshall

Table 2.2: Superpave compaction design criteria [McGennis et al., 1994]

Compaction level	**Criterion for %G_{mm}**
N_{ini}	< 89.0
N_{des}	$= 96.0$
N_{max}	< 98.0

mix design method. The Superpave minimum VMA criterion for a 19 mm nominal maximum mix is 13 percent. The Superpave VFB requirement for high design traffic is between 65 - 75 percent. The window satisfying the Superpave requirements has been shaded. If one examines the mix from the Superpave point of view, the binder content required to achieve 4 percent voids at N_{des} (130 gyrations) is slightly less than 5 percent, the optimum of 4.7 percent would therefore satisfy the Superpave requirement.

Figure 2.3 also sheds light on the Superpave philosophy, which is not always very transparent. It can be inferred that the minimum VMA criteria are established to ensure adequate binder for durability and workability. This is not immediately apparent from this example if one applies the 13 percent criterion but becomes clearer if the minimum VMA was set to 14 percent say. The upper VFB criterion places a limit on the binder content or restricts the use of too high a binder content and the lower VFB criterion sets the traffic capacity of the mix.

The two different approaches used for the volumetric mix design of HMA mixes are discussed in Section 2.2. Another important volumetric aspect is optimisation of the filler:binder ratio of HMA mixes, addressed in Section 2.3.

2.1.7 Performance optimisation

The next stage of the mix design process is measuring the behaviour of the mix by means of simulation or fundamental type tests. The performance of HMA mixes are judged in terms of limiting criteria established for acceptable performance. These criteria are also often used to establish optimum binder contents for mixes in design methodologies with higher level stages e.g. Superpave level 2 and 3.

There are a number of mix performance properties that must be considered for

specific mix design situations. These include stiffness, resistance to permanent deformation or rutting, fatigue resistance, resistance to (reflective) cracking, permeability, durability, workability, segregation and low temperature response. These mix properties have a direct influence on the structural and functional behaviour of HMA and will be discussed briefly. Other mix properties influencing the functional performance of HMA include skid resistance, riding quality and noise.

Performance optimisation serves as an analysis tool in the mix design process. It may be used to test the validity of the volumetric optimisation stage. Aspects of the performance evaluation of HMA mixes are discussed in Chapter 6.

Mixture stiffness

Stiffness characteristics of asphalt materials are dependent on time of loading (frequency) and temperature because of the visco-elastic nature of these materials. Stiffness dictates the performance (load spreading ability) of an asphalt mix in a pavement structure. It is required to determine the stresses and deformations in the asphalt layer due to traffic and environmental loading.

A number of different test methods may be used to evaluate the stiffness characteristics of asphalt. These include:

1. Axial resilient stiffness,
2. Diametral resilient stiffness,
3. Flexural dynamic stiffness, and,
4. Shear dynamic stiffness tests.

Resistance to permanent deformation

Rutting or permanent deformation is the accumulation of plastic strain due to repetitive loading. Rutting in HMA is a combination of:

1. Densification - consolidation characterised by a decrease in volume and consequently an increase in density.

2. Shear deformation - permanent deformation characterised by no volume change.

Mechanical tests to evaluate the resistance to permanent deformation of HMA include static and dynamic creep, triaxial, Hveem stabilometer, Superpave shear and wheel tracking tests. These tests are usually done at elevated temperatures between 40 °C to 60 °C.

Fatigue resistance and cracking

Fatigue resistance is the ability of a mix to bend repeatedly without fracture. Fatigue cracking is caused by the repetitive application of traffic loads. For heavy duty pavements, fatigue is a result of tensile stresses and/or strains at the bottom of the asphalt layer(s). The maximum principal tensile strain is considered to be the primary determinant of fatigue cracking [SHRP, 1994].

Various tests have been developed to evaluate the fatigue characteristics of asphalt mixes. These include:

1. Simple flexure testing

2. Supported flexure testing

3. Direct axial testing

4. Diametral testing

5. Triaxial testing

6. Fracture mechanics testing, and

7. Wheel-track testing

Fatigue distress generally accumulates most rapidly under moderate to cool temperatures and rapid traffic loading. For this reason, fatigue tests are typically done at temperatures ranging between 10 to 20 °C. Another option is to do fatigue tests at the critical temperature anticipated at highly stressed locations within the pavement structure. Higher temperatures lower fatigue life in the case of thick asphalt pavements.

Besides fatigue properties, the tensile strength of HMA is used to evaluate resistance to cracking caused by load, environment or external influences such as cracking in asphalt bases initiated by shrinkage cracks reflecting through stabilised subbase layers. Asphalt materials must have sufficient tensile strength to resist or retard this cracking.

Durability and permeability

Durability can be considered to be the resistance of an asphalt mixture to environmental influences and to the abrasive action of traffic. It is influenced by the hardening of the binder due to oxidation and volatilisation and also by changes to the aggregate characteristics due to degradation and the influence of moisture as related to stiffness reduction or stripping. The latter influence is more critical for HMA bases as these are usually not directly exposed to climatic influences. Two key mechanisms contribute to the deterioration of HMA by water: 1) reduction in adhesion and stiffness of the binder matrix; and 2) loss of adhesion between the binder and the aggregate surface. Durability is promoted by high binder contents, dense aggregate gradations and well compacted mixtures. These factors contribute to ensure that the mix is impervious to air and moisture.

Change in stiffness can be used to quantify environmental influences on pavement response. The modified Lottman test [Lottman, 1982] (ASTM D4867 or AASHTO

T283) is used in South Africa for this purpose [SABITA, 1997]. This involves diametral indirect tensile splitting tests. Other tests used to evaluate the moisture susceptibility of HMA include:

- NCHRP 274, Indirect tensile tests with Tunnicliff and Root [1984] conditioning
- Boiling water test (ASTM D 3625; TxDOT method 530-C)
- Immersion-Compression test (ASTM D 1075; AASHTO T 165)
- Freeze-thaw pedestal test [Kennedy et al., 1982]
- Static immersion test (AASHTO T 182; ASTM D 1664)
- Conditioning with stability test (AASHTO T 245)
- SHRP Environmental Conditioning System [Al-Swailmi and Terrel, 1992]
- Wet wheel tracking tests [Smit et al., 2002b]

The Hamburg wheel tracking test is routinely used by the Texas Department of Transportation (TxDOT) to evaluate the rutting and stripping potential of HMA. The test is done on gyratory compacted specimens (7 percent VIM) or field cores that are submerged in water at a temperature of 50 °C. A steel wheel under a fixed load tracks over the specimens and the deformation per wheel pass is monitored. Besides indicating the potential for rutting, the creep curve is used to calculate a "stripping inflection point" indicated by a change in the slope of the creep curve as shown in Figure 2.4. Wet MMLS tests have also been used to evaluate the moisture susceptibility of asphalt mixes [Smit et al., 2002b].

In South Africa the permeability of HMA materials is not routinely evaluated in the laboratory as part of mix design procedures. Air permeability tests as outlined in an appendix to TRH8 [CSRA, 1987] are used to test 100 mm diameter laboratory

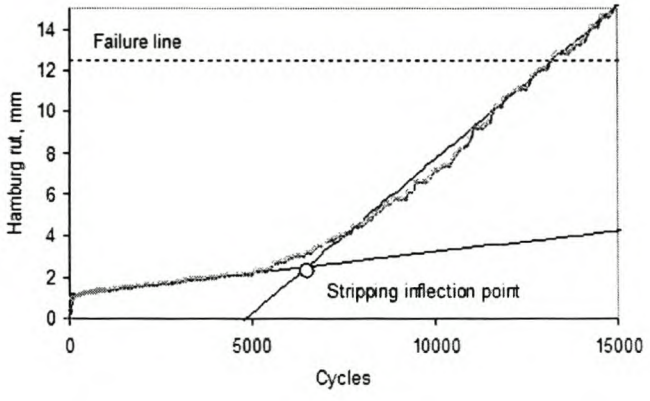

Figure 2.4: Hamburg test result

compacted Marshall specimens or field cores. Permeability is evaluated in the field (post construction) using the MARVIL permeability test. Cooley et al. [2002] report extensively on the permeability of coarse graded Superpave mixes. They conclude that the permeability of these mixes may be related to mix density, nominal aggregate size and lift thickness. Cooley [1999] discusses the use of four different field permeameters and ranks these in terms of correlation with laboratory results, repeatability and ease of use.

Segregation

Kennedy et al. [1987] found that mixture design is not a primary cause of segregation but that certain mixes are more inclined to segregate than others do. They point out that the two prime mixture design factors are bitumen content and gradation. Lower bitumen contents generally cause reduced cohesion. In addition, coarse-graded aggregates with large maximum size and gap-graded aggregates are prone to segregation.

The cause of segregation in asphalt mixes is complex and varied and can even be traced back to the production of the aggregate at quarries. VBW-Asfalt [1999a] list potential instances when segregation can occur during the production through to the

construction of asphalt:

1. Mining/blasting of aggregate deposits at quarries
2. Crushing and sieving of aggregate at quarries
3. Stockpiling of aggregate at quarries
4. Transport of stockpiled material to asphalt plants
5. Stockpiling of aggregate at asphalt plants
6. Loading of front-end loaders into aggregate bins
7. Sieving of aggregate from bins (screening)
8. Dumping of aggregate onto conveyer belt cold feeders
9. Drying of aggregate in dryer drum
10. Feeding mixers or pugmills
11. Feeding hot or surge bins
12. Loading asphalt onto trucks
13. Loading asphalt into paver hoppers
14. Paving operation

The "Skanska" apparatus is a new device used to measure the segregation potential of asphalt mixes [VBW-Asfalt, 1999b]. About 10 kg of asphalt is placed in a funnel and dropped from a height of about 1 m onto a flat base plate. A circular disk (diameter of 140 mm) on the base plate is opened pneumatically allowing the core of the asphalt on the base plate to be collected in a container placed beneath the circular opening. This "fine" asphalt sample collected in the container is roughly

about 4 kg. Following this, another circular disk (diameter of 220 mm) is opened pneumatically and the middle part of the asphalt sample remaining on the base plate is collected in a separate container. The mass of this sample is about 2 kg. Finally, the remaining outer "coarse" asphalt on the base plate is collected by scooping it through the opening in the base plate into a third container. The binder contents of the "fine" and "coarse" samples are determined separately and the calculated difference in binder contents between the "fine" and "coarse" samples is the segregation value. It is reported that the segregation value allows the relative sensitivity of asphalt mixes to segregation to be quantified.

2.1.8 Performance prediction based on volumetric properties

The results of the volumetric optimisation stage discussed previously permit one to arrive at the performance of the material in the pavement using appropriate volumetric prediction models. Prediction models allow a preliminary evaluation of HMA performance during the design phase prior to performance testing. This allows refinement in the selection of the most suitable mixes, although the information must be validated experimentally. Predictive equations have been developed for mixture stiffness, fatigue and permanent deformation. Appendix C contains a summary of some models that may be used for performance prediction.

2.1.9 Quality control/assurance

Verification of quality prescribed by performance type specifications or standards is the decisive stage in obtaining the final product in the mix design process. This is represented by the formula (job mix formula), which is subsequently processed to define the design curve and the related tolerances. Luminari [1997] emphasises that once the mix is accepted and is in production, the factors critical to the success of the

pavement are the conditions under which the mix is prepared in plant, transported and laid. These factors must therefore also be subject to quality control.

Quality in asphalt mix design must be defined in terms of acceptable long term performance in service. In other words the mix design process must deliver reliable mixes. For the *structural* design of pavements, risk may be allocated for different road categories depending on anticipated design traffic and climatic conditions. The TRH4 [CSRA, 1996] structural design approach is an example. It allocates risk to the different road categories, which is related to the length of the road that will not exceed the specified terminal functional performance criteria at the end of the design period. Reliability in asphalt *mix* design is usually used to assess the performance potential of asphalt mixes (the optimum job mix) in terms of fatigue or rutting. The approach adopted by SHRP [1994] is an example. Satisfactory mix performance demands that the mix resistance (N_{supply}) equals or exceeds the traffic demand (N_{demand}). A multiplicative factor is applied to N_{supply} to account for the fact that neither N_{supply} nor N_{demand} is known with certainty and to accommodate the desired level of design reliability. Thus for a satisfactory mix, the following must be met:

$$N_{supply} \geq M \cdot N_{demand} \tag{2.5}$$

The reliability multiplier (M) can be calculated from the following equation:

$$\ln(M) = Z_R \left[\text{Var}\left\{\ln(N_{supply})\right\} + \text{Var}\left\{\ln(N_{demand})\right\}\right]^{0.5} \tag{2.6}$$

where

Z_R = Function of the reliability level (use normal distribution tables)

$\text{Var}\left\{\ln(N_{supply})\right\}$ = Variance of the natural logarithm of N_{supply}

$\text{Var}\left\{\ln(N_{demand})\right\}$ = Variance of the natural logarithm of N_{demand}

The risks directly associated with the mix design process itself are usually accounted for in product (end-result) specifications. The South African COLTO specifications [COLTO, 1998] address risks with regard gradation, compaction density, binder content and voids in the mix (VIM).

In mix design, the critical aspects defining risk may be related to the performance of the mix in the field. Compaction density influences both the stability and durability of the mix. Binder content may in turn influence the compactibility and workability of the mix in the field. Too high a binder content may also lead to excessive rutting but too low a binder content may have a negative influence on the durability of the mix. The same applies to VIM. Specifications therefore aim to balance conflicting influences to reduce the client's risk. Where product specifications fail (in the author's opinion) is in identifying the consequences of combined variability, even when individual mixture properties may fall within required specification limits. Variables influencing asphalt mixtures are not always mutually exclusive. A classic example is the obvious relationship between filler and binder content. Specification limits are set for the filler and binder contents of mixes and even (in some cases) the filler:binder ratio, but little regard is given to the possible influence of the combined effect of both filler and binder variability. This shortcoming in HMA mix design is addressed in the dissertation. It is argued that the combined effect of the variability of all variables (or at least the most significant) should be taken into account. The variabilities inherent in the properties (gradation, densities, binder contents, volumetric properties, to name a few) of asphalt pavement materials and mixes must be accounted for in the risk management of the mix design process.

Product specifications

Specifications are used as a basis for competitive bidding for the delivery of products or services and are used to measure compliance to specifications. There are four

types of specifications generally recognised in the construction industry: proprietary product, method, end result, and, performance specifications. Proprietary product specifications tend to be conservative. The client has complete control over the final product and consequently bears most of the risk whilst the contractor has little latitude for innovation. These specifications tend to limit competition, which increases cost. Performance specifications on the other hand are those in which the product payment is directly dependent upon its actual performance. The contractor therefore carries considerable risk during the warranty period in ensuring performance albeit through maintenance and repair. The COLTO specifications [COLTO, 1998] used in South Africa combine elements of method and end-result specifications. Product characteristics (asphalt density, binder content and void content, for example) must fall within specified limits that agencies judge to be satisfactory based on statistical techniques. In some cases elements of method specifications are incorporated to guard against early failure of the product (for instance, specifying the thickness of the pavement layers). No matter which type of specification is applied though, identifying and controlling product variability is the objective to achieve the desired degree of quality.

Specifications in Section 4200 of COLTO [1998] cover all the work in connection with the construction of asphalt bases and surfacings in South Africa. In the COLTO specifications, the combined aggregate and filler grading may not deviate from the approved target grading for the working mix by more than that given in Table 2.3. The table refers to material passing a specific sieve and the permissible percent deviation from the approved target grading. The mean grading of each lot of the working mix (minimum of six tests per lot) must be determined from samples obtained in a stratified random sampling procedure.

Compaction densities, binder contents and voids in the mix must be within limits specified in an applicable judgement scheme. The COLTO specification provides

Table 2.3: COLTO grading specifications (after [COLTO, 1998])

Sieve size, mm	Specification
26.500	± 5.0
19.000	± 5.0
13.200	± 5.0
9.500	± 5.0
6.700	± 5.0
4.750	± 4.0
2.360	± 4.0
1.180	± 4.0
0.600	± 4.0
0.300	± 3.0
0.150	± 2.0
0.075	± 1.0

two judgement schemes, the first will be discussed. COLTO applies a single lower specification limit (L_s) to compaction density and both lower (L_s) and upper (L'_s) specification limits to bitumen content and voids. These are shown in Table 2.4 for continuously graded HMA mixes.

Table 2.4: COLTO specification limits (after [COLTO, 1998])

Property	Sample size	Spec. limits	ϕ, %
Relative compaction	6	L_s = (97-Design VIM) of Rice	15
Binder content	6	L_s = Specified binder - 0.3% L'_s = Specified binder + 0.3%	15
Voids	4	L_s = Specified voids - 1.5% L'_s = Specified voids + 1.5%	15

The table shows the minimum samples required for acceptance calculations. These samples are used to calculate the standard deviation S_n and the mean $\bar{x}$ of the sample values. The ϕ values shown in Table 2.4 are the maximum percentage of the statistical

population of values of a product property permitted to lie outside the specification limits where the product may still be regarded as being acceptable. Acceptance and rejection limits are established to determine conditional acceptance criteria for part payment. Although not apparent, these limits are established based on the anticipated variabilities associated with the mix being judged. Variabilities associated with the mix design of HMA are discussed in more detail in Chapter 4.

2.2 Mix design approaches

This section reviews the volumetric mix design of HMA mixes. There are two analytical approaches in asphalt mix design to determine the optimum binder content of a mix. The first considers the minimum VMA in the aggregate skeleton of a mix and the volume of binder or mastic required to fill it. The second approach considers the minimum film thickness required to coat the aggregate. Both approaches aim to ensure the durability of HMA mixes i.e. to limit excessive ageing of the mix by limiting the volume of voids and binder. A critical review of both approaches is given.

2.2.1 Minimum VMA approach

The VMA of a mix consists of the voids between the mineral aggregate particles (stone, sand and filler). This volume or space is easily defined and simple to visualize when the aggregates consist of single sized particles or if the gradation is open. With dense continuously graded mixes, however, the smaller sand and filler particles are arranged within the voids or interstices of larger stone particles creating a complex voids distribution. Binder added to the mix occupies this volume. The VMA of the mix is therefore the sum of the VIM and volume of effective binder (Vbe) i.e. binder not absorbed by the aggregate. This definition is based on the classic theoretical spatial model (Model 1) illustrated in Figure 2.1 and is a simplified model of the actual

spatial composition of HMA mixes. Figure 2.5 compares the classic model to some other spatial models used to describe the composition of HMA mixes. These other models assume that the voids in the combined stone and sand aggregate fractions comprise the voids in the mix and the volume of mastic comprising the binder and filler in the mix. Model 2 is a simplification of that used in the Belgium mix design method OCW [1997]. Model 3 accounts for the influence of binder absorption. These latter models may be refined further as indicated in Figure 2.6 which illustrates the spatial model of a mastic system.

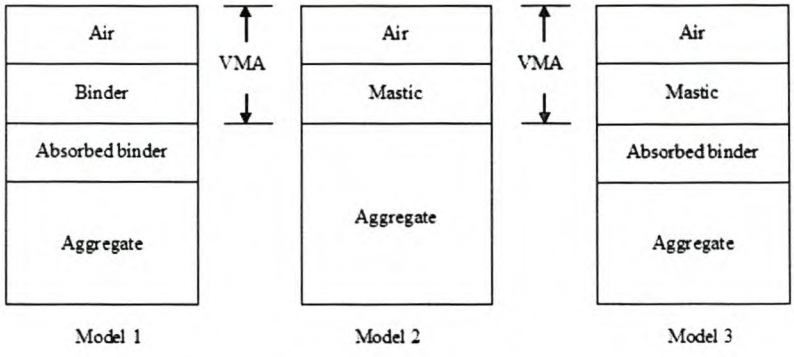

Figure 2.5: Spatial models used to describe the composition of HMA

Despite the different approaches used to model the spatial composition of dense continuously graded HMA, the basic principle is the same i.e. the aggregate structure or framework provides stability through interparticle contact and the binder or mastic component binds the aggregate structure providing cohesion and durability. This is the reasoning behind mix designs adopting minimum VMA criteria i.e. to ensure that there are sufficient VMA for the binder or mastic to ensure durability, taking into account that the VMA of the mix decreases with compaction during construction and in service.

In 1957, McLeod [1957] presented a modified Marshall mix design methodology

that listed a minimum design VMA requirement of 15 percent (irrespective of aggregate size) with volume of air voids between 3 percent and 5 percent (50 blows MArshall). In 1959, Mcleod [1959] related VMA to nominal maximum aggregate size which was adopted by the Asphalt Institute in 1964 [AI, 1964]. Superpave also specifies minimum design VMA criteria depending on maximum aggregate size [McGennis et al., 1994]. These criteria are roughly 1 percent lower than those originally prescribed by the Asphalt Institute since Superpave mixes are designed for design VIM of 4 percent instead of 5 percent.

The formulation of VMA specifications is complicated since the VMA of a mix depends on the packing characteristic of the aggregates. This is influenced not only by aggregate size, but also by the gradation, shape (angularity) and surface texture of the aggregate [Lefebvre, 1957]. Aschenbrenner and McKean [1994] examined laboratory mixes to study the effects of different variables on VMA. They found that gradation played a role in influencing VMA but got such poor correlation that VMA could not effectively be predicted from gradation. They found that filler content has a significant effect on VMA, particularly for gradations on the fine side of the maximum density line. They recommended that the fine aggregate be kept well off the maximum density line. They found aggregate angularity to substantially affect the VMA, with crushed aggregates providing more VMA than rounded aggregates. The fine aggregate angularity was more influential for coarse mixes or mixes following the maximum density line than for mixes on the fine side of the maximum density line.

Mallick et al. [2000] looked at an alternative approach for specifying VMA for dense-graded HMA Superpave mixes. They point out that coarse graded Superpave mixes (with gradations significantly below the restricted zone), if designed with the minimum VMA criteria based on nominal maximum aggregate size, could result in mixes with very thick binder film because these mixes have relatively lower surface area. Consequently these mixes may have low resistance to rutting. They concluded

that substantial differences in VMA exist among different (Superpave) permissible gradations of mixes with the same nominal maximum aggregate size. They postulate that a more rational way of specifying the minimum design VMA will be to specify VMA on the basis of percent passing the 2.36 mm sieve rather than the nominal maximum aggregate size. This will ensure about equal binder film thickness in all mixes regardless of gradation to ensure reasonable durability of the mixes. It was recommended that minimum VMA requirements, some of which are shown in Table 2.5, be followed for specifications. The VMA values for the different mixes are given on the basis of percent passing the 2.36 mm sieve (P2.36), and 4.0 percent air voids in compacted mix. It was suggested that the VMA in the design mix should not exceed the minimum specified VMA by more than 2.0 percent to minimise a potential rutting problem. This approach is yet to be validated.

Table 2.5: Recommended design VMA for dense-graded mixes with nominal maximum aggregate size [Mallick et al., 2000]

Passing 2.36 mm	Max size 19.0 mm	Passing 2.36 mm	Max size 25.0 mm	Passing 2.36 mm	Max size 37.5 mm
49-44	14.0	45-40	13.8	41-36	13.6
44-39	13.7	40-35	13.4	36-31	13.2
39-34	13.4	35-30	13.1	31-26	12.8
34-29	13.1	30-25	12.7	25-21	12.2
29-23	12.7	25-19	12.3	21-15	11.7

The rationale behind adopting alternative measures against which to specify VMA is because of reports of problems experienced in meeting current Superpave minimum VMA requirements, particularly for coarse graded mixes passing below the restricted zone. Kandhal et al. [1998a] suggest that some of these problems may be caused by the increased compactive effort of the Superpave gyratory compactor. It must be remembered that in Superpave, VMA is defined based on a simplified model of

the actual spatial composition of HMA mixes (Model 1 in Figure 2.5). This model does not account for the volume of filler which in some cases contributes to the aggregate structure of a mix but in other cases acts more like a binder. This is the dual nature of mastics and is one of the reasons why the Belgium mix design procedure considers the voids in the stone and sand fractions rather than VMA. Given the problems experienced, some researchers have found that minimum VMA requirements are restrictive [Hinrichsen and Heggen, 1996] and suggest that rigid enforcement of a minimum VMA criterion should be discouraged [Coree and Hislop, 1999]. Other researchers have opted to drop minimum VMA criteria in place of a minimum average film thickness [Kandhal et al., 1998a, b].

2.2.2 Film thickness mix design considerations

A film thickness mix design approach focuses on evaluating the quantity of binder needed to coat the aggregates in a mix with a specified average film thickness. Film thickness is a measure of the *average* binder thickness surrounding aggregate particles in asphalt mixes. The thickness is no more than a few micrometers and is therefore difficult to measure accurately. Besides this, it is also influenced by a number of factors that are often difficult to quantify, including particle shape, roughness and binder viscosity. For this reason it is usually calculated based on the assumption that each aggregate particle, including the filler, is spread apart each with its own coating of bitumen. An average binder film thickness for an asphalt mix may be estimated using the highly empirical approach as originally outlined by the Asphalt Institute [AI, 1995]:

$$FT = \frac{B_e}{100 - B} \cdot \frac{1}{A} \cdot \frac{10^6}{G_b} \tag{2.7}$$

where

FT = Film thickness, μm

B_e = Effective binder content, percent by mass of mix

B = Total binder content, percent by mass of mix

A = Surface area of aggregate blend, m^2/kg

G_b = Density of the binder at 25 C, kg/m^3

The surface area of the aggregate is calculated from:

$$A = (2 + 0.02a + 0.04b + 0.08c + 0.14d + 0.30e + 0.60f + 1.60g)\,0.20482 \qquad (2.8)$$

where

A = Surface area of aggregate blend, m^2/kg

a = Percentage passing the 4.75 mm sieve

b = Percentage passing the 2.36 mm sieve

c = Percentage passing the 1.18 mm sieve

d = Percentage passing the 0.60 mm sieve

e = Percentage passing the 0.30 mm sieve

f = Percentage passing the 0.15 mm sieve

g = Percentage passing the 0.075 mm sieve

As with the minimum VMA mix design approach, the purpose of the minimum film thickness approach is to ensure mix durability. Huber [1991] points out that the reason why the Asphalt Institute does not use film thickness as a criterion for durability is the influence of compaction. This is understandable since the film thickness of loosely and well compacted mixes are the same when calculated using Equation 2.7, however, loosely compacted mixes will have higher voids. This promotes ageing and may have

a negative influence on durability. It is therefore necessary to specify compaction criterion together with film thickness criterion to ensure durability.

If the compaction level is set and the bulk relative density of the aggregate is known it is possible to calculate the binder content of a mix required to satisfy a specified film thickness (usually in the order of 8 micrometer). Hinrichsen and Heggen [1996] present equations that account for both aggregate gradation and the volumetric properties of the materials to judge the proper VMA requirement for unique blends of materials. They point out that setting minimum VMA requirements on the basis of the nominal maximum sizes of the aggregates is confining. By doing so an agency often eliminates a significant percentage of aggregate combinations that will produce acceptable HMA. If the minimum VMA is set too high the result may be mixes with high percentages of sand requiring high binder contents. Their method allows the calculation of the minimum VMA required in a particular aggregate combination based on the volumetric properties of the components and the required air voids and film thickness. To accomplish this, the film thickness equation of the Asphalt Institute [AI, 1993] is modified so that a minimum film thickness is assumed and the equation is then solved for the percentage binder (P_b). The result is the minimum percentage binder required to achieve the minimum film thickness:

$$P_{bm} = \frac{10\,(SA)\,(FT) + 100\,(P_{ba})}{100 + P_{ba}} \tag{2.9}$$

where

P_{bm} = Minimum percentage binder by weight of the total mix

SA = Calculated surface area, m^2/kg

FT = Minimum film thickness required, micron

P_{ba} = Percentage binder absorption

The surface area coefficients recommended by the Asphalt Institute [AI, 1993] are used for the calculations, combined with the following equation proposed by Hinrichsen and Heggen [1996] that allows the expression of film thickness in terms of the effective binder content, P_{be}, of the mix (by weight of total mix):

$$FT = \frac{10\,(P_{be})}{SA} \tag{2.10}$$

This equation is combined with the absorbed binder as follows:

$$P_{be} = P_b - \frac{(P_{ba})\,(100 - P_b)}{100} \tag{2.11}$$

where

P_{be} = Effective binder content, percentage by weight of total mix

P_b = Total binder content, percentage by weight of total mix

P_{ba} = Percentage binder absorption

Once the minimum binder content has been determined, it can be entered into the following equation to determine the minimum VMA required to allow sufficient space for that amount of binder and the correct air void level:

$$\mathrm{VMA_{min}} = \frac{100 P_{bm} G_{se} G_{sb} + (100 - P_{bm})\,G_b G_{se} V_t - 100\,(100 - P_{bm})\,G_b\,(G_{se} - G_{sb})}{(100 - P_{bm})\,G_b G_{sb} + P_{bm} G_{se} G_{sb}} \tag{2.12}$$

where

G_{se} = Effective relative density of the aggregate

G_{sb} = Bulk relative density of aggregate

G_b = Relative density of the binder

V_t = Target percentage air voids

Hinrichsen and Heggen [1996] mention that the VMA criteria currently used in the Superpave mix design procedure appear to be derived from materials with a relative density of 2.65. When all the other variables are held constant and only the relative density of the aggregate is changed, they found that the VMA required to allow space for the required binder changes more than 1 percent over the range of relative densities of 2.5 to 2.8. Based on this they propose that the equations be improved by adjusting the surface area by the relative density of the aggregate. Thus Equation 2.10 becomes:

$$FT = \frac{10\,(P_{be})}{SA \cdot R} \tag{2.13}$$

where R is equal to $2.65/G_{sb}$. Then, by adding this improvement to Equation 2.9, the following results:

$$P_{bm} = \frac{10\,(SA)\,(FT)\,(R) + 100\,(P_{ba})}{100 + P_{ba}} \tag{2.14}$$

Not addressed in the preceding is how the mix design approaches (both minimum VMA and film thickness) relate to durability. In this regard, Goode and Lufsey [1965] related binder hardening (ageing) to voids, permeability, and film thickness. They defined a bitumen index as the ratio of the mass of binder (pounds) in a mix to the surface area of the aggregate (square foot). Their study indicated that a combined factor of the ratio of the air void to the bitumen index could be related to the binder hardening characteristics in the HMA mixture. They suggested that the Marshall method of mix design could be improved by incorporating a maximum value of voids:bitumen index ratio in place of a maximum value of air voids alone and they suggested a value of 4 as the maximum for this ratio, to ensure reasonable resistance to ageing. Kumar and Goetz [1977] also looked at binder hardening as related to permeability and binder film thickness. They defined a film thickness factor as the ratio of the percent effective binder content of a mix to the surface area of the aggregate and related this factor to permeability. These measures address the

problem of durability directly and it is unfortunate that not more attention has been given to establishing mix design criteria in terms of these.

2.3 Filler-binder interaction

The significant influence of filler-binder interaction on the durability and workability of asphalt mixes *must* be addressed in mix design procedures. A critical parameter in mix design, the filler content, will define this interaction. In practice, it is often not cost effective to control the filler content of a mix and consequently, filler contents are fixed by the filler contents of the finer particle stockpiles such as the crusher dust. In South Africa, crusher dust may constitute up to 35 percent, by mass, of the mix. As a result, high filler contents (6 - 7.5 percent) are not uncommon in mixes used in the Western Cape of South Africa, for example. This was one of the reasons identified for the compactibility problems experienced with surfacing mixes in this region [Smit et al., 2000, 2002a].

Another reason for considering filler-binder interaction is that it allows one of the many parameters in mix design to be fixed i.e. either the filler content or the binder content. This aspect is applied in international mix design methodologies. The Superpave mix design method specifies a dust proportion of between 0.6 - 1.2 [McGennis et al., 1994]. This is a filler:binder ratio on a mass basis. The Belgium (BRRC) mix design method accounts for the filler-binder interaction to determine the mastic composition of an asphalt mix [OCW, 1997]. The section discusses specific research undertaken to characterise fillers and filler-binder systems. Two of the more commonly used methods to evaluate the stiffening effect of fillers are:

1. A stiffening ratio using kinematic viscosities of a mortar and neat bitumen.

2. The increase in the ring and ball softening point temperature due to the addition

of fillers.

It should be noted that the systems described in this section assume that binder absorption into filler is negligible. If this is not the case, the volume of free bitumen available will decrease, which would result in a stiffer mastic. The calculations of percent bulk volume of filler won't reflect this though resulting in faulty judgements if criterion are set based on the percentage bulk volume of filler.

2.3.1 Characterisation of fillers and filler-binder systems

As early as 1937, Traxler [1937] assumed that any stiffening (of mortars) should be related to the physical properties of the fillers, such as particle size, grain-size distribution, and shape but did not find any reasonable relationships between these filler properties and stiffening. Rigden [1947] described the volumetric properties of dry compacted fillers. When fillers are dry compacted to their maximum density (using the Rigden test), the void volume within the compacted filler is at a minimum. The volume of binder required to fill the voids within the compacted filler is referred to as "fixed" binder. This is illustrated in Figure 2.6. Rigden theorised that if a filler were mixed with less binder than required to fill these minimum voids, a dry stiff mortar would result. Binder in excess of the fixed amount is called "free" binder and decreases the stiffness of the binder-filler mortar. This amount of free binder can be considered the binder available to lubricate the mastic. Higher values of bulk volume of filler result in more fixed binder and less free binder for a given binder content. As the filler:binder ratio changes, so does the amount of free binder. Kallas and Puzinauskas [1961] studied the use of mineral filler in the mix. They focussed on the different roles that the filler can play by contributing to the development of contact points between aggregate particles. They found that fillers that caused the highest increase in the viscosity of binders at lower temperatures also produce the

highest VMA in paving mixtures.

Bolk et al. [1982] report research on manufactured fillers in the Netherlands. The fillers are classified according to their capacity to absorb bitumen and the influence on viscosity of the mastic. Fillers are classified as weak (low viscosity-influencing behaviour) to strong (high viscosity influencing behaviour). Table 2.6 shows the Dutch filler specifications:

Table 2.6: Dutch filler specifications [VBW, 1992]

Filler type	**Weak filler**		**Average filler**		**Strong filler**		**Unit**
	Min	Max	Min	Max	Min	Max	
Grain distribution:							
on 2 mm sieve	-	0	-	0	-	0	% (m/m)
on 0.09 mm sieve	-	15	-	15	-	15	% (m/m)
on 0.063 mm sieve	5	25	5	25	5	25	% (m/m)
Water number	28	38	40	50	54	60	% (m/m)
Rigden voids	29	-	36	-	44	-	-
Mass loss @ 150 °C	-	1.5	-	1.5	-	1.5	% (v/v)
Water sensitivity	-	10	-	10	-	10	% (m/m)
Swell	-	3	-	3	-	3	% (m/m)
Soluble in hydroxide	-	-	-	-	25	-	% (m/m)
Soluble in water	-	10	-	10	-	10	% (m/m)

In the Netherlands, characterisation of the viscosity-influencing behaviour of fillers is also determined by means of the water ("bitume") number and the Rigden voids of the filler. The test used for the determination of the water number employs apparatus similar to that used in the bitumen penetration test, the difference is that instead of a penetration needle, a thin solid metal rod is used to. The test is conducted at constant loads at various percentages of water added to the filler until a specified penetration is achieved. The mass ratio between the water and the filler is defined as the water number, which serves as an indicator of the influence of the filler on the

viscosity of the binder-filler system at mixing temperature.

Anderson et al. [1982] state that the type and fineness of the mineral dust plays an important role in the design, construction and performance of asphalt mixes. Fine mineral dust ($< 10\mu$m) can affect mix design and can extend the bitumen. They conclude:

1. Fineness is not always a measure of the magnitude of stiffening that will result when a dust is added to bitumen. The stiffening that occurs in filler-bitumen mixtures is more apparent in the softening point test results than in viscosity or penetration test results.

2. Fine mineral dusts may act as a bitumen extender even though they stiffen the bitumen. The filler:binder ratio may be a better control criteria than a limit on the percentage of baghouse fines, especially since the characteristics of the baghouse fines are a function of the aggregate, plant operations, and efficiency of the primary collector.

3. When fine dusts are used as a bitumen extender, the mix properties can be very sensitive to changes in bitumen content. Limited evidence indicates that gap-graded dusts may be better extenders than well graded dusts.

4. Maximum and minimum filler:binder ratios must be based on the effect of the fine dust on fatigue, creep, compactibility and other mixture properties.

Anderson [1987] developed guidelines for the use of dust in HMA. He contends that the gradation of the dust fraction should be measured. He also points out that the percentage free bitumen in the dust fraction should be maintained at 40 percent or less to ensure mixes with adequate mechanical properties and workability. Kandhal [1981] showed that baghouse fines must be specified in order to identify the detrimental ones. Kandhal's study used viscosity measurements and change in

softening point temperatures to show transitions in the stiffening effect of fillers at approximately 60 percent bulk volume. Based on this, Kandhal suggested a limiting value of 50 percent bulk volume. He further suggested limiting criteria on changes in softening point temperature of 11.5 °C. Values above this may result in mortars that are too stiff. These stiff mortars in HMA may require "higher mixing and compaction temperatures, prompt rolling, etc." Huschek and Angst [1980] described the important role of the mastic in the mix. Relative density, Rigden voids and solid volumes were used to relate filler-binder interaction to mix performance. They showed that the rank ordering of filler types tested was different at high and low temperatures. They used the tensile strength and elongation at rupture of binder-filler mortars at a temperature of -15 °C to conclude that the tensile strength of HMA reaches a maximum at a percent bulk volume of filler of 60. Cooley et al. [1998] also reported that the percent bulk volume from dry compaction tests on fillers, as defined in Figure 2.6, has been shown to be an indicator of a filler's stiffening potential. A limiting value of bulk volume of filler was selected as 55 percent based on tests at both high service temperatures (softening point) and mixing, transport and compaction temperatures.

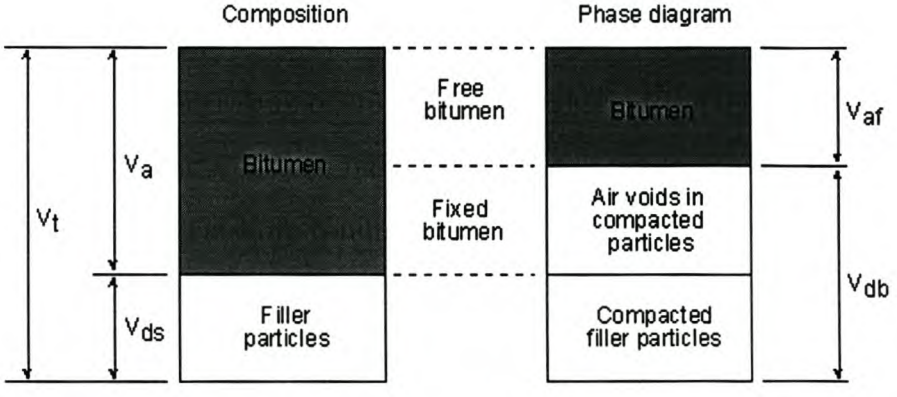

Figure 2.6: Parameters to describe voids in filler-binder mortar [Cooley et al., 1998]

From Figure 2.6, the following filler properties may be defined:

$$\%V_{dv} = \frac{V_{db} - V_{ds}}{V_{db}} \cdot 100 \tag{2.15}$$

$$\%V_{db} = \frac{V_{db}}{V_a + V_{ds}} \cdot 100 \tag{2.16}$$

$$\%V_{af} = 100 - \%V_{db} \tag{2.17}$$

where

V_t = Total volume

V_a = Volume of binder

V_{ds} = Volume of dust particles

V_{db} = Bulk volume of compacted filler

V_{af} = Volume of free binder

$\%V_{dv}$ = Percent voids in compacted filler (Rigden voids)

$\%V_{db}$ = Percent bulk volume of filler

$\%V_{af}$ = Percent free binder

Figure 2.7 shows the relationship found by Cooley et al. [1998] between change in ring and ball softening point temperature and percent bulk volume of the compacted fillers. The four different filler:binder ratios tested are expressed on a volume basis. On a mass basis, this would cover a range of filler:binder ratios from about 0.5 to 1.3.

In the Belgium (BRRC) mix design method [OCW, 1997], the determination of the mastic composition entails finding the optimum filler:binder ratio, K = f/b, by volume. BRRC [OCW, 1997] point out that the increase in the softening point (Ring and ball) of a filler and binder mixture depends on the filler:binder ratio and the volume of voids in the filler (Rigden voids). It has been shown that the following

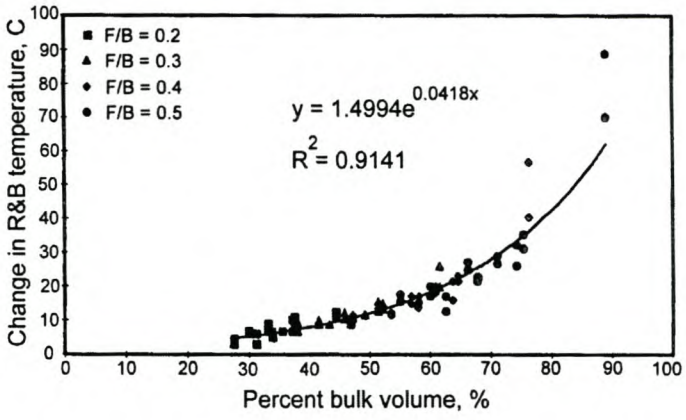

Figure 2.7: Relationship illustrating stiffening of filler-binder mortar [Cooley et al., 1998]

relationship holds:

$$K = \frac{f}{b} = \frac{(100 - h_F\%) \cdot \Delta RK}{(1021.2 + \Delta RK \cdot h_F\%)} \tag{2.18}$$

where

h_F = Voids in the filler

ΔRK = Increase in softening point due to the addition of filler

Typical results of this equation that may be applied in practice are shown in Figure 2.8. BRRC [OCW, 1997] state, that based on experience, a mastic composition that ensures an increase in softening point of between 12 and 16 is required to balance the mix requirements in terms of durability (flexible mastic) and stability (stiff mastic).

The influence of the filler-binder interaction is taken into account in the new South African HMA design guidelines [PMGHDP, 2000; Jooste et al., 2000]. From tests carried out on a range of South African fillers, it has been shown that filler-binder systems stiffen dramatically beyond a certain filler:binder ratio. Figure 2.9 indicates that at a temperature of 60 °C the viscosity ratio (defined as the filler-binder

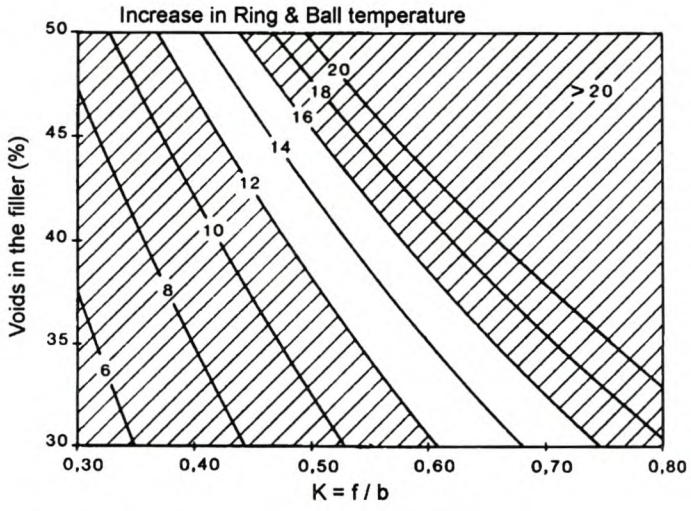

Figure 2.8: Increase in softening point as a function of K and h_F

viscosity divided by the binder viscosity) increases significantly when the filler:binder ratio exceeds 1:2. Figure 2.10 indicates that at a temperature of 135 °C the viscosity ratio increases when the filler binder exceeds 1:1, although there is a lot of scatter in the data at a filler:binder ratio of 2:1. These two temperatures can be likened to upper limits of road performance and average field compaction temperature.

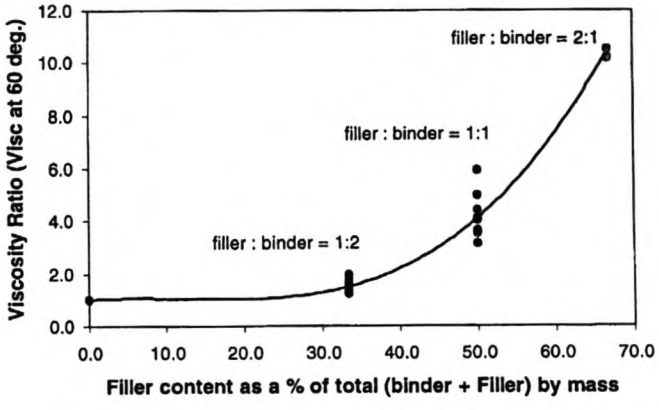

Figure 2.9: Influence of filler:binder ratio on mastic viscosity at 60 °C [PMGHDP, 2000]

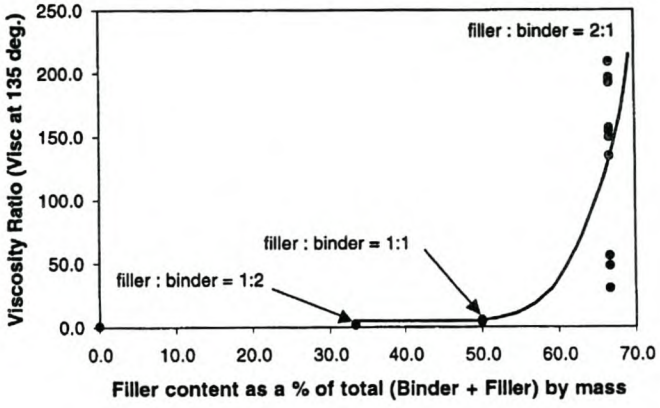

Figure 2.10: Influence of filler:binder ratio on mastic viscosity at 135 °C [PMGHDP, 2000]

Shashidhar and Romero [1998] report on an alternative method of evaluating the stiffening potential of mineral fillers. They cite a number of factors affecting the stiffening potential of binders, including:

1. Average particle size. The stiffening effect of the fillers increased with decreasing particle sizes below 10 μm. Above 10 μm, such dependencies were not significant.

2. Gradation. This has a strong effect on the packing of powders.

3. Binder-filler interface. They point out that the same filler can behave differently in two different binders.

4. State of particle dispersion. The magnitude of interparticle attraction determines the stability of the binder-filler system. A poorly dispersed system is not a stable system.

5. Agglomerates. These are clusters of particles that are formed due to particles mutual attraction to each other. Particles in these clusters are poorly packed and lead to stiffening.

6. Particle shape. As the aspect ratio of particles (ratio of longest dimension to smallest dimension) increases, the ability of the particles to pack efficiently decreases, which results in an increase in the stiffening potential of the filler.

The influence of filler-binder interaction was investigated in a project to improve the compactibility of wearing course mixes in the Western Cape, South Africa [Smit et al., 2000, 2002a]. At the onset of the project it was believed that one of the primary causes of the compactibility problems experienced in the Western Cape was the nature of the filler material and the difficulty of controlling the filler content. To investigate this assumption, a number of tests were done on the filler and filler-bitumen systems. Based on the findings of this study it was concluded that optimum filler:binder ratios may be determined based on limiting criteria on changes in softening point temperature of 12 °C. This was confirmed based on APT using the MMLS3 Smit et al. [2002a].

2.4 References

AI. *Mix Design Methods for Asphalt Concrete and Other Hot Mix Types.* Asphalt Institute, 1964.

AI. *Mix design methods for asphalt concrete and other hot-mix types, MS-2.* Asphalt Institute, Lexington, Kentucky, 6 edition, 1993.

AI. *Superpave level 1 mix design, SP-2.* Asphalt Institute, Asphalt Institute, Lexington, Kentucky, 1995.

S. Al-Swailmi and R. L. Terrel. Evaluation of water damage of asphalt concrete mixtures using the environmental conditioning system (ECS). *Association of Asphalt Paving Technologists*, Vol. 61, 1992.

D. A. Anderson. Guidelines for use of dust in hot-mix asphalt concrete mixtures. *Proceedings Association of Asphalt Paving Technologists*, Vol. 56, 1987.

D. A. Anderson, J. P. Tarris, and J. D. Brock. Dust collector fines and their influence on mixture design. *Proceedings Association of Asphalt Paving Technologists*, Vol. 51, 1982.

T. Aschenbrenner and C. McKean. Factors that effect the voids in the mineral aggregate of hot-mix asphalt. Transportation Research Record 1469, Transportation Research Board, 1994.

Austroads. Selection and design of asphalt mixes: Australian provisional guide. APRG Report No. 18, Austroads and Australian Road Research Board, 1997.

H. U. Bahia, T. P. Friemel, P. A. Peterson, and J. S. Russell. Optimization of constructibility and resistance to traffic: A new design approach for HMA using the Superpave compactor. *Proceedings of the Association of Asphalt Paving Technologists*, Vol. 67, 1998.

P. B. Blankenship, C. K. Mahboub, and G. A. Huber. Rational method for laboratory compaction of hot mix asphalt. Transportation Research Record 1454, Transportation Research Board, Washington, D.C., 1994.

N. J. N. A. Bolk, J. P. J. van der Heide, and M. C. Zantvliet. Basic research into the effect of filler on the mechanical properties of dense asphaltic concrete. *Proceedings Association of Asphalt Paving Technologists*, Vol. 51, 1982.

E. R. Brown, I. R. Hanson, and R. B. Mallick. An evaluation of SHRP gyratory compaction of HMA. *Paper presented to the annual meeting of the Transportation Research Board, Washington, D.C.*, 1996.

E. R. Brown and R. B. Mallick. An initial evaluation of N-design Superpave gyratory compactor. *Proceedings of the Association of Asphalt Paving Technologists*, Vol. 67, 1998.

M. Butcher. Determining gyratory compaction characteristics using the Servopac gyratory compactor. *Department of Transport, South Australia*, 1997.

COLTO. *Standard specifications for road and bridge works for state road authorities.* Committee for Land Transport Officials, Department of Transport, Johannesburg, South Africa, 1998.

L. Cooley, M. Stroup-Gardiner, E. R. Brown, D. Hanson, and M. Fletcher. Characterization of asphalt-filler mortars with Superpave binder tests. *Proceedings Association of Asphalt Paving Technologists*, Vol. 67, 1998.

L. A. Cooley. Permeability of Superpave mixtures: Evaluation of field permeameters. Technical Report NCAT Report 99-1, National Center for Asphalt Technology, Auburn University, Alabama, 1999.

L. A. Cooley, B. D. Prowell, and E. R. Brown. Issues pertaining to the permeability characteristics of coarse graded superpave mixes. *Association of Asphalt Paving Technologists*, 2002.

K. E. Cooper, S. F. Brown, and G. R. Pooley. The design of aggregate gradings for asphalt basecourses. *Proceedings of the Association of Asphalt Paving Technologists*, Vol. 54, 1985.

B. J. Coree. HMA volumetrics revisited - a new paradigm. *Presented to the Annual meeting, Transportation Research Board, Washington, D.C.*, 1998.

B. J. Coree and W. P. Hislop. The difficult nature of minimum VMA: A historical perspective. *Presented to the Annual meeting, Transportation Research Board, Washington, D.C.*, 1999.

CSRA. *TRH8: Selection and design of hot-mix asphalt surfacing for highways.* Committee of State Road Authorities, Pretoria, South Africa, 1987.

CSRA. *Draft TRH4- Structural design of flexible pavements for interurban and rural roads.* Committee of Land Transport Officials, Pretoria, 1996.

C. W. Curtis, K. Ensley, and J. Epps. Fundamental properties of asphalt-aggregate interactions including adhesion and absorption. Technical report, Strategic Highway Research Program, 1993.

R. de Sombre, D. E. Newcomb, B. Chadbourn, and V. Voller. Parameters to define the laboratory compaction temperature range of hot-mix asphalt. *Proceedings of the Association of Asphalt Paving Technologists*, Vol. 67, 1998.

Duriez. *Traité des matériaux de construction.* DUNOD, Paris, 1950.

M. Gauer. Compaction of asphalt in the Darmstadt gyratory compactor. *International Workshop on the use of the Gyratory Shear Compactor, LCPC, Nantes*, 1996.

J. F. Goode and L. A. Lufsey. A new graphical chart for evaluating aggregate gradations. *Proceedings of the Association of Asphalt Paving Technologists*, Vol. 31, 1962.

J. F. Goode and L. A. Lufsey. Voids, permeability, film thickness vs. asphalt hardening. *Association of Asphalt Paving Technologists*, Vol. 34, 1965.

J. Harvey, C. L. Monismith, and J. Sousa. An investigation of field and laboratory compacted asphalt rubber, sma, recycled and conventional asphalt concrete mixes

using SHRP project A-003A equipment. *Proceedings of the Association of Asphalt Paving Technologists*, Vol. 63, 1994.

J. A. Hinrichsen and J. Heggen. Minimum voids in mineral aggregate in hot-mix asphalt based on gradation and volumetric properties. Transportation Research Record 1545, Transportation Research Board, Washington, D.C., 1996.

I. Horvli. Gyratory testing of cold mix asphalt. *International Workshop on the Use of the Gyratory Shear Compactor, LCPC, Nantes*, 1996.

G. A. Huber. Marshall mix design criteria changes. *Asphalt magazine, Asphalt Institute*, 1991.

F. Hugo. A critical review of bituminous mixtures at present being used for surfacing pavements, with proposals for the composition and design of mixtures suitable for South African conditions. Masters thesis, Department of Civil Engineering, University of Natal, Durban, 1970.

F. Hugo, M. F. C. van de Ven, and A. D. F. Smit. N2 north coast contracts investigation: LAMBs. a limited comparative study between Hugo hammer and Superpave gyratory compactor. Prepared for Sabita, Institute for Transport Technology, University of Stellenbosch, 1996.

S. Huschek and C. Angst. Mechanical properties of filler-bitumen mixes at high and low service temperatures. *Proceedings Association of Asphalt Paving Technologists*, Vol. 49, 1980.

F. J. Jooste, A. Taute, B. Verhaeghe, A. Visser, and P. Myburgh. A new hot-mix design method for Southern Africa. *Paper presented at the 1st International Conference on World of Asphalt Pavements, Sydney, Australia*, 2000.

B. F. Kallas and V. P. Puzinauskas. A study of mineral fillers in asphalt paving mixtures. *Procedings of the Association of Asphalt Paving Technologists*, Vol. 30, 1961.

P. S. Kandhal. Evaluation of baghouse fines in bituminous paving mixtures. *Proceedings Association of Asphalt Paving Technologists*, Vol. 50, 1981.

P. S. Kandhal, K. Y. Foo, and R. B. Mallick. A critical review of VMA requirements in Superpave. NCAT Report No. 98-1, National Center for Asphalt Technology, 1998a.

P. S. Kandhal, K. Y. Foo, and R. B. Mallick. Critical review of voids in mineral aggregate requirements in Superpave. Technical Report Transportation Research Record 1609, Transportation Research Board, Washington, D.C., 1998b.

P. S. Kandhal and M. A. Khatri. Evaluation of asphalt absorption by mineral aggregates. *Proceedings of the Association of Asphalt Paving Technologists*, Vol. 60, 1991.

T. W. Kennedy, R. B. Mcgennis, and R. J. Holmgreen. Asphalt mixture segregation; diagnostics and remedies. *Proceedings of the Association of Asphalt Paving Technologists*, Vol. 56, 1987.

T. W. Kennedy, F. L. Roberts, and K. W. Lee. Evaluation of moisture susceptibility of asphalt mixtures using the texas freeze-thaw pedestal test. *Association of Asphalt Paving Technologists*, Vol. 51, 1982.

A. Kumar and W. H. Goetz. Asphalt hardening as affected by film thickness, voids and permeability in asphaltic mixtures. *Association of Asphalt Paving Technologists*, Vol. 46, 1977.

J. Lefebvre. Recent investigations of the design of asphalt paving mixtures. *Proceedings of the Association of Asphalt Paving Technologists*, Vol. 26, 1957.

R. P. Lottman. Predicting moisture-induced damage to asphaltic concrete. Technical Report NCHRP 192, Transportation Research Board, Washington, D.C., 1982.

M. Luminari. Mix design: State-of-the-art and RILEM interlaboratory test program. In H. Di Benedetto and L. Francken, editors, *Mechanical tests for bituminous materials*, Lyon, France, May 1997. A. A. Balkema, Rotterdam.

R. B. Mallick, M. S. Buchanan, P. S. Kandhal AndR. L. Bradbury, and W. McClay. A rational approach of specifying the voids in mineral aggregate (VMA) for dense-graded hot mix asphalt. *Presented at 79th Annual meeting of the Transportation Research Board, Washington, D.C.*, 2000.

R. B. McGennis, R. M. Anderson, T. W. Kennedy, and M. Solaimanian. *Superpave Asphalt Mixture Design and Analysis.* National Asphalt Training Center, Federal Highway Administration, FHWA-SA-95-003, Washington, D.C., 1994.

N. W. McLeod. Relationship between density, binder content, and voids properties of compacted paving mixtures. *Proceedings of the Highway Research Board, Washington, D.C.*, Vol. 35, 1957.

N. W. Mcleod. Void requirements for dense-graded bituminous paving mixtures. *American Society of Testing and Materials, STP-252*, 1959.

J. L. McRae. Procedures for establishing family of voids curves for hot mix bituminous pavement. *Association of Asphalt Paving Technologists*, Vol. 25, 1956.

F. Moutier. The French bituminous mix design method. *Fifth Eurobitume Congress, Stockholm*, 1993.

NCHRP. Superpave gyratory compaction guidelines. *Research Results Digest, National Cooperative Highway Research Program, Washington, D.C.*, (237), March 1999.

L. W. Nijboer. *Plasticity as a factor in the design of dense bituminous road carpets.* Elsevier Publishing Company, Inc, 1943.

OCW. *Handleiding voor de formulering van dichte bitumineuze mengsels.* Opzoekingscentrum voor de Wegenbouw, Brussels, Belgium, 2 edition, 1997.

PMGHDP. Interim guidelines for the design of hot-mix asphalt in South Africa. Technical report, Project Management Group of the Hot-Mix Asphalt Design Project, 2000.

B. D. Prowell and J. E. Haddock. Superpave for low volume roads and base mixtures. *Association of Asphalt Paving Technologists*, 2002.

P. J. Rigden. The use of fillers in bituminous road surfacings - a study of filler-binder systems in relation to filler characteristics. *Journal of the Society of Chemical Industry*, Vol. 66, 1947.

SABITA. *LAMBs - The Design and Use of Large Aggregate Mixes for Bases.* Southern African Bitumen and Tar Association, Cape Town, 2 edition, 1997.

N. Shashidhar and P. Romero. Factors affecting the stiffening potential of mineral fillers. Transportation Research Record 1638, Transportation Research Board, Washington, D.C., 1998.

SHRP. Accelerated performance-related tests for asphalt-aggregate mixes and their use in mix design and analysis systems. SHRP Report SHRP-A-417, National Research Council, Washington, D.C., 1994.

A. D. F. Smit, W. J. Douries, K. J. Jenkins, and J. C. Wise. Asphalt mix design and analysis towards improving compactibility of wearing course mixes in the western cape. *SATC*, 2002a.

A. D. F. Smit, F. Hugo, K. Jenkins, and L. Walubita. The model mobile load simulator as a tool for evaluating asphalt performance under wet conditions. *Presented at ISAP*, 2002b.

A. D. F. Smit, K. Jenkins, and M. F. C. van de Ven. Mix design laboratory compaction of continously graded large aggregate mixes with temperature variation. *Proceedings of the 7th Conference on Asphalt Pavements for Southern Africa, Zimbabwe*, 1999.

A. D. F. Smit, M. F. C. van de Ven, R. Burger, W. Douries, and C. T. Weston. Asphalt mix design and analysis towards improving compactibility of wearing course mixes in the western cape. Technical Report ITT Report 1-2000, Institute for Transport Technology, University of Stellenbosch, 2000.

H. R. Smith and A. C. Edwards. A study of bitumen and bituminous mixes for road pavements in Kenya. Project Report PR/OSC/567/96, Transport Research Laboratory, Crowthorne, Berkshire, 1996.

J. Sousa, A. Tayebali, J. Harvey, P. Hendricks, and C. L. Monismith. Sensititvity of SHRP A-003A proposed testing equipment to mix design parameter for permanent deformation and fatigue. Transportation Research Record 1384, Transportation Research Board, National Research Council, Washington, DC, 1993.

R. N. Traxler. The evaluation of mineral powders as fillers for asphalt. *Proceedings of the Association of Asphalt Paving Technologists*, Vol. 8, 1937.

D. G. Tunnicliff and R. E. Root. Use of antistripping additives in asphaltic concrete mixtures. Technical Report NCHRP 274, Transportation Research Board, Washington, D.C., 1984.

VBW. *Asfalt Onderzoek*. Vereniging voor Bitumineuze Werking, 1992.

VBW-Asfalt. Elke korrel rolt anders (dutch) every particle rolls differently. *Asfalt*, 2/1999, 1999a.

VBW-Asfalt. Ontmengingsapparaat van VBW-asfalt (dutch) segregation apparatus of VBW-asfalt. *Asfalt*, 4/1999, 1999b.

Chapter 3

Aggregate packing

3.1 Introduction

The Oxford dictionary defines packing as filling a space by pressing tightly together. In the context of this dissertation it refers to the filling of aggregate (and binder) within a confined space, either a container (mould) or a pavement layer by compaction, which presses the aggregate particles together. The spaces or voids between the packed aggregates are defined as voidage or porosity. Porosity is the voids in the mineral aggregate or VMA of the mix when no binder has been added. The packing arrangement of the particles making up the mix is related to the particle distribution or gradation.

Van Gurp [1995] looked at the packing characteristics of granular materials. He points out that determination of the actual packing of granular materials is hampered because particles are usually angular and not rounded, and contain various distributions of particle sizes. With a balanced gradation, smaller particles fill the voids left by the larger particles. These arrangements are random and complex. The effect of packing may be better understood by examining various kinds of packing with uniform spheres. Van Gurp points out that five modes of regular packing of uniform (same sized) spheres can be achieved. Figure 3.1 shows the types of packing while Table 3.1 presents values of density and porosities for these packing arrangements.

The values are defined in terms of the radius (R) of the spheres.

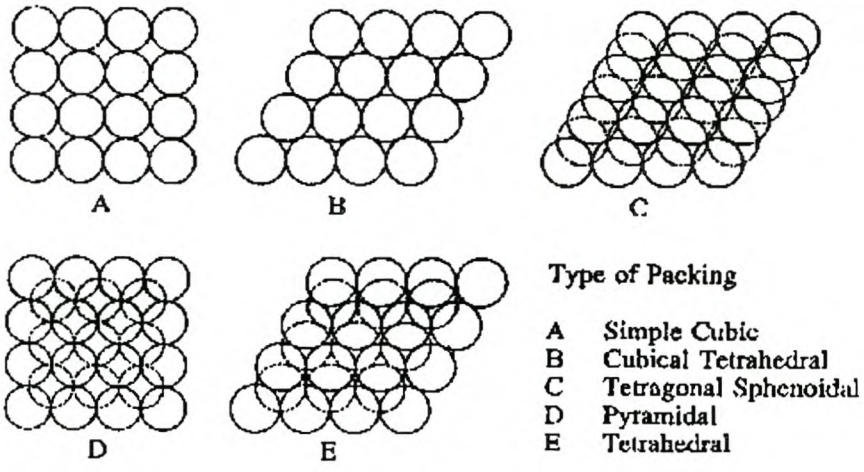

Figure 3.1: Models of packing of equal spheres [Van Gurp, 1995]

Table 3.1: Spheres packing arrangements [Van Gurp, 1995]

Type of packing	**Spacing of layers**	**Volume of unit prism**	**Density**	**Porosity (%)**
Simple cubic	2R	$8R^3$	$\pi/6$	47.64
Cubic tetrahedral	2R	$4\sqrt{3}R^3$	$\pi/3\sqrt{3}$	39.54
Tetragonal sphenoidal	$R\sqrt{3}$	$6R^3$	$2\pi/9$	30.19
Pyramidal	$R\sqrt{2}$	$4\sqrt{2}R^3$	$\pi/3\sqrt{2}$	25.95
Tetrahedral	$2R\sqrt{2/3}$	$4\sqrt{2}R^3$	$\pi/3\sqrt{2}$	25.95
Random	-	-	-	36 - 38

Some of the earliest work on packing of aggregates was carried out from 1901 to 1907 by Fuller and Thompson [1907] in connection with their studies of the best aggregate proportions for Portland Cement Concrete. In 1928 Furnas [1928] developed a model for the prediction of voids in binary systems. He showed that the voids in a binary mixture of broken solids depends on the size ratio and the relative proportions

of the constituents as shown in Figure 3.2. From the figure it can be seen that each curve has a clear minimum and for any given proportion of fine to coarse aggregate, the voids in the mix decrease with decreasing size ratio. The lowest minimum point is that for the size ratio of zero. The chapter expands on the further development of this approach based on the packing of binary systems.

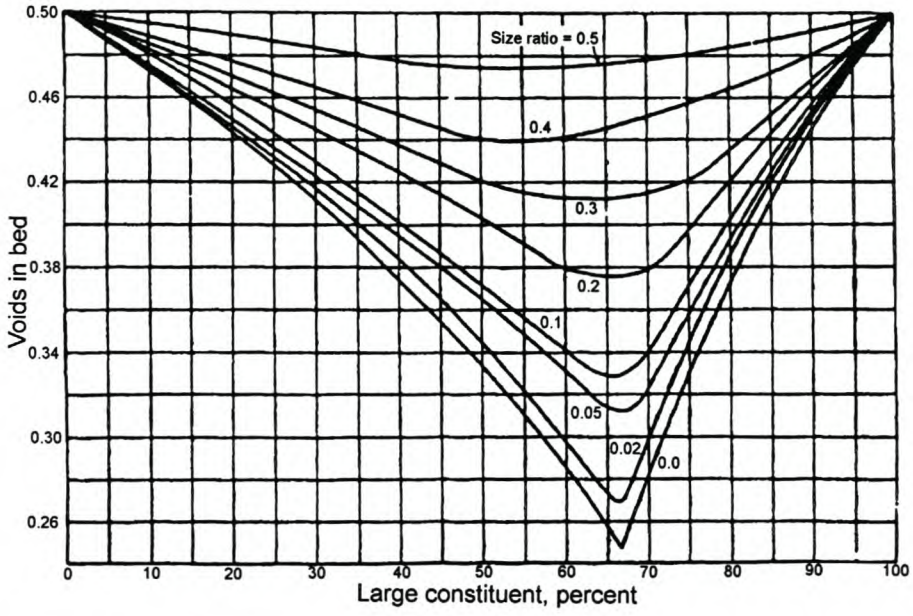

Figure 3.2: Relation between voids and size composition [Furnas, 1928]

The particle packing theory developed by Furnas [1929] describes the ideal packing of spherical particles. Consider the packing of a mixture of two materials, 1 and 2, consisting of spherical particles with diameters $d_1 \ll d_2$, volume fractions r_1 and r_2, and packing densities ϕ_1 and ϕ_2. In this mixture two limiting cases may be considered:

1. The volume fraction of small particles is large ($r_1 \gg r_2$)

2. The volume fraction of coarse particles is large ($r_2 \gg r_1$)

In case 1, the mixture may be considered to consist of a matrix of smaller particles containing discrete larger particles. The matrix of smaller particles will have a packing

density ϕ_1 and contributes to the specific volume of the mixture as r_1/ϕ_1. The larger particles contribute to the volume by the solid volume fraction of coarse particles r_2.

The specific volume and packing density of the mixture therefore are:

$$\nu = \frac{r_1}{\phi_1} + r_2 \tag{3.1}$$

$$\phi = \frac{1}{\frac{r_1}{\phi_1} + r_2} \tag{3.2}$$

In case 2, the particle mixture may be considered to consist of a matrix of the smaller particles distributed in interstices between the larger particles. The smaller particles, as they are contained within the interstices, do not contribute to the overall specific volume of the mixture, whereas the larger particles contribute with the specific volume of a monodisperse packing of large particles. The specific volume, and hence the packing density, of the mixture are:

$$\nu = \frac{r_2}{\phi_2} \tag{3.3}$$

$$\phi = \frac{\phi_2}{r_2} \tag{3.4}$$

From the equations it can be seen that the packing density of the mixture in either case is larger than for the individual components. The maximum value of the packing density is found for the value $r^* = r_1 = 1 - r_2$, which for both cases gives the packing density:

$$r_1^* = \frac{\phi_1^* (1 - \phi_2)}{\phi_2 + (1 - \phi_2) \cdot \phi_1} \tag{3.5}$$

With the composition corresponding to $r_1 = r_1^*$ all interstices between larger particles are filled with packed smaller particles and the maximum packing density ϕ^* of the binary mixture is obtained:

$$\phi^* = \phi_2 + (1 - \phi_2) \cdot \phi_1 \tag{3.6}$$

The packing model by Furnas is only valid in cases of $d_1 \ll d_2$. If this condition is not fulfilled the packing density of the binary mixture will also depend on the diameter ratio d_1/d_2. When the difference in diameter of the two sizes of sphere is large,

the smaller spheres pack into the interstices of the assembly of larger spheres, and partially occupy the void volume. When the sphere sizes are more closely comparable, the interstices of the larger spheres are not only no longer filled, but also even enlarged by the attempted intrusion of the smaller spheres, resulting in expansion. The maximum contraction (difference in voids before and after mixing) that occurs in any particular binary mixture is plotted against sphere diameter ratio in Figure 3.3. This figure shows the data from a number of different researchers. Epstein and Young suggest a logarithmic relation between contraction and diameter ratio that implies an infinite contraction or zero voids at zero diameter ratio. Ridgeway and Tarbuck [1968], supported by the data of Furnas indicate that this end value is finite having a value of about 0.23. The significance of this number is that at a diameter or size ratio of about 0.23, the finer spheres fits within the interstices of the coarser spheres. The data of Furnas is for broken solids. The best quadratic regression line to fit the data shown in Figure 3.3 is:

$$\left(\frac{\Delta\varepsilon}{0.23}\right) = 1 - 2.35\phi + 1.35\phi^2 \tag{3.7}$$

where

$\Delta\varepsilon$ = Maximum contraction

ϕ = Diameter ratio

This equation is similar to Furnas' equation. The similarity between data for broken solids and for spheres shows that the difference between the packing of regular and irregular materials is not necessarily as great as is often thought.

Following the pioneering work on packing by Furnas, numerous other packing models have been developed based on the packing of binary systems. The chapter reviews some of these. Following the review, a critical evaluation of the packing

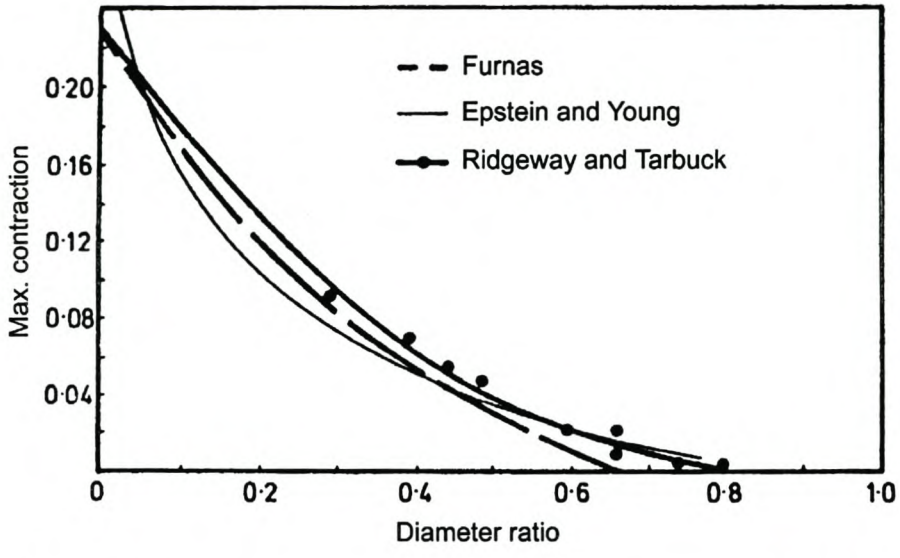

Figure 3.3: Contraction of binary mixtures (after Ridgeway and Tarbuck [1968])

models is undertaken towards the selection of an appropriate model for incorporation into PAVDAM. This is followed by a discussion of aspects to consider in the application of the PAVDAM packing model, particularly factors influencing the packing of aggregates in HMA.

3.2 A review of aggregate packing models

This section reviews different analytical packing models based on binary systems that could be used in a mix design procedure for the definition and control of the volumetric aspects of asphalt mixes. The following models are discussed:

1. Nijboer's packing model
2. Hudson and Davis packing model
3. The packing procedure of Lees
4. Francken and Vanelstraete's PRADO model

3.2.1 Nijboer's packing model

The first practical procedure for predicting voids in asphalt mixes was proposed by Nijboer [1943] in 1943. Nijboer studied aggregate gradations plotted on a log-log gradation chart with percentage passing plotted against sieve opening in microns. The gradation used in the study plotted as straight lines on the log-log scale. Regardless of whether an angular crushed stone or rounded gravel was used, the gradation with minimum VMA plotted as a straight line with a slope (n) of 0.45.

It can be shown that if n is the slope of a gradation curve between two successive sieve sizes $i-1$ and i then:

$$n_i = \frac{\Delta \log(Y)}{\Delta \log(K)} = \frac{\log\left(\frac{Y_i}{Y_{i-1}}\right)}{\log\left(\frac{K_i}{K_{i-1}}\right)} \tag{3.8}$$

where

n_i = Gradation curve slope

K_i and K_{i-1} = Size of two successive fractions

Y_i and Y_{i-1} = Percentage passing of two successive fractions

Starting from the finest fraction of the aggregates (the filler) the decrease of the voids can be followed step by step when the different size fractions making up the mix-grading are progressively added. Considering the grading curve as consisting of the combination of N aggregate fractions, this procedure, published by Nijboer in a graphical form, can be computed from a product of $N-1$ factors such that:

$$\text{VMA} = \varepsilon_f \times \prod_{i=2}^{i=N} \left(\frac{K_i}{K_{i+1}}\right)^p = \varepsilon_f \cdot \prod_{i=2}^{N} F_i \tag{3.9}$$

where

ε_f = Voids in the filler

K_i and K_{i+1} = Size of two successive fractions

p = Exponent depending on the slope of the grading curve

F_i = Reduction factor

Francken [1991] outlines the procedure developed by Nijboer. He points out that the p-exponent used in Eq 3.9 is related to the gradation exponent, n, in Eq 2.1 as shown in Table 3.2 for rounded and cubical aggregates (p1) and elongated or flaky aggregates (p2).

Table 3.2: Relationship between p and n exponents [Francken, 1991]

n	0	0.1	0.2	0.3	0.4	0.5	0.6	0.7	0.9
p1	0	0.06	0.11	0.15	0.17	0.17	0.15	0.14	0.12
p2	0	0.04	0.08	0.11	0.13	0.14	0.12	0.11	0.08

To determine the VMA of a mixture, the gradation of the mix, voids in the filler or Rigden voids [Anderson, 1997] and shape of the particles must be known. Nijboer's method involves the successive combination of binary systems starting with the two finest fractions of the mix, for example the 0.075 mm and 0.15 mm particles. This combined fraction is then blended with the 0.3 mm particle fraction and the procedure repeated until all of the fractions have been blended. The algorithm to calculate the VMA of a mixture based on Nijboer's packing method may be summarised as follows:

1. Sieve sizes and percentage passing sieves are required.

2. Calculate the slope of the gradation curve for each of the successive fractions using Equation 3.8.

3. Determine the p-exponent corresponding to the slope of the gradation for each successive fraction. See Table 3.2.1.

4. Calculate reduction factors using Equation 3.9.

5. Multiply the reduction factor from the first fraction with the voids in the filler to determine the VMA of the first binary system. Multiply this VMA with the reduction factors of the successive fractions to determine the reduction in VMA with the addition of successive fractions.

Table 3.3 shows an example of the Nijboer packing method for a mix gradation with round or cubical aggregate and voids in the filler of 40 percent. Table 3.4 shows an example of the Nijboer packing method for the same mix gradation with elongated or flaky aggregate and voids in the filler of 40 percent. The examples indicate, as expected, that the VMA of rounded aggregate is considerably lower than that of flaky aggregate for the same gradation and voids in the filler.

Table 3.3: Nijboer packing of mix with rounded or cubical aggregate

i	K_i	K_{i+1}	Y_i	q_i	p_i	F_i	**VMA**
1	0	0.075	6.100	-	-	-	40.0
2	0.075	0.150	8.300	0.444	0.170	0.889	35.6
3	0.150	0.300	11.400	0.458	0.170	0.889	31.6
4	0.300	0.600	15.600	0.453	0.170	0.889	28.1
5	0.600	1.180	21.100	0.447	0.170	0.891	25.0
6	1.180	2.360	28.800	0.449	0.170	0.889	22.3
7	2.360	4.750	39.500	0.452	0.170	0.888	19.8
8	4.750	9.500	53.900	0.448	0.170	0.889	17.6
9	9.500	19.000	73.600	0.449	0.170	0.889	15.6
10	19.000	37.500	100.000	0.451	0.170	0.891	13.9

The main shortcoming of the Nijboer model is that it has a limited application. The reduction factors used in the model were determined using a limited number of aggregates from specific sources.

Table 3.4: Nijboer packing of mix with elongated or flakey aggregate

i	K_i	K_{i+1}	Y_i	q_i	p_i	F_i	**VMA**
1	0	0.075	6.100	-	-	-	40.0
2	0.075	0.150	8.300	0.444	0.134	0.911	36.4
3	0.150	0.300	11.400	0.458	0.136	0.910	33.2
4	0.300	0.600	15.600	0.453	0.135	0.911	30.2
5	0.600	1.180	21.100	0.447	0.135	0.913	27.6
6	1.180	2.360	28.800	0.449	0.135	0.911	25.1
7	2.360	4.750	39.500	0.452	0.135	0.910	22.8
8	4.750	9.500	53.900	0.448	0.135	0.911	20.8
9	9.500	19.000	73.600	0.449	0.135	0.911	18.9
10	19.000	37.500	100.000	0.451	0.135	0.912	17.3

3.2.2 Hudson and Davis' packing model

In 1965, Hudson and Davis [1965] studied the relationship between VMA and gradation. They used a similar incremental procedure to Nijboer but with a standard variation curve for each fraction added to the mix as shown in Figure 3.4.

From Figure 3.4 it can be seen that the successive VMA values are calculated using specific voidage reduction factors. Hudson and Davis [1965] provided a table of voidage reduction factors for both rounded/cubical and angular/elongated aggregates. These factors (determined experimentally), shown in Table 3.5 are expressed as a function of the ratio (R) obtained by dividing the percent passing one sieve by the percent passing the next smaller sieve $\frac{Y_i}{Y_{i-1}}$ in the specified sieve series.

As with the packing model of Nijboer outlined previously, the VMA of the aggregate blend may be estimated by applying:

$$\text{VMA} = \varepsilon_f \cdot \prod_{i=2}^{N} F_i \tag{3.10}$$

where

ε_f = Voids in the filler

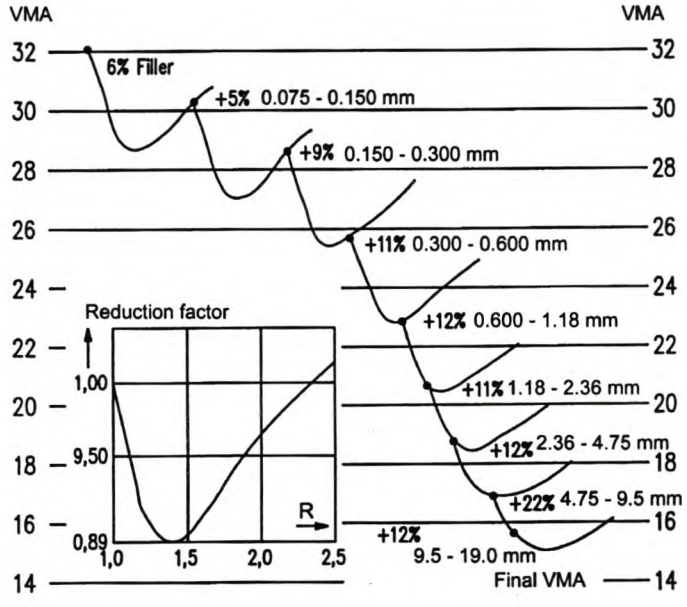

Figure 3.4: Incremental VMA calculation procedure [Hudson and Davis, 1965]

F_i = Voidage reduction factor (see table 3.5).

To determine the VMA of a mixture, the gradation of the mix, voids in the filler (Rigden voids) and shape of the particles must be known. The method of Hudson and Davis involves the successive combination of binary systems in the same manner as Nijboer's method outlined previously. The algorithm to calculate the VMA of a mixture based on the Hudson and Davis packing method may be summarised as follows:

1. Calculate the R ratio by dividing the percent passing one sieve by the percent passing the next smaller sieve for the successive fractions.

2. Depending on the shape of the aggregate, determine the voidage reduction factor corresponding to the calculated R for each successive fraction. See Table 3.5.

3. Multiply the reduction factor from the first fraction with the voids in the filler to determine the VMA of the first binary system. See Equation 3.10.

Table 3.5: Voidage reduction factors (after [Hudson and Davis, 1965])

R	**Rounded**	**Angular**
1	1	1
1.1	0.9583	0.970
1.2	0.9098	0.935
1.3	0.8945	0.920
1.4	0.8908	0.919
1.5	0.8971	0.921
1.6	0.9107	0.924
1.7	0.9260	0.931
1.8	0.9400	0.947
1.9	0.9528	0.970
2.0	0.9647	0.985
2.1	0.9757	1.000
2.2	0.9805	
2.3	0.9905	
2.4	1.0000	

4. Multiply this VMA with the reduction factors of the successive fractions to determine the reduction in VMA with the addition of successive fractions.

Table 3.6 shows an example of the Hudson and Davis packing method for a mix gradation with round or cubical aggregate and voids in the filler of 40 percent. Table 3.7 shows an example of the Hudson and Davis packing method for the same mix gradation with elongated or flaky aggregate and voids in the filler of 40 percent. As with the Nijboer packing method, the examples indicate, as expected, that the VMA of rounded aggregate is considerably lower than that of angular aggregate for the same gradation and voids in the filler. The VMAs estimated using the Hudson and Davis packing model are slightly higher than those estimated with the Nijboer packing model for comparable gradation and aggregate shape.

Table 3.6: Hudson and Davis packing of mix with rounded aggregate

i	K_i	K_{i+1}	Y_i	R	F_i	**VMA**
1	0	0.075	6.100	-	-	40.0
2	0.075	0.150	8.300	1.361	0.892	35.7
3	0.150	0.300	11.400	1.373	0.892	31.8
4	0.300	0.600	15.600	1.368	0.892	28.4
5	0.600	1.180	21.100	1.353	0.893	25.3
6	1.180	2.360	28.800	1.365	0.892	22.6
7	2.360	4.750	39.500	1.372	0.892	20.2
8	4.750	9.500	53.900	1.365	0.892	18.0
9	9.500	19.000	73.600	1.365	0.892	16.0
10	19.000	37.500	100.000	1.359	0.892	14.3

Table 3.7: Hudson and Davis packing of mix with angular aggregate

i	K_i	K_{i+1}	Y_i	R	F_i	**VMA**
1	0	0.075	6.100	-	-	40.0
2	0.075	0.150	8.300	1.361	0.919	36.8
3	0.150	0.300	11.400	1.373	0.919	33.8
4	0.300	0.600	15.600	1.368	0.919	31.1
5	0.600	1.180	21.100	1.353	0.919	28.6
6	1.180	2.360	28.800	1.365	0.919	26.3
7	2.360	4.750	39.500	1.372	0.919	24.2
8	4.750	9.500	53.900	1.365	0.919	22.2
9	9.500	19.000	73.600	1.365	0.919	20.4
10	19.000	37.500	100.000	1.359	0.919	18.8

3.2.3 Lees' packing methodology

In 1970 Lees [1970] made a study of the factors affecting the packing and porosity of particles. He provides a general theory for the combining of aggregates of varying shapes and sizes to achieve *minimum* VMA.

Lees expands on the theoretical case when the size ratio of binary components is zero (as shown in Figure 3.2). A size ratio of zero implies an infinitely small fine aggregate (or infinitely large coarse aggregate). By recalculating the voids value of the separate components as volume per unit weight (of the mixture), it follows that for a size ratio of zero, the partial relative or specific volume of the fine component is zero i.e., theoretically, weight can be added without an increase in bulk volume, and for the coarse component the partial specific volume is the reciprocal of its specific or relative density. These are theoretical points of partial specific volume. In other words, both cases assume that the considered component causes no dilation in the structure of the other component. Lees mentions that similar arguments apply to the specific void volume. Specific voids are calculated as:

$$s = \frac{e}{1-e} \tag{3.11}$$

where

s = Specific voids

e = Unit voids or porosity of the mixture

Specific voids graphs may be drawn, an example of which is shown in Figure 3.5 based on the data of Furnas (Figure 3.2).

Lees points out that the use of the specific voids graph has advantages over the specific volume graph in that differences in relative density of particles are eliminated. In a specific voids graph the theoretical minimum points corresponding with those for

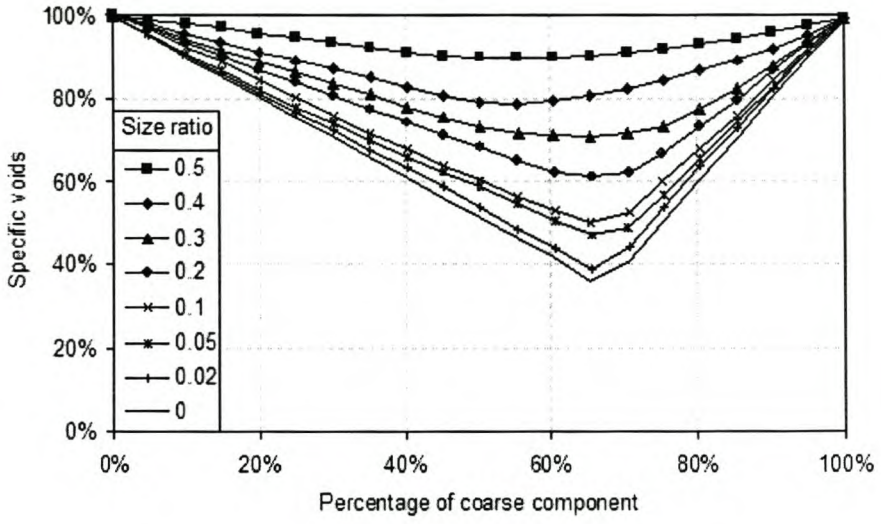

Figure 3.5: Relation between specific voids and size composition

the specific volume graph, are -1 and 0 for the fine and coarse components respectively. In both graphs the position of the intersection of the boundary lines for a size ratio of zero locates the minimum theoretical porosity (in the aggregate blend) and the mix proportions to produce that minimum. The minimum possible porosity of binary systems is the product of the porosities of the respective fractions. All real cases, of finite size ratio, lie within the triangle connecting this point with the specific voids content values of the separate individual components.

Figure 3.6 shows the benefits of the specific voids graph. The influence of the porosity of the fractions making up the binary system may be deduced. In the graph shown there are four intersections where lines from the coarse and fine fractions cross. As indicated, these represent the minimum possible porosity of the binary systems and differ given the porosity of these fractions.

Using the specific void graph, Lees was able to draw general conclusions regarding packing of binary systems:

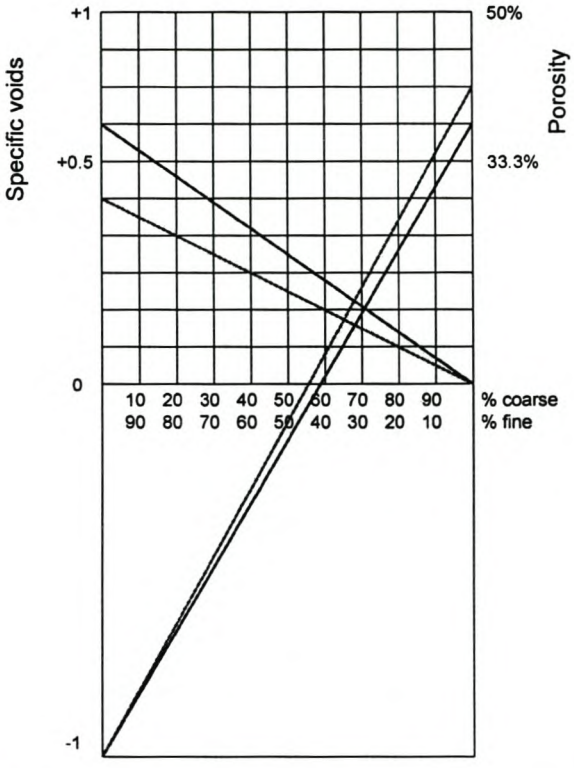

Figure 3.6: Application of specific voids graph

- The actual value of the porosity of the separate component aggregates has a marked influence on the position of the point of intersection.
- Even if the average porosity of the coarse and fine components remains the same, increasing differences between the values produce large changes in the proportion for minimum voids.
- A system of angular coarse aggregate and angular fine aggregate will require a higher percentage of fines for minimum voids than a system of rounded gravel and rounded sand (rounded particles pack to a lower voids content).
- A system of angular coarse aggregate and rounded fines will require a higher percentage of fines than if they too are angular.

- The proportions in which to mix two components for maximum density can change appreciably with the compaction effort applied.
- An aggregate laid in a thin layer, having a high surface area/volume ratio will show a higher porosity than the same aggregate in a thick layer. This will result in an increase in the proportion of fines required for maximum density.
- Decreasing the layer thickness has a greater effect on the coarse component than on the fine, indicating the need for a still higher fines requirement.
- The binder content that will give maximum aggregate density at an early stage of the pavement life (say after rolling) cannot also be the binder content to achieve the same condition at a later stage when traffic has completed the process of aggregate compaction.
- The difference in void content between the continuous and the gap grading is likely to be small.

Based on the above points, Lees makes the following statement that reflects on the spatial composition of asphalt mixes:

> "Consequently it has been considered essential that any laboratory (or field) test upon whose results the prediction of optimum proportions is to be made must imitate as faithfully as possible the dimensions of the section in which the mix is to be placed (especially its least dimensions), the intensity, duration and the type of the compactive effort, and must employ as representative a sample as can be obtained of the aggregate in question."

Lees carried out a full series of experiments with a variety of aggregate combinations over a wide range of size ratios. For the benefit of general application to

all mixes, Lees looked at the reduction in bulk volume that results on blending the two components of binary systems at their optimum proportions compared with the sum of their separate bulk volumes. The ratio of this reduction to the theoretical maximum possible reduction, at size ratio = 0, is termed the relative contraction. Thus:

$$\text{Relative contraction} = \frac{a-c}{a-b} = \frac{\text{actual reduction}}{\text{possible reduction}} \tag{3.12}$$

where

a = Porosity at minimum point at size ratio = 1

b = Porosity at minimum point at size ratio = 0

c = Porosity at minimum point at size ratio = x

x = Actual size ratio of components

It follows that for two components of size ratio = 1, i.e., of the same size, the relative contraction = 0, and that for the theoretical case when size ratio = 0, the relative contraction = 1. In the equation, a is the lower of the two porosities measured for the separate fine and coarse aggregates (since this would necessarily be the minimum porosity when the size ratio = 1). Lees has shown that the relative contraction is dependent upon size ratio and upon P_{diff}, the difference between the porosities of the coarse and fine components respectively. He constructed a graph (Figure 3.7) showing the relationship between these three quantities. From known values of size ratio and P_{diff}, the porosity at the minimum point can be calculated from the value of relative contraction read from the graph and by applying Equation 3.13.

$$c = a - [(a-b) \times \text{ relative contraction}] \tag{3.13}$$

Lees points out that the minimum possible porosity is the product of the porosities

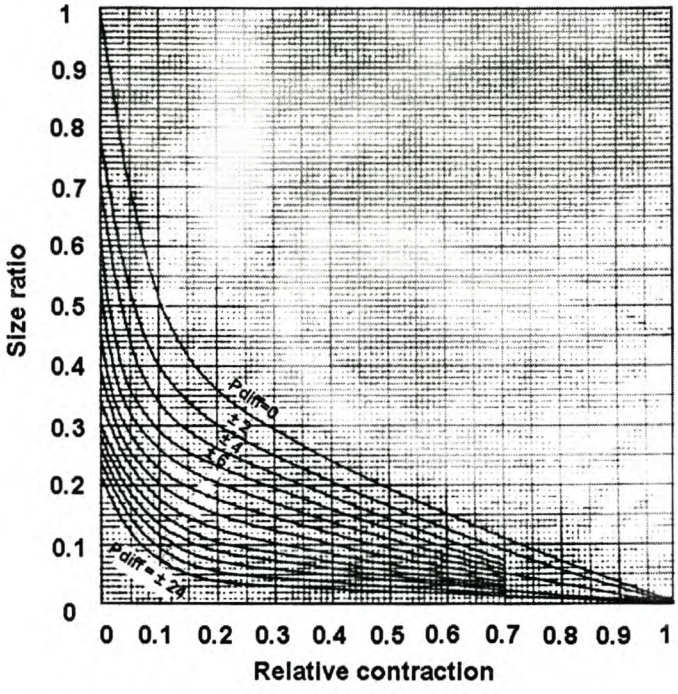

Figure 3.7: Relative contraction as a function of size ratio and P_{diff} [Lees, 1970]

of the individual fractions:

$$b = \frac{P_{coarse} \times P_{fine}}{100} \tag{3.14}$$

Combining these equations the resultant porosity (c) is calculated as

$$c = a - \text{ relative contraction} \left[a - \left(\frac{P_{coarse} \times P_{fine}}{100} \right) \right] \tag{3.15}$$

The method as proposed by Lees enables one to establish gradations for minimum VMA. His approach provides a means of estimating the VMA of a mix from the aggregate gradation. This will be outlined later in the chapter after first introducing some essential packing concepts discussed in the next section.

3.2.4 Francken and Vanelstraete's PRADO model

The Belgian mix design procedure allows an estimation of the VMA of an asphalt mix based on the aggregate gradation and particle angularity. As with the previous

packing procedures discussed in this section, the estimation follows the combination of binary systems. Francken and Vanelstraete [1993] outline the analytical approach in which the mixing law of binary mixes is described in terms of specific voids by simple relationships as represented graphically in Figure 3.8.

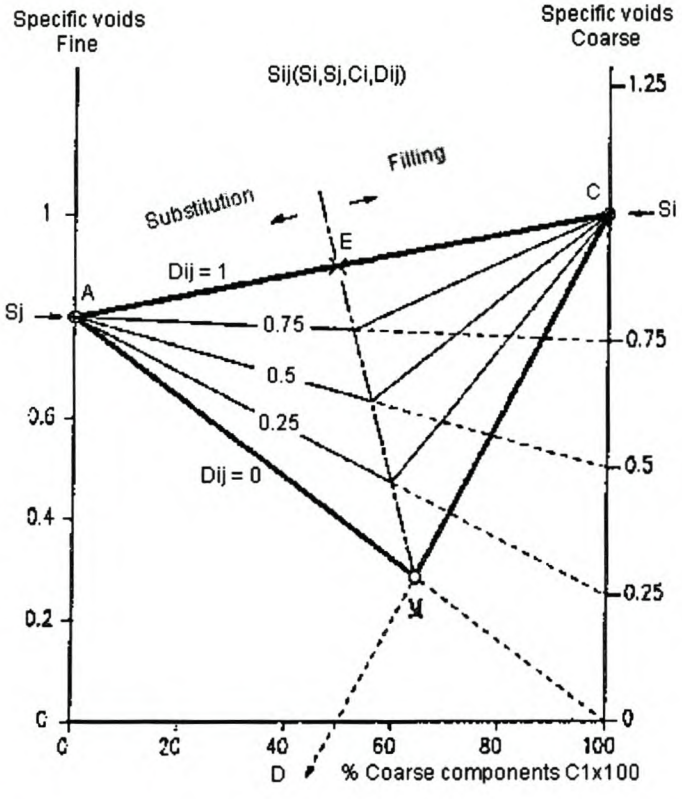

Figure 3.8: Specific voids graph of a binary mixture [Francken and Vanelstraete, 1993]

In both packing modes (substitution or filling), the specific voids S_{ij} of a mix are linearly dependent on the concentration C_i of the coarse fraction and a function of the size ratio D_{ij}. For the substitution mode, constant D_{ij} lines are distributed in a bunch crossing at point A (Figure 3.8) and defined by:

$$S_{ij}\,(S_i,\, S_j, C_i, D_{ij}) = S_j - \left(S_j - \, S_i D_{ij}^{\alpha}\right) C_i \tag{3.16}$$

Francken and Vanelstraete point out that according to experimental observations, the limit between the packing modes is fixed by the line EM joining the middle point

E (S for $D_{ij} = 1$ and $C_i = 0.5$) to the point of minimal voids M. For the filling mode (right wing of the D_{ij} contour lines) specific voids follow a bunch of lines starting from EM and crossing in C. It is important to note that in PRADO, that size ratios (D_{ij} contour lines) are proportioned linearly between 0 and S_i. This is a theoretical assumption that is not necessarily correct but, as will be shown later in the chapter, is adequate for the evaluation of continuously graded mixes.

The PRADO approach considers the aggregate gradation as the combination of a set of narrow fractions, each characterised by their specific voids. It assumes that the specific voids of a mix of particles with different sizes (as defined by the grading curve) can be obtained as a result of successive binary mixes from fine to coarse, in which the fine element is a partial mix of the previous fractions. Starting from the finest fraction of the aggregates (the filler) the decrease of the voids can be followed step by step when the different size fractions making up the mix are progressively added. In other words, the approach assumes that the specific voids of a mix of particles with different sizes can be obtained as the result of blending successive binary mixes in which the fine element is a partial mix of i-1 first fractions and the coarse element is an additional fraction i. At each step, the size d_i of the coarse component is progressively increased until the final fraction of size d_N is reached. This process starting from the finest component (the filler) involves N (i=1, 2, ... N) successive steps in which the mixing law presented in Figure 3.8 is applied. The specific voids S_{Mi} of a partial mix at step i is obtained in a recurrent way from the specific voids S_{Mi-1} of the preceding partial mix i-1 on the basis of the formula:

$$S_{Mi} = \sum_{j=2}^{i=1} f_{ij} S_{ij} (S_i, S_j, C_i, D_{ij}) \qquad (3.17)$$

where

i = Index of the next coarse component added to the mix of the i-1 fractions.

j = Index of each individual component fraction of the partial mix at step i-1

f_{ij} = Probability of finding a particle of fraction j in partial mix i-1 ($2 < j <$i-1)

S_{ij} = Specific voids of the binary mix (Equation 3.16)

S_j = Specific voids of partial mix of the i-1 first components

S_i = Specific voids of component i

S_1 = Specific voids of filler

D_{ij} = Size ratio of particle fractions

Ten specific sieve sizes are used to characterise the aggregate fractions: 0.063; 0.125; 0.25; 0.5; 1; 2; 4; 8; 16 and 32 mm. Standard or reference voids for the different fractions are used as shown in Table 3.8 and differ depending on whether the aggregate is rounded or angular. Note that the specific voids values shown in Table 3.8 correspond to a fixed Marshall compaction level. Validation of Table 3.8 was recently performed on the basis of 126 mixes (72 sand skeleton mixes and 54 stone skeleton mixes) taken from actual construction sites [Van de Ven et al., 1999]. This resulted in the modification of the set of reference voids presented in Table 3.8. The adjustments made led to a standard deviation in estimated VMA of less than 1 percent for the sand skeleton mixes and 1.25 percent for stone skeleton mixes. These standard deviations, although not particularly large, are significant when one considers the strict limits set for minimum VMA.

For each successive binary mixture, the mechanism of substitution or filling is accounted for, together with the concentrations and particle sizes of the mix components. Substitution occurs when large stones take the place of fine aggregates. This happens for low concentrations in coarse aggregates. Filling occurs when the fine aggregates are taking the place of the voids between large particles. The packing of particles is adjusted to take account of influences such as angularity and binder lubrication.

Inputs required by the BRRC packing model are the sieve sizes, the percentages

Table 3.8: PRADO reference voids for gradation fractions

Index	Fraction	% Voids		Specific voids	
i	mm	Round	Angular	Round	Angular
1	< 0.0625	Rigden voids of filler			
2	0.0625 - 0.125	43	50	0.75	1
3	0.125 - 0.25	42	49	0.72	0.96
4	0.25 - 0.5	40	48	0.67	0.92
5	0.5 - 1	36	51	0.56	1.04
6	1 - 2	36	51	0.56	1.04
7	2 - 4	37	50	0.59	1
8	4 - 8	40	50	0.67	1
9	8 - 16	41	52	0.69	1.08
10	16 - 32	42	55	0.72	1.22

passing a specific sieve and the corresponding porosities of the individual fractions. The model as applied in PRADO uses the specific voids values shown in Table 3.8. For the purpose of this dissertation, the BRRC packing model was modified to allow the user to specify the specific voids of the different fractions. These values may be calculated from the porosities determined for individual fractions using Equation 3.11. Porosities of the fractions may be determined using any compaction method and effort. Porosities would typically be determined at compaction levels at which VMA is to be estimated. As an example, consider estimating the VMA of a mix at the Superpave N_{des} compaction level. The individual fractions of the mix would then be gyratory compacted (aggregate only) to the N_{des} compaction level and the porosities of the compacted aggregate fractions determined. These would then serve as input to the model.

The algorithm to estimate VMA using the BRRC method is more complex than that of the previous models discussed. As before, the model considers the combination of binary systems (fine to coarse). The following outlines the steps to be taken in

estimating VMA using the BRRC model:

1. Calculate the percentage coarse component for each of the fractions based on the percentages retained on the sieves.

2. The porosities of the different fractions must be converted to specific voids using Equation 3.11.

3. Calculate the size ratios for the respective fractions. This is the ratio of the particle sizes (fine/coarse) to be blended.

4. Based on the size ratio determine the specific voids of the blend based on the geometric linear relations as described in Figure 3.8. Note that it is necessary to determine the mode of packing (substitution or filling) since this controls which linear relationship to apply.

5. Determine the probability of finding a particle of fraction j in partial mix i-1. This is achieved by applying the following equation:

$$f_{ij} = \frac{(y(j) - y(j-1))}{(y(i-1) - 0)} \tag{3.18}$$

where

f_{ij} = Probability of finding a particle of fraction j in partial mix i-1

$y(i,j)$ = Percentage passing the sieve size of the fraction j or partial mix i

6. Calculate the VMA reduction factor. This is an iterative process as shown in Equation 3.17.

7. Multiply the reduction factor from the first fraction with the voids in the filler to determine the VMA of the first binary system. Multiply this VMA with the

reduction factors of the successive fractions to determine the reduction in VMA with the addition of successive fractions.

As part of the dissertation, the packing model used in PRADO was computerized with the assistance of Dr. Louis Francken of BRRC. The source is given in Appendix A. The process of estimating the VMA of a mix using the BRRC packing model is best explained using an example. Section B.1 of Appendix B shows the output from a computer run. Table 3.9 summarises the results of the BRRC packing model example. The porosities of each of the individual fractions were assumed to be 40 percent. From the output shown in Appendix B it can be seen that the software converts the input gradation to the sieves commonly used in the Belgian mix design procedure. The smallest sieve size is 0.063 mm and subsequent sieve sizes are always an order of 2 greater than the previous size. The first step establishes the voids in the filler fraction (passing the 0.063 mm sieve). In the second step, the filler is blended with the particles retained on the 0.063 mm sieve, which is the coarser fraction of the two. The following symbols are defined:

i = Partial mix.

j = Fraction to be added to the partial mix.

Ci2 = Percentage of the blend that is coarse.

Si1 = Specific voids of the partial mix.

Si2 = Specific voids of the coarser fraction to be added to the partial mix.

f(i,j) = The probability of finding a particle of fraction j in partial mix i-1.

rs(j) = Ratio of the specific voids resulting from the blend of fractions

fact(j) = f(i,j) * rs(j) for each fraction added to the partial mix

Clim = Limit of percentage coarse fraction below which substitution occurs.

Mode = Packing mode: Sub is substitution, Fill is filling.

VMA = VMA or porosity of the partial mix after blending fraction.

Table 3.9: Packing method of Francken (BRRC)

i	K_i	K_{i+1}	Y_i	F_i	**VMA**
1	0.0	0.063	6.10	-	40.0
2	0.063	0.125	7.72	0.895	37.4
3	0.125	0.250	10.58	0.821	32.9
4	0.250	0.500	14.50	0.820	28.7
5	0.500	1.000	19.75	0.833	25.1
6	1.000	2.000	26.96	0.847	22.1
7	2.000	4.000	36.87	0.866	19.7
8	4.000	8.000	50.33	0.887	17.9
9	8.000	16.000	68.72	0.906	16.5
10	16.000	32.000	93.84	0.923	15.4

To determine the porosity of the partial mixes, a probabilistic approach is applied. Consider Step 3 in the output of the example shown in Appendix B. At this stage, the 0.063 mm particles have been added to the filler particles resulting in a partial mix (Step 2). The porosity of this partial mix is 37.37 percent, which converts to a specific voids of 0.597. The 0.125 mm particle fraction must now be added to this partial mix. The porosity of the 0.125 mm particles is 40 percent, which converts to a specific voids of 0.667. In this blend, the 0.125 mm particles are coarser than the partial mix and make up 27.1 percent of the blend (from the gradation). Particles making up this blend consist of the filler fraction, the 0.063 mm particles and the 0.125 mm particles. Consider the case if the 0.125 mm particles are added to the filler fraction (substep j=1). An assumption is made with regards the size of the filler particles. The size of the filler particles are assumed to be half that of the 0.063 mm particles i.e. 0.03125 mm. The size ratio for this subset is 0.03125 / 0.125 = 0.25. The probability (f(i,j)) of finding a filler particle in the partial mix (composed of filler and 0.063 mm particles) is roughly 79 percent (calculated using Equation 3.18). The

specific voids resulting from the blend of 0.125 mm and filler particles is 0.481. This specific voids is divided by the specific voids of the partial mix resulting in rs(j) = 0.481 / 0.597 = 0.805. Next, consider the case if the 0.125 mm particles are added to the 0.063 mm fraction (substep j=2). The size ratio for this subset is 0.063 / 0.125 = 0.5. The probability of finding a 0.063 mm particle in the partial mix (composed of filler and 0.063 mm particles) is roughly 25 percent. The specific voids resulting from the blend of 0.125 mm and 0.063 mm particles is 0.526. This specific voids is divided by the specific voids of the partial mix resulting in rs(j) = 0.526 / 0.597 = 0.881. The voidage reduction factor may then be calculated as the sum of the probabilities multiplied by rs(j) determined for the two cases considered. This reduction factor is multiplied by the specific voids of the previous blend which is then converted to VMA (e=s/(1+s)) and the process continues until each of the fractions have been added.

The probabilistic approach as outlined above was also used for the blending of successive binary systems in the Aim and Toufar packing models to be discussed in the following section.

3.2.5 Aim and Toufar's packing models

In 1997 Goltermann et al. [1997] presented two models, the Aim and Toufar models (named after researchers of aggregate packing), to determine the packing degree of fine and coarse aggregate gradation combinations. Aim and Toufar's packing models were used together to develop concrete packing models as part of the concrete research under SHRP [Roy and Idorn, 1993]. These models represent the packing state-of-the-art in the concrete industry. In concrete, the densest packing of aggregate is often desirable. Furthermore, in general, less stockpiles are used to produce concrete mixes compared to asphalt mixes.

Aim's model (as with the Furnas model outlined in the introduction to the chapter)

considers two cases:

1. The amount of fine particles is much less than the amount of coarse particles.

2. The amount of fine particles is much higher than the amount of coarse particles.

In the first case, the fine particles fill some of the voids between the coarse particles (filling), whereas in the second case, the fine particles act as a media in which the coarse particles are embedded (substitution). The volume concentration of fine particles at maximum packing density of the mix is found as:

$$r^* = \frac{p}{(1+p)} \tag{3.19}$$

$$p = \frac{\phi_1}{\phi_2} - \left(1 + 0.9\frac{d_1}{d_2}\right)\phi_1 \tag{3.20}$$

where

r_1, r_2 = Volume fraction of the fine and coarse aggregates respectively

ϕ_1, ϕ_2 = Packing density of the fine and coarse aggregates respectively

d_1, d_2 = Characteristic diameter of the fine and coarse aggregates respectively

This equation is the same as that presented by Furnas (Equation 3.5) when $d_1 \ll d_2$. The factor $(1+0.9d_1/d_2)$ is used to take the wall effect into account. The packing degree can, in the two cases (filling and substitution), be calculated as:

$$\phi = \frac{\phi_2}{(1-r_1)} \text{ for } r_1 < r^* \tag{3.21}$$

$$\phi = \frac{1}{\left[\frac{r_1}{\phi_1} + (1-r_1)\left(1+0.9\frac{d_1}{d_2}\right)\right]} \text{ for } r_1 \geq r^* \tag{3.22}$$

Toufar's model predicts the packing degree as:

$$\phi = \frac{1}{\left[\frac{r_1}{\phi_1} + \frac{r_2}{\phi_2} - r_2\left(\frac{1}{\phi_2} - 1\right)k_d k_s\right]} \tag{3.23}$$

where

y_1/ϕ_1 = Specific volume of the fine particles

y_2/ϕ_2 = Specific volume of the coarse particles

$y_2(1/\phi_2 - 1)$ = Void volume between the coarse particles

k_d = A factor that determines the influence of the diameter ratio

k_s = A statistical factor

Toufar states that

$$k_d = \frac{(d_2 - d_1)}{(d_1 + d_2)} \tag{3.24}$$

and that each of the fine particles are placed between four of the coarse particles, leading to:

$$k_s = 1 - \frac{(1 + 4x)}{(1 + x)^4} \tag{3.25}$$

where x = (specific volume of the fine particles) / (void volume between the coarse particles) or:

$$x = \frac{\left(\frac{r_1}{r_2}\right)\left(\frac{\phi_1}{\phi_2}\right)}{1 - \phi_2} \tag{3.26}$$

When x = 1, the volume of fine particles equals the volume of voids between the coarser particles. Tests have shown that Toufar's model predicts that the packing degree of a sample of coarse particles does not increase when a small amount of fine particles is added to the coarse particles. This is due to the assumption that each fine particle is placed in a space, which is limited by four coarse particles. This unrealistic behaviour can best be corrected by introducing a minor modification of the k_s-expression based on experimental data:

$$k_s = \left(\frac{x}{x_0}\right) k_0 \text{ for } x < x_0 \tag{3.27}$$

$$k_s = 1 - \frac{(1 + 4x)}{(1 + x)^4} \text{ for } x \geq x_0 \tag{3.28}$$

where $x_0 = 0.4753$ and $k_0 = 0.3881$.

The Aim packing model is considered more accurate than the Toufar model for size ratios less than 0.22. At about this size ratio, the fine fraction fits within the interstices of the coarser fraction. The theoretical models are based on a number of assumptions, where the following three conflict with the practical combination of realistic aggregates:

1. Aggregates are perfect spheres
2. Aggregates are monosized
3. Fine and coarse aggregates are of a different size

The first two assumptions can be overcome by introducing a characteristic diameter for the aggregates and by using the measured packing degrees for the aggregates. Goltermann et al. [1997] point out that many crushed particles within a single stockpile have the size distribution curves presented by the Rosin-Raimmler-Sperling-Bennett distribution:

$$P(d) = \exp\left(-\left(\frac{d}{d'}\right)^n\right) \tag{3.29}$$

where

$P(d)$ = Cumulative probability that the diameter is less than d

d = Particle diameter

d' = Position parameter = sieve size for which there is 36.8 percent retained

Goltermann et al. [1997] recommend that the position parameter be used to determine the characteristic diameter for the aggregates. This recommendation was made based on experimental evidence. They point out that the third assumption mentioned previously may lead to problems when the two aggregates have overlapping fractions (i.e. when a substantial part of the fine aggregates is of the same size as a substantial part of the coarse aggregates) and when their characteristic diameters are fairly

different. The models should then overestimate the packing of the combined mix in the area where $y_1 < y^*$, although the estimate will not be affected much for larger y_1-values.

Anderson and Johansen [1993] present a guide to determining the optimal gradation of concrete aggregates using the Aim and Toufar models. The guide presents tables based on a computer model for the theoretical packing of spherical particles takes into account their size and specific gravity (as outlined above). To find the optimal composition of sand and coarse aggregates, the following steps are followed:

1. Determine the characteristic diameter from a Rosin-Raimmler plot of the sieve analysis of the materials:
   (a) Plot the results of a sieve analysis onto the Rosin-Raimmler graph.
   (b) Draw the best straight line through all points.
   (c) Determine the particle diameter from the straight line equivalent to 63 weight percent of the material passing.
2. Determine the packing density of the sand and coarse aggregates. The following procedures should be followed:
   (a) Determine the void volume of each material using the dry rodding procedures described in ASTM Test Method C29.
   (b) Calculate dry weight packing density = 1 - (% voids/100).

Roy and Idorn [1993] discuss the Aim and Toufar models that were used to develop packing models for the concrete industry as part of the concrete research under SHRP. They point out that the method proposed to determine the characteristic diameter from the Rosin-Raimmler graph is not always very accurate. The author has modified the Aim and Toufar packing model so that characteristic diameters of blends do not

need to be determined. Although the Aim and Toufar packing models are applicable to the blending of stockpiles (this requires determining the density and porosity of the compacted stockpile fractions), the models were modified and used to estimate the VMA resulting from the blending of individual aggregate fractions making up the gradation of a mix.

For the purpose of the dissertation, the Aim and Toufar packing models were modified by adopting the probabilistic approach as used in the BRRC packing model discussed previously. This eliminates the need to determine the characteristic diameters of the blends. In fact, the procedure adopted was identical to that used for the BRRC packing model, the only difference in the approach being the method by which specific voids were calculated. The Aim packing model was applied when the size ratio of fractions was less than 0.22. An output of a computer run using the modified Aim and Toufar (MAT) packing models with the input parameters as previously defined for the BRRC packing models is shown in Appendix B. Table 3.10 summarises the results of the packing exercise using the same inputs as for the PRADO model discussed previously.

Table 3.10: Packing method of Aim and Toufar

i	K_i	K_{i+1}	Y_i	F_i	**VMA**
1	0.038	0.075	6.10	-	40.0
2	0.075	0.150	8.30	0.868	36.7
3	0.150	0.300	11.40	0.829	32.4
4	0.300	0.600	15.60	0.835	28.6
5	0.600	1.180	21.10	0.846	25.3
6	1.180	2.360	28.80	0.855	22.5
7	2.360	4.750	39.50	0.871	20.2
8	4.750	9.500	53.90	0.892	18.4
9	9.500	19.000	73.60	0.911	17.0
10	19.000	37.500	100.000	0.930	16.0

From the table it can be seen that the final VMA estimated using the MAT models is slightly higher than that estimated using the BRRC packing model shown in Table 3.9.

3.3 Critical evaluation of the packing models

The previous section reviewed the theory underlying a number of packing models that may be used to estimate the VMA of asphalt mixes. In the search for an analytical packing model for PAVDAM, a number of prerequisites had to be met:

1. Applicability: The model has to be applicable for a broad range of aggregate characteristics, including gradation, shape, size and surface texture.

2. Accuracy: The model has to be consistently accurate. Model VMA estimates have to be in line with measured VMA.

3. Flexibility: The model has to be flexible enough to be incorporated into PAVDAM. As such, it was necessary that the model be computerized.

4. Speed: PAVDAM, as will be discussed in the next chapter, uses Monte Carlo simulation. The packing model will therefore be called upon to estimate the VMA of a mix thousands of times during one simulation run.

General applicability was the reason why empirical packing models are not discussed in the chapter. Examples of empirical packing models include the COMPACT model by Semmelink [1991] and Bailey's packing method [Vavrik et al., 2001].

The Nijboer and Hudson and Davis packing models apply different reduction factors depending on the angularity of the aggregate. These reduction factors were determined based on the packing of a limited number of aggregates from specific sources. This severely restricts the general applicability of these models. These

simple models are useful for quickly predicting the effect of changes in gradation on aggregate porosity.

As mentioned previously, a packing model based on the theory presented by Lees [1970] may be developed using the approaches adopted in the BRRC and modified Aim and Toufar packing methods. Figure 3.7 may be used to determine the minimum possible porosity of a binary system. Although not presented in this dissertation, Lees [1970] presented a number of figures to determine the percentage of the finer or coarser fraction at which this minimum possible porosity occurs for different size ratios. These figures would need to be modelled or alternatively the approach adopted in the BRRC packing method may be employed i.e. proportioning the size ratio lines based on the porosity of the coarser fraction. The porosity of the blend at any percentage of the coarser fraction may then be determined by assuming linear relationships between the porosities of the individual fractions and the minimum possible porosity as is done in the BRRC method. It would also be necessary to model the relationships defined in Figure 3.7. A disadvantage of this approach is that it would be difficult to model the various relationships required accurately and furthermore the model would be based on assumed linear relationships that are not realistic. For these reasons it was decided against developing a packing model based on Lees' theory.

The method of successively packing binary systems employed in the BRRC and modified Aim and Toufar (MAT) approaches is efficient since algorithms may be programmed for computer analysis. The probabilistic approach employed to determine the porosities of partial mixes based on size ratio in the modified Aim and Toufar models is also more accurate and efficient than determining characteristic diameters from a Rosin-Raimmler plot. Use of the Rosin-Raimmler plot may be feasible when mixes are composed of materials from limited stockpiles. Both the BRRC and MAT models have general application since the estimated porosity of a mix is determined

based on the porosities of the individual fractions making up the mix. The disadvantage of these approaches, however, is that laboratory work is required to determine these porosities. These two models therefore satisfy most of the prerequisites imposed but the question of accuracy remains.

An evaluation of the output from the different packing models reviewed in the chapter indicates differences in the estimated VMA of a mix with the same gradation. Figures 3.9 (size ratios from 0 to 0.1) and 3.10 (size ratios from 0.2 to 0.5) summarize the packing model estimates of the different models reviewed. The models are compared to packing results of Furnas [1928] presented previously and as shown in Figure 3.2.

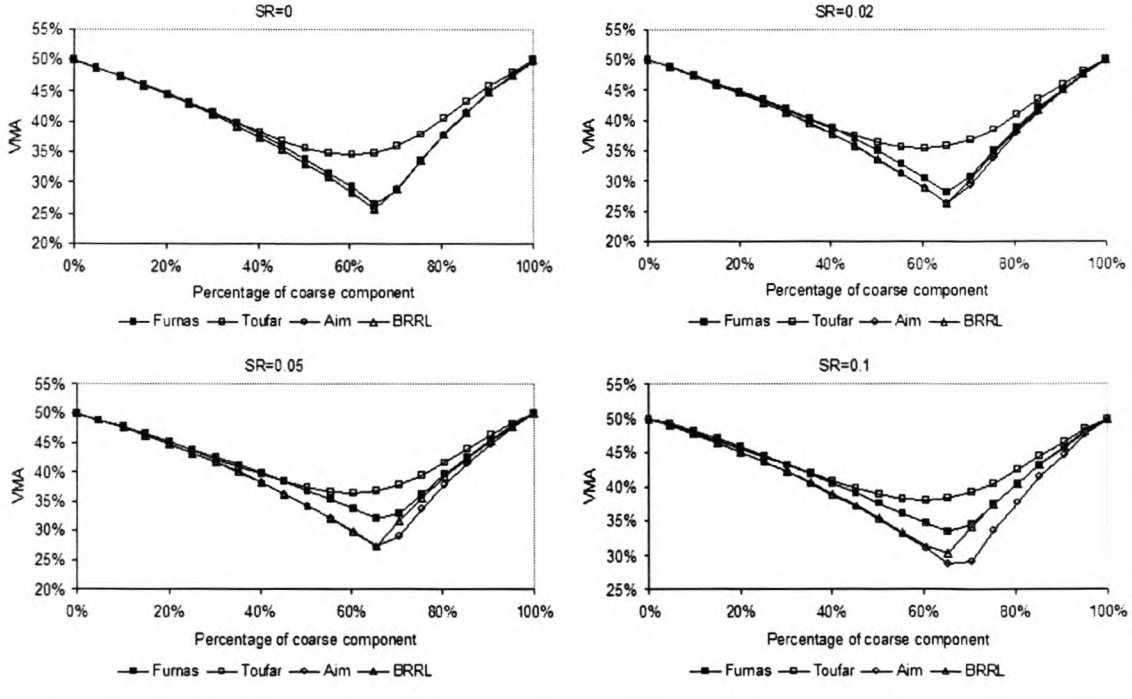

Figure 3.9: Comparison of packing model VMA estimates, Size ratio: 0 - 0.1

From the figures it can be seen that the packing model estimates differ from Furnas' experimentally determined results to various degrees depending on the size ratio. The important aspect to consider is the percentage of the coarse component

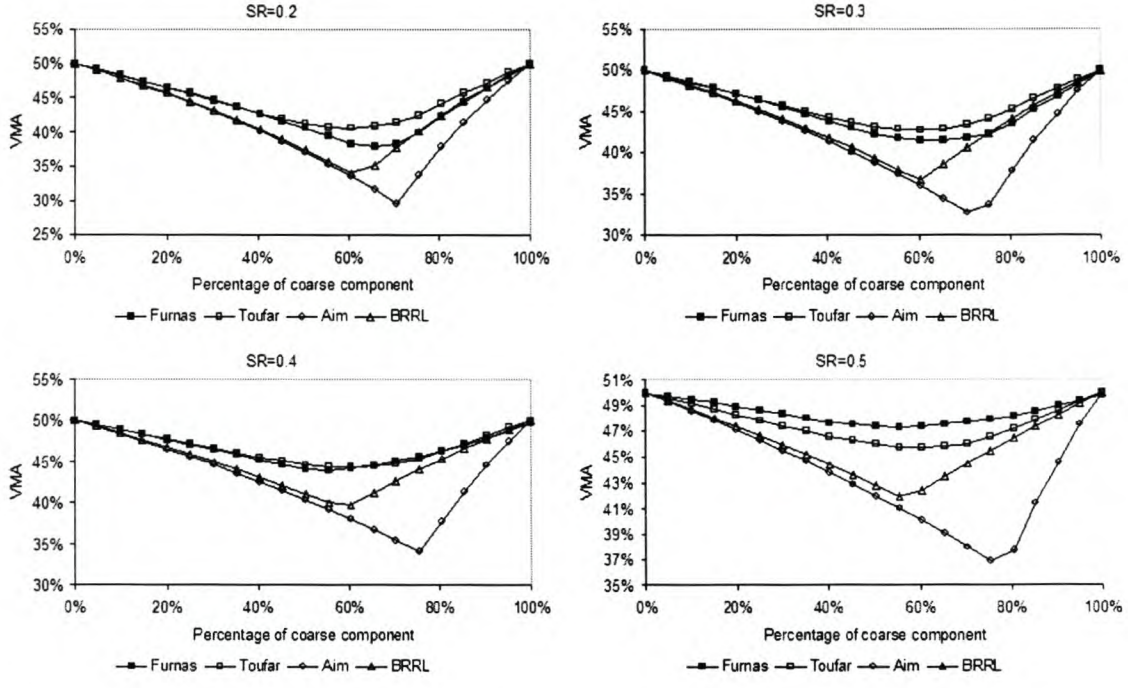

Figure 3.10: Comparison of packing model VMA estimates, Size ratio: 0.2 - 0.5

and how the packing model estimates compare as this changes. At size ratios less than 0.2, all of the packing models compare reasonably well with the experimental results with the exception of the Toufar model between percentages of coarse fraction from 40 to 80 percent. At sizes ratios less than 0.22, Aim's model is used instead of the Toufar model as discussed previously. At or above a size ratio of 0.2, the Toufar model provides the best estimate at any percentage of the coarse fraction. The figures are for a single binary system. The successive combination of binary systems would increase the difference in estimated VMA. It is therefore advantageous to have the model estimate as close to the actual VMA of the mix as possible. For the successive packing of binary systems for continuously graded mixes, the size ratios are always less than or equal to 0.5. For these mixes the percentage of coarse fraction is also nearly always less than 40, even for coarser gradations with high gradation exponents. From a packing model point of view this is beneficial since as can be seen in Figures 3.9

and 3.10, the model estimates are generally very close to the experimental results for percentages of the coarse fraction less than 40.

From the preceding it may be concluded that either the BRRC or MAT packing models may be used to estimate the VMA of continuously graded mixes. These models are therefore suitable for use with PAVDAM. The MAT packing model may be the better model for more open graded type mixes. The MAT packing model is also directly based on the packing of uniform spheres whereas the BRRC model incorporates linear relationship assumptions regarding the influence of size ratio. Packing experiments were also done on aggregates from the Contermanskloof quarry in South Africa to investigate the application of the packing models. These are discussed in the next section.

3.4 Packing model application

For practical application of the BRRC or modified Aim and Toufar (MAT) packing models it is necessary to consider different influencing factors. Packing characteristics of HMA mixes are important because of the general association between mixture properties and density. Various researchers have identified the most relevant factors influencing the packing characteristics of aggregates. These include:

1. Size and distribution (gradation),
2. Shape (flat or elongated),
3. Angularity,
4. Surface texture,
5. Rugosity, and,
6. Compaction effort.

It is assumed that each of these factors are accounted for in both the BRRC and MAT packing models since the listed factors influence the packing characteristics and hence porosities of the individual fractions making up the mix. This section outlines specific details for application of these packing models.

3.4.1 Porosities of individual aggregate fractions

Following on the research of Tons and Goetz [1968] and Tons et al. [1970], Ishai and Gelber [1982] looked at the effect of geometric irregularity of aggregates on the properties and behaviour of HMA. The research undertaken focussed on two aggregate factors: a) particle volume and b) particle geometry (shape, angularity and surface texture). The packing volume (V_p) of a particle was defined as the volume that a rock particle occupies in a mass of monovolume (one-size) particles. In their words: "Since irregular particles usually touch one another at the peaks of the surface roughness, the packing volume encompasses not only the solids and the surface capillaries (micro surface voids), but also the volume of surface macro dips and valleys (macro surface voids)." The packing volume can be visualised as the volume enclosed by a dimensionless membrane surrounding the particle as shown in Figure 3.11. Based on the packing volume of a particle (V_p), the packing specific gravity was defined as $G_p = W/V_p$, where W is the dry weight of the particle.

The packing volume was used to develop a concept that defines the behaviour of one-sized particles in bulk. The concept was verified experimentally by Tons and Goetz [1968]. This concept is important to the analytical packing model used for PAVDAM and can be stated as follows:

> Different types on one-size aggregates will be compacted to the same bulk volume when they possess identical total packing volume ($\sum V_p$) under identical compaction procedure.

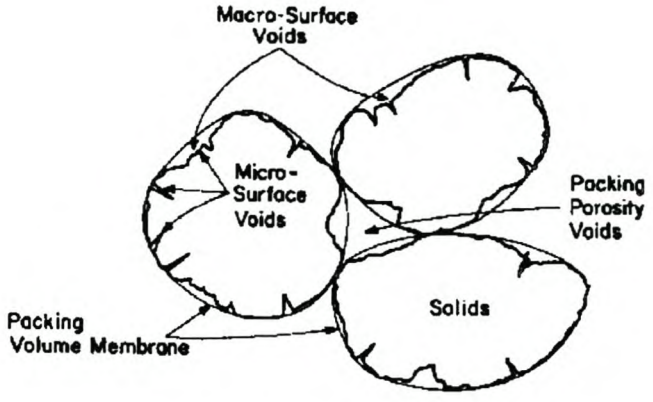

Figure 3.11: Description of specific rugosity parameters [Ishai and Gelber, 1982]

Therefore, if $\sum V_p$ is constant, the following equation can be written:

$$\sum V_p = \frac{\sum W_1}{G_{p1}} = \frac{\sum W_2}{G_{p2}} = \ldots = \frac{\sum W_i}{G_{pi}} = \text{constant} \tag{3.30}$$

where

$\sum W_i$ = Weight of the i-th one-size fraction that occupies the same bulk volume,

G_{pi} = Packing specific gravity of the i-th one-size fraction.

As a consequence, if for different aggregates $\sum V_p$ is constant and the bulk volume that the particle occupies (V_b) is constant (monosized particles), then the different types of aggregate particles will also have *identical* packing porosity (P_p):

$$P_p = \frac{V_b - \sum V_p}{V_b} = \text{constant} \tag{3.31}$$

Figure 3.12 shows experimental results of Tons and Goetz [1968]. Three different types of rock (crushed limestone, crushed gravel and rounded gravel) with single sizes of 19 mm, 9.5 mm and 3.2 mm were vibratory compacted. The results indicated that regardless of rock type or size, the porosities obtained at each of the indicated cycles were similar. As a check, 12.5 mm diameter glass marbles (without rugosity) were

included in the compaction tests. The marbles behaved similarly to the single sized rocks.

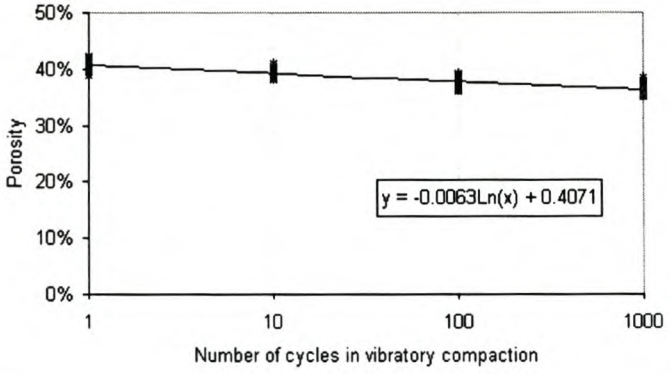

Figure 3.12: Porosities of different single sized aggregates under vibratory compaction (after [Tons and Goetz, 1968])

From the results in Figure 3.12, the average porosity of the particles after 1 vibratory cycle was 40.6 percent with a standard deviation of 0.7 percent and after 1000 vibratory cycles, the average and standard deviation of the particles porosity were 36.4 and 0.8 percent respectively. Hence the difference in (average) porosity with compaction was in the order of 4.2 percent.

To further investigate the packing characteristics of individual fractions, gyratory compaction tests were done on aggregate from the Contermanskloof quarry in the Western Cape, South Africa. The porosities of individual aggregate fractions were determined using *dry* gyratory compaction tests within 150 mm diameter moulds. Three different samples were compacted for each individual fraction. Figure 3.13 illustrates the results of the gyratory compaction tests in terms of porosities determined at specific compaction levels. The results for the different fractions have been combined.

A regression line fitted to the data takes the following form:

$$\text{VMA} = a + b \cdot \ln(N) \tag{3.32}$$

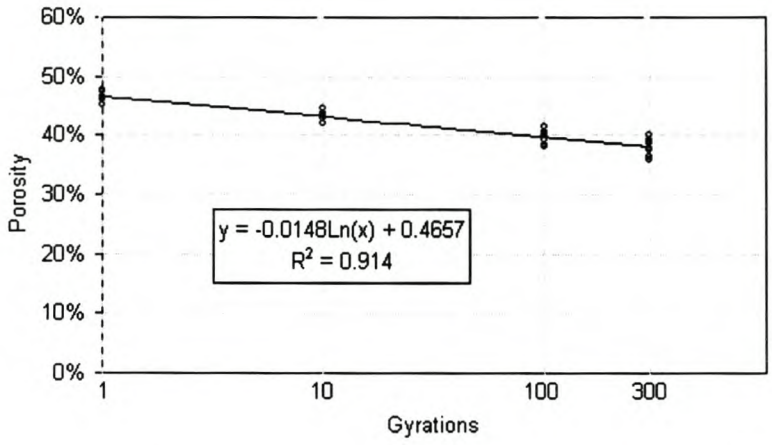

Figure 3.13: Combined gyratory compaction porosities of individual fractions

where

VMA = Voids in the mineral aggregate compacted dry = VMA = VIM

N = Number of gyrations

a, b = Regression constants

For the Contermanskloof aggregates therefore, the following compaction characteristic was determined for gyratory compaction of the individual fractions:

$$\text{VMA} = 0.4657 - 0.0148 \cdot \ln(N) \tag{3.33}$$

The average porosity of the fractions after 1 gyration (which is equivalent to placing the aggregate in the mould and applying a pressure of 600 kPa) was 46.5 percent with a standard deviation of 0.8 percent. The average porosity after 300 gyrations was 38.1 percent with a standard deviation of 1.4 percent. The difference in (average) porosity with compaction was therefore in the order of 8.4 percent. Hornfels aggregate has a high crushing strength, but slight degradation of the aggregate was apparent under gyratory compaction, particularly at the sharp edges of the stone sized

particles i.e. particles greater than 2.36 mm. Crushing of the aggregate would obviously influence the measured porosities since the bulk volume of the packed aggregate would decrease slightly, therefore the use of the gyratory compactor to determine the porosities of softer aggregates is questionable. Use of lubricants or even low bitumen contents may aid in reducing crushing of the aggregate.

The compaction results shown in Figure 3.13 are encouraging and confirm the finding of Tons and Goetz [1968]. It is obvious though that the determined porosities depend on the compaction method and effort applied.

3.4.2 Compaction of individual fractions

The influence of compaction on the porosity of the individual fractions is an important consideration. The estimate of the VMA of an aggregate blend using the BRRC or MAT packing models is directly related to the porosities used for the individual aggregate fractions.

Various researchers have applied different compaction methods. Recent research undertaken by Vavrik et al. [2001] looked at rodding of individual aggregate fractions to determine porosities. They describe a procedure in which the packing characteristics of the fractions are measured by determining the loose and rodded weights for the aggregates. The procedure used is basically the same as that established in AASHTO T19. Loose weight is the unit weight of aggregate when poured into an empty container. It is recommended that the container used should have a diameter at least 10 times the nominal maximum particle size to minimize edge effects relating to particle packing. Vavrik et al. [2001] recommend a circular metal bucket of known volume, ranging from 0.007-0.009 cubic meter for coarse aggregates with a 25 mm or smaller nominal maximum particle size and the use of a 100 mm diameter, standard proctor mould of known volume, approximately 0.001 cubic meter, for fine aggregates with a

nominal maximum particle size of 4.75 mm or less. A 15 mm diameter metal rod is used for leveling the top of the sample. A representative sample of the lab-dried aggregate is poured into the corresponding container until overflowing and then struck off level with the metal rod, being careful not to compact the aggregate. The sample is then weighed to determine the loose unit weight (e.g., kilograms/cubic meter). This test is conducted a minimum of three times to determine an average. Rodded weight is the unit weight of aggregate when it is rodded into an empty container. Aggregate is poured into the container in three lifts with each one rodded 25 times. After the third lift is rodded, the container is struck level and weighed. This test is also conducted a minimum of three times to establish an average. New material should be used for each test if there is a concern that the aggregate will degrade from the rodding procedures. Both the loose and rodded weight tests are performed for each individual aggregate being used in the blend. They found the following ranges to apply:

- Voids at the loose unit weight - 43 to 48 percent
- Voids at the rodded unit weight - 37 to 42 percent
- Difference in voids between the loose and rodded unit weights - 4 to 8 percent

NCHRP [1997] research on large stone mixes also incorporated dry rodding according to AASHTO T19 to establish the bulk volume (or porosity) of large coarse particles. Research by Seward et al. [1996] incorporated dry rodding as well as a pressure of 600 kPa in the gyratory compactor to determine bulk volumes for aggregate fractions. Semmelink's [1991] COMPACT procedure uses shake-tamping of the individual fractions. The dry rodding or shake tamping procedures are beneficial in that aggregate degradation is limited. A disadvantage of this procedure, however, is that the degree of compaction and potential for further compaction of the aggregate skeleton is unknown. Having a gauge on the change in porosity with compaction is useful

if VMA is to be estimated at specific compaction levels, for example at N_{ini}, N_{des} or N_{max}, the Superpave gyratory compaction criteria levels. Rodding or shake tamping procedures only provide aggregate porosities at one compaction level, the degree of which cannot be defined unless the aggregate skeleton is compacted to refusal.

To explore this argument, binary systems consisting of 0.15 mm (fine component) and 9.5 mm (coarse component) aggregate particles (from the Contermanskloof quarry in the Western Cape, South Africa) were dry compacted using the gyratory compactor. Having compacted the individual fractions of both the 0.15 mm and 9.5 mm sized particles previously, the change in porosity of these fractions with compaction was known as indicated in Figure 3.13. The 0.15 mm fraction was mixed with increasing percentages of the coarser 9.5 mm fraction. The specific voids diagram shown in Figure 3.14 illustrates the binary system of these two fractions. The binary systems are shown at three gyratory compaction levels i.e. after 1, 10 and 100 gyrations. From the figure it can be seen (as anticipated) that the porosities of the blend at the different compaction levels depend on the porosities of the individual fractions at the different compaction levels.

Estimates of the porosity of aggregate blends using packing models may be defined at specific compaction levels. The packing model estimate will depend on the porosities of the individual fractions at these compaction levels. Figures 3.15 through 3.18 show the laboratory determined porosities of the binary systems consisting of 0.15 mm and 9.5 mm sized particles at different compaction levels compared to the porosities estimated using the MAT packing model, which depended on the porosities of the individual fractions at the different compaction levels. The figures illustrate that the porosities estimated using the MAT packing model are slightly lower (about 4 percent lower) than the actual laboratory measured porosities. The porosity estimate, however, clearly relates to the actual porosity at the different compaction levels.

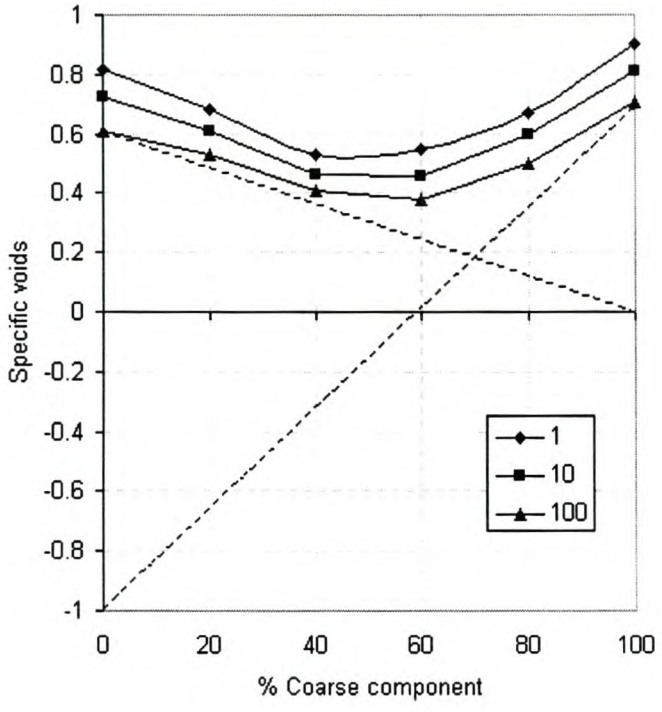

Figure 3.14: Specific voids diagram of 0.15 mm and 9.5 mm binary system

One option therefore is to determine the change in porosity of the individual fractions with compaction. As pointed out, this is beneficial if porosity estimates are required at different compaction levels. This may be done by fitting the compaction data (of mixes or individual fractions) to a mathematical model as shown in Figure 3.13. It has been found that gyratory compaction data fit well to sigmoidal or "S-shaped" growth curve models. These curves start at a fixed point and increase their growth rate monotonically to reach an inflection point. After this, the growth rate approaches a final value asymptotically. Examples of sigmoidal models investigated include the so-called MMF model:

$$y = \frac{(ab + cx^d)}{(b + x^d)} \tag{3.34}$$

and the Weibull model:

$$y = a - b \cdot \exp\left(-cx^d\right) \tag{3.35}$$

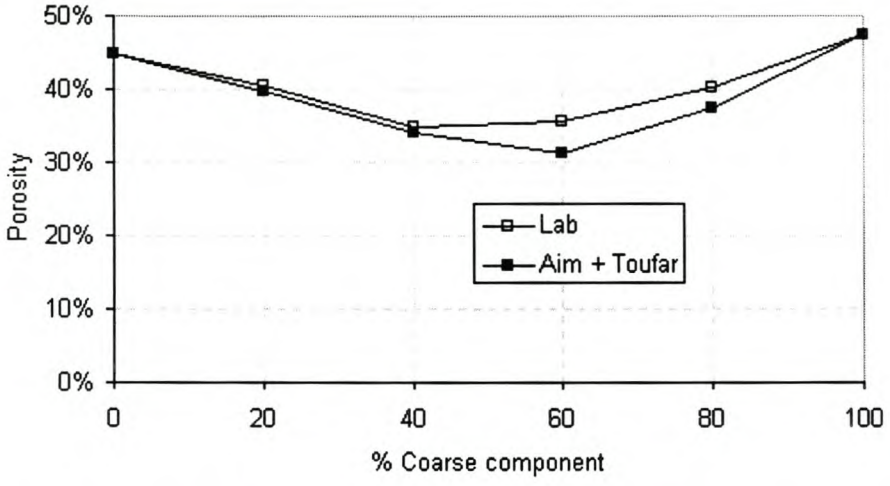

Figure 3.15: Binary system laboratory determined and packing model estimated porosities after 1 gyration

These models are non-linear and are defined by regression coefficients a, b, c and d. MMF fitting of gyratory compaction data is accurate as illustrated in Figure 3.19. The figure shows an example of the compaction of an asphalt mix at a specific binder content.

Another option for the application of packing models is to estimate porosities of aggregate blends at specific compaction levels. The packing model applied in the Belgian PRADO procedure, for example, uses reference porosities of the individual fractions as outlined in Table 3.8. The first option was adopted in PAVDAM i.e. allowing the estimation of the VMA of a mix at any compaction level. This represents a departure from previous approaches and sets the packing model used in PAVDAM apart from other models used to estimate the VMA of asphalt mixes.

Another factor to consider in the application of packing models is the influence of binder content on aggregate packing. This is addressed in the next chapter.

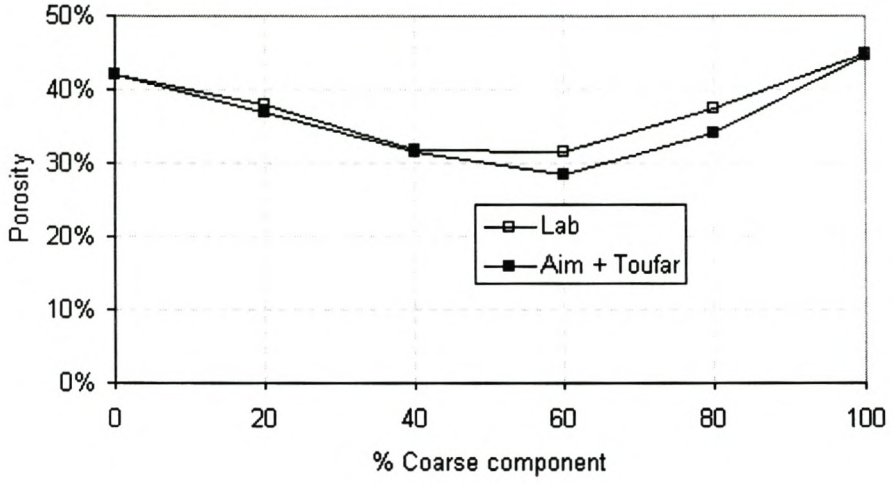

Figure 3.16: Binary system laboratory determined and packing model estimated porosities after 10 gyrations

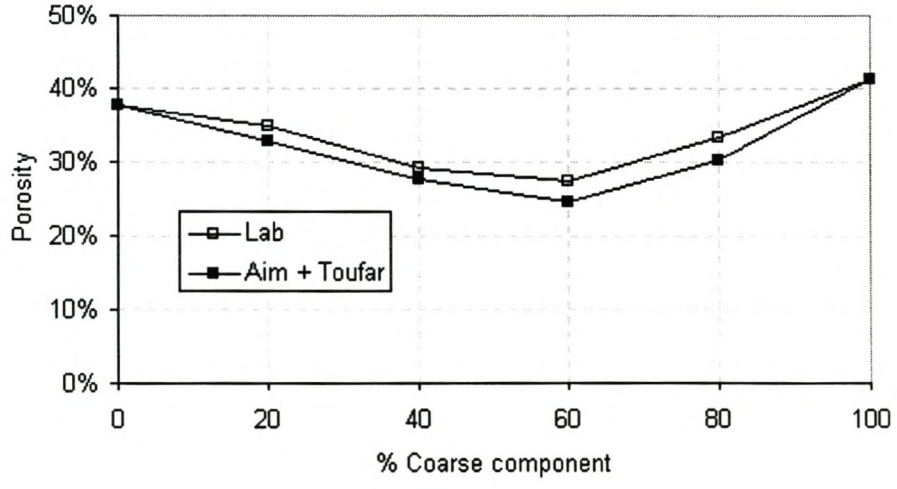

Figure 3.17: Binary system laboratory determined and packing model estimated porosities after 100 gyrations

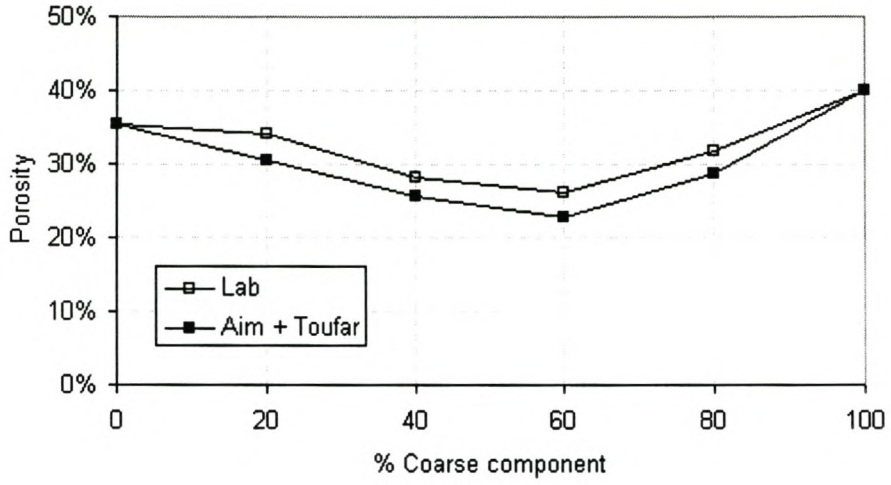

Figure 3.18: Binary system laboratory determined and packing model estimated porosities after 288 gyrations

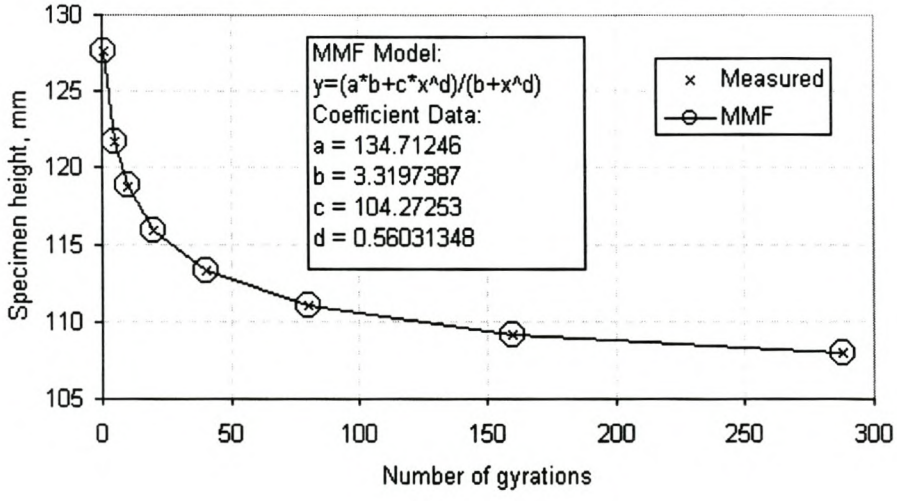

Figure 3.19: MMF curve fitting of gyratory compaction characteristic

3.5 Summary

The importance of defining the spatial composition of an asphalt mix was the underlying theme of the chapter. The VMA of a mix determines the space available for the volume of effective binder and the voids in the mix. An accurate estimation of the VMA of an asphalt mix during the design stage is therefore desirable. It was pointed out that the VMA of a mix is difficult to estimate accurately since it is difficult to quantify the factors influencing VMA such as gradation, particle shape, angularity, texture and rugosity.

The chapter outlined a number of different approaches that may be used to estimate the VMA of an asphalt mix. Most of these approaches make use of the gradation of the asphalt mix and the voids in the compacted filler (Rigden voids). Some of the models take account of the angularity of the particles whereas some of the more sophisticated models require the porosities of the individual fractions to estimate VMA.

The approaches used by Nijboer and Hudson and Davis are classic in their simplicity. Both approaches take account of the angularity of the aggregate and are based on the combination of successive binary systems. The approaches are limited in that packing is only related to aggregate angularity.

Lees made use of the specific void graph to illustrate the influence of the size ratios, porosities, proportions and angularities of binary mixtures on the spatial packing of these mixtures. He points out that an aggregate laid in a thin layer, having a high surface area/volume ratio will show a higher porosity than the same aggregate in a thick layer. This will result in an increase in the proportion of fines required for maximum density. Decreasing the layer thickness has a greater effect on the coarse component than on the fine, indicating the need for a still higher fines requirement. Lees developed a method to estimate the VMA of an aggregate gradation based on the combination of successive binary systems when the porosities of the individual

fractions are known.

The Belgian (PRADO) analytical mix design procedure allows an estimation of the VMA of an asphalt mix based on the aggregate grading curve, angularity of the aggregate and compaction level. As with most of the other approaches discussed in the chapter, the estimation of VMA follows the combination of binary systems. The advantage of this analytical packing model is that the packing mode (substitution or filling) may be defined. The strength of this packing model is that it is based on a theoretical approach that incorporates probability and is therefore applicable to a wider range of applications than some other packing models discussed, which were primarily developed based on the blending of specific aggregates (shape and texture).

The chapter discusses in detail the Aim and Toufar packing models. These models are used in the concrete industry for optimising the packing of aggregates from blends of stockpiles. The models are based on the theory of the packing of spheres and take into account the wall effect. The Aim packing model is considered more accurate than the Toufar model for size ratios less than 0.22. At this size ratio, the fine fraction fits within the interstices of the coarser fraction. These models were modified to make them more applicable for use in estimating the VMA of HMA mixes.

Tons and Goetz verified experimentally a concept that defines the behaviour of one-sized particles in bulk. They showed that different types on one-size aggregates will be compacted to the same bulk volume when they possess identical total packing volume ($\sum V_p$) under identical compaction procedure. This concept is relevant to the dissertation as most of the packing models require as input the porosities of the individual fractions for VMA estimation. Differences in the porosities of packed single-sized particles may therefore be related to differences in the rugosity of the particles.

The modified Aim and Toufar (MAT) packing model was selected for incorporation into PAVDAM. Furthermore, the author elected to use gyratory compaction of

the individual fractions (dry) to determine the porosities of these fractions with compaction. The compaction characteristics of the individual fractions may be modelled using either MMF or Weibull relationships and incorporated directly into PAVDAM.

As discussed in the chapter, the estimation of HMA VMA is difficult given the different influencing factors. To overcome some of these difficulties, PAVDAM takes into account the variabilities of the influencing factors. The MAT model and PAVDAM are therefore interactive and VMA estimations of the MAT model cannot be discussed without first understanding the PAVDAM approach. This is explained in the next chapter.

3.6 References

D. A. Anderson. Guidelines on the use of baghouse fines. Information Series 101-11/87, National Asphalt Pavement Association, Maryland, 1997.

P. J. Anderson and V. Johansen. A guide to determine the optimal gradation of concrete aggregates. Technical Report SHRP-C-334, Strategic Highway Research Program, Washington, D.C., 1993.

L. Francken. Korrelverdeling en mengselontwerp. *Bituminfo*, (60):3–21, 1991.

L. Francken and A. Vanelstraete. New developments in analytical asphalt mix design. *Proceedings of the Fifth Eurobitme Conference, Stockholm*, 1993.

W. B. Fuller and S. E. Thompson. The laws of proportioning concrete. *Transactions of the American Society of Civil Engineers*, Vol. 59, 1907.

C. C. Furnas. Relations between specific volume, voids and size composition in systems of broken solids of mixed sizes. Report of Investigations 2894, US Bureau of Mines, 1928.

C. C. Furnas. Flow of gasses through beds of brocken solids. *Bureau of Mines Bulletin*, Vol. 307, 1929.

P. Goltermann, V. Johansen, and L. Palbøl. Packing of aggregates: An alternative tool to determine the optimal aggregate mix. *ACI Materials Journal*, 1997.

S. B. Hudson and R. L. Davis. Relationship of aggregate voidage to gradation. *Proceedings of Association of Asphalt Paving Technologists*, Vol. 34, 1965.

I. Ishai and H. Gelber. Effect of geometric irregularity of aggregates on the properties and behaviour of bituminous concrete. *Proceedings of the Association of Asphalt Paving Technologists*, Vol. 51, 1982.

G. Lees. The rational design of aggregate gradings for dense asphaltic compositions. *Proceedings of Association of Asphalt Paving Technologists*, Vol. 39, 1970.

NCHRP. Design and evaluation of large stone asphalt mixes. Report 386, National Cooperative Highway Research Program, Washington, D.C., 1997.

L. W. Nijboer. *Plasticity as a factor in the design of dense bituminous road carpets.* Elsevier Publishing Company, Inc, 1943.

K. Ridgeway and K. J. Tarbuck. Particulate mixture bulk densities. *Chemical and Process Engineering Journal*, 1968.

D. M. Roy and G. M. Idorn. Concrete microstructure. Technical Report SHRP-C-340, Strategic Highway Research Program, Washington, D.C., 1993.

C. J. Semmelink. *The Effect of Material Properties on the Compactibility of some Untreated Road Building Materials.* PhD thesis, University of Pretoria, South Africa, 1991.

D. L. Seward, J. A. Hinrichsen, and J. L. Ries. Structural analysis of aggregate blends using strategic highway research program gyratory compactor. Transportation Research Record 1545, Transportation Research Board, Washington, D.C., 1996.

E. Tons and W. H. Goetz. Packing volume concept for aggregates. Technical Report Highway Research Record 236, Highway Research Board, 1968.

E. Tons, W. H. Goetz, and V. L. Anderson. Flow in aggregate-binder mixes. *Association of Asphalt Paving Technologists*, Vol. 39, 1970.

M. F. C. van de Ven, K. J. Jenkins, and A. D. F. Smit. Conceptualisation of spatial composition. ITT Report 2-1999, Institute for Transport Technology, University of Stellenbosch, Stellenbosch, 1999.

C. A. P. van Gurp. *Characterisation of seasonal influences on asphalt pavements with the use of falling weight deflectometers.* PhD thesis, TU Delft, Netherlands, 1995.

W. R. Vavrik, W. J. Pine, G. Huber, H. Carpenter S, and R. Bailey. The bailey method of gradation evaluation: The influence of aggregate gradation and packing characteristics on voids in the mineral aggregate. *Association of Asphalt Technologists*, Vol. 70, 2001.

Chapter 4

Probabilistic and Volumetric Design of Asphalt Mixes

4.1 Introduction

Ang and Tang [1975] define reliability as the probability of no failure. Probability is the conceptual and theoretical basis for modelling and analysing uncertainty. Asphalt materials are inherently heterogeneous. Aggregates vary in shape, size and surface texture. Plant gradations vary from design target gradations and binder contents cannot be controlled exactly. These variations alone will influence the compactibility of the mix but uncertainties abound with compaction itself, particularly in the field. And then there are the variables associated with traffic and climatic influences and of course human error.

Reliability design of asphalt mixes allows variabilities inherent in the material properties (and design) of these mixes to be taken into account. An understanding of this variability becomes increasing important with the industry trend towards the implementation of end result and performance related specifications or warranty projects where the contractor is responsible for the performance of the mix. The development of a probabilistic approach, the Probabilistic and Volumetric Design of Asphalt Mixes or PAVDAM, is the focus of this chapter.

The chapter begins by motivating the use of a probabilistic approach for mix design. It then outlines and defines the variabilities associated with HMA materials. Statistical techniques to evaluate the influence of these variabilities are also addressed. The defined variabilities and statistical techniques are used to develop a strategy for implementation of a reliability based approach to the mix design of HMA using the analytical volumetric packing model (MAT) developed previously. The influence of binder content on packing is addressed and a strategy to account for this influence is suggested. An example of the use of PAVDAM is given, followed by a summary of the salient points addressed in the chapter.

4.2 Reliability based mix design of HMA

Reliability is addressed in the quality control and assurance of HMA as previously discussed in Section 2.1.9. As such, it is used to evaluate the quality of the final product. PAVDAM is an attempt to address reliability during the mix design phase. To do this, the variabilities inherent in the properties (gradation, densities, binder contents, volumetric properties, etc) of HMA materials and mixes must be accounted for. This section expands on the different variabilities and the effects of test variability on mixture volumetric properties and mix design verification. These variabilities must be catered for in PAVDAM.

Hand and Epps [2000] reported on the effects of test variability on mixture volumetric properties and mix design verification. In order to calculate the volumetric parameters for a given mixture, the following properties are required:

1. Relative density of the binder content (G_b)
2. Relative density of the combined aggregate (G_{sb})
3. Bulk relative density of the compacted mix (G_{mb})

4. Maximum theoretical density of the compacted mix (G_{mm})

Hand and Epps [2000] mention that the American Society of Testing and Materials (ASTM) and the American Association of State Highway and Transportation Officials (AASHTO) both have well established test methods for measuring the density properties as listed. There are, however, variabilities associated with the measurement of these properties. This variability has a significant impact on the calculated mixture volumetric properties, and this in turn can substantially affect the optimum mixture selected. For this reason, both institutions have established specification limits for the measured properties. These take the form of precision statements within and between laboratories. The within laboratory standard deviations for the different properties are shown in Table 4.1. Note that these are relative densities and hence unitless.

Table 4.1: Summary of relevant USA within laboratory mix property standard deviations (after Hand and Epps [2000])

Property	**Stdev**
G_b	0.0008
Coarse aggregate G_{sb}	0.009
Fine aggregate G_{sb}	0.011
G_{mb}	0.0124
G_{mm}	0.0040

4.2.1 Monte Carlo simulation

Hand and Epps [2000] made use of Monte Carlo simulation to ascertain the combined effects of variability in materials and mixture property measurements on volumetric properties and optimum binder content selection. The Monte Carlo procedure is used in PAVDAM and is illustrated by example.

Consider the calculation of percent voids in the mix (VIM). VIM is a function of the relative density of the mix (G_{mb}) and the maximum theoretical density or Rice's

density (G_{mm}) as follows:

$$\text{VIM} = \frac{G_{mm} - G_{mb}}{G_{mm}} \tag{4.1}$$

Given measured values for both G_{mb} and G_{mm} and the standard deviation limits as shown in Table 4.1 associated with each of the tests used to measure the properties, normal probability distributions may be developed for each property. Once the G_{mb} and G_{mm} normal distributions have been established, they are repeatedly sampled in a random fashion and VIM calculated using Equation 4.1. A distribution of VIM is eventually generated after taking multiple samples and calculating corresponding VIM values. The VIM distribution produced represents the combined effects on VIM of the variability associated with G_{mb} and G_{mm} measurements.

Hand and Epps [2000] used Monte Carlo simulation to evaluate a 19 mm Superpave surfacing mix design. This particular mix met all the Superpave requirements at the optimum binder content of 5.75 percent. Their analyses indicated that variability associated with measurement of the properties required to determine mixture volumetrics can have a significant impact on calculated volumetric properties (using the property variabilities established by the ASTM and AASHTO control agencies). They found possible differences in VIM and VMA values of approximately 1 percent, which would translate into potential differences in selected optimum binder contents of 0.7 percent!

4.2.2 Variability of HMA

Mahoney [1997] has reported results from various agencies and road tests in the USA that provide insight into the variability of pavement materials. These are shown in Table 4.2. The standard deviation (Stdev) and coefficient of variation (COV) are shown.

Table 4.2: Summary of reported variabilities for asphalt materials (after [Mahoney, 1997])

Property	**Stdev**	**COV, %**
Extracted binder content, %	0.25	4
Percentage passing		
25 mm	5	5
19 mm	2	2
13.2 mm	2	2
9.5 mm	2	2-3
4.75 mm	4	1-10
2.36 mm	3	5-10
1.18 mm	3	5-10
0.60 mm	2	5-10
0.30 mm	2	10
0.15 mm	1	10
0.075 mm	1	10-20
Bulk relative density	0.030	1
Theoretical maximum density	0.010	1
VIM, %	1	10-65
VFB, %	5	6

The magnitudes of the variabilities for the different material properties are relevant and coincide to a large extent with variabilities used in the South African COLTO specifications COLTO [1998] as discussed previously in Section 2.1.9. The variability of HMA properties is expected to be more pronounced in the field than in the laboratory. Laboratory mix designs done with sieved fractions allow a tight control of the mix gradation, which is not possible with plant mixes.

4.3 PAVDAM procedure

The purpose of asphalt mix design is to identify a suitable aggregate gradation and an optimum binder content that satisfies mix property criteria established for different design traffic classes. Monte Carlo simulation may be used to evaluate the influence of parameter variability on estimated binder contents of asphalt mixes.

Figure 4.1 illustrates the PAVDAM procedure to estimate the binder content of a mix using the concepts already developed in the chapter.

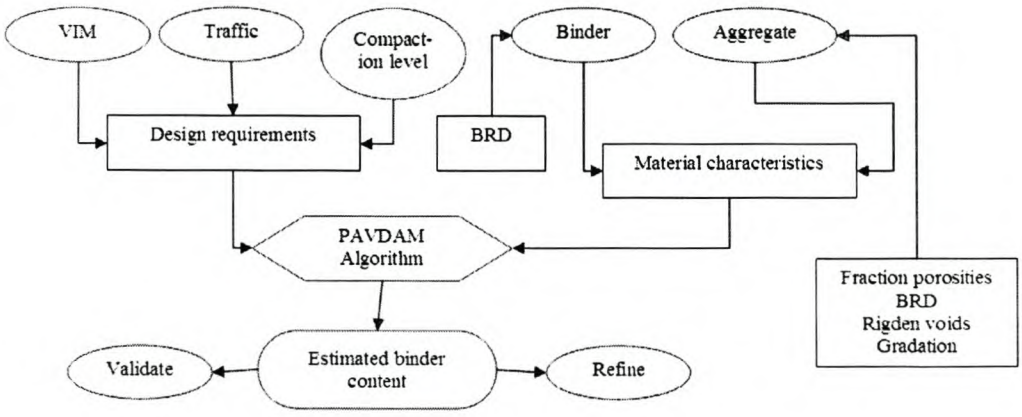

Figure 4.1: Flowchart of PAVDAM procedure

The elements of the PAVDAM flowchart are as follows:

1. **Establish design traffic level.** The design traffic level of a pavement will influence the choice of binder content for HMA mixes thereof. Pavements for higher design traffic will have lower binder contents than pavements for lower design traffic levels. In Table 2.1, the design traffic level establishes gyratory compaction levels for Superpave mixes. The design VMA of these mixes therefore depends on traffic level. PAVDAM determines the porosities of the individual fractions used by the packing model for VMA estimation based on design traffic level.

2. **Establish desired air voids (mean and standard deviation) and compaction level.** The estimated binder content will depend on the available VMA of a specific mix. Since V_{be} = VMA - VIM, the desired VIM at a specific compaction level is required. The desired VIM at specific compaction levels are usually specified by Superpave. For example, at N_{des}, the desired VIM are 4 percent. At N_{max} the VIM must be greater than 2 percent. Since it is unrealistic to assume that there will not be a standard deviation on the VIM at a specific compaction level, this needs to be accounted for. Table 4.2 shows that the standard deviation of measured VIM may be as high as 1 percent. Using Monte Carlo simulation, the variability of the properties (VMA and VIM) may also be accounted for.

3. **Establish material characteristics.** The estimated binder content of a mix is a function of the bulk relative densities of the aggregate and the bitumen. To determine the influence of variability of these parameters on the estimated binder content using Monte Carlo simulation, the mean and standard deviations of the material characteristics are required. Standard deviations for the aggregate and bitumen bulk relative densities as defined by ASTM or AASHTO may be used.

4. **Establish grading curve.** The grading curve is required by the packing model to estimate the VMA of the mix. Presently, the percentage passing each of the following sieve sizes are required: 0.075 mm, 0.15 mm, 0.3 mm, 0.6 mm, 1.18 mm, 2.36 mm, 4.75 mm, 9.5 mm, 19 mm and 37.5 mm. The standard deviation on each of the sieves may be used to determine the influence of gradation variation on estimated binder content. For field variation, the COLTO specifications outlined in Section 2.1.9 (see Table 2.3) may be used.

5. **Establish porosities of the individual fractions.** The modified Aim and

Toufar (MAT) packing model requires the porosities of the individual fractions and the voids in the filler (Rigden's voids). For the purpose of this dissertation, these porosities were determined using gyratory compaction of the individual fractions, for example as outlined in Section 3.4.1. Aggregate stockpiles are sieved into the individual fractions, which are then gyratory compacted dry. This is a critical step in the PAVDAM process. If aggregates from different quarries are to be used or if new aggregates are introduced, the porosities of the new individual fractions must be determined. It is also important to relate the porosities of the individual fractions to compaction. With higher compaction effort, the porosities of the fractions will decrease, which reflects the decrease in VMA with traffic compaction. It was found that the Weibull distribution described by Equation 3.35 is useful in estimating the porosity of the individual fractions at different compaction levels although a simple logarithmic equation such as that shown in Figure 3.13 may suffice.

The variability in the porosities of the gyratory compacted individual fractions should also be taken into account. Extensive testing may be required to determine these standard deviations accurately. This can only be achieved in a properly managed mix design process. It is envisaged that the use of PAVDAM will initially entail extensive laboratory compaction (and sieving) to characterise the packing nature of the individual fractions. Monitoring these characteristics over time will allow refinement of the model and as a consequence laboratory testing will only be required to calibrate the model for specific requirements.

6. **Account for binder absorption.** If necessary, binder absorption may be accounted for. Mean and standard deviation values of binder absorption are used for the binder content estimation calculations.

7. **Refine the packing model estimate.** This step is required to improve or

validate the accuracy of the estimated VMA and properties at PAVDAM estimated binder contents. Having designed a mix using PAVDAM, specimens may be fabricated in the laboratory. Calibration factors may be used to refine property estimates compared to measured values.

4.3.1 PAVDAM algorithm

PAVDAM estimates the binder content of a mix based on specific inputs as outlined previously. Monte Carlo simulation is used to determine the influence of the different variabilities on the estimated binder content. The number of iterations to be used will depend on the extent of the variations of the different parameters. The greater the variations or standard deviations, the more iterations will be required. The mix designer may increase the number of iterations until the difference in the estimated binder content from successive runs is within acceptable tolerances. Typically 50000 to 100000 iterations are necessary for the estimated binder content to stabilise.

Having estimated the VMA of the mix using the MAT packing model, the volume of effective binder (V_{be}) of the mix may be determined since the voids in the mix (VIM) have been fixed i.e. V_{be} = VMA - VIM (expressed as volume percentages). In fact, PAVDAM samples representative values of VIM based on the normal distribution and input VIM mean and standard deviation as part of the Monte Carlo simulation. Representative values of aggregate and bitumen bulk relative density and binder absorption (P_{ba}) are also sampled in a similar manner. The aim of the simulation is to estimate an optimum binder content given these and the other input parameters, including the mix gradation, which is also sampled statistically based on the mean and standard deviations of the percentages passing the respective sieves. To estimate an optimum binder content the following calculation steps are taken:

1. Calculate the effective relative density of the mix (G_{se}):

$$G_{se} = \frac{-100 \cdot G_b \cdot G_{sb}}{(P_{ba} \cdot G_{sb} - 100 \cdot G_b)} \tag{4.2}$$

2. Calculate the volume of bulk aggregate (V_{sb}):

$$V_{sb} = \frac{(100 - V_{be} - VIM)}{100} \tag{4.3}$$

3. Calculate the mass of aggregate (M_s):

$$M_s = V_{sb} \cdot G_{sb} \tag{4.4}$$

4. Calculate the volume of effective aggregate (V_{se}):

$$V_{se} = \frac{M_s}{G_{se}} \tag{4.5}$$

5. Calculate the volume of absorbed binder (V_{ba}):

$$V_{ba} = V_{sb} - V_{se} \tag{4.6}$$

6. Calculate the total binder volume (V_{tb}):

$$V_{tb} = \frac{V_{be}}{100} + V_{ba} \tag{4.7}$$

7. Calculate the mass of binder (M_b):

$$M_b = V_{tb} \cdot G_b \tag{4.8}$$

8. Calculate the maximum theoretical density of the mix (G_{mm}):

$$G_{mm} = \frac{(M_s + M_b)}{\left(\frac{V_{be}}{100} + V_{sb}\right)} \tag{4.9}$$

9. Calculate the bulk relative density of the mix (G_{mb}):

$$G_{mb} = \frac{G_{mm} \cdot (100 - VIM)}{100} \tag{4.10}$$

10. Calculate the percentage aggregate, by mass of total mix (P_s):

$$P_s = \frac{(100 - V_{be}) \cdot G_{sb}}{G_{mm}} \tag{4.11}$$

11. Finally, calculate the percentage binder, by mass of the total mix (P_b):

$$P_b = 100 - P_s \tag{4.12}$$

12. The effective binder, as a percentage of the total mass of the mix, may be calculated (P_{be}):

$$P_{be} = P_b - \left(\frac{P_{ba} \cdot P_s}{100}\right) \tag{4.13}$$

A FORTRAN computer source code of the PAVDAM model is included in Appendix A.

4.3.2 Influence of binder content on packing

Consider Figure 4.2. The figure shows a specific void diagram of a binary system consisting of the aggregate blend (coarse fraction) and bituminous binder (fine fraction). The VMA or porosity of the aggregate blend before the addition of binder is at Q. The porosity of the binder without voids entrapped is zero. The thick solid line QP0 therefore represents the packing characteristic of the binary system at different combinations of aggregate and binder. As binder is added to the mix, the porosity of the binary system decreases from Q and is zero at point P. At this point the voids in aggregate structure are saturated with binder. If at this point more binder is added to the mix, the VMA of the mix will indeed increase (although not shown on the figure) since the aggregate particles will be forced apart and "float" within the binder mass. We are only concerned with what happens between P and Q though. The binary relationship defined by line QP0 is a simple model and Lees points out that in practice more complicated relationships exist.

Lees makes the point that the addition of binder to an aggregate blend results in either lubricating or dilating effects at different proportions and different compactive efforts. As mentioned previously, small additions of binder may lead to dilation of the aggregate structure (represented by the dashed line from Q). Further addition of binder may lead to lubrication such that, in some cases, the aggregate packs even more densely under the given effort than when compacted without binder, suggested by the fall of the dashed line below the level of the theoretical line QR. This leads to saturation (zero voids) being reached at a lower binder content than would have been predicted from the intersection of QR with the horizontal base line. Note that this same condition could have been reached if the porosity of the aggregate was at point U before the addition of binder. Lees uses this argument to emphasize the importance of heavy compaction during construction to better define the optimum

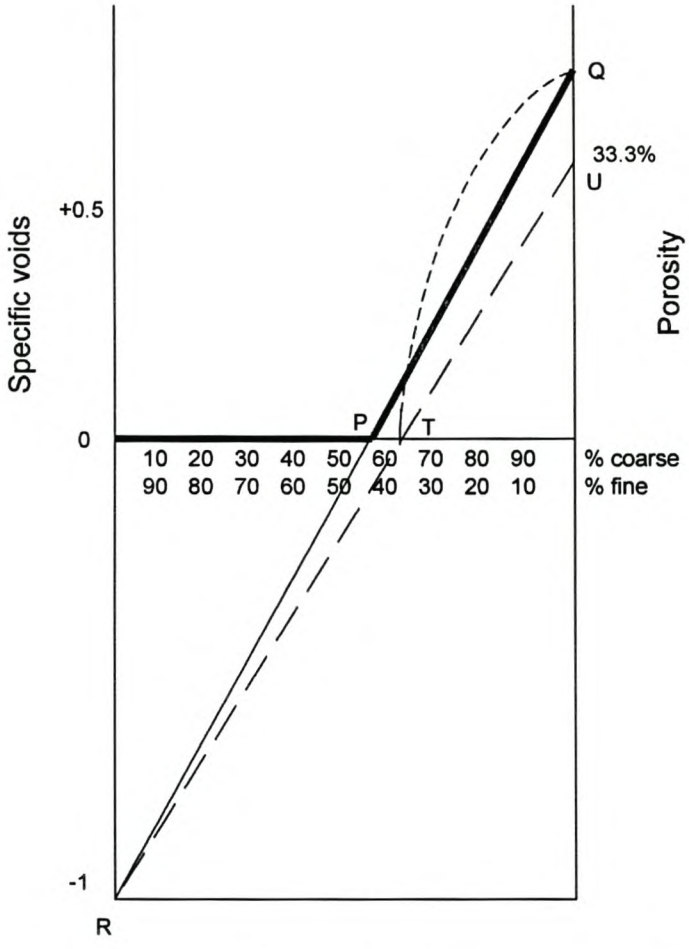

Figure 4.2: Specific void diagram - aggregate-binder combination (after [Lees, 1970])

binder contents of mixes and to prevent the voids in mixes becoming overfilled with binder in service under conventional traffic.

The relationships as outlined above are mentioned to illustrate how the packing model may account for the influence of binder content. Remember that the model estimate of VMA is used to establish an optimum binder content for a particular mix. If the VIM has been set at a specific level, 4 percent say, then the volume of effective binder (V_{be}) may be calculated: V_{be} = VMA - VIM. The curved dashed line from Q may be used to establish the influence of binder content on the VMA of a mix. This relationship is difficult to model since it would change for different gradations and

even compactive efforts. This is a complex problem that will need to be addressed if one wants to understand the interaction between the mix components in asphalt mixtures. A simplistic solution to the problem is to assume the reduction that would occur in VMA with the addition of binder. This may be done by dropping the VMA of the aggregate blend (without binder) by an assumed percentage i.e. the drop from Q to U in Figure 4.2. The magnitude of the drop must be related to the amount of binder added to the mix. Thus once the porosity of the aggregate blend has been established using the modified Aim and Toufar packing model, the volume of effective binder in the mix is determined with reference to the specific voids diagram shown in Figure 4.2 (line QP). Depending on the volume of binder, the VMA of the asphalt mix (with binder) may be calculated.

Given the difficulty of accurately accounting for the influence of binder content on aggregate packing, for the dissertation it is assumed that it has no influence. PAVDAM therefore assumes that the packing model VMA estimate is the same as the VMA at the estimated binder content. To account for the influence of binder content (and compaction) on VMA, PAVDAM makes use of calibration factors that are calculated to relate estimated and measured VMA. This requires that mixes be compacted at the PAVDAM estimated binder content and the volumetric properties at the designed compaction level be measured and compared to the estimated properties. Use of these calibration factors is expanded upon in the next chapter.

4.4 An example of the use of PAVDAM

To illustrate the use of PAVDAM, consider designing an HMA mix with the following inputs:

Design traffic level	= 1 - 30 million ESALs
Desired air voids (mean and stdev)	= 4 %, 0.5 %

Desired compaction level	= N_{des} = 100 gyrations
Aggregate bulk relative density (mean and stdev)	= 2.682, 0.010 (See Table 4.1)
Bitumen bulk relative density (mean and stdev)	= 1.026, 0.0008 (See Table 4.1)
Binder absorption (mean and stdev)	= 0.2 %, 0.001 %
Rigden's voids	= 40 %
Porosity standard deviation	= 0.5 %

A continuous target gradation for the mix is shown in Table 4.3 and Figure 4.3. The COLTO gradation specification limits (see Table 2.3) have been included in the Table and Figure (dotted lines) to show the allowable variation on the different sieve sizes.

Table 4.3: Target gradation and deviation of example mix

Sieve size, mm	**Target**	**- stdev**	**+ stdev**
0.075	5.7	4.7	6.7
0.150	9.0	7.0	11.0
0.300	14.0	11.0	17.0
0.600	20.0	16.0	24.0
1.180	27.0	23.0	31.0
2.360	36.0	32.0	40.0
4.750	53.0	49.0	57.0
9.500	82.0	77.0	87.0
19.00	100.0	100.0	100.0

For the example, the gyratory compaction characteristic required to determine the porosities of the individual fractions was assumed to be the same as that defined in Equation 3.33.

PAVDAM uses the mean and standard deviations of the input parameters to sample representative values (based on a normal distribution) that are then used to

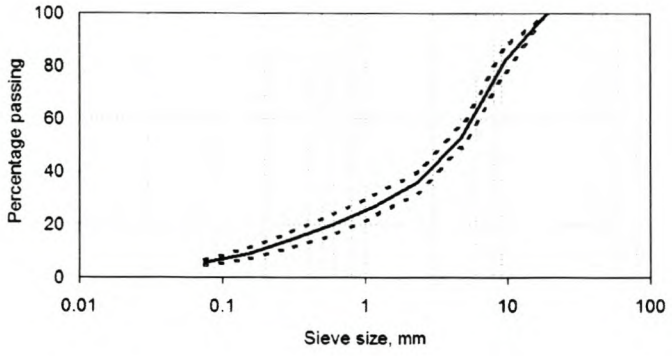

Figure 4.3: Target and allowable variation of example mix gradation

calculate estimated binder contents. Running the inputs through PAVDAM gave the estimated results shown in Table 4.4. Using 100,000 iterations, the histogram of estimated binder contents is shown in Figure 4.4. The figure illustrate the possible binder contents that satisfy the input parameters and the spread is indicative of the influence of variability of the different mix design parameters.

Table 4.4: PAVDAM estimated results of example mix

Property	**Stats**	**Result**
VMA	mean	16.88%
	stdev	0.30%
P_b	mean	5.19%
	stdev	0.27%
G_{mm}	mean	2.464
	stdev	0.012
G_{mb}	mean	2.366
	stdev	0.010
P_{be}	mean	5.00%
	stdev	0.27%

The relevance of the PAVDAM output will be discussed in more detail in the next chapter. An important consideration in the application of PAVDAM is the validity of

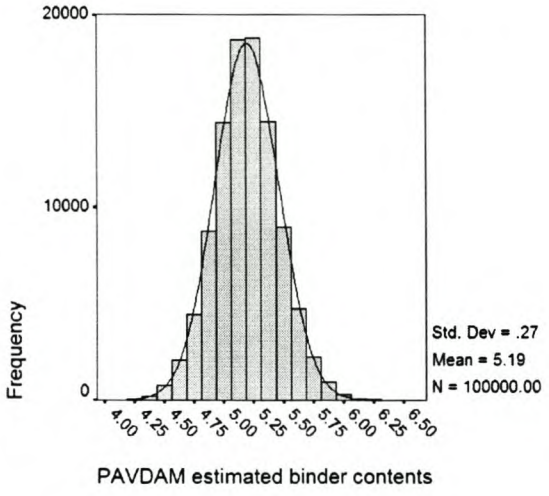

Figure 4.4: Histogram of PAVDAM estimated binder contents for example problem without binder absorption

the normally distributed sampled values. These values are sampled based on the mean and standard deviation of an input parameter. In the case of gradation parameters it is possible to sample incorrectly. For example, consider the gradation of the mix shown in Table 4.3. Using random sampling based on the normal distribution it is possible that the percentage passing the 0.3 mm sieve is 17 percent. At the same time, PAVDAM may randomly sample a value of 16 percent for the 0.6 mm sieve. Theoretically this is impossible, the percentage passing the smaller sieve must always be equal to or less than the next larger sieve. To cater for this possibility, PAVDAM tests for this situation and resamples until a valid value is obtained. For the example in question, this occurred 6.4 percent of the times during sampling of the gradation values. Obviously, the randomness of the sampling during the Monte Carlo simulation is an important consideration and becomes questionable as soon as the sampled values are controlled. To ensure validity of the solution, however, is was necessary to control the sampled gradation.

Further examples of the use of PAVDAM are discussed in the following chapter towards calibration and validation of the model.

4.5 Summary

The objective of this chapter was to present a probabilistic and volumetric model that may be used for the reliability design of HMA. To achieve this it was necessary to define the different variabilities influencing the volumetric properties of HMA mixes and to incorporate a packing model for estimation of VMA. The result was PAVDAM, a model that incorporates Monte Carlo simulation to estimate the binder content of an asphalt mix at specific compaction levels based on the gradation of the mix and properties of the mix components, taking into account the variabilities associated with these components.

In asphalt mix design, reliability is usually considered as part of the quality control or assurance phase or in the case of systems such as Superpave, the reliability of a mix is judged in terms of performance, be it fatigue or rutting. Performance evaluation is a high level (Level 2 or 3) requirement and as such, testing is done on the selected gradation to evaluate the influence of binder content after weaning other candidates in the low level (Level 1) screening process. In this way PAVDAM may serve as a low level reliability evaluation of candidate gradations.

Given the nature of asphaltic materials, variability is inherent but control is necessary for conformity. Control is established through product specifications detailing specific aspects of an asphalt mix. Tight controls are placed on the gradation of a mix because of the critical influence of gradation on the volumetric properties, particularly the finer fractions and the filler content. The COLTO gradation specifications are used in PAVDAM to evaluate the influence of gradation variability on

estimated binder content. PAVDAM also requires the variabilities of other mix component properties, specifically the bulk relative densities of the aggregate and binder and binder absorption. No specification limits are set for these properties in South African specifications and for this reason the limits suggested by ASTM and AASHTO are currently applied in PAVDAM.

The modified Aim and Toufar (MAT) packing model was selected for use in PAVDAM. The packing model requires as input the porosities of the individual fractions making up the gradation of a mix. PAVDAM uses gyratory compaction of the individual fractions to assess porosity but also accounts for the fact that different types of one-size aggregates will compact to the same bulk volume when they possess identical total packing volume under identical compaction procedure. Laboratory (gyratory) compaction tests on these fractions are required to establish compaction characteristics before PAVDAM application.

The chapter discusses the algorithm and procedure used in PAVDAM to estimate the binder content of a mix from various input parameters. The influence of binder on mix VMA may be accounted for in PAVDAM using a simplistic approach although this aspect of the packing model must be refined and developed further. For this reason, in the application of PAVDAM, it is assumed that the packing model estimate of the VMA is not influenced by binder content.

4.6 References

A. H-S. Ang and W. H. Tang. *Probability Concepts in Engineering Planning and Design. Volume 1 - Basic Principles.* John Wiley & Sons, Inc., New York, 1975.

COLTO. *Standard specifications for road and bridge works for state road authorities.* Committee for Land Transport Officials, Department of Transport, Johannesburg, South Africa, 1998.

A. J. Hand and A. L. Epps. Effects of test variability on mixture volumetrics and mix design verification. *Journal of the Association of Asphalt Paving Technologists*, Vol. 69, 2000.

G. Lees. The rational design of aggregate gradings for dense asphaltic compositions. *Proceedings of Association of Asphalt Paving Technologists*, Vol. 39, 1970.

J. P. Mahoney. *Statistical Methods for Pavements and Material Applications.* University of Washington, 1997. Course material prepared for the Division of Roads and Transport Technology, CSIR, Pretoria.

Chapter 5

Application, calibration and validation of PAVDAM

5.1 Introduction

This chapter discusses the application of PAVDAM towards validation of the model. Calibration of the PAVDAM model is also addressed. Two case studies are included. In the first, a comparison is given between the Marshall mix designs of two large aggregate mixes used for bases and a PAVDAM analysis. In the second, MMLS3 testing at the NCAT test track is discussed with emphasis on the use of PAVDAM for evaluation of mixture performance at the volumetric design level.

PAVDAM estimates the volumetric properties of mixes based to a large extent on the gyratory compaction characteristics of the aggregates. The dilemma of comparing gyratory compaction of mixes in the laboratory with performance of the mix in the field was discussed previously (see Section 2.1.5). Bahia et al. [1998] saw in the gyratory compactor the possibility of evaluating the post construction compaction of mixes at ambient temperatures in the field, notwithstanding the obvious differences such as compaction temperature, effort or long term climatic influences. For this reason, the validation of PAVDAM is not in terms of performance under wheel trafficking but rather in terms of reliability from a volumetric point of view.

Consider an HMA mix designed for a specific level of traffic. If the actual level of traffic exceeds the design estimate, there is a possibility that the mix may fail. The voids in the mix may reduce such that the mix becomes overfilled with bitumen leading to instability. If on the other hand the actual level of traffic is underestimated the voids in the mix may be too high leading to durability related problems. The optimum binder content of the mix must therefore be selected to balance the associated risks. The VIM of a mix at a specific compaction level will depend on the binder content of the mix, which can be estimated using PAVDAM.

Figure 5.1 illustrates the concept of failure. Assuming normal distributions for design limits (the optimum binder content of a mix for example) and failure limits (the binder content at which failure occurs), failure is related to those conditions where the distributions are overlapping i.e. the probability that the optimum binder content range exceeds the failure binder content range.

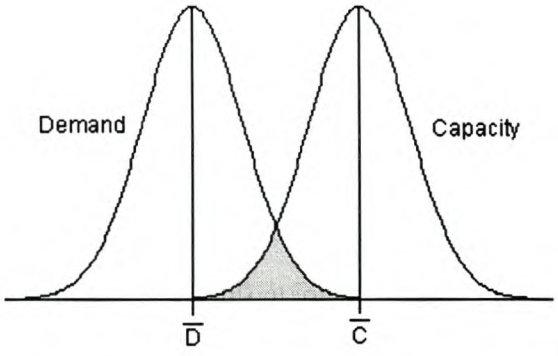

Figure 5.1: Statistical representation of failure

In order to be able to calculate the occurrence of failure, we define reliability (R) as the chance that the design optimum binder content (Pb) is higher than the failure binder content, then the probability of failure is defined as:

$$P(F) = 1 - R \tag{5.1}$$

$$R = P[(\text{Design Pb} - \text{Failure Pb}) > 0] \tag{5.2}$$

$$D = \text{Design Pb} - \text{Failure Pb} \tag{5.3}$$

The function $f(D)$ is called the difference density function. The mean value μ_D and standard deviation σ_D of this difference function can be written as:

$$\mu_D = \mu_A - \mu_B \tag{5.4}$$

$$\sigma_D = \sqrt{\sigma_A^2 + \sigma_B^2} \tag{5.5}$$

where

μ_A = Mean design Pb

μ_B = Mean failure Pb

σ_A = Standard deviation of design Pb

σ_B = Standard deviation of failure Pb

The shape of the difference density function is shown in Figure 5.2. Reliability is given by the area to the right of zero while the probability of failure is given by the area to the left of zero.

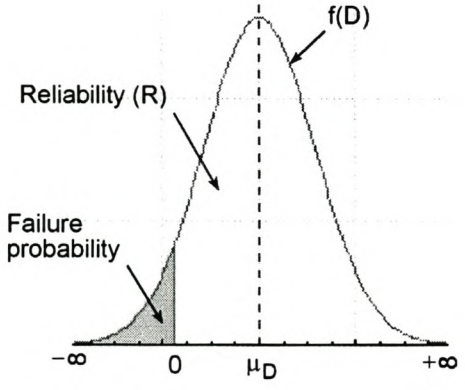

Figure 5.2: Difference density function

It can be shown that the reliability can be calculated from the standard normal distribution:

$$R = \frac{1}{\sqrt{2\pi}} \int_{\frac{-\mu_D}{\sigma_D}}^{\infty} e^{-\left(z^2/2\right)} dz \tag{5.6}$$

where

$$z = \left(D - \mu_D\right) / \sigma_D \tag{5.7}$$

These formulations are used to evaluate the performance of the mixes (in terms of volumetrics) tested using the MMLS3 at the NCAT test track.

5.2 Mix design of large aggregate mixes

Two mix designs of large stone base mixes received from Much Asphalt Ltd., an asphalt contractor in the Western Cape in South Africa, were evaluated using PAVDAM. Appendix D contains details of the two mixes. Both mixes were designed using aggregate from the Contermanskloof quarry and 60/70 pen bitumen from the CALREF refinery in the Western Cape, South Africa. Appendix D includes the gradations of the mixes, bulk relative densities of mix components and volumetric property details. The mixes were Marshall compacted at varying binder contents (75 blows per specimen face). The mixes are designated CK4 and CK6, the respective reference numbers as noted on the mix design sheets. CK4 is a bitumen treated basecourse (BTB) mix having a maximum aggregate size of 26 mm. CK6 is a large aggregate mix for bases (LAMBS) having a maximum aggregate size of 37.5 mm. If one were to design lean rut resistant mixes then based on the Marshall mix designs, the optimum binder content of CK4 would possibly be in the order of 4.5 percent. At this binder content, the VIM are about 4 percent, VMA is on the dry side of the minimum VMA curve and stability is optimised. Using the same criteria, the optimum binder content of CK6 could be 4.2 percent. These binder contents are typical for large stone asphalt bases in South Africa. At these binder contents, the calculated film thickness values

for both mixes are well below 8 micron. The binder absorption values for mix CK6 in the mix design sheets are probably incorrect and would more likely be in the order of 0.3 percent and not 3 percent as tabulated (see Appendix D).

PAVDAM was used to estimate the optimum binder contents for both CK4 and CK6. A high design traffic level (> 30 million ESALs) was used to evaluate the base mixes. The VIM at the N_{des} were fixed at 4 percent. Voids in the filler (Rigden voids) of 42 percent were determined for Contermanskloof filler (from which the mix designs originated) using the Anderson approach [Anderson, 1997]. The compaction characteristic used to determine compaction porosities of the individual fractions is defined by Equation 3.33. This was determined previously for Contermanskloof aggregate. The percentages passing each of the sieves were given permissible COLTO standard deviations as previously reported in Table 2.3. The standard deviations of the aggregate porosities were set at 1 percent. Based on the values reported in Table 4.1 the standard deviations of the bulk relative densities of the aggregate and bitumen were set at 0.01 and 0.0008 respectively. A total of 100000 iteration cycles were applied. Table 5.1 shows the results of the PAVDAM analyses on both CK4 and CK6. The mean and standard deviations of the calculated mix properties are given.

Table 5.1: Results of PAVDAM evaluation of CK4 and CK6

Property	**CK4**		**CK6**	
	Mean	Stdev	Mean	Stdev
VMA %	16.99	0.42	16.20	0.42
P_b %	5.16	0.29	4.93	0.29
G_{mm}	2.493	0.013	2.509	0.013
G_{mb}	2.393	0.011	2.409	0.011

A comparison of the estimated VMA of the mixes (corresponding to 130 gyrations) and the measured VMA (2 x 75 Marshall hammer blows as shown in Appendix D) indicates that the packing model underestimates this value for both of the mixes. To

correct this a simple multiplier or calibration factor (f) may be applied:

$$f = \frac{\text{Measured VMA}}{\text{Estimated VMA}} \tag{5.8}$$

The PAVDAM VMA estimate may hence be adjusted by applying:

$$\text{Adjusted VMA estimate} = f \cdot \text{Estimated VMA} \tag{5.9}$$

From Appendix D, appropriate VMA values for CK6 and CK6 at the Marshall design level (2 x 75 blows) are 14.5 percent and 13 percent respectively. Hence the calibration factors calculated for CK4 and CK6 are 0.85 and 0.80 respectively. Applying these calibration factors within PAVDAM gives the adjusted values for the mix properties shown in Table 5.2.

Table 5.2: Adjusted results of PAVDAM evaluation of CK4 and CK6 at N_{des}

Property	**CK4**		**CK6**	
	Mean	Stdev	Mean	Stdev
VMA %	14.51	0.36	13.12	0.34
P_b %	4.15	0.26	3.69	0.25
G_{mm}	2.537	0.013	2.564	0.013
G_{mb}	2.435	0.011	2.461	0.011

The spread in binder contents estimated for CK4 and CK6 are shown in Figures 5.3 and 5.4 respectively.

5.2.1 Discussion of the PAVDAM results

Apparent from the results is the fact that the modified Aim and Toufar (MAT) packing model used in PAVDAM underestimated the VMA of both mixes. This was expected given the nature of the model as discussed in the previous chapter and also because the influence of binder content and compaction on packing is not considered

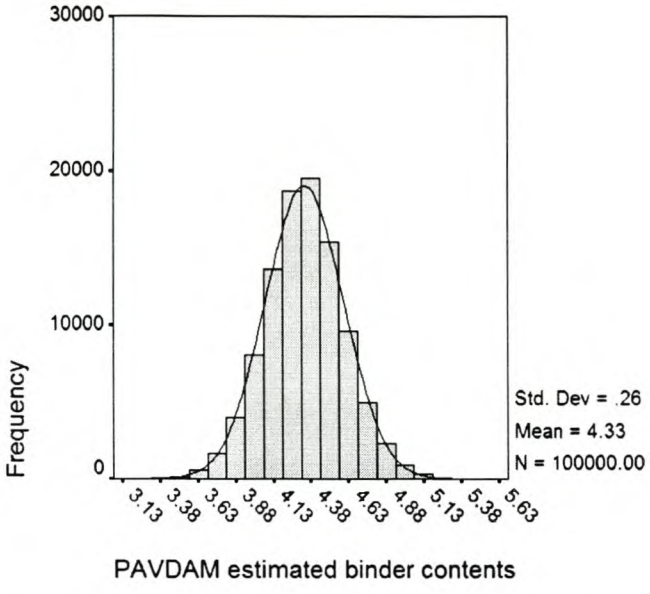

Figure 5.3: Binder content spread from PAVDAM evaluation of CK4

in PAVDAM. This shortcoming was easily corrected though through application of a multiplier to correct the estimated VMA of the mixes. After this correction, the resultant PAVDAM estimated binder contents are more in line with what one would expect for the given mixes. The quality of the PAVDAM VMA estimate is addressed in more detail later in the chapter.

Using the Marshall mix design approach, the optimum binder contents for mixes CK4 and CK6 were judged to be 4.5 percent and 4.2 percent respectively. The lower binder contents suggested by PAVDAM (4.2 percent and 3.7 percent respectively) may be related to the greater compaction effort applied in PAVDAM i.e. 130 Superpave compactor gyrations compared to 2 x 75 blows per face Marshall hammer. The Marshall design VIM are also higher than the 4 percent limit used in the PAVDAM analysis which could also explain the slightly higher Marshall design binder contents.

The spread of PAVDAM estimated binder contents shown in Figures 5.3 and 5.4 are indicative of the influence of mix design variability. For both mixes, the standard

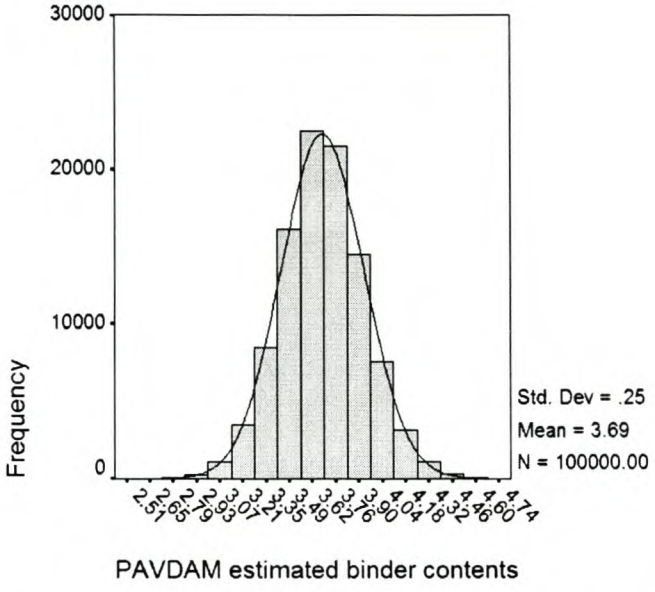

Figure 5.4: Binder content spread from PAVDAM evaluation of CK6

deviation of the estimated binder contents were in the order of 0.3 percent. It is interesting to note that this is the typical variation from target field binder contents and the COLTO allowable deviation (see Table 2.4). It is important, however, to understand the difference between the PAVDAM estimated binder content standard deviation and the expected deviation of binder contents in the field. In PAVDAM, the binder deviation is as a result of the different possible combinations of mix properties (variations in gradation, bulk densities etc) to achieve 4 percent VIM at a specific compaction level. The field standard deviation of binder content is related to the precision with which binder is applied to the aggregate during the manufacturing stage. In order to take the influence of the latter into account it would be necessary to approach the problem slightly differently i.e. fix the binder content (mean and expected standard deviation) and use PAVDAM to explore the resulting deviation in VIM. This option was not explored as part of the dissertation.

The VMA adjustment factor shown in Equation 5.8 is a simple calibration factor

that allowed a better estimate of the VMA of the mixes. This approach was used since gyratory compaction trials were not available for the mixes in question. A more effective calibration approach is discussed in the next section.

5.3 MMLS3 testing at the NCAT test track

The following section discusses a series of MMLS3 tests done at the National Center for Asphalt Technology (NCAT) test track in Opelika, Alabama. One of the many objectives established for this testing was validation of the PAVDAM model developed as part of the dissertation. The section therefore only discusses aspects of the study relevant for this validation and does not address the other objectives of the study, which included a comparison of MMLS3 and full-scale performance. Interested readers are referred to [Smit, 2002; Smit et al., 2002] for additional information. Before the PAVDAM evaluation of MMLS3 NCAT sections is addressed, some background information regarding the test track is given. This includes construction aspects as well as full-scale performance of the MMLS3 NCAT sections.

5.3.1 Sections selected for MMLS3 testing

Figure 5.5 shows a plan view of the NCAT test track. The track was divided up into 46 different flexible pavement sections, each about 60 m in length. The sections comprise various mixes from different states. Mixes were constructed from materials imported to the test track from these states.

Five sections on the track were selected for MMLS3 testing. The sections selected are shown in Table 5.3 together with specific construction and performance information. More information on the construction and performance details of the selected sections may be found in Appendices E and F respectively. A synthesis of the construction and performance details of the sections is given later in the chapter. A

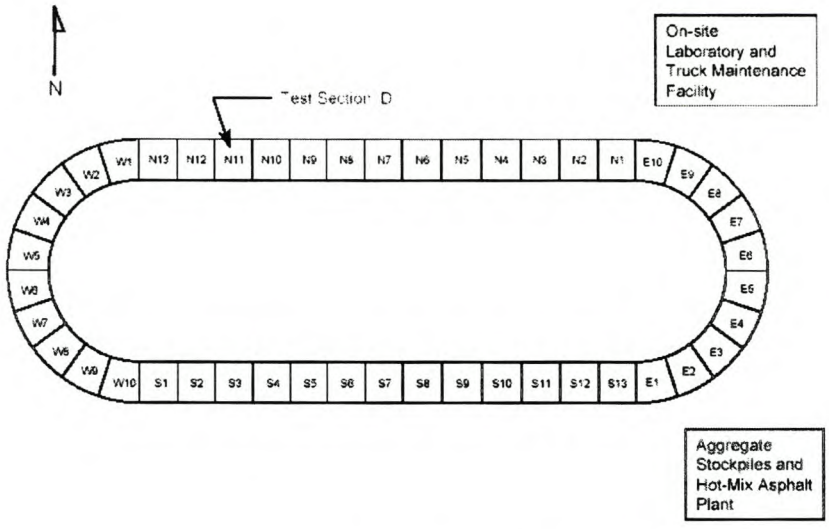

Figure 5.5: Layout of the NCAT test track

study of the VIM in the field after compaction indicated that this varied considerably for the different sections evaluated. Details are given later in the chapter.

The sections for MMLS3 testing were selected based on the following criteria:

- Each of the sections comprised one type of aggregate (granite) only. Other sections consisted of blends or combinations of more than one aggregate type. Southbound sections (S9 and S10) consisted of granite from Jamestown, North Carolina whereas eastbound sections (E2, E6 and E8) consisted of granite from Columbus, Georgia.

- Each of the sections are made with mixes comprising PG 67-22 binder. Other sections included mixes with modified binders.

- The sections had varying gradations passing above, through and below the Superpave restricted zone (see Table 5.4). The gradation curves of the respective selected sections are shown in Figure 5.6.

Table 5.3: Selected section construction and performance details

SECT	Pb	F/B	G_{mb}	G_{mm}	RUT
S9	4.7	1.2	2.419	2.510	4.4
S10	5.2	1.3	2.407	2.488	3.6
E2	4.7	0.9	2.434	2.505	2.0
E6	5.0	0.9	2.411	2.510	1.8
E8	5.6	0.9	2.372	2.477	1.9
SECT	Section number				
Pb	Binder content, percentage by mass (as constructed)				
F/B	Filler/binder ratio, by mass				
G_{mb}	Bulk relative density (after 100 gyrations)				
G_{mm}	Maximum theoretical density				
RUT	NCAT ARAN field rutting after 5.3 million ESALs, mm				

Test sections S9 and S10 have a 75 mm thick surfacing layer. The eastbound sections (E2, E6 and E8) have a 100 mm thick surfacing layer. Beneath the surfacing layer the pavement structure consisted of a 150 mm HMA (upper) base, a 225 mm HMA (lower) base, a 125 mm permeable black base, a 150 mm crushed aggregate base and a 300 mm improved roadbed over the subgrade. The total thickness of the HMA construction is in the order of 600 mm.

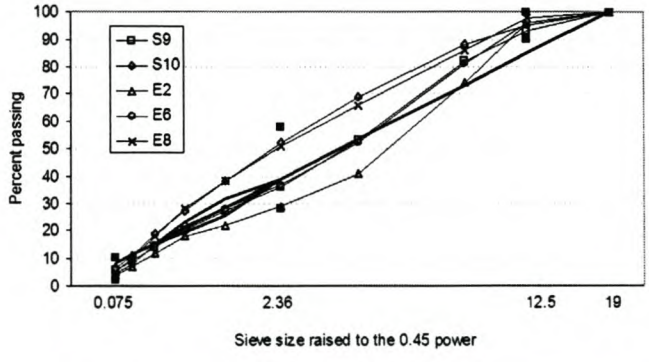

Figure 5.6: Gradations of selected NCAT test sections

Table 5.4: NCAT-MMLS3 section gradations

Size,mm	S9	S10	E2	E6	E8
0.075	5.7	6.6	4.1	4.3	5.2
0.150	9	11	7	8	10
0.300	14	19	12	15	18
0.600	20	27	18	22	28
1.180	27	38	22	28	38
2.360	36	52	29	37	51
4.750	53	69	41	52	66
9.500	82	88	74	81	86
13.20	93	95	96	96	98
19.00	100	100	100	100	100

5.3.2 Full-scale performance

The rutting performance of the NCAT test sections was monitored on a weekly basis during trafficking. Measurements were made using the ARAN vehicle laser profilometer and dipstick device.

ARAN rutting measurements

Figure 5.7 shows the average ARAN rutting monitored on all of the sections and the 7 day average maximum high air temperatures during trafficking. From the figure it can be seen that at the onset of trafficking, the air temperature was relatively high but dropped after the application of about 200,000 ESALs. It is interesting to note, however, that even during this cool spell, rutting of the sections was apparent. This initial rutting was most likely due to consolidation of the pavement after construction since the pavement rutting tapered off with an increase in air temperature. From Table 5.3 the ranking of the section mixes in terms of rutting performance (best to worst) is: E6, E8, E2, A10 and S9.

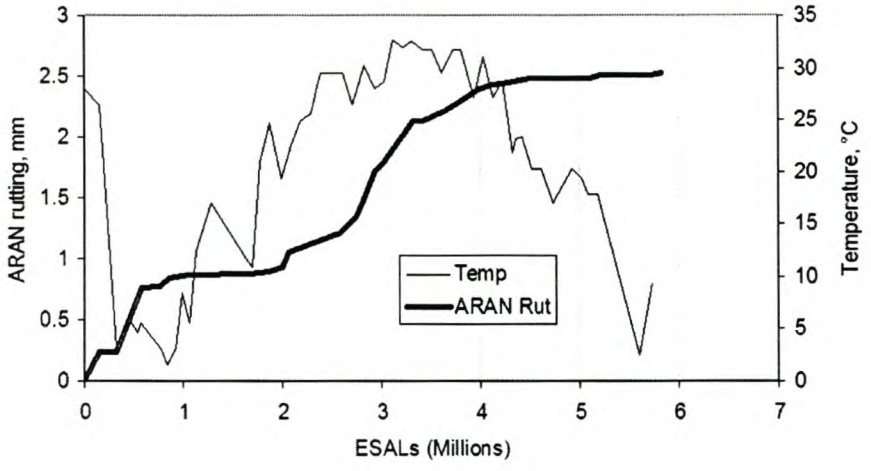

Figure 5.7: Temperature and section ARAN rutting monitored during full-scale trafficking

Dipstick rutting measurements

An indication of the rutting performance of the sections selected for MMLS3 testing was obtained from dipstick measurements taken on these sections. Dipstick measurements were taken on a weekly basis at three random points on each of the NCAT test sections. Based on these data, estimates were made of the downward rutting in the left and right wheelpaths of the MMLS3 sections after the application of 5 million ESALs. These estimates are illustrated in Figure 5.8.

Apparent from the figure is the higher rutting in the right hand wheelpaths on each of the sections but particularly for the eastbound sections on the curved superelevation. The slope on the eastbound sections was such that the mass inertia of the vehicles tended towards the right. Based on the dipstick data, after the application of 5 million ESALs, the mixes rank in terms of rutting performance (from best to worst) as S9, E8, E6, E2, S10. There does not appear to be a significant difference in the rutting performance of mixes E8, E6 and E2. This ranking differs substantially from that obtained using the ARAN. The dipstick rutting measurement is considered

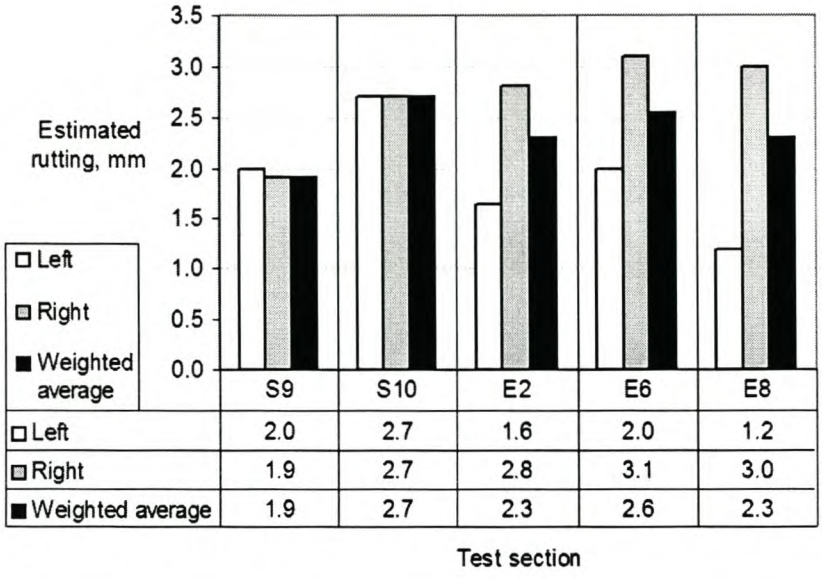

	S9	S10	E2	E6	E8
Left	2.0	2.7	1.6	2.0	1.2
Right	1.9	2.7	2.8	3.1	3.0
Weighted average	1.9	2.7	2.3	2.6	2.3

Figure 5.8: Estimate of dipstick downward rutting after 5 million ESALs

more accurate than the ARAN since actual physical measurements are taken..

5.3.3 Densification of the test sections under full-scale trafficking

The densities of the surfacing asphalt layers were monitored with trafficking from cores extracted from the trafficked right wheelpath. Figure 5.9 shows the apparent change in density of the upper lift of the MMLS3 NCAT sections respectively, based on a limited number of observations. Densities are expressed as a percentage of the respective maximum theoretical densities. The data have been extrapolated to 10 million ESALs. The figure indicates that the initial compaction densities of the sections varied considerably and influenced the density of the section mixes throughout the trafficking period. The rate of densification of the upper lift for the different sections is similar.

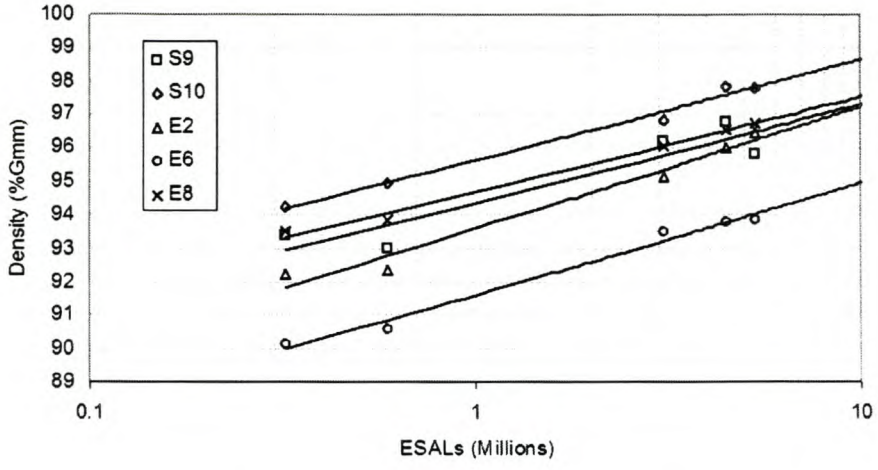

Figure 5.9: Density of upper lift with trafficking (extrapolated)

5.3.4 Superpave mix designs

During field compaction of the asphalt mixes, material was sampled in the field and gyratory compacted in the laboratory. The number of specimens compacted per section and mix information is indicated in Table 5.5. The binder content used for section E8 was greater than the Superpave design binder content whereas that for sections E2 and E6 was lower than that determined for design. These deviations from design binder contents were part of the NCAT experiment. In the Superpave mix design procedure, design binder contents are chosen to achieve 4 percent voids in the mix (VIM) at the design compaction level (N_{des}). Section mixes were designed for a traffic level of between 10 - 30 million ESALs. The dynamic nature of the volumetric properties with compaction (means and standard deviations) of the section mixes is illustrated in Figures G.1 through G.7 in Appendix G. Table 5.6 and Table 5.7 summarise the gyratory compaction properties of the section mixes after the initial (N_{ini}) and design (N_{des}) number of gyrations respectively. None of the section mixes included lime as an additive.

Table 5.5: Section mix information

Info	**S9**	**S10**	**E2**	**E6**	**E8**
n	6	12	12	12	9
Gsb	2.682	2.682	2.686	2.690	2.696
Pbd, %	4.7	5.3	5.3	5.6	5.3
Pb, %	4.7	5.2	4.7	5.0	5.6
G_{mm}	2.510	2.480	2.490	2.510	2.480
n	Number of specimens compacted				
Gsb	Aggregate bulk relative density				
Pbd	Design binder content (percentage by total mix mass)				
Pb	Field binder content (percentage by total mix mass)				
G_{mm}	Theoretical maximum density (Rice)				

Superpave requires that the minimum voids in the mineral aggregate (VMA) of mixes with nominal aggregate sizes of 12.5 mm be greater than 14 percent. The mix on section S9 only just satisfies this criterion whereas the mix on section E2 fails with a VMA of 13.5 percent. The VIM of these mixes at N_{des} are well below 4 percent. The Superpave VFB requirement of between 65 - 75 percent is satisfied for each of the mixes. It is interesting to note that for section E8, even though the binder content used was 0.3 percent higher than the design binder content, the VIM of this mix at N_{des} is still slightly greater than 4 percent. The filler-binder ratios of the section mixes were given in Table 5.3. These ratios for mixes on sections S9 and S10 are at and above the maximum Superpave limit (1.2) if binder absorption is accounted for. The gyratory and volumetric properties of the mixes are discussed in more detail later in the chapter. The experiments (both full- and model-scale) provided an opportunity to investigate the relationship between the performance of the test sections and the gyratory compaction characteristics of the mixes.

Table 5.6: Gyratory compaction volumetric properties at N_{ini} (8 gyrations)

Section	Stats	%Gmm	%VIM	%VMA	%VFB
S9	mean	88.3	11.7	21.3	44.8
	stdev	0.4	0.4	0.4	1.0
S10	mean	90.0	10.0	21.0	52.2
	stdev	0.6	0.6	0.5	1.7
E2	mean	89.3	10.7	20.8	48.5
	stdev	0.7	0.7	0.3	2.6
E6	mean	89.4	10.6	20.7	49.0
	stdev	0.3	0.3	0.2	0.7
E8	mean	89.7	10.3	22.1	53.3
	stdev	0.2	0.2	0.2	0.5

Table 5.7: Gyratory compaction volumetric properties at N_{des} (100 gyrations)

Section	Stats	%Gmm	%VIM	%VMA	%VFB
S9	mean	94.6	3.6	14.1	74.2
	stdev	0.5	0.5	0.5	3.0
S10	mean	97.0	3.0	14.8	79.6
	stdev	0.6	0.6	0.4	3.2
E2	mean	97.5	2.5	13.5	81.8
	stdev	0.6	0.6	0.2	4.2
E6	mean	96.2	3.8	14.7	74.4
	stdev	0.2	0.2	0.2	1.2
E8	mean	95.6	4.4	16.9	74.2
	stdev	0.2	0.2	0.2	0.8

5.3.5 The MMLS3

Figure 5.10 shows a schematic of the MMLS3. It consists of four recirculating axles, each with a single 300 mm diameter wheel. The wheels can be laterally displaced across 150 mm in a normal distribution about the centre-line to simulate traffic wandering. The tyres may be inflated up to a pressure of 800 kPa. Axle loads varying between 2.1 kN to 2.7 kN are possible. The axle loads are automatically kept constant at a predetermined value by the special suspension system. Nominal wheel speed is 2.5 m/s, applying about 7200 loads per hour. A single 1.5 kW variable speed motor drives the chain of four wheels.

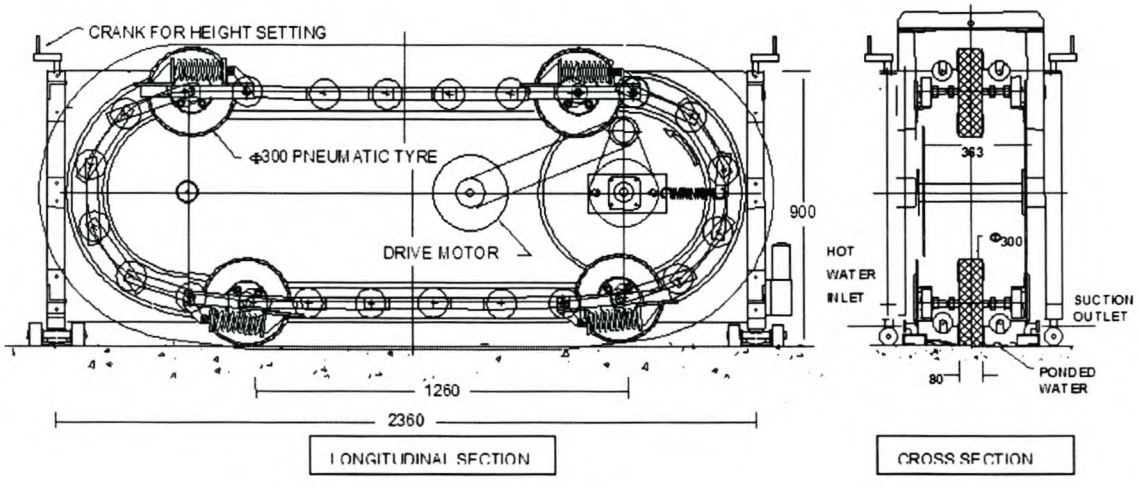

Figure 5.10: Schematic of the MMLS3

The following specifications were used for the MMLS3 tests at NCAT:

Wheel load	:	2.7 kN
Tire pressure	:	690 kPa
Rate of loading	:	7200 axles per hour
Test temperature	:	51 °C - 53 °C (wet and dry)

No lateral wandering of the wheel was applied during testing.

For the dry tests, heat is applied to the surface of pavement through plenums positioned alongside the MMLS3. Heated air is forced through one plenum and sucked through another so that there is a constant stream of heated air circulating beneath the MMLS3. The direction of heated air flow is alternated every 15 minutes. For the wet tests, heated water is passed through a perforated pipe onto the surface of the pavement on one side of the MMLS3 and collected, under vacuum, through another on the other side of the MMLS3. Depending on temperatures in the field, a period of between 2 to 5 hours is required for pavement temperatures to stabilise before testing can commence.

5.3.6 Experimental design

Table 5.8 shows the NCAT test track sections tested using the MMLS3, the order in which the tests were done and the type of test i.e. whether dry or wet. Two dry tests were done on section S9. One dry test was done on section S10. Three tests were done on section E2; two dry and one wet. One wet test was done on section E6. Two tests (wet and dry) were done on section E8.

Table 5.8: MMLS3 test matrix

Test no.	Date	Section	Wet/Dry
1	03/04/2002	S9	Dry
2	03/11/2002	S10	Dry
3	03/18/2002	E2	Dry
4	03/25/2002	S9	Dry
5	04/02/2002	E6	Wet
6	04/15/2002	E2	Dry
7	04/15/2002	E2	Wet
8	04/22/2002	E8	Dry
9	04/22/2002	E8	Wet

5.3.7 Temperature control

Test temperatures were controlled using thermocouples attached onto and within the pavement at various depths using quick drying epoxy. For the dry tests, the temperature at a depth of 25 mm beneath the surface was maintained between 51 °C and 53 °C. Figure 5.11 shows temperatures within the pavement monitored using i-button temperature probes for one of the dry MMLS3 tests i.e. MMLS3 test 4 on NCAT section S9. From the figure it can be seen, as expected, that the temperature fluctuation on the surface is greater than that with depth.

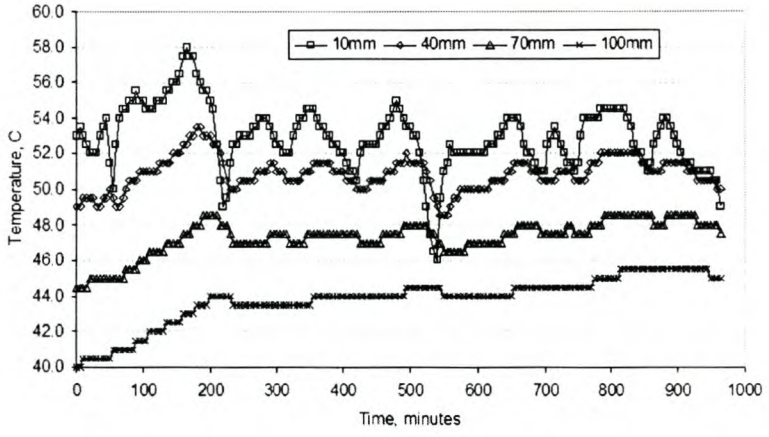

Figure 5.11: Temperature control on test S9 (Dry MMLS3 test 4)

For the wet tests, a control thermocouple was placed at a depth of 25 mm beneath the surface. The wet test heating system adjusts the temperature of the water sprayed onto the surface to maintain the control temperature as shown in Figure 5.12. Pavement temperatures for the wet tests were typically one degree Celsius higher at the respective depths compared to the dry tests.

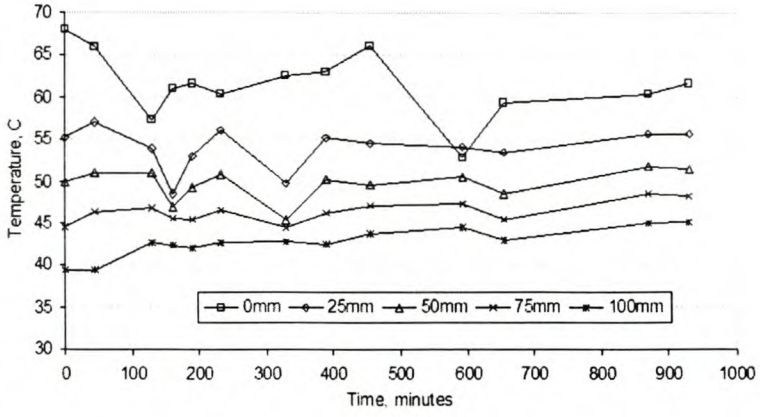

Figure 5.12: Temperature control on test E6 (wet test)

5.3.8 Profilometer measurements and rutting definition

During an MMLS3 test, profilometer measurements are taken prior to trafficking and thereafter at specific intervals during trafficking to allow an accurate definition of the cumulative rutting curve. Since the maximum number of axles to be applied for the test series was limited to about 100,000 per test, it was decided to take readings after the following number of axles: 0; 5,000; 20,000; 50,000 and ± 100,000. Three transverse profilometer measurements were taken after each interval.

Rutting profiles or surface elevations with trafficking are developed relative to the transverse profiles taken prior to MMLS3 trafficking i.e. 0 axles reading. The maximum rut depths (total rut) reported were determined by applying an imaginary straightedge over the maximum surface elevations and calculating the vertical distance to the lowest surface elevation as shown in Figure 5.13. Down rutting results are also reported that were determined as the depth of the rut measured from the original surface profile.

If necessary, minor adjustments were made to the rutting profiles to take account

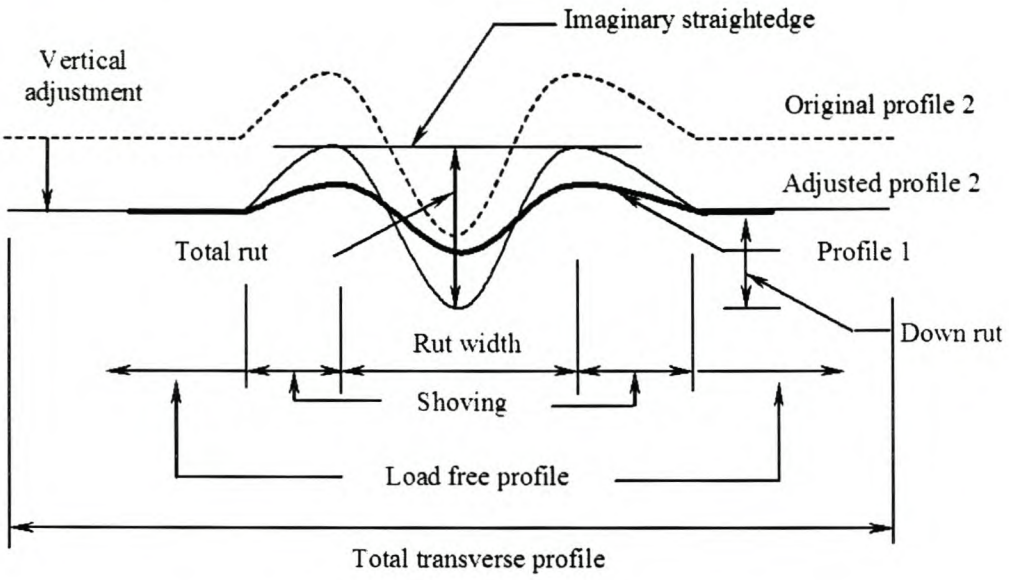

Figure 5.13: Adjustment to vertical rutting profiles

of errors resulting from temperature effects and misalignment. The profilometer measures a transverse surface profile across a total width of about 750 mm. The rutting profile is centred across 80 - 100 mm on this total profile. Shoving is usually apparent at the edges of the rut extending a distance as shown in Figure 5.13. The profile beyond the shoving range is not influenced by loading and may be used as a reference for adjusting vertical deviations. The difference in the sum of squares of two load free profiles is minimised to adjust vertical profiles.

The profilometer used for the rutting measurements is accurate to 0.1 mm in the horizontal and vertical directions.

5.3.9 MMLS3 rutting test results

As mentioned previously, transverse rutting profiles were measured at three positions beneath the MMLS3 intermittently during MMLS3 trafficking i.e. before testing and after the application of 5 000, 20 000, 50 0000 and ± 100 000 load applications. The

rutting profiles measured on each of the MMLS3 tests as well as cumulative rutting profiles are given in Appendix H. Figure 5.14 summarises the mean cumulative (total) MMLS3 rutting on the NCAT sections.

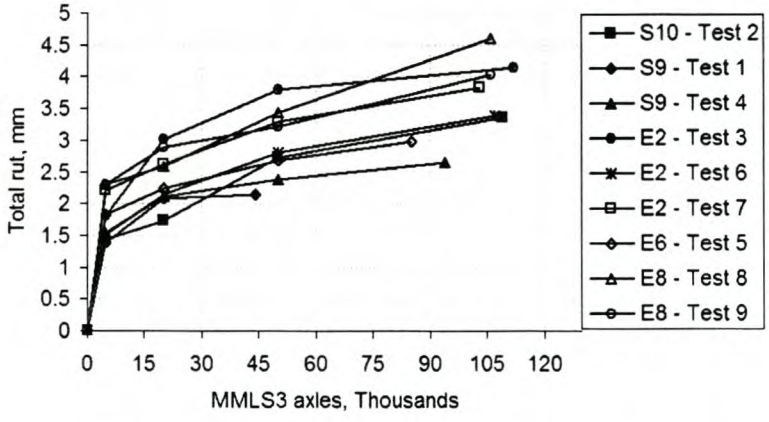

Figure 5.14: Mean cumulative MMLS3 rutting on the NCAT sections

The MMLS3 rutting results are discussed in more detail later in the chapter. Results of the MMLS3 tests were used to characterise the rutting potential and rank the mixes on the different NCAT sections. A synthesis is given later in the chapter, suffice it to say that a difference between MMLS3 and full-scale ranking of rutting resistance was evident. Density measurements were done on cores taken alongside the MMLS3 tests on untrafficked areas of each of the sections as well as on the MMLS3 trafficked wheelpaths after termination of the MMLS3 tests. It was found that the densities of the untrafficked cores on *all* the MMLS3 sections were in the order of 95 percent of the maximum theoretical densities of the respective mixes. Furthermore, no evidence of further densification of the mixes under MMLS3 trafficking was observed. From Figure 5.9 it can be seen that the post construction densities of some of the mixes were way below 95 percent. The reason for the apparent increase in density of the section mixes without trafficking is unknown.

5.3.10 Synthesis of Superpave mix design and performance

Asphalt mixes on the MMLS3 sections were designed using the Superpave procedure. Design binder contents were established to achieve 4 percent voids in the mix (VIM) after 100 gyrations (N_{des}). Table 5.9 shows the design binder contents of the MMLS3 sections and the binder contents of the mixes as used in the field. The mixes on section E2 and E6 were constructed with binder contents 0.6 percent less than design and that on E8 has a 0.3 percent higher than design binder content. One would expect the leaner mixes to have better rutting performance. As will be shown latter in the chapter, under the MMLS3 the leaner mixes did appear to rut less than E8 although under full-scale (based on dipstick data), E8 performed better than the leaner E2 and E6.

Table 5.9: Design and field binder contents of MMLS3 section mixes

Section	Design	Field
S9	4.7	4.7
S10	5.3	5.2
E2	5.3	4.7
E6	5.6	5.0
E8	5.3	5.6

The surfacing mixes have a nominal maximum aggregate size of 12.5 mm. The gradations of the mixes on section S10 and E8 are similar, falling above the restricted zone. The gradations of mixes from sections S9 and E6 are also similar but pass through the restricted zone. The mix on section E2 falls below the restricted zone. Rutting results from the MMLS3 and full-scale tests indicated that the performance of mixes passing through the restricted zone (S9 and E6) was comparable or better than that of mixes passing above or below the restricted zone.

The binder content of the mix on section E8 is 0.4 percent higher than that on

section S10. The field density of S10 was 1 percent higher than that of E8. With the higher binder content and lower field density one would expect more rutting on section E8 compared to section S10. This was the case under the MMLS3 but not under full-scale trafficking.

The harshness of the E8 mix in the gyratory compactor (at N_{des}) could well be misleading as its high volume of binder may result in conditions that boost the effective shear stress state of this mix. The author has noted this behaviour in other high binder content fine graded mixes in the gyratory compactor. The mix in the mould is highly confined and the rapid application of the load (pressure) may lead to pore pressure buildup within the mix that cannot be dissipated. In the field, however, the mix is not as highly confined and pore pressures can dissipate which could mean that the mix may not be as resistant to shear failure as suggested by the gyratory compaction results.

5.3.11 Synthesis of pavement densification in the field

The density of the pavement sections prior to trafficking (after construction) is an important parameter influencing the ultimate performance of these sections. Apparent from Figure 5.9 is the difference in the initial compaction densities of the surfacing layers of the different MMLS3 sections. The trend lines in Figure 5.9 indicate that the MMLS3 sections that had the lowest density prior to trafficking had the lowest density after the application of 5 million ESALs.

It is important to note that the rate of densification of the upper lift of the sections was similar up until the application of 5 million ESALs. It appears therefore that the rate of densification of the sections was not unduly influenced (unlike the section rutting) by seasonal temperature fluctuations during trafficking.

Another consideration is the stage during the life of an asphalt mixture when the

voids in the mixture fall below the 2 or 3 percent level. At this stage there is a risk that the mixture may become unstable and susceptible to shear failure. Figure 5.9 shows that the density of the mix on section S10 reached 97 percent density after the application of about 3 million ESALs.

The densification of the sections may be used to establish a performance ranking. The pavement sections were designed for a design traffic of 10 million ESALs. If one uses the 97 percent density limit as a failure criterion then the probability of failure of the sections may be defined in terms of the Weibull distribution of failure:

$$F_W(t) = 1 - \exp\left[-\left(\frac{n}{N}\right)^{\beta}\right] \tag{5.10}$$

where

$F_w(t)$ = Probability that failure has occurred before time t,

n = Number of load applications at time t,

N = Number of load applications at which a defined failure occurs,

β = Curvature parameter.

Applying a 1 percent standard deviation in density, Figure 5.15 indicates the probability of failure of the sections based on the densification trends observed in the upper lift of the surfacing i.e. probability that the voids in the section mixes fall below 3 percent.

After the design traffic, the figure ranks the performance of the sections (best to worst) as E6, E2, S9, E8 and S10. There does not appear to be a significant difference in the performance of sections E2, S9 and E8.

5.3.12 Comparison of compaction gyrations and ESALs

Prowell et al. [2002] have related the densification characteristics of mixes under

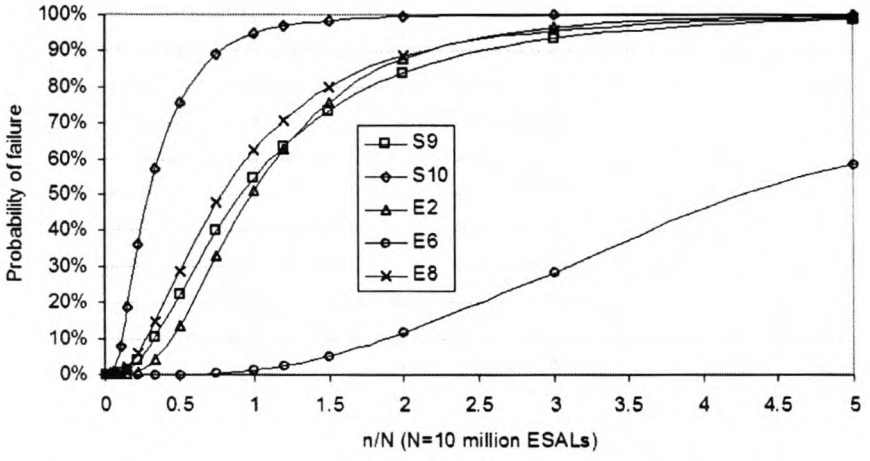

Figure 5.15: Probability that VIM in section mixes fall below 3 percent

full-scale trafficking at the NCAT test track to the laboratory gyratory compaction characteristics. They concluded that the as-constructed densities of the mixes at the track were significantly affected by gradation and that the densification data appeared to verify the current Superpave specifications at design traffic levels of 0.3 to 3 million ESALs. Data were collected from cores extracted from the right wheelpath during trafficking. Only one core was extracted after the different loading intervals. These data were used to construct Figure 5.9 reported previously.

Prowell et al. [2002] looked at the overall densification of the track. Using the gyratory compaction results reported previously (gyratory compaction of specimens sampled in the field), the author compared the densification of the MMLS3 section mixes in the field (as reported by Prowell et al. [2002]) to laboratory gyratory compaction results. The number of gyrations required to compact the mixes to field densities were back-calculated. The means and standard deviations of these are shown in Table 5.10. Figure 5.16 compares the ESALs and mean number of gyrations for the MMLS3 sections for equivalent densities.

Table 5.10: Statistics of back-calculated gyrations to achieve field density

ESALs/Section	Stats	S9	S10	E2	E6	E8
0.05 million	mean	20	38	16	5	23
	stdev	2	6	1	1	2
0.32 million	mean	38	64	26	11	45
	stdev	4	12	2	1	5
0.59 million	mean	46	80	35	15	59
	stdev	6	16	2	2	7
1.58 million	mean	72	112	47	23	96
	stdev	12	26	3	2	13
3.09 million	mean	98	155	61	31	140
	stdev	20	40	4	3	23
4.49 million	mean	125	196	70	38	201
	stdev	30	56	5	4	39
5.30 million	mean	131	209	81	38	237
	stdev	32	62	5	4	50

Figure 5.16 shows that, as discussed previously, the gyratory compaction characteristic of the section E8 mix is probably incorrect and is perhaps better defined by the dotted line indicated on the figure. This would mean that the E8 mix is not nearly as harsh as suggested by the gyratory compaction results and that the mix densifies more readily in the field.

Table 5.11 lists power regression equations fitted through the curves for the MMLS3 section data shown in Figure 5.16. The regression equation for mix E8 was based on the first 5 readings only. The table also shows the number of gyrations for each section equivalent to the application of 10 million ESALs.

The comparison between number of gyrations in the laboratory and ESALs applied in the field is complicated given obvious differences in loading conditions and spatial composition. A highly confined mix in a mould will exhibit vastly different

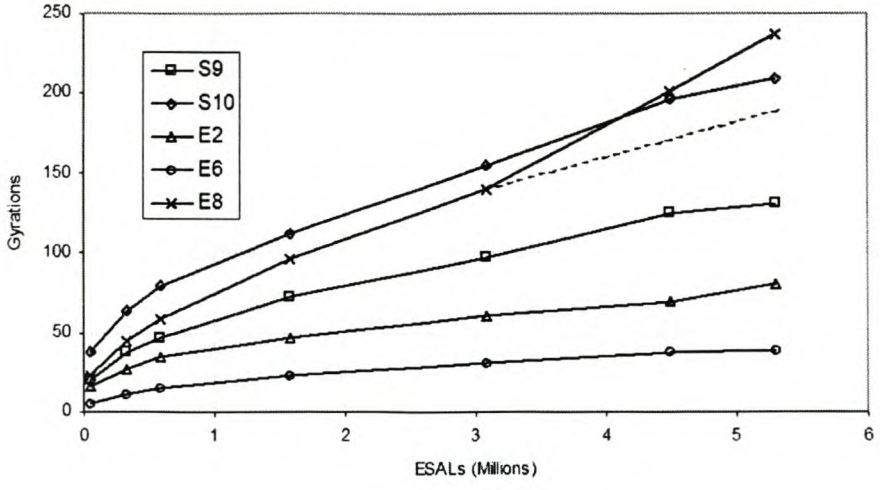

Figure 5.16: Track ESALs vs. backcalculated number of laboratory compaction gyrations

shear behaviour to a mix in the field. It is evident from Figure 5.16 that the relationship between the number of gyrations and ESALs is influenced by the initial compaction density of the mix in the field. The relationship between the section mixes with fine gradations, E8 and S10, is similar. The same cannot be said of the relationship between the other mixes. The comparison between gyratory compaction and equivalent ESALs was used in the PAVDAM analyses of the NCAT MMLS3 sections described later in the chapter.

5.3.13 Influence of temperature on MMLS3 rutting

At the onset of MMLS3 testing at the track, concern was expressed over the different climatic conditions under which field testing was to be done. To investigate the influence of temperature it was decided to repeat the dry MMLS3 test on section S9. Figure 5.17 shows that even though the first test was done under significantly colder conditions, the rutting performance of section S9 measured on the two tests was similar. This indicates that the heat applied to the surface of the pavement before

Table 5.11: Power regression equations relating gyratory compaction and ESALs for the MMLS3 test sections

Section	Equation	Gyrations for 10 mESALs
S9	$Y = 62.886X^{0.4094}$	161
S10	$Y = 104.24X^{0.3695}$	244
E2	$Y = 41.967X^{0.3438}$	93
E6	$Y = 18.752X^{0.4443}$	52
E8	$Y = 79.282X^{0.4353}$	216
Y	Number of gyrations	
X	ESALs, Millions	

and during MMLS3 trafficking is the controlling environmental factor influencing the performance of the mix. This is feasible given the limited depth of influence within the pavement of the MMLS3.

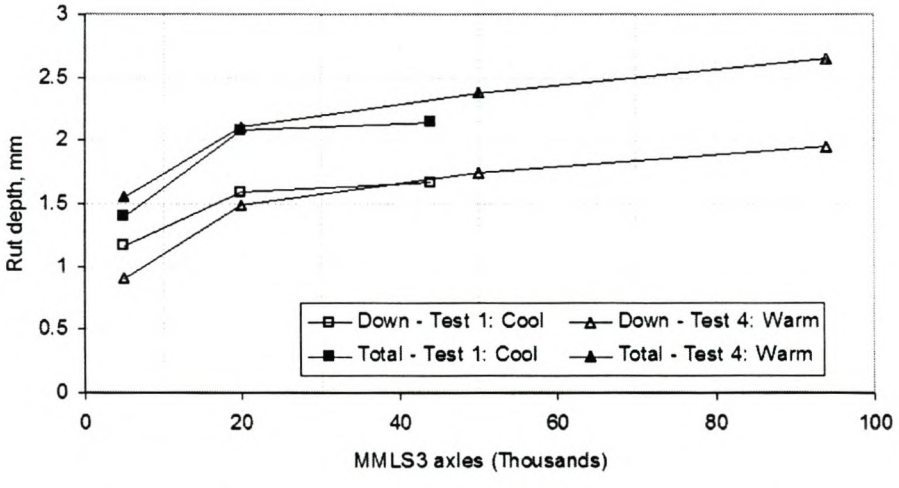

Figure 5.17: Combined average rutting for section S9 (Only dry)

5.3.14 Influence of wet/dry testing on MMLS3 rutting

It was found that the MMLS3 rutting of specific sections tested wet and dry were similar. This is shown in Figure 5.18 for section S9 and Figure 5.19 for section E8.

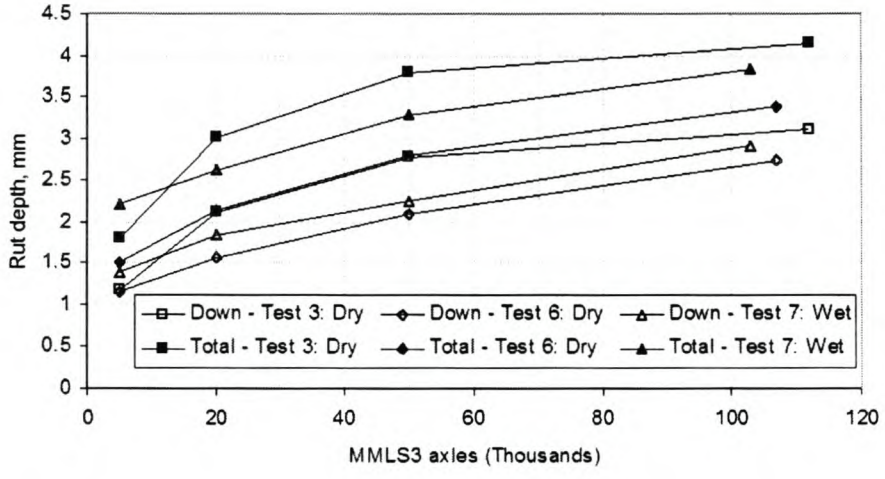

Figure 5.18: Combined average rutting for section E2 (Dry and wet)

The similar rutting behaviour of the wet and dry sections is probably because the sections mixes were relatively impervious, which mitigated the impact of the water on rutting. Given the similar rutting performance of the replicate tests on the sections, it was decided to combine the results of MMLS3 tests on similar sections and perform analyses on the combined results.

5.3.15 Regression analysis of MMLS3 rutting results

Power functions were fitted to the combined MMLS3 rutting results (both down and total rutting) on the various sections. The regression equations of these functions together with the correlation (r^2 values) are given in Table 5.12

Using the regression equations, Figures 5.20 and 5.21 were drawn, extrapolating the rutting data up to 10 million ESALs.

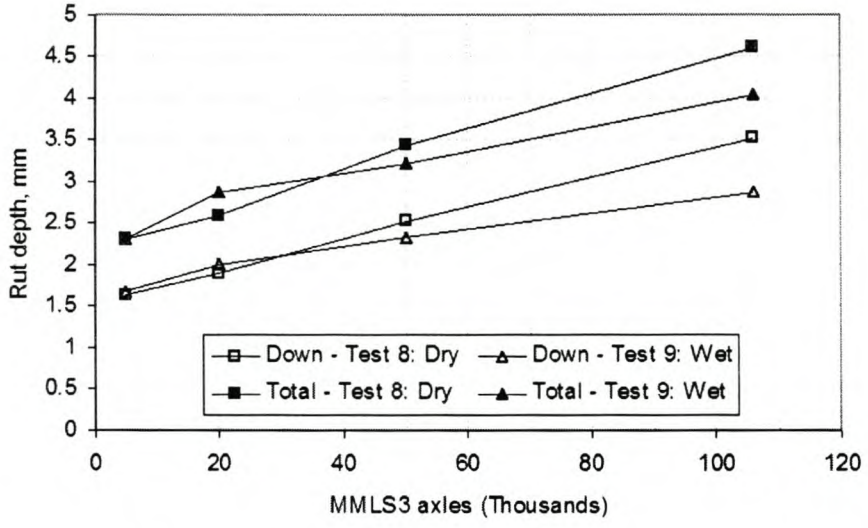

Figure 5.19: Combined average rutting for section E8 (Dry and wet)

5.3.16 MMLS3 rutting performance

Epps et al. [2001] established MMLS3 rutting criteria to judge the performance of asphalt mixes. These criteria were based on MMLS3 (total) testing at the critical pavement temperature for permanent deformation. Depending on the number of rut depth measurements taken (sample size), an acceptable mean rut depth after the application of 100,000 axles is specified. This is shown in Table 5.13.

Applying a rutting criteria of 3.5 mm total rutting after the application of 100,000 MMLS3 axles, and a standard deviation of 0.2 mm, the probability of failure (using the Weibull distribution defined previously) of the MMLS3 sections was determined as shown in Figure 5.22. The figure ranks the performance of the mixes (best to worst) as S9, E6, S10, E2 and E8.

In previous MMLS3 research undertaken in the field in Jacksboro, Texas (Smit et al. [1999]), a total of 1 million axles were applied to an asphalt pavement under hot temperature conditions. It was found that extrapolation of the rutting results after the application of 100,000 MMLS3 axles gave a good estimation of the ultimate

Table 5.12: Regression equations of MMLS3 rutting data

Section	Rut	Equation	Correlation
S9	Total	$Y = 1.0980X^{0.1960}$	$r^2 = 0.94$
	Down	$Y = 0.7386X^{0.2224}$	$r^2 = 0.89$
S10	Total	$Y = 0.8391X^{0.2897}$	$r^2 = 0.94$
	Down	$Y = 0.4701X^{0.3237}$	$r^2 = 0.97$
E2	Total	$Y = 1.2436X^{0.2415}$	$r^2 = 0.82$
	Down	$Y = 0.7822X^{0.2819}$	$r^2 = 0.91$
E6	Total	$Y = 1.3643X^{0.1736}$	$r^2 = 0.99$
	Down	$Y = 0.9359X^{0.1448}$	$r^2 = 0.95$
E8	Total	$Y = 1.5948X^{0.1998}$	$r^2 = 0.91$
	Down	$Y = 1.1286X^{0.2070}$	$r^2 = 0.89$
Y	Rut depth, mm		
X	MMLS3 load applications, Thousands		

Table 5.13: Rut depth criteria for MMLS3 after 100k load repetitions (after Epps et al. [2001])

Sample size	Acceptable mean rut depth, mm
2	3.0
3	3.5
4	3.7
5	3.9

rutting of the pavement after 1 million axles. Based on the findings of this research it is hypothesized that long term predictions of MMLS3 rutting may be made after the application of only 100,000 axles if relatively high pavement temperatures are maintained. The basis for this hypothesis is that the material response may be related to the rate of rutting (secondary rutting slope) which should remain relatively constant up until failure of the asphalt mixture.

Table 5.14 compares the ranking of the MMLS3 and field rutting performance of the mixes under full-scale trafficking. The MMLS3 ranks S9 the best but differs with

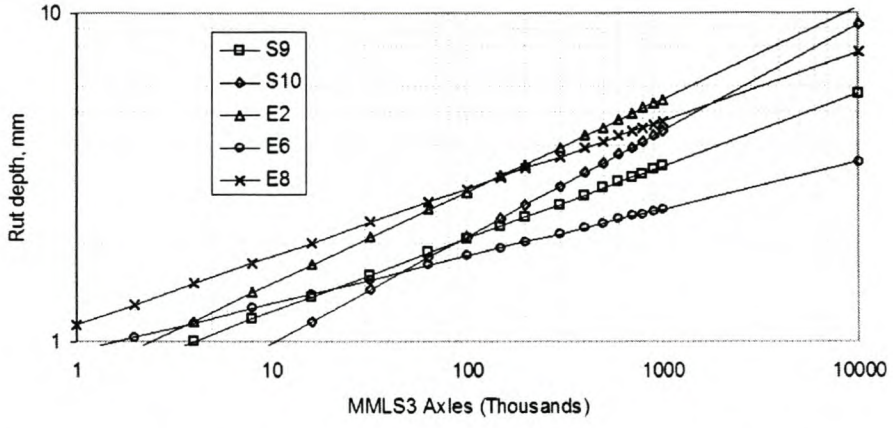

Figure 5.20: MMLS3 section down rutting (Extrapolated)

the field ranking of the fine (above restricted zone) mixes E8 and S10. This difference in the ranking between the MMLS3 and full-scale trafficking is relevant. The MMLS3 tests were done under controlled temperature conditions and the performances of the section mixes were not influenced by wander patterns. For this reason it may be assumed that the MMLS3 ranking is perhaps a more direct ranking and a better indicator of the true relative performances of the section mixes.

Table 5.14: Ranking of MMLS3 and field rutting performance

Rank	**MMLS3**	**Truck**
1	S9	S9
2	E6	E8
3	S10	E6
4	E2	E2
5	E8	S10

An important consideration in the interpretation of the MMLS3 rutting results was the density of the sections prior to trafficking. If the initial densities shown in Figure 5.9 are indicative of the densities on the MMLS3 sections (based on limited

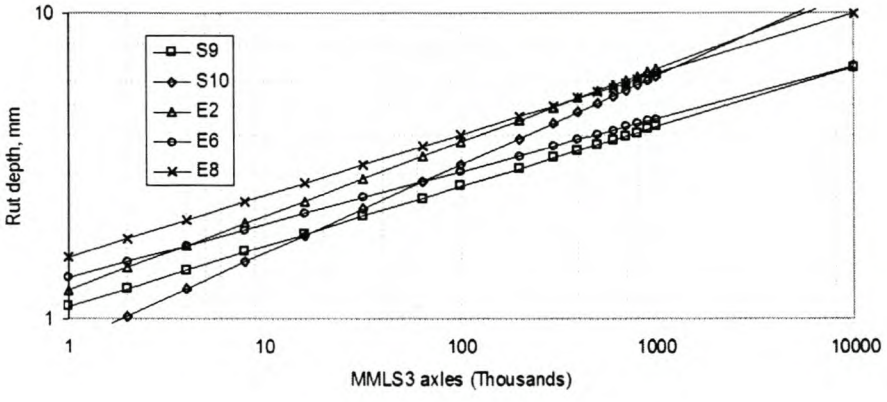

Figure 5.21: MMLS3 section total rutting (Extrapolated)

data), it could be argued that the better MMLS3 rutting performances of sections S9 and S10 may be because these sections had been compacted to a higher density than the other sections. Yet, as mentioned previously, the densities of *all* the untrafficked MMLS3 sections appeared to be similar (about 95 percent of maximum theoretical density) when MMLS3 tests were initiated. This complicates the interpretation of the MMLS3 rutting results.

5.4 PAVDAM evaluation of the NCAT MMLS3 sections

This section outlines the input parameters used in the PAVDAM analyses. Calibration of PAVDAM using results of gyratory compaction tests on the NCAT section field mixes is discussed. Having calibrated the model it is used to evaluate the reliability of the different NCAT MMLS3 sections in terms of volumetric performance. This performance was judged in terms of field densification. Firstly PAVDAM was used to evaluate binder contents as used in the field on the various test sections, whether these would provide sustainable VIM in the field i.e. 4 percent after the application

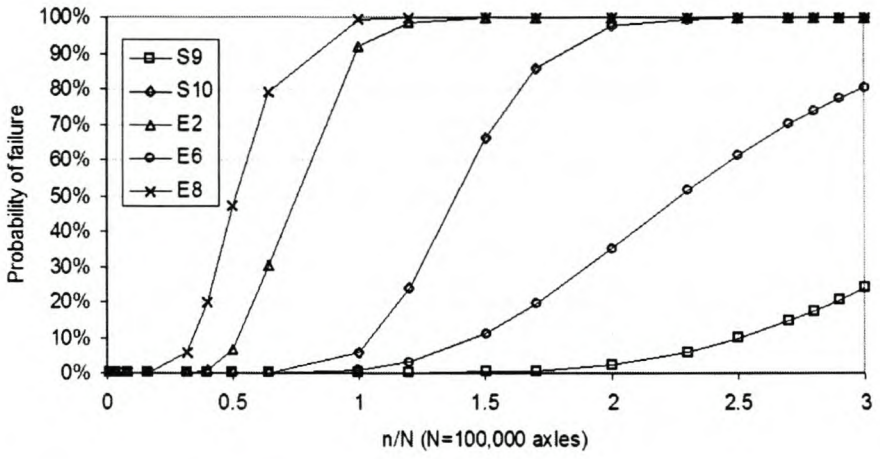

Figure 5.22: Weibull probability of MMLS3 total rutting failure

of the design 10 million ESALs. Secondly PAVDAM was used to judge reliability of the section mixes in terms of overfilling of the VIM of the mixes at the design traffic level. It was assumed that when the VIM of a particular mix fails below 2 percent there is a possibility that the mix may become unstable and have reduced resistance to rutting which would be evident from the results of full-scale and MMLS3 testing on the sections.

5.4.1 PAVDAM input parameters

As mentioned previously, the Southbound sections (S9 and S10) consisted of granite from Jamestown, North Carolina whereas eastbound sections (E2, E6 and E8) consisted of granite from Columbus, Georgia. Although from different sources, both granites were similar in shape and texture. Dry gyratory compaction tests were done on individual fractions from both granites. The compaction characteristics of both were similar and for this reason it was decided to combine the results to obtain a single characteristic describing both sources as shown in Figure 5.23. The figure also shows the standard deviation with compaction from three compaction trials on both

sections (six in total). Fractions compacted separately included the 0.6 mm, 2.36 mm and 4.75 mm aggregate sizes. A total of 300 gyrations were applied. The figure indicates that the standard deviation of the porosity of the fractions increased slightly with compaction effort, which could be because of aggregate crushing at the higher compaction efforts. A value of 1 percent for porosity standard deviation was applied in the PAVDAM analyses.

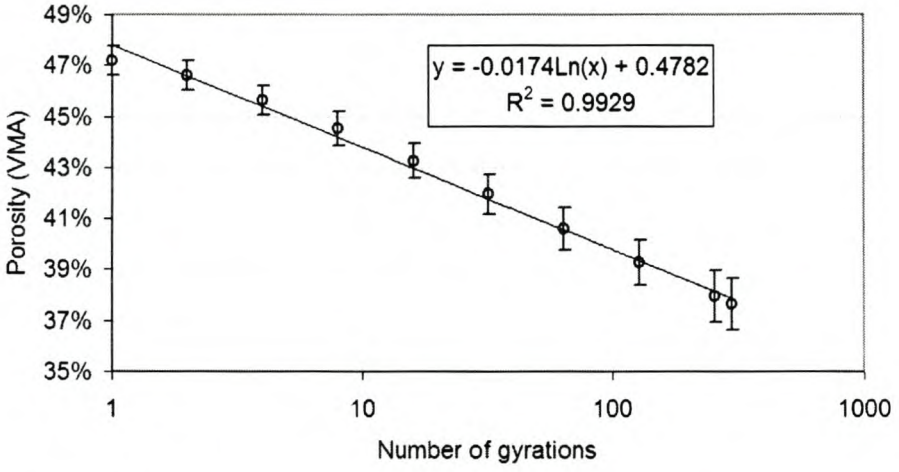

Figure 5.23: Dry gyratory compaction characteristic of NCAT aggregates

Voids in the filler (Rigden voids) for both granites were determined using the Anderson approach [Anderson, 1997] to be 40 percent. Bulk relative densities of the aggregates from the Southbound and Eastbound sections were 2.682 and 2.686 respectively. The bulk relative density of the PG 67-22 binder used on both sections was 1.026. Binder absorption determined for both sources was about 0.35 percent by mass of total aggregate.

5.4.2 PAVDAM calibration

From previous examples it is evident that the packing model used in PAVDAM underestimates the VMA of HMA mixes. One reason for this is that the influence of binder

is not accounted for. Another reason is the influence of compaction. Figure 5.24 compares the PAVDAM estimated VMA for a particular mix with actual measured VMA under gyratory compaction. The figure indicates that actual measured VMA decreases significantly more than the PAVDAM VMA estimate with compaction. The PAVDAM estimate is similar to the measured VMA between 20 and 30 gyrations. Design levels for HMA mixes are typically in the region of 100 gyrations. It is clear therefore that the PAVDAM estimate must be calibrated to allow more accurate estimates of VMA at expected design levels to account for the influence of binder content and compaction on aggregate packing.

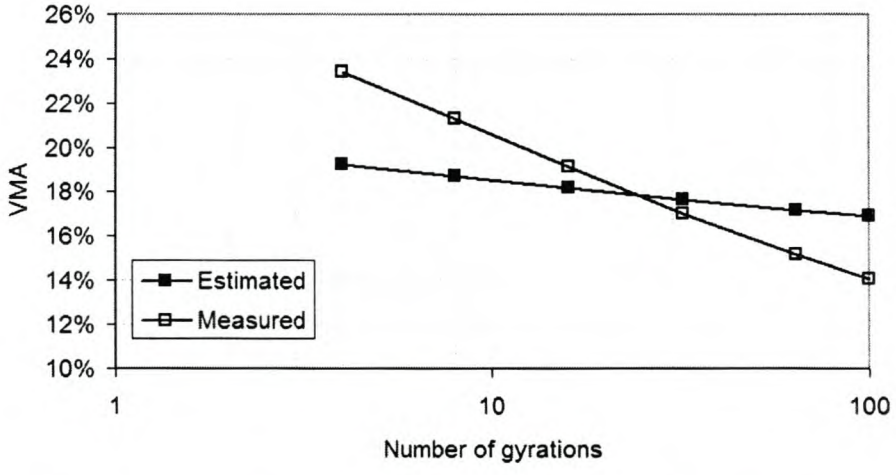

Figure 5.24: PAVDAM estimated vs. measured VMA with gyratory compaction

In order to calibrate the PAVDAM model it is necessary to gyratory compact an asphalt mix (evaluated using PAVDAM) at a binder content estimated using PAVDAM without the use of calibration factors. Having done this, the PAVDAM estimated VMA is compared to the measured VMA at different compaction levels e.g. 4, 8, 16, 32, 64 and 100 gyrations. The calibration takes the form of the following function:

$$\text{Adjusted VMA} = \frac{\text{PAVDAM Estimated VMA}}{f} \tag{5.11}$$

where

$$f = a \cdot N^b \tag{5.12}$$

The constants a and b may be determined by minimizing the difference between the measured and estimated VMA using a solver routine. Table 5.15 lists the constants determined for the NCAT MMLS3 mixes. The measured VMA of the mixes were taken as shown in Figure G.3 in Appendix G.

Table 5.15: PAVDAM calibration constants

Mix	a	b
S9	0.69	0.12
S10	0.74	0.098
E2	0.70	0.12
E6	0.74	0.093
E8	0.75	0.068
Mean	0.72	0.10
Stdev	0.03	0.02

The calibration constants shown in the table are discussed later in the chapter towards general applicability of PAVDAM.

5.4.3 PAVDAM reliability analyses

Having calibrated the model for the different mixes, analyses were done to estimate binder contents for the respective mixes using PAVDAM. Estimated binder contents were determined to achieve 4 percent VIM at compaction levels determined based on a comparison of the gyratory compaction and field densification trends as indicated in Figure 5.16. The respective compaction levels for the equivalent application of 10 million ESALs (design traffic level) were used in the analyses. The results are shown in Table 5.16 together with the actual binder contents applied in the field. A total of 100000 iterations were used in PAVDAM analyses.

Table 5.16: PAVDAM estimated binder contents for densification of NCAT MMLS3 sections to 4% VIM at the design traffic level

Section	Mean P_b, %	Stdev P_b, %	Field P_b %
S9	3.8	0.23	4.7
S10	3.83	0.23	5.2
E2	4.05	0.25	4.7
E6	4.97	0.26	5.0
E8	4.79	0.25	5.6

The table indicates the binder contents estimated by PAVDAM that are required to achieve 4 percent VIM of the MMLS3 sections after the application of 10 million ESALs. The actual binder contents applied in the field for the sections are, with the exception of section E6, considerably higher. This indicates that the mixes would probably densify to below 4 percent VIM after the application of 10 million ESALs. The probability of this occurring may be calculated using the reliability equations outlined in the introduction to the chapter. Assuming the standard deviations of the field binder contents are 0.3 percent, Table 5.17 shows the probabilities of "failure" for the different MMLS3 sections defined as the risk that the VIM of the sections fall below 4 percent at the design traffic level.

Table 5.17: Probability of MMLS3 section mixes falling below 4 % VIM at the design traffic level

Section	Probability, %
S9	99.1
S10	100.0
E2	95.2
E6	53.0
E8	98.1

Hence PAVDAM ranks the MMLS3 sections in terms of reliability (best to worst)

as E6, E2, E8, S9 and S10. There is not much difference in the ranking between mixes E2, S9 and E8. This ranking is in terms of over-densification in the field after the application of the design traffic i.e. 10 million ESALs. This is much the same ranking determined previously for the MMLS3 sections based on the densification trends discussed in Section 5.3.11.

If the risk of failure due to rutting is assumed to be related to the probability that the VIM of a mix falls below 2 percent then PAVDAM may be used to evaluate this. Using a similar approach as outlined for the previous analysis, Table 5.18 shows the PAVDAM estimated binder contents (means and standard deviations) required to achieve 2 percent VIM of the NCAT MMLS3 sections after 10 million ESALs. These are "failure" binder contents.

Table 5.18: PAVDAM estimated binder contents for densification of NCAT MMLS3 sections to 2% VIM at the design traffic level

Section	**Mean P_b, %**	**Stdev P_b, %**
S9	4.77	0.25
S10	4.79	0.25
E2	5.02	0.27
E6	6.00	0.28
E8	5.81	0.27

Table 5.19 shows the probabilities (for the different MMLS3 sections) that the binder contents as used in the field may result in VIM less than 2 percent after the application of 10 million ESALs.

The results indicate that the reliabilities of the section mixes to resist overfilling of the VIM rank from best to worst as E6, E2, E8, S9 and S10. This ranking neither matches that for the resistance to rutting determined using the MMLS3 nor that under full-scale trafficking with the exception of the S10 mix that appeared to perform relatively poorly under full-scale trafficking. The E6 mix, indicated by PAVDAM to

Table 5.19: Probability of MMLS3 section mixes falling below 2 % VIM at the design traffic level

Section	Probability, %
S9	42.9
S10	85.3
E2	21.4
E6	0.7
E8	30.1

be the most reliable in terms of resistance to overfilling and hence probable failure due to rutting performed well under MMLS3 trafficking and reasonably well under full-scale trafficking. The "outlier" is the S10 mix. PAVDAM indicates this mix to be the least reliable of the mixes yet it performed relatively well under the MMLS3. Only a single MMLS3 test was done on section S10. To improve confidence in the MMLS3 results more tests on this section and the others would be recommended. It must be concluded, however, that although PAVDAM was useful in identifying the reliabilities of the mixes in terms of densification in the field, based on the results of the MMLS3 testing at NCAT, it cannot be used with confidence to rank rutting performance. This was not unexpected given the obvious differences between gyratory compaction characteristics of mixes determined in the laboratory and densification of mixes in the field.

The fact that the densification trends of the NCAT sections under full-scale trafficking do not tally with the rutting trends observed under full-scale and MMLS3 trafficking deserves further attention. It was assumed that both densification and rutting in the field could be related to the level at which VIM fall below 2 percent, which in turn could be evaluated using gyratory compaction. Based on the findings of the NCAT study it must be concluded that the 2 (or 3) percent level suggested as the limit below which mixes may become susceptible to rutting should be scrutinised

and not accepted as fact.

5.4.4 General applicability of PAVDAM

The average constants shown in Table 5.15 were used to investigate the sensitivity of calibration constants on estimated binder content. The PAVDAM binder content estimates shown in Table 5.16, calculated using the calibration factors determined from gyratory compaction tests on the section mixes to achieve 4 percent VIM at the design traffic level, were compared to estimates determined using the mean constant values. The difference between the estimates determined using the actual calibration constants and the mean constants is shown in Table 5.20.

Table 5.20: PAVDAM estimates determined using actual and mean calibration constants

Section	**Pb using actual constants**	**Pb using mean constants**	Difference
S9	3.8 %	4.1 %	+0.3 %
S10	3.8 %	3.9 %	+0.1 %
E2	4.1 %	4.5 %	+0.4 %
E6	5.0 %	5.0 %	0.0 %
E8	4.8 %	4.0 %	-0.8 %

With the exception of the E8 mix, the table indicates that using the mean constants determined for the NCAT mixes allows a reasonable estimate of binder content compared to the estimates determined using the calibration constants determined from the gyratory compaction tests. The average constants shown in Table 5.15 may therefore be a good first approximation to use with PAVDAM if gyratory compaction test results are not available since the standard deviations of both constants are relatively low (see Table 5.15). Further evaluations on a variety of continuously graded HMA mixes with different aggregates and binder contents should be done to better

define these constants and their sensitivity on VMA estimation.

5.5 Summary

The chapter presents two case studies to describe the application of PAVDAM. In the first, PAVDAM is used to evaluate two large aggregate base mixes. The PAVDAM analysis is compared to that of Marshall mix designs. In the second, PAVDAM is used to evaluate mixes tested using the MMLS3 at the NCAT test track. In the second case study calibration and validation of the model are discussed.

The MAT packing model used in PAVDAM underestimates the VMA of asphalt mixes. The reason for this is that the combined influence of binder content and compaction on VMA are not directly considered. To correct for this it is necessary to calibrate the model, preferably by gyratory compaction of mixes evaluated using PAVDAM. The chapter outlines two procedures that may be used for calibration. The first makes use of a single calibration factor whereas the second is a more effective approach to better relate PAVDAM estimated and measured VMA. It was found that the calibration factors determined for most of the NCAT MMLS3 mixes evaluated were very similar. This is promising and suggests that PAVDAM may have general applicability, although it is recommended that evaluations on a variety of continuously graded HMA mixes with different aggregates and binder contents be done to better define these constants and their sensitivity on VMA estimation.

In order to validate the PAVDAM model, analyses were done to determine the reliability of each of the NCAT MMLS3 test section mixes in terms of densification in the field under full-scale trafficking. PAVDAM estimated binder contents were determined for each of the NCAT MMLS3 section mixes to achieve 4 percent VIM at the design traffic level i.e. 10 million ESALs. Since PAVDAM estimates are based on the gyratory compaction characteristics of mixes, to allow a more realistic evaluation

of field densification it was necessary to compare densification of the section mixes in the gyratory compactor and in the field. An analysis of field densification data allowed relationships to be established for each of the section mixes between gyratory compaction and applied ESALs. A comparison of PAVDAM estimated and field binder contents allowed a ranking of the reliabilities of the different section mixes to achieve 4 percent VIM at the design traffic level. This ranking compared favourably with that obtained from an analysis of actual densification trends monitored in the field under full-scale trafficking.

Additional analyses were done to ascertain whether PAVDAM was able to rate the reliabilities of the section mixes in terms of resistance to rutting or performance in the field. It was assumed that resistance to rutting may be evaluated by calculating the probability that mixes in the field would compact to below 2 percent VIM at the design traffic level. At these low VIM asphalt mixes have been known to become unstable and susceptible to shear failure. The PAVDAM analyses, however, were unable to conclusively rank the mixes in terms of rutting performance. This was anticipated given that PAVDAM is based on volumetric procedures and cannot directly account for performance of pavement structures in the field. The fact that the densification trends of the NCAT sections under full-scale trafficking do not tally with the rutting trends observed under full-scale and MMLS3 trafficking may indicate, however, that the 2 (or 3) percent level suggested as the limit below which mixes may become susceptible to rutting should be scrutinised and not accepted as fact.

5.6 References

D. A. Anderson. Guidelines on the use of baghouse fines. Information Series 101-11/87, National Asphalt Pavement Association, Maryland, 1997.

H. U. Bahia, T. P. Friemel, P. A. Peterson, and J. S. Russell. Optimization of constructibility and resistance to traffic: A new design approach for HMA using the Superpave compactor. *Proceedings of the Association of Asphalt Paving Technologists*, Vol. 67, 1998.

A. L. Epps, T. Ahmed, D. C. Little, and F. Hugo. Prediction with the MMLS3 at westrack. Technical Report Report 2134-1, Texas Department of Transportation, 2001.

B. D. Prowell, E. R. Brown, and M. H. Huner. In-place densification of hot mix asphalt and verification of superpave n(design). *ISAP*, 2002.

A. D. F. Smit. Results and synthesis of MMLS3 testing at the NCAT test track. Technical report, Texas Department of Transportation, 2002.

A. D. F. Smit, F. Hugo, and A. L. Epps. Report on the first Jacksboro MMLS tests. Technical report, Center for Transportation Research, University of Texas at Austin, 1999.

A. D. F. Smit, F. Hugo, D. Rand, and B. Powell. MMLS3 testing at the NCAT test track. *Presented for publication at the Annual Meeting of the Transportation Research Boad, Washington, D.C.*, 2002.

Chapter 6

The semi-circular bending (SCB) test

The primary objective of the dissertation is the development of a probabilistic and volumetric mix design procedure for HMA. This is only a subset of the mix design process. Following the volumetric design stage is the performance evaluation and optimisation stage. This was outlined briefly in Chapter 2. This chapter discusses the development of the SCB test. The SCB has the potential for evaluating both the strength and stiffness properties of HMA. The SCB test is a well-known test in soft rock mechanics [Lim et al., 1994]. In the asphalt research field, the development of the SCB was initiated by Krans et al. [1996]. In this research the possibilities of the SCB as a practical crack growth test were investigated and the results of this research were positive. Butcher et al. [1998] have also used the SCB to evaluate the fracture of asphalt mixes. Erkens et al. [2002] have used non-linear finite element methods to simulate damage development and propagation in an SCB specimen.

There is an international trend towards performance related mix design procedures. These procedures incorporate the use of sophisticated equipment to determine the fundamental performance characteristics of asphalt mixes. Many test methods are available for the accurate determination of these characteristics. Most of these

tests, however, are relatively expensive, require specialised equipment, are time consuming and suitable test specimens are often difficult to obtain. The consequence is that these tests are mainly used for specific purposes or fundamental research but not necessarily for evaluating mix designs or for quality control purposes.

For quality control measurements during a manufacturing or design process, it is important to procure test results quickly in order to make any necessary corrections. Simple tests on cores and briquettes are favoured as these specimens are often produced as part of the process. The above reasoning partly explains why a "simple" test such as the Indirect Tensile Strength test (ITS) is in common use worldwide. The ITS is used in South Africa to evaluate the tensile strength of HMA. A minimum tensile strength of 800 kPa determined using the test is often specified [CSRA, 1987; SABITA, 1997]. The ITS, however, has disadvantages:

1. The stress state during a diametral test on a specimen under loading is complex and not a realistic representation of the stress state in the pavement structure. A biaxial state of stress exists, the maximum horizontal tensile stress at the centre of the specimen is one third the vertical compressive stress at the same point. This situation must be realised and can be anticipated on.

2. If the compressive strength of the material under loading is lower than three times the tensile strength, specimen fracture will probably be initiated by compressive failure.

3. High stresses at the supports in the ITS may cause local compressive failure at these points.

Partly, because of these disadvantages, the SCB test was developed as an alternative means to determine the tensile strength properties of asphalt mixes. The chapter begins by introducing the concept behind the SCB test and discusses the development of the SCB test configuration. It then discusses finite element approaches used

to characterise the tensile strengths of materials tested using the SCB. These initial approaches were based on linear elastic analysis assuming a single modulus for the material modelled isotropically. SCB strength and fatigue testing is then reported. A comparison between SCB and ITS results is also given. These were based largely on linear elastic solutions derived as part of the initial finite element analyses. The chapter then addresses concerns expressed regarding the initial approach adopted to characterise tensile strength using linear elastic FEM and an alternative non-linear approach is discussed based on CAPA-3D FEM analyses undertaken at the Delft Technical University in the Netherlands to better characterise material strengths using the SCB.

6.1 Development of the SCB test configuration

A schematic of the mechanical set-up of the SCB is shown in Figure 6.1.

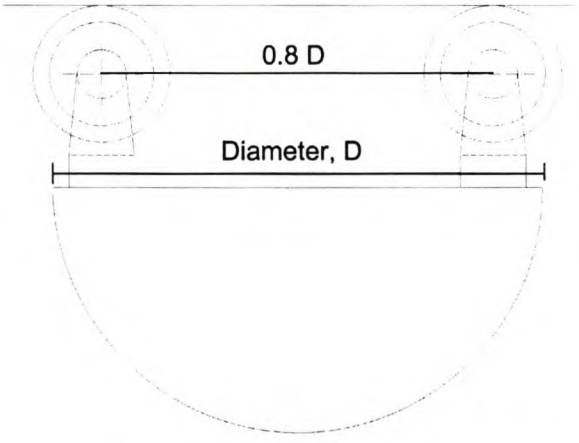

Figure 6.1: Schematic of the SCB test configuration

The mechanical scheme shown in Figure 6.1 suggests a simple test arrangement, but this is misleading. The configuration of the roller supports that rotate and translate under vertical loading is of critical importance. The roller supports have to move

horizontally without friction and to rotate freely when test specimens are loaded. If this movement and rotation are restricted because of friction and/or other second order effects, relatively large horizontal forces can develop in the support system, which can have a negative influence on the accuracy of the test results. Testing the SCB test setup with different support configurations using finite elements validated this. A special calibration instrument was developed by Tolman and Versluis [1996] to investigate the magnitude of the horizontal force for different supports under vertical loading. SCB tests on a sand asphalt at 0 °C and 30 °C with different support types were done to investigate the influence of the supports on the measured test results. The maximum vertical force measured at failure of these tests is reported in Table 6.1. The friction coefficients determined with the calibration apparatus are also shown. The mean of 5 tests per factor and the standard deviations are given between brackets. These SCB tests were deformation controlled at a speed of 0.085 mm/s to minimize interia effects.

Table 6.1: SCB tests on sand asphalt to determine the influence of support configuration (after Tolman and Versluis [1996])

Support type	$\mathbf{F_{max}}$ **(T=0 °C)**	$\mathbf{F_{max}}$ **(T=30 °C)**	**Friction coefficient**
Free rollers	6592 (401)	992 (69)	0.071 (0.01)
Fixed support	8520 (478)	1553 (314)	0.151 (0.006)
Bearing rollers	6965 (255)	922 (34)	0.024 (0.006)

From Table 6.1 it can be seen that the free rollers and bearing rollers almost gave the same maximum loads. This was observed both at temperatures of 0 °C and 30 °C. Calibration measurements showed that the free rollers gave slightly higher horizontal forces than the bearing rollers. The influence of the horizontal forces depends strongly on the horizontal displacements that will occur during a test.

Another factor influencing the horizontal forces at the supports is the vertical

distance from the point the support touches the specimen to the centre point of support rotation. The influence of this factor was investigated using a finite element approach. Figure 6.2 illustrates this influence under a load of 1 MPa for specimen stiffness values of 1000 MPa, 5 000 MPa and 10 000 MPa. From the figure it can be seen that the horizontal force at the support is minimised when the vertical distance from the rotation point to support contact is greater than 25 mm. At this distance, specimen stiffness does not have an influence. Theoretically, it is possible to have no horizontal force at the supports if the distance is approximately 5 mm, however, the configuration is unstable at this point.

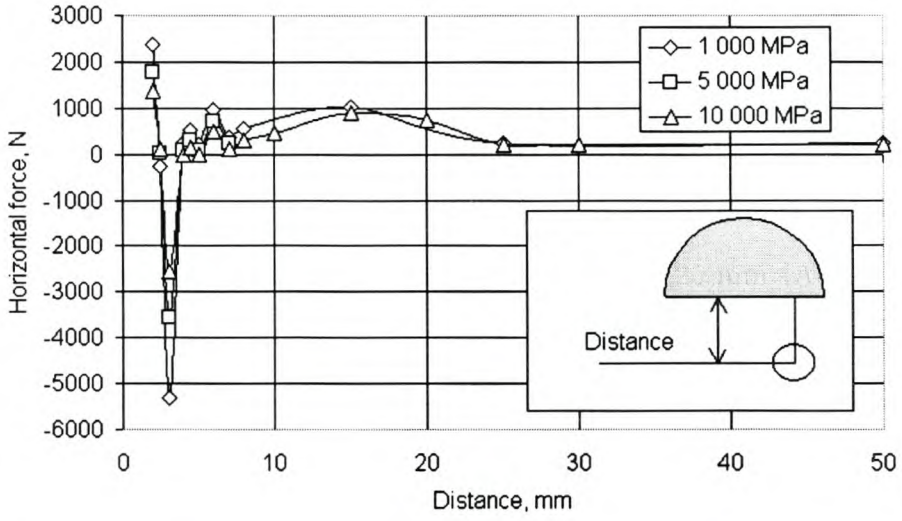

Figure 6.2: Influence of support distance on horizontal forces

Given the above information, the latest SCB testing apparatus incorporates bearing rollers and a distance from support rotation point to support contact point of 35 mm. The width of both the supports and loading strip are 20 mm for 150 mm diameter SCB specimens (and 10 mm for 100 mm diameter specimens). The distance from centre to centre between the supports is 0.8 times the specimen diameter. This ensures that the supports are at least 5 mm from the edges of the specimen to

eliminate edge effects.

6.2 Modelling with finite elements - Linear elastic approaches

Unlike the indirect tensile strength test, to the author's knowledge, there is no analytical solution for the three-point loading stress/strain response on semi-cylindrical specimens. It is possible, however, to calculate an approximate maximum horizontal tensile stress based on the three point bending moment formula for linear elastic beams as shown in Equation 6.1 with a theoretical support length of D. The maximum horizontal tensile stress under ITT loading is shown in Equation 6.2.

$$\sigma_x = \frac{6 \cdot P}{D} \tag{6.1}$$

$$\sigma_x = \frac{2 \cdot P}{\pi \cdot D} \tag{6.2}$$

where

σ_x = Maximum horizontal tensile stress

P = Load per unit thickness of specimen

D = Support length or diameter of specimen

Comparing Equations 6.1 and 6.2 the SCB with a theoretical support length of D requires an applied load that is approximately 9 times lower compared with the ITT to obtain the same maximum horizontal tensile stress. To interpret the test results it was decided to develop load-stress relations using the finite element program ABAQUS [1996].

6.2.1 2-D FEM analysis - linear-elastic approach

A 2-D finite element model used to analyse a semi cylindrical specimen with a diameter of 150 mm is shown in Figure 6.3 before loading and in Figure 6.4 after loading, with an exaggerated displacement magnification factor. To simplify the model, symmetry may be used in one direction to analyse the SCB. Roller supports were supplied at each node along the vertical plane of symmetry. The vertex of the support was free to rotate and also to translate horizontally. A pressure load was applied on the loading strip. Plane strain elements were used, which assumes that out-of-plane strains are negligible. The plane strain model is suitable for structures that are relatively thick in the out-of-plane direction, in contrast to the plane stress model, which is more suitable for modelling plate or sheet objects. The materials were modelled as being isotropic and elastic under axisymmetric stress conditions.

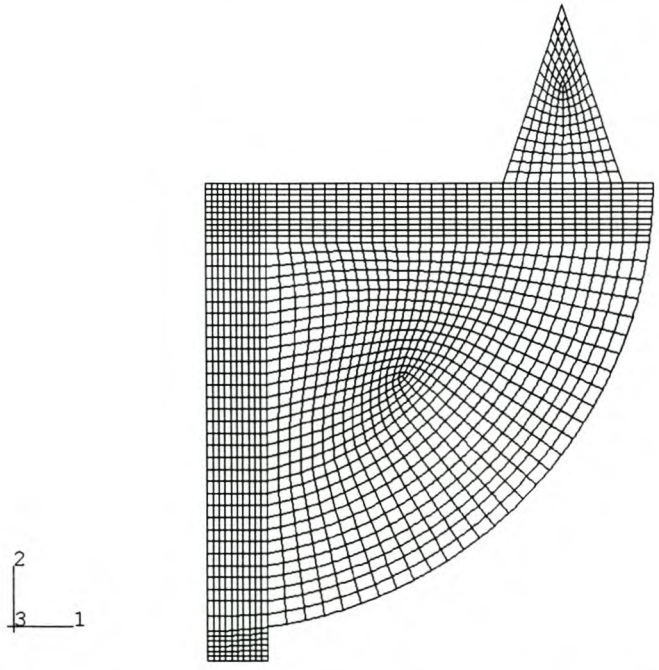

Figure 6.3: SCB finite element model before loading

Figures I.1 through I.6 in Appendix I illustrate the 2-D finite element method

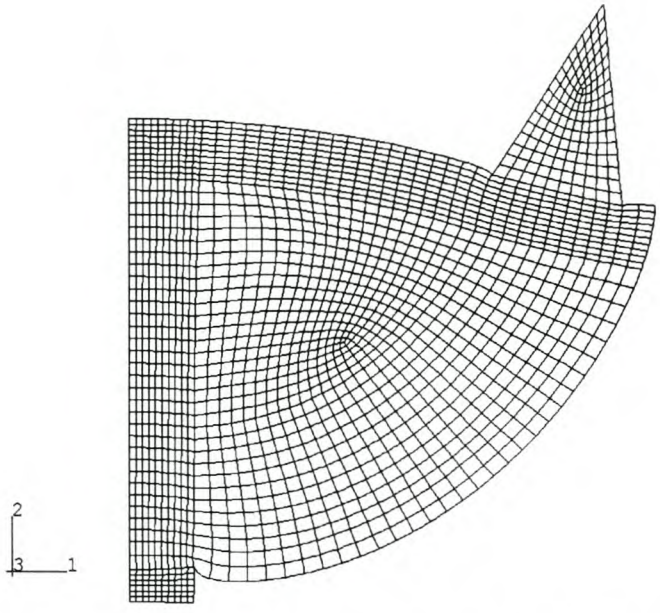

Figure 6.4: SCB finite element model after loading

(FEM) solutions of the SCB stress, strain and deflection distributions in the vertical and horizontal planes with a Poisson's ratio of 0.35. The steel loading head and support was given a stiffness of 206 GPa and a Poisson's ratio of 0.30. Given the plane strain condition imposed on the model, the out of plane stresses and strains (σ_{33} and ϵ_{33}) are not necessarily correct and were later validated using a 3-D finite element model. The relative directions of the different stresses and strains are as shown in Figure 6.3.

Figure I.1 shows that the stress distributions over the height of the semi-cylindrical specimen are not linear. A 150 mm diameter SCB specimen was modelled, hence the distance along the vertical symmetry plane is 75 mm, the maximum stress is expected at the free boundary (0 mm) with the load applied at 75 mm. The horizontal stress (σ_{11}) is non-uniform and changes from a tensile stress to a compressive stress about midway along the vertical symmetry plane. As expected, the vertical compressive stress (σ_{22}) degenerates to zero at the free boundary. It should be noted that the

stiffness of the modelled asphalt specimen does not influence the stress distributions although the influence of specimen thickness and Poisson's ratio can only be determined using a 3-D FEM model. From Figure I.2 it can be seen that the strain distributions vary along the vertical symmetry axis. The horizontal strain (ϵ_{11}) remains tensile throughout the specimen but becomes compressive in the region of loading. The vertical strain (ϵ_{22}) remains compressive throughout the specimen. The strains are a function of the stiffness of the asphalt specimen. Figure I.3 shows the vertical deflection along the vertical symmetry axis, which is also influenced by the stiffness of the asphalt specimen.

The stresses and strains along the horizontal symmetry plane are shown from the point of maximum stress (0 mm) up until they become significantly influenced by the SCB supports (at about a distance of 50 mm). It is positive to note from Figure I.4 that both the horizontal and vertical stresses along the horizontal plane are tensile and are fairly constant up until a distance of about 10 mm from the point of maximum stress. Likewise, the horizontal and vertical strains shown in Figure I.5 remain fairly constant, which is positive when consideration is given to strain measurements using strain gauges. Along the horizontal plane, the horizontal strain is tensile and the vertical strain remains compressive. The horizontal (δ_1) and vertical (δ_2) deflections along the horizontal symmetry plane are shown in Figure I.6. It can be seen that there is no horizontal deflection at the point of maximum stress but that this deflection increases linearly towards the supports. The maximum vertical deflection in the horizontal plane is at the point of maximum stress and decreases as expected towards the supports.

6.2.2 3-D FEM analysis - linear-elastic approach

Figure 6.5 shows the 3-D FEM mesh used to model the SCB. The model is essentially the 2-D model extruded into the 3-plane. Symmetry was used in the 1- and 3-planes to simplify the model.

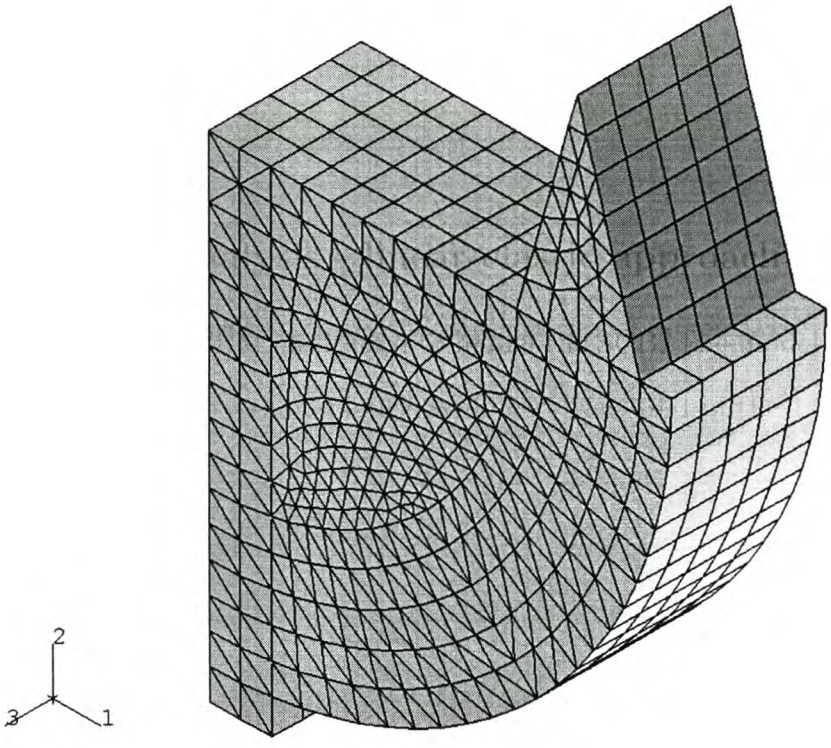

Figure 6.5: 3-D FEM mesh of SCB

As with the 2-D analysis, the stresses, strains and displacements in three principal directions were determined using finite elements. Tables I.1, I.2 and I.3 in Appendix I give the results of the 3-D FEM analysis for specimen thicknesses of 10 mm, 25 mm and 50 mm, respectively. The maximum horizontal tensile stress (S11) and vertical deflection (U2) with variation in asphalt stiffness, thickness and Poisson's ratio are tabulated. The results of the 3-D analyses are also shown in Figures I.7 through I.27 in Appendix I for an asphalt stiffness of 4000 MPa, a Poisson's ratio of 0.35 and under

a load of 1 MPa. The stress/strain responses were determined for three thicknesses and, included in the figures for the 1- and 2- plane directions, are the previously calculated 2-D responses.

In the 1- symmetry plane, the 2-D and 3-D stresses, strains and vertical deflections in the 1- and 2- plane directions compare well although the stress in the 3- plane direction (S33) differs significantly, primarily because of the plane strain assumption used for the 2-D modelling. The 3-D FEM solution of the S33 stress in the out of plane direction is zero, which confirms the uniaxial stress state at the centre of SCB specimens under loading. In general, the influence of specimen thickness on stress, strain and deflection response is limited although it becomes emphasised in the region of the supports.

In the 2- symmetry plane, the 2-D and 3-D stresses, strains and vertical deflections for the 2-D and 3-D FEM solutions compare well with the exception of 1) the stresses in the out of plane direction (S33) as was the case for the 1- symmetry plane and 2) the shear stresses (S12). This is the shear stress vertically within the specimen, and although relatively small, is not zero as the 2-D solution would suggest.

In the 3- symmetry plane only the 3-D FEM solutions are shown with thickness variation. The influence of specimen thickness on the stresses, strains and deflections in the out of plane direction is clearly evident. This again emphasises the importance of testing relatively thinner specimens since the stress, strain and deflection distributions across the specimen would then be fairly constant. The non-linear stress distribution apparent under SCB loading motivated the determination of relationships, based on finite element analyses, between:

1. Maximum horizontal tensile stress and applied load, and,

2. Stiffness and maximum vertical deflection.

These two parameters (maximum tensile stress and stiffness) can be determined in

the laboratory using the SCB test. The influence of specimen thickness and Poisson's ratio on these parameters must be determined using 3-D FEM. For this reason, a 3-D FEM analysis was done by varying the asphalt stiffness, thickness and Poisson's ratio as shown in Table 6.2.

Table 6.2: FEM 3-D analysis matrix

Stiffness MPa	**Thickness mm**	**Poisson's ratio**
1000	10	0.2
2000	25	0.35
4000	50	0.45
8000		

Figure 6.6 illustrates the influence of Poisson's ratio and thickness on the maximum horizontal tensile stress at the point of maximum tensile stress within an SCB specimen under loading. It can be seen that the influence of these parameters (at a constant stiffness level) is less at lower thicknesses and Poisson's ratios, but that the influence is limited. Note that the expression of the y-axis is expressed as the quotient of maximum horizontal tensile stress (S11) and applied load or pressure and is therefore without units.

Figure 6.7 shows that the stiffness of the asphalt has a small but distinct influence on the maximum horizontal stress. From this figure and Tables I.1 through I.3, the percentage difference in maximum horizontal tensile at extreme conditions of thickness and Poisson's ratio is less than 4 percent.

Figure 6.8 illustrates the influence of thickness and Poisson's ratio on maximum vertical deflection under SCB loading at a constant stiffness. From the figure it can be seen that the influence of Poisson's ratio is less at a lower thickness. This suggests that specimens for SCB tests should preferably have a thickness less than 30 mm to restrict the influence of Poisson's ratio.

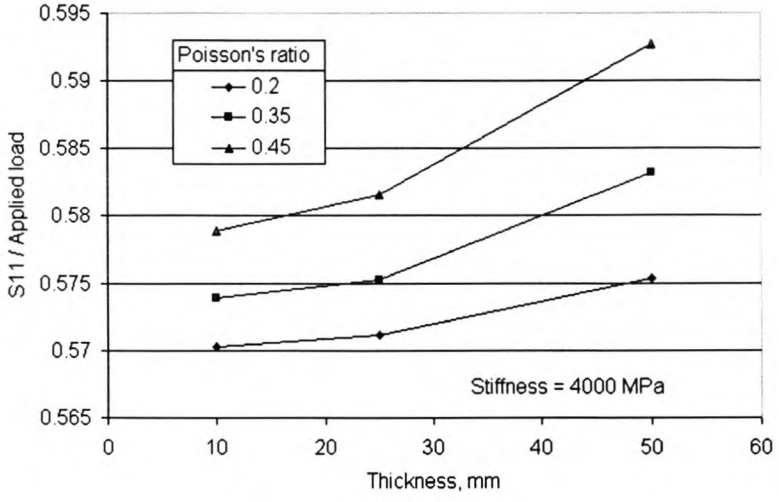

Figure 6.6: 3-D FEM stress solution of SCB with variation of thickness and Poisson's ratio

The influence of stiffness on vertical deflection is shown in Figure 6.9. As expected, stiffness has a significant influence on vertical deflection, and if the influence of thickness and Poisson's ratio is taken into account (from Tables I.1 through I.3), the percentage difference in maximum deflection at extreme conditions of thickness and Poisson's ratio is slightly greater than 10 percent.

From the 3-D FEM analysis, relationships for maximum horizontal tensile stress and stiffness were derived for the SCB test as shown in Equations 6.3 and 6.4 respectively. These equations are only applicable for the SCB test configuration as described and modelled using finite elements. The distance between the support centres must be 0.8 times the diameter of the specimen and the support and loading-head widths must be 20 mm.

$$\sigma_x = \frac{4.314 \cdot P}{t \cdot D} \tag{6.3}$$

$$E = \frac{2.25 \cdot P}{t \cdot \Delta v} \tag{6.4}$$

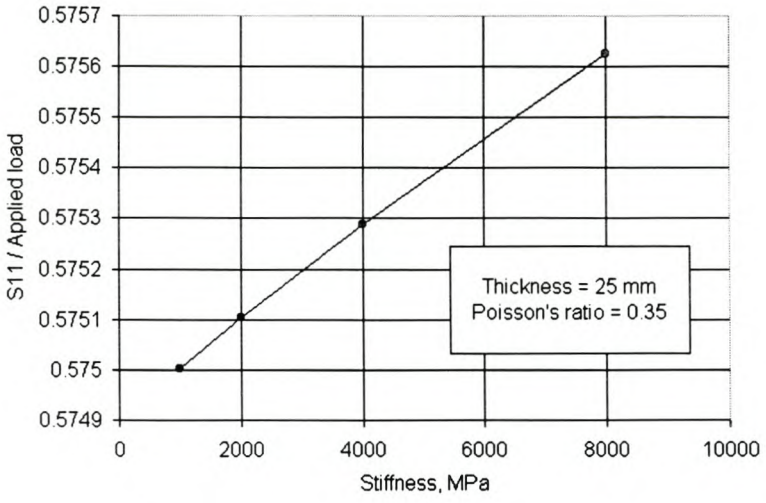

Figure 6.7: 3-D FEM stress solution of SCB with variation of stiffness

where

σ_x = Maximum horizontal tensile stress, MPa

P = Applied load, N

t = Specimen thickness, mm

D = Specimen diameter, mm

Δv = Vertical deflection, mm

Specimen diameter has been included as a variable in Equation 6.3, although the 3-D FEM analysis did not consider variation in specimen diameter (only 150 mm diameter specimens were modelled). This was considered feasible as previous FEM analyses were done using a specimen diameter of 100 mm that gave comparable results [Smit et al., 1997].

Determining the stiffness of SCB specimens from the maximum deflection of these specimens under loading is not straightforward from a practical point of view. This is because the rollers are designed to rotate and translate under loading in order to

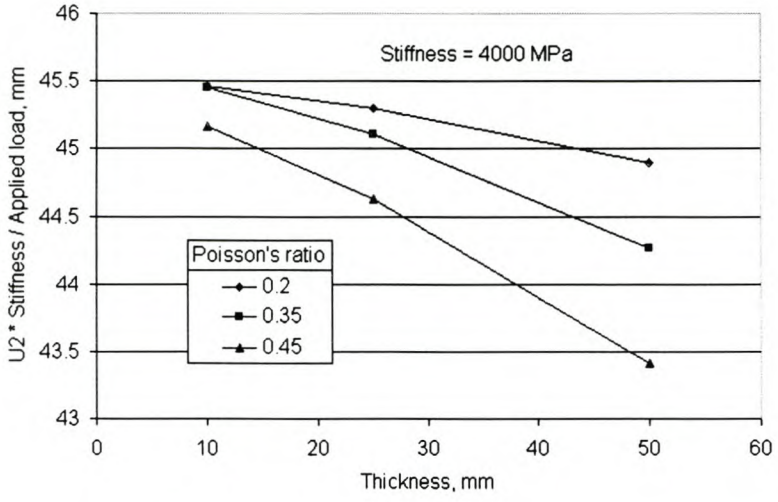

Figure 6.8: 3-D FEM vertical deflection solution of SCB with variation of thickness and Poisson's ratio

counter the horizontal forces acting on the specimen. Deflection measurements must therefore be taken directly from the specimen. A light aluminium frame glued to the specimen may be feasible. Deflection measurements from a source not attached to the specimen will unfortunately include the deflection of the rollers under loading. An alternative approach is to make use of strain gauges attached to the specimen enabling stiffness to be calculated by applying Equation 6.3.

The equations presented above were determined using a linear elastic isotropic finite element material model. The following section discusses why the use of the equations may lead to incorrect estimations for material strengths and moduli and presents an alternative approach to determine material parameters using the SCB test.

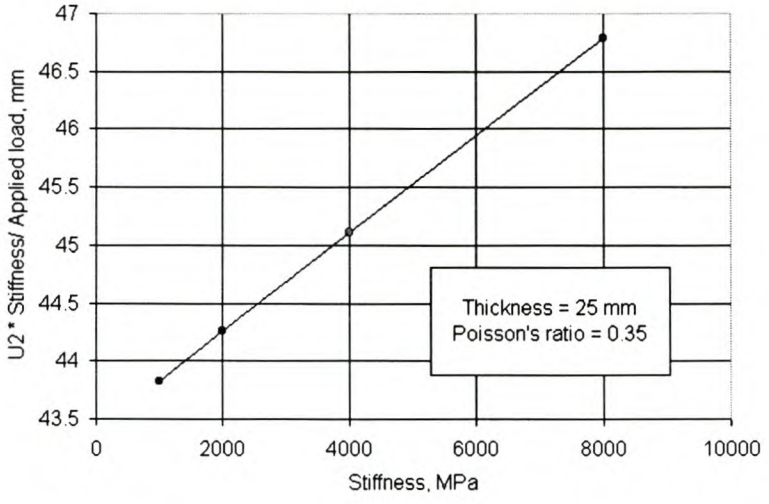

Figure 6.9: 3-D FEM vertical deflection solution of SCB with variation of stiffness

6.3 SCB testing

The following section discusses SCB testing to evaluate the strength and fatigue characteristics of HMA. A comparison between SCB and ITS results is given. The SCB tensile strengths reported in this section were calculated using Equation 6.3. It will be seen that in many cases these strengths are extremely high. This is misleading and for this reason an alternative finite element approach was adopted to better characterise material strengths determined using the SCB. This alternative approach is discussed in the next section.

6.3.1 A comparison of ITS and SCB strength test results

From the finite element analysis of the horizontal tensile stress it is clear that the SCB test gives a simple horizontal uniaxial tensile stress at the free boundary of the specimen. This is in contrast to the biaxial stress situation in the ITS, with a three times higher compressive than tensile stress. According to Arand [1990] and

Heukelom [1966], the ratio between compressive and tensile strength of asphalt mixes increases with decreasing temperature. In general the ratio (compressive to tensile strength) will be around three at a temperature below 15 °C and around 6 at a temperature below -10 °C. This implies that with the ITS, accurate tensile strength determination can only take place at temperatures well below 15 °C. The SCB test, on the other hand, does not have this restriction.

The SCB test is a relatively new test in South Africa. Studies have been undertaken to ascertain the repeatability of the test and how it compares with the ITS [Smit et al., 1997; van de Ven et al., 1997]. Much of the development work on the SCB resulted in an improved test configuration and procedure. Test results from older test configurations indicated significant variation in SCB results compared to ITS results. Some interesting results have been found and these will be illustrated and discussed.

Figure 6.10 shows a comparison between tensile strengths determined using the SCB compared with those determined with the ITS. The results are from tests done on a South African "TPA" medium mix used for routine maintenance patching. The samples were obtained and tested over a period of two months and variation in grading, binder and active filler content caused the spread of the data shown in the figure. The briquettes were Marshall compacted and tested at 25 °C. A regression analysis was done, the result of which is also shown in the figure. A good correlation was found between the ITS and SCB test results. The ITS results are in the order of 20 percent lower than those determined using the SCB. The constant in the regression equation is a function of the friction in the test set-up and the ratio of tensile to compressive stresses in the ITS test. It should be noted that the ITS results vary between 1 to 2 MPa whereas the SCB test results vary between 2 and 6 MPa, a much greater range. This may indicate that the SCB test is particularly more sensitive to the tensile strength of the material being tested. It must be said, however, that the

tensile strengths calculated from the SCB tests were based on Equation 6.3 and as pointed out may overestimate the actual strengths of the materials tested.

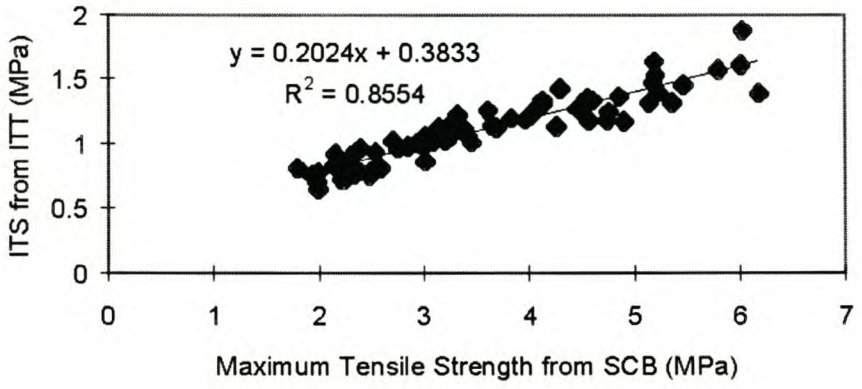

Figure 6.10: Comparison of tensile strength test results using the ITS and SCB

Figure 6.11 shows the results of SCB splitting tests on various asphalt mixtures used in Gauteng, South Africa. The vertical deformation of the specimens during loading at the standard Marshall speed of 50.8 mm/minute was monitored. This allowed the calculation of the fracture energies of the different mixtures.

The variation in the repeatability of a performance related test should preferably be minimal. Figure 6.12 shows the results of SCB splitting tests on halves of a single sawn briquette. These test results form part of those reported previously (see Figure 6.10). From Figure 6.12 it is apparent that a good correlation exists between the results of the tests done on the halves. This reflects on the repeatability of the test. It can also be seen that the variability in the test results is greater at the higher tensile strengths. This greater variability is related to the higher frictional forces that developed in the support configuration of the prototype SCB equipment.

The coefficient of variation (COV) of all the SCB test results shown in Figure 6.10 is 0.33 compared to a COV of 0.23 for the ITS. If one considers only the SCB test results less than 4 MPa then the COV is 0.21, which is comparable with the COV

	Binder	Grade	Modifier	Filler	Voids
SMA	6.5%	60/70	0.3% Fibre	3% OPC	6%
TPA Medium	5.3%	60/70	-	-	3%
Semi-gap	5.7%	60/70	2% SBR	1% Lime	4%
Porous	5.7%	80/100	22% Rubber	-	22%

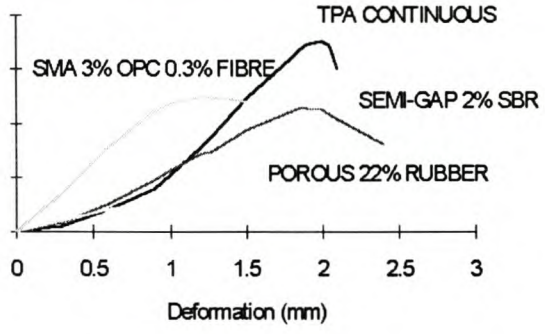

Figure 6.11: SCB splitting tests on various asphalt mixtures

of the ITS. These figures suggest that the variation in the repeatability of SCB is comparable to that of the ITS.

In another study to compare SCB and ITS test results, both an asphalt surfacing mixture with a maximum grain size of 9.5 mm and a base course mix with a nominal maximum grain size of 37.5 mm were evaluated. Details of the mixes have been reported [Van de Ven et al., 1997]. The test program consisted of ITS and SCB splitting tests on 100 mm and 150 mm specimens at temperatures of 5 °C and 25 °C. These tests were deformation controlled at a speed of 0.83 mm/s. Additional tests at a speed of 0.083 mm/s were done on 150 mm specimens at 5 °C. The vertical deformation of the specimens under loading was also measured. This enabled the calculation of the area beneath the force-deformation curve. Stiffness tests on SCB specimen were also done, however, these were discontinued when it became apparent that the measurement system (used at the time) was not accurate enough to measure the small vertical deflections under SCB loading. The system has subsequently been modified. SCB fatigue tests on the 100 mm specimen at 5 °C were also done. The

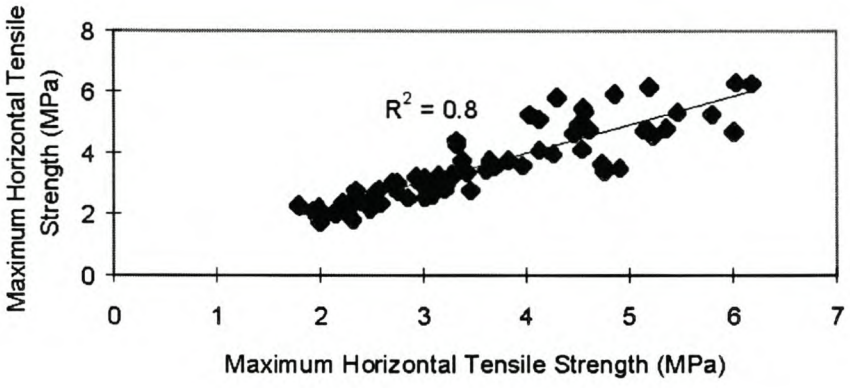

Figure 6.12: SCB tests on the two halves of a Marshall compacted briquette

results of the ITS and SCB tests on 100 mm and 150 mm specimens at 5 °C and 25 °C are shown in Table 6.3. The total number of tests done, the mean, standard deviation (STD) and coefficient of variation (COV) for each test series are tabulated. As before it can be seen that the SCB tensile strengths are overestimated.

Table 6.3: Summary of ITS and SCB test results

Test	**D** **mm**	**Temp** **°C**	**Rate** **mm/min**	**n**	**Mean** **kPa**	**STD** **kPa**	**COV** **%**
ITS	100	5	50	3	4007	136	3.4
SCB	100	5	50	3	7615	1219	16.0
ITS	150	5	50	4	3579	244	6.8
SCB	150	5	50	6	7862	1873	23.8
ITS	100	25	50	4	1133	210	18.6
SCB	100	25	50	7	4943	403	8.2
ITS	150	25	50	4	835	56	6.7
SCB	150	25	50	8	5133	513	10.0
SCB	150	5	5	5	9786	1209	12.4

Typical force-displacement curves for 100 mm and 150 mm SCB specimens tested at 5 °C and 25 °C are shown in Figures 6.13 and 6.14 respectively. The curve for

a test at a speed of 0.083 mm/s on a 150 mm specimen at 5 °C is also shown in Figure 6.14.

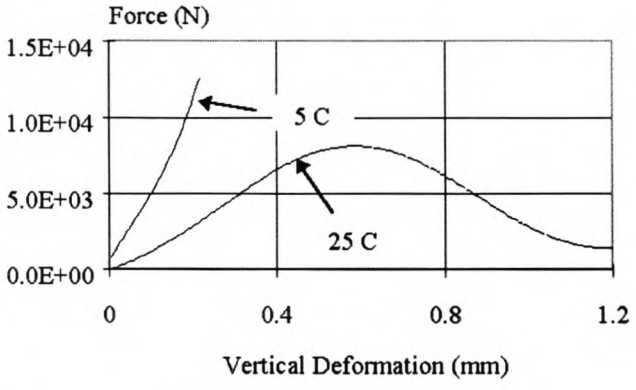

Figure 6.13: Force-displacement curves for 100 mm SCB specimens

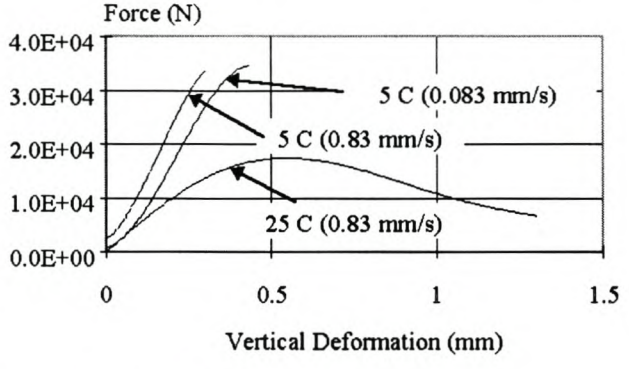

Figure 6.14: Force-displacement curves for 150 mm SCB specimens

The area beneath the force-displacement curves for the SCB splitting tests was calculated in order to get an indication of the brittleness and toughness of the materials tested. Table 6.4 shows the statistics of these results for 100 mm and 150 mm specimens tested at 5 °C and 25 °C. The statistics i.e. mean, standard deviation (STD) and coefficient of variation (COV) of the vertical deformation measurements until failure of the tested specimens are shown in Table 6.5.

Table 6.4: Statistics of area beneath SCB force-displacement curves

D mm	Temp C	Rate mm/min	n	Mean Nmm/mm	STD Nmm/mm	COV %
100	5	50	3	15	4	23.8
150	5	50	6	35	11	30.2
100	25	50	7	85	4	4.5
150	25	50	8	160	27	16.7
150	5	5	5	74	18	24.9

Table 6.5: Statistics of SCB vertical deformation measurements prior to specimen failure

D mm	Temp C	Rate mm/min	n	Mean micron	STD micron	COV %
100	5	50	3	173	42	24.0
150	5	50	6	260	39	15.2
100	25	50	7	544	70	12.9
150	25	50	8	731	109	14.9
150	5	5	5	498	192	38.5

The tensile strength coefficients of variation (COVs) of the SCB tests at 5 °C are greater than the COVs at 25 °C. The tensile strength COVs of the SCB are generally higher than those calculated for the ITS, the tests on 150 mm specimen at 25 °C being the exception. This reflects on the repeatability of the SCB test results. The tensile strength COVs for the 150 mm specimens are higher than those for the 100 mm specimens for both the SCB and the ITS. This may be attributed to the large aggregate used in the 150 mm specimens in contrast to the finer grading of the 100 mm specimens. The maximum size of the aggregate used in a specimen will influence the path followed by the crack initiated under loading.

From the tests results it can be seen that the tensile strengths determined using the SCB are always higher compared to those determined using the ITS. The difference

between the strengths is greater for the tests done at 25 °C (in the order of 5 times greater) than at 5 °C (in the order of 2 times greater). Furthermore, the ratio of the tensile strengths at 5 °C to those at 25 °C are in the order of 3.5 times greater for the ITS and 1.5 times greater for the SCB tests on the 100 mm specimens. This ratio increases to about 4 times greater for the ITS tests but remains at about 1.5 times greater for the SCB tests on 150 mm specimens.

The differences in the tensile strengths between the SCB and ITS tests may be attributed to a number of different factors. As was pointed out, part of the problem lies in the assumption that material response may be modelled using linear elastic approaches. This applies for the SCB and ITS. Different stress states develop within the respective specimens under loading. In the ITS there is a more unform distribution of horizontal tensile stress along the vertical principal axis compared to the SCB. In the SCB, however, there is a higher stress localisation at the point of maximum tensile stress. The material response and strength is a function of the strain rates that develop with the specimen and the magnitude of these strain rates. These factors were not accounted for in the calculation of the strengths reported.

The area beneath the force-displacement curves gives an indication of the energy required to split the specimens. This then reflects on the brittleness and toughness of the specimens as the crack is continuously growing under tensile stress as indicated by Krans et al. [1996]. It can be seen that the specimens at 5 °C undergo brittle fracture.

The vertical deflection of the 100 mm specimens under the maximum load is in the order of 200 micron. This deflection is relatively small, which emphasises the importance of accurate deflection measurements for stiffness calculations where the deflection will be much smaller. The deflection of the specimens tested at 25 °C is in the order of three times greater than those measured for the specimens tested at 5 °C.

Although the tests for this study were done on a Materials Testing System (MTS) electro-hydraulic apparatus, it appears as if it may well be feasible to perform the SCB splitting tests on a standard Marshall press with adequate capacity. The maximum force applied to the 150 mm SCB specimens at 5 °C was in the order of 30 kN in contrast to a maximum force of 90 kN measured for the ITS specimens.

6.3.2 Comparison of SCB, ITS and bending beam fatigue testing

In a study undertaken for the Provincial Administration of the Western Cape (PAWC) in South Africa, the fatigue characteristics of a large aggregate asphalt base mixture were evaluated using the SCB together with repeated load indirect tensile (both stress controlled tests) and strain controlled four point bending beam fatigue tests (the beam fatigue tests were done by the CSIR in South Africa). The fatigue test results were compared to theoretical fatigue curves determined using the SHELL method [Bonnaure et al., 1980], which makes use of the macro volumetric properties of a mix to estimate it's fatigue life. The asphalt base mixture had a maximum aggregate size of 26 mm and the design binder content was 4.9 percent. At this binder content a large stone mix may be rut resistant but prone to fatigue distress. Details of the asphalt base mixture have been reported elsewhere [Smit et al., 1998].

The ITS and SCB fatigue tests were done at 10 °C as in most cases the greatest contribution to fatigue of asphalt layers is at lower to ambient temperatures. The test frequency for these tests was set at 10 Hz. Tests were done at three stress levels anticipating a fatigue life ranging between 10^4 and 10^6 load cycles. Four repetitions at each stress level were done in order to predict a regression line on log-log scale. The four point bending fatigue tests were done in strain controlled mode with sinusoidal loading. The test temperature was 20 °C and the test frequency was 10 Hz. Strain

levels were selected to characterise the fatigue behaviour of the specimens under various loading conditions, from light loads to heavy loads. Strain levels ranged from 281 microstrain to 474 microstrain. In controlled stress tests, stiffer mixtures exhibit longer fatigue lives while in controlled strain tests the more flexible mixtures have longer fatigue lives. In cases where the specimens are identical the controlled stress loading will result in a shorter fatigue life. This may be explained in terms of total energy dissipation. The controlled stress test dissipates energy much faster although equal amounts of energy are dissipated at the end of each test.

ITS fatigue testing involves applying a compressive load across the diametrical axis of a cylindrical specimen. The mechanics of the test are such that a nearly uniform state of tensile stress is achieved across the diametrical plane. Porter and Kennedy [1975] found that the repeated-load indirect tensile test produces results comparable with other fatigue tests if the state of stress developed in the specimen is considered. They point out that the large differences between test results obtained from the repeated-load indirect tensile test and from other tests were explained in terms of the biaxial state of stress that develops in the indirect tensile test, resulting in higher shear stresses as discussed previously. By expressing stress as a stress difference, it was found that a large portion of the variation was eliminated. The stress difference is the deviator stress (σ_d) calculated by subtracting the horizontal principal stress responses (σ_3) from the vertical principal stress response (σ_1) i.e. $\sigma_d = \sigma_1 - \sigma_3$. They postulate that the biaxial state of stress more closely simulates the stress conditions produced at the bottom of a layer by a moving wheel load.

The SHELL method [Bonnaure et al., 1980] allows an estimation or prediction of the fatigue life of an asphalt mix based on the volumetric properties of the mix, binder properties and the stresses involved. Formulae for initial strain giving failure

after N cycles have been derived. For constant strain tests:

$$\varepsilon = \alpha \cdot S_m^{-0.36} \cdot N^{-0.2} \tag{6.5}$$

For constant stress tests:

$$\varepsilon = \beta \cdot S_m^{-0.28} \cdot N^{-0.2} \tag{6.6}$$

where

ε = Initial strain

α = (4.102 x PI - 0.205 x PI x V_b + 1.094 x V_b - 2.707)

β = (0.300 x PI - 0.015 x PI x V_b + 0.080 x V_b - 0.198)

PI = Penetration Index of the binder in the mix

V_b = Volumetric bitumen content of the mix

S_m = Stiffness modulus of the mix

N = Fatigue life

Equation 6.6 was used to determine the SHELL fatigue curves for the ITS and SCB test specimens and Equation 6.5 was used for the four point bending beam test specimens. For the stress controlled tests, the initial strain was converted to an initial stress using elastic theory : $\sigma = S_m \cdot \varepsilon$. This conversion was deemed acceptable at the low temperatures and high frequencies applied.

Equations 6.5 and 6.6 were determined from a statistical analysis of fatigue tests in which the specimens were loaded sinusoidally producing tension and compression stresses at the points of maximum stress. This is in contrast to the ITS and SCB tests in which haversine loading is applied. Figure 6.15 illustrates the difference between the two types of loading.

For load controlled fatigue tests on metals and concrete, the Smith diagram [Van de Ven and Montauban, 1994] is often used to illustrate stress/fatigue relationships. The Smith diagram, an example of which is shown in Figure 6.16, is only

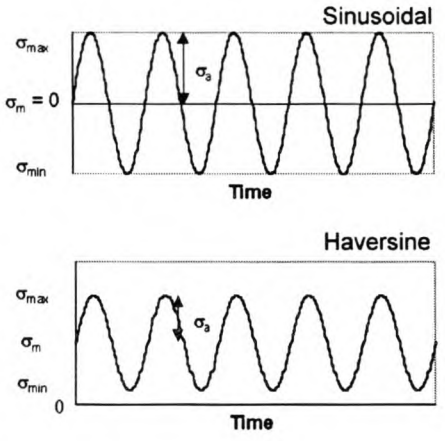

Figure 6.15: Sinusoidal and haversine loading

applicable if the specimens tested undergo no creep deformation under loading. The Smith diagram illustrates the influence of sinusoidal and haversine loading on the fatigue performance of specimens. From the diagram it can be seen that the amplitude (σ_a) under haversine loading is lower than for sinusoidal loading at a specific N (fatigue life) value. In other words, under ITS or SCB loading, the material is subjected to a mean tensile stress (i.e. σ_m is not zero as is the case for sinusoidal loading) and the stress range must be decreased to preserve the same N. This principle is also known as Goodman's Rule.

Assuming Goodman's Rule applies, it may be used to compare the fatigue results of the ITS and SCB tests with those of the SHELL fatigue curves. Van de Ven and Montauban [1994] have shown that the fatigue performance under haversine loading with a specific amplitude falls between that determined under sinusoidal loading with the same amplitude and sinusoidal loading under twice the amplitude. This satisfies Goodman's Rule and allows a means of adjusting the SHELL fatigue curves to account for the difference in loading mode. The SHELL fatigue curves were adjusted by calculating fatigue life (using Equation 6.6) based on twice the stress amplitude as applied for the SCB tests. The ITS fatigue test results were also adjusted by applying

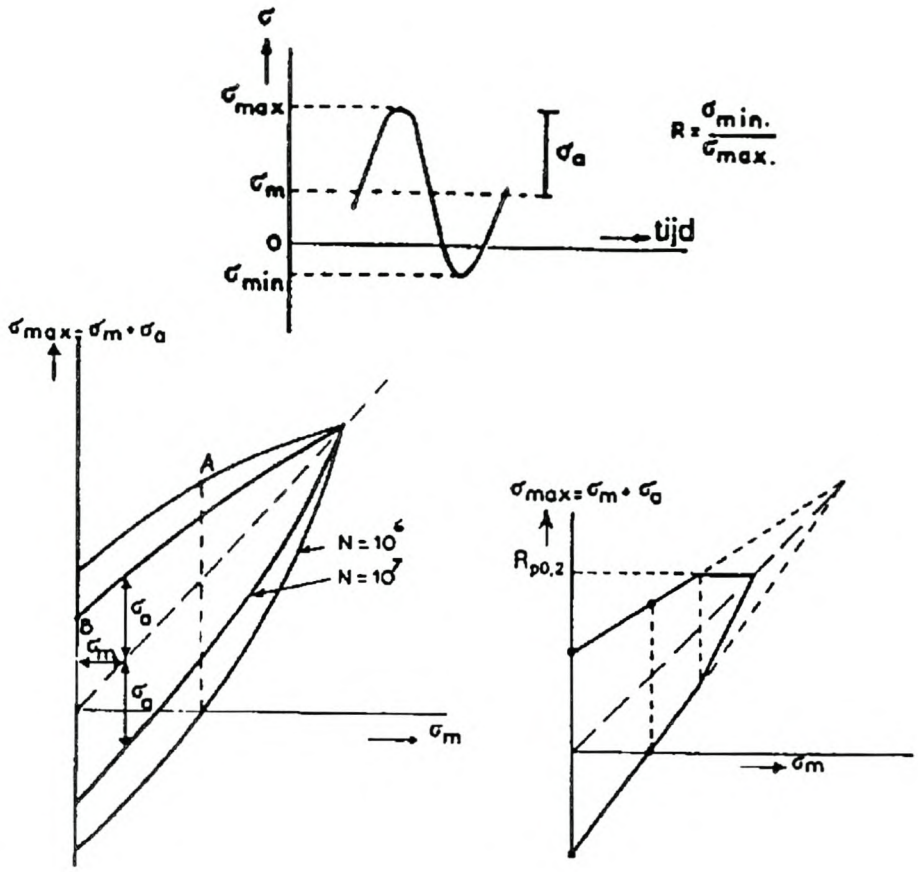

Figure 6.16: Smith diagram

the stress difference or deviator stress. The effects of these adjustments are shown in Figure 6.17.

Figure 6.18 shows the four point bending beam fatigue test results together with the predicted SHELL fatigue curve.

From the test results shown in Figure 6.17 it can be seen that the ITS tends to underestimate the fatigue life whereas the SCB overestimates the fatigue life compared with the SHELL fatigue curves. This phenomenon has been reported previously for fatigue tests on large aggregate mixes [Van de Ven et al., 1997; Hugo et al., 1996]. Applying the deviator stress results in an ITS fatigue performance that is comparable

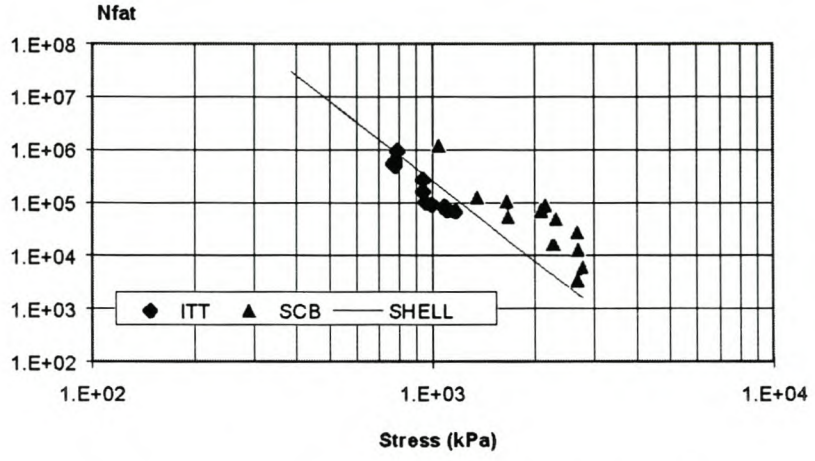

Figure 6.17: SCB and ITS fatigue test results

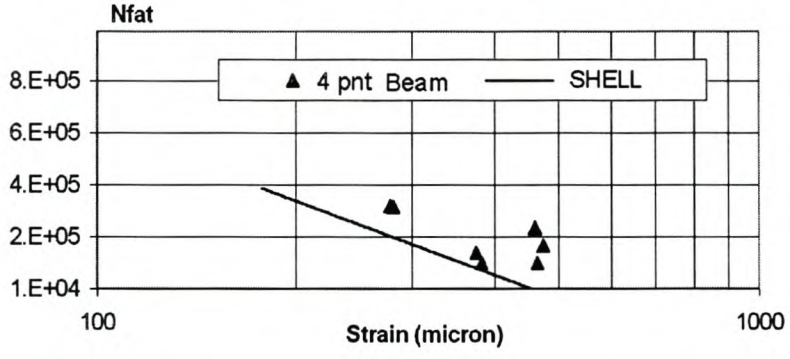

Figure 6.18: Bending beam fatigue test results

with the SHELL fatigue curve. The four point bending beam fatigue test results are scattered and do not show any significant fatigue relationship. For the limited amount of data shown, the resulting fatigue lives are higher than the predicted SHELL fatigue lives. It is clear that the beam fatigue testing should also have been done at lower and higher stress/strain levels for a more accurate assessment of fatigue behaviour. It was postulated that the possible reason for the scatter of these results was due to the large aggregate used in the mix. The compacted beam is 50 mm in height and a large percentage of the aggregate in the mix is between 19 and 26.5 mm. As noted, the SCB

gives the highest fatigue performance prediction. These higher results are perhaps excessive as the SCB test configuration is such that horizontal restraining stresses may develop within test specimens as a result of horizontal frictional forces at the load supports. These stresses counter the maximum horizontal tensile stress resulting in longer fatigue lives. From the other side, creep can have a negative influence on the SCB fatigue life. With this in mind, the actual fatigue performance of the mix in question may be less than the SCB results.

The plotted SHELL fatigue curve is perhaps the best indicator or predictor of the fatigue performance of the mix as it falls between the SCB and ITS results. The fatigue characteristic of the design mix in question was determined by evaluating the SHELL fatigue curve shown in Figure 6.17. The fatigue characteristic of the design mix is shown in Figure 6.19. Comparing the design mix fatigue characteristic with the SHELL fatigue characteristics [SHELL, 1985] it was noted that the design mix has better fatigue characteristics at lower mix stiffnesses compared to that at higher mix stiffnesses. It was concluded that the design mix therefore has satisfactory fatigue characteristics although the mix is not ideally suited for fatigue performance.

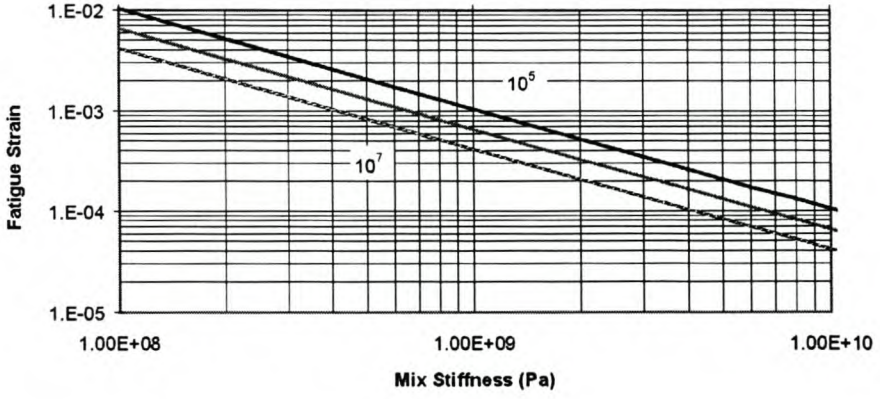

Figure 6.19: Fatigue characteristic of a large stone design mix

6.4 SCB non-linear FEM analysis

Erkens et al. [2002] have developed a material model to describe the response of asphaltic materials in terms of elasticity, visco-plasticity and cracking. They evaluated the SCB test configuration as part of the model verification and were able to simulate damage development and propagation in an SCB specimen under a constant rate of loading. They found that significant localisation of (tensile) strains results in "intense localisation of cracking" along the diameter of the specimen. Erkens, in communication with the author, pointed out that the SCB will probably result in more reliable indications of "tensile-type" failure than the ITS. This is because of the localisation effect. In the ITS this effect is less pronounced and a lot of energy is spent in causing compressive failure in the loading area and support. In the SCB it appears that most of the energy is spent in splitting the specimen.

Using non-linear FEM analysis with the CAPA-3D finite element package developed at the Technical University of Delft in the Netherlands by Scarpas and Kasbergen [Scarpas, 1992], Erkens et al. [2002] were able to define the highly non-linear fracturing force-displacement response of SCB specimens. They point out that using elastic models, the absence of softening renders the response of the linear elastic material several times higher than that of the asphaltic material. For this reason, the finite element solutions presented in Equations 6.3 and 6.4 are subject to error since they have been derived using elastic response modelling.

This argument was taken further by Molenaar et al. [2002] who point out that because of the very complex stress state in an SCB specimen under loading it will be very difficult to determine parameters like tensile strength and modulus from test results. They indicate that the strain rates are not constant over the height of the specimen even under a constant vertical displacement rate typically used for splitting tests. This is a critical disadvantage of the SCB test since the modulus of HMA is not

only dependent on the temperature but also on the strain rate (the dependency on loading time is in fact a dependency on strain rate). Based on a CAPA-3D analysis using a strain dependent material model, Molenaar et al. [2002] indicated that the use of Equation 6.3 estimated a tensile strength for a material that was twice the real tensile strength. They conclude that the SCB can be a very useful test in mix design and for QA/QC purposes provided that a parametric analysis be performed to support the evaluation of the SCB results.

In light of these observations it was decided to re-evaluate the SCB test using an alternative FEM approach to explore the influence of non-linearity. Time limitations did not warrant the use of the non-linear material model implemented by Molenaar et al. [2002]. For this reason a finite element model of the SCB was developed using a quasi-isotropic material model but imposing non-linearity in terms of tension and compression stiffness response and accounting for tensile and compressive failure. This section discusses the development of this model and the approach used towards better definition of material parameters obtained using the SCB.

6.4.1 CAPA-3D finite element model

As a first step, an SCB model was developed for use with the CAPA-3D finite element system. Figure 6.20 illustrates the finite element model.

The model consists of different sections: the (asphalt) core, the (steel) loading head and support and interfaces between the loading head and support and the core. The asphalt and steel parts are modelled using 20-noded parabolic brick elements whereas the interface is modelled using special interface elements to control the transfer of frictional forces between the loading head and support and the core. This is achieved by controlling the stiffness of the interface element in three directions. The loading head was made longer than usual to ensure a uniform transfer of loading onto the

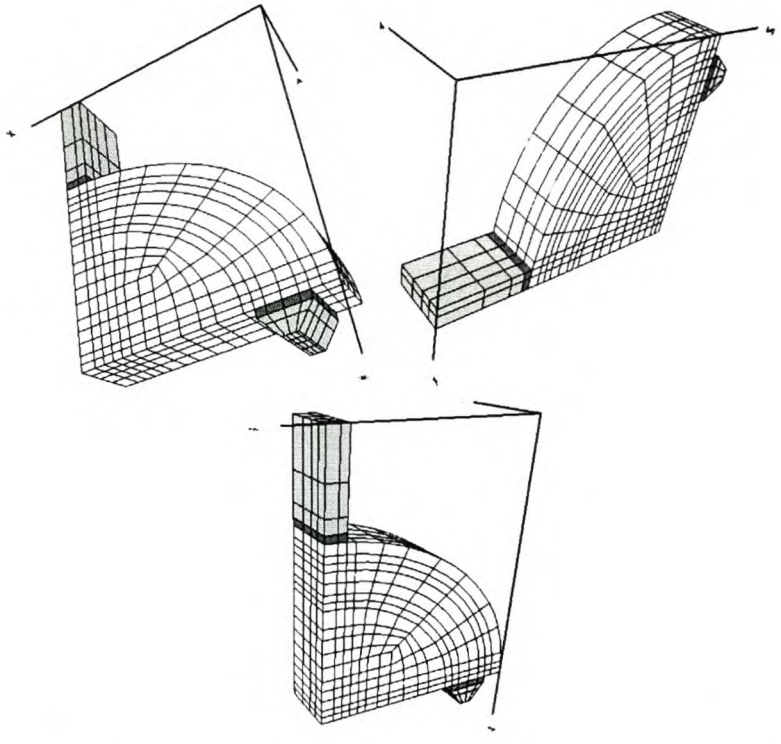

Figure 6.20: CAPA 3-D finite element model of the SCB

core. The diameter of the model is 100 mm and the support width is 10 mm. The support was placed such that it was 5 mm from the edge of the specimen. Symmetry is used in the x (length) and y (width) directions so that only one quarter of the SCB needed to be modelled. The width of the symmetrical model was set at 15 mm i.e. 30 mm total thickness. The support was constrained to allow translation movement in the x direction only and rotation about the y direction. The model consists of 820 elements of which 740 make up the asphalt core. The loading head and support were modelled as isotropic materials having a stiffness of 206 GPa and a Poisson's ratio of 0.3. The core elements were also modelled using isotropic materials although each element was given a unique material property. The reason for this approach will be discussed shortly. The SCB model, including the core, loading head, support and interface elements therefore consisted of 742 materials.

6.4.2 Tension and compression stiffness response

Figure 6.21 shows the horizontal strains that develop in an SCB specimen under loading. The shaded area beneath the loading head is in compression and the unshaded area is in tension. The grayed area represents the neutral axis dividing the compression and tension zones. The SCB specimen is therefore partly in compression and partly in tension and one can expect different material behaviour in these zones. Given this difference it was deemed necessary to use different modulus values in tension and compression in the analysis of the SCB.

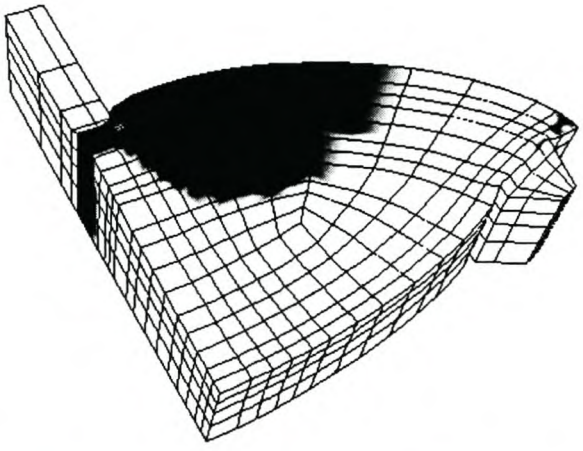

Figure 6.21: Horizontal strains in an SCB specimen under loading

Khanal and Mamlouk [1997] studied the tension and compressive nature of flexible pavements under rolling wheel loads using bimodular analysis. They suggest that the compressive and tensile modulus depends on temperature and used the values as given in Table 6.6 for their analyses. They also assumed Poisson's ratio to be the same in both tension and compression.

A strategy was required to account for the influence of compressive and tension moduli on SCB response. Unfortunately, no test data on mixes tested with the SCB

Table 6.6: Compressive and tensile moduli of asphalt concrete for bimodular analysis (after Khanal and Mamlouk [1997])

Temperature level	**Compressive modulus, GPa**	**Tensile modulus, GPa**
25 °C	6.90	4.13
40 °C	1.72	0.62

were readily available to implement this strategy. For this reason it was decided to make use of existing data, albeit from tests on mixes not previously tested with the SCB. Molenaar [1983] performed tensile and compressive tests on various asphalt mixes. These tests were done at 4 different temperatures i.e. 5 °C, 15 °C, 25 °C and 35 °C. Using the test results, the author was able to derive master curves of tension and compression modulus values obtained at the different test temperatures for the different mixes based on a Arrhenius type equation [Francken and Clauwaert, 1987]:

$$\log(\alpha_T) = \frac{0.4343\Delta H}{R}\left(\frac{1}{T} - \frac{1}{T_s}\right) \tag{6.7}$$

where

ΔH = Apparent activation energy (in the order of 50 kcal/mole = 210 kJ/mole),

R = Universal gas constant (8.27 J/mole/K)

T = Test temperature, Kelvin

T_s = Reference temperature, Kelvin.

Figures 6.22 and 6.23 show the tension and compression master curves determined for one of the mixes, a continuously graded dense asphalt concrete surfacing mix, at two temperatures i.e. 15 °C and 25 °C respectively. The gradation of this particular mix is shown in Figure 6.24 together with the Fuller gradation. By mass of aggregate, the mix was composed of crushed gravel (57%), riversand (9%), crushed riversand

(26%) and filler (8%). By mass of total mix, the mix contained a binder content of 6.4 percent of 80/100 pen bitumen. The mean void content of tested specimens was 4.4 percent.

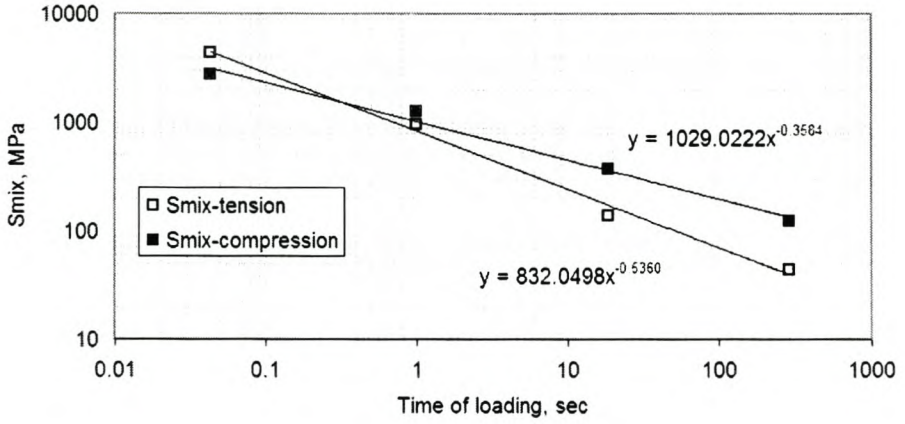

Figure 6.22: Master curves for tension and compression stiffness at 15 °C

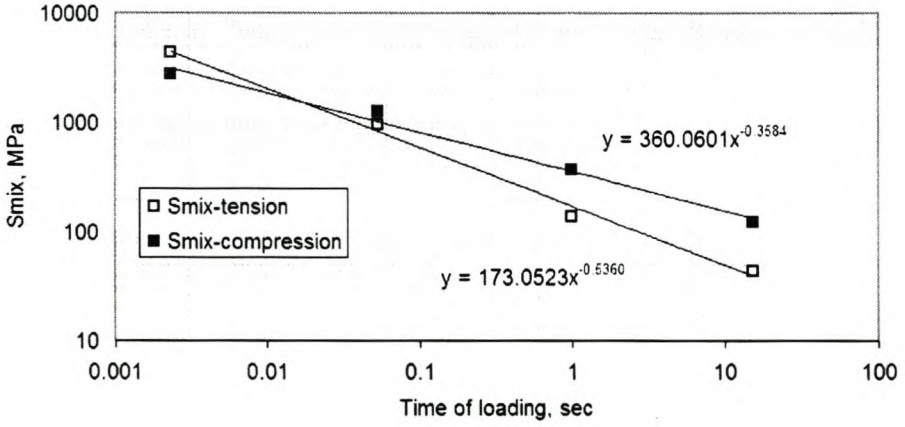

Figure 6.23: Master curves for tension and compression stiffness at 25 °C

A comparison of the master curve figures indicates that the difference between the tension and compressive moduli increases with an increase in temperature at a specific frequency or time of loading, as expected. At lower temperatures one could

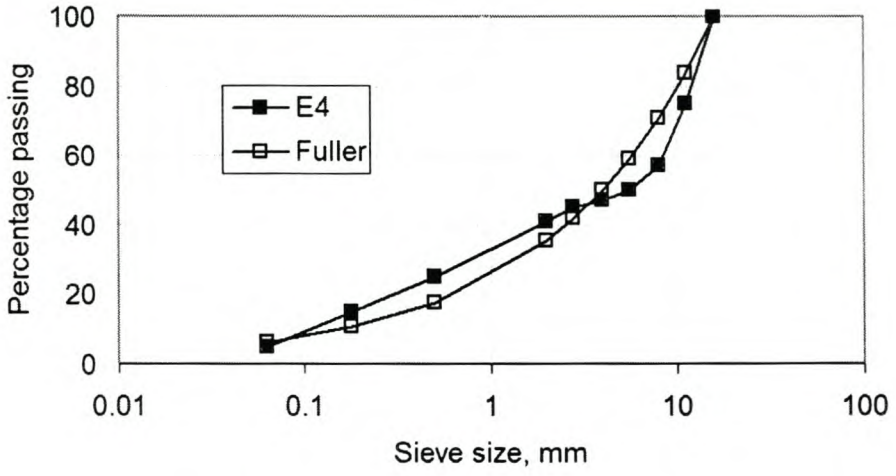

Figure 6.24: Gradation of reference mix

expect similar tension and compression moduli. A temperature of 15 °C was used in the analyses that follow.

Given the different regions of compression and tension within an SCB specimen under loading it was necessary to develop a model that would allow bimodular assignment. One option considered was to identify general regions within an SCB specimen with similar stress response and assign to these similar material properties. This would have limited the number of materials needed for modelling but at the same time would severly restrict the range of moduli that could be applied since it would be necessary to average moduli over a particular region. To over come this limitation it was decided to assign each element comprising the asphalt core a unique material property. Preliminary FEM analyses were done to determine appropriate element sizes to allow an accurate response within a reasonable processing time. Poisson's ratios of 0.35 were assigned to the core elements.

Having divided the asphalt core into 740 seperate elements, using the master curves it was possible to assign moduli values to the different elements depending on the frequency of loading within an element or indeed the strain rate within that

element. The SCB splitting test is typically a displacement controlled test. The test may be done using a Marshall press with a displacement rate of 50.8 mm/minute or 0.847 mm/s. CAPA-3D allows stresses and strains within an SCB specimen to be calculated after a given time interval at a specific displacement of the loading head. These stresses and strains are calculated in the three global directions x, y and z. By dividing the strain in any element by the rate of loading within that element one is able to calculate an effective strain rate for that element. So, for example, using the Marshall speed displacement rate of 0.847 mm/s, after 0.05 seconds the displacement of the loading head is 0.0424 mm. This causes the development of stresses and strains within the specimen in the three global directions. Dividing the CAPA-3D calculated strain in a element by the time (0.05 seconds) one is able to determine the strain rate within that element.

Having calculated the strain rate within an element the next step was to assign a stiffness to the element based on this strain rate. Since master curves were available to determine the modulus of an element depending on whether it was in tension or compression a procedure was required to calculate the time of loading within the element. There was no way to calculate this time of loading other than to assume an "apparent" loading time calculated using the follow equation:

$$t_i = \frac{\sigma_i}{\dot{\varepsilon}_i \cdot E_i} \tag{6.8}$$

where

t_i = Apparent time of loading in global direction i, sec

σ_i = Normal stress in global direction i, MPa

$\dot{\varepsilon}_i$ = Strain rate in global direction i, s^{-}1

E_i = Modulus in global direction i, MPa

i = x, y or z global directions.

The term "apparent" is used since the element's response to the imposed strain

rate would depend on the modulus of the element at any particular moment. The modulus at the same time is a function of the imposed strain rate and would change as the strain rate changes. This is the complex nature of strain dependant materials. To account for this it was necessary to apply an iterative procedure that would take into account the changing strain rates in an element, adjust the moduli depending on the strain rate, recalculate the strain rate based on the adjusted moduli and so on until a stable condition was reached when subsequent changes in moduli were small.

Having calculated the apparent time of loading within an element, the modulus of the element may be determined using the master curves depending on whether the element is in tension or compression. Given that CAPA-3D calculates stresses and strains in the three global directions it would appear to be feasible to apply an anisotropic material model that allows definition of element moduli in the three global directions, since these may be calculated given the strain rates in the three global directions. Unfortunately this approach was not possible given that the Poisson's ratios in the three directions are required and that these are not necessarily the same to satisfy the laws of thermodynamics.

Given this restriction, isotropic material models had to be used for the elements in the CAPA-3D analyses. The problem, however, was assigning a stiffness to the element since strain rates were available in the three global directions. One option considered was to calculate a "resultant" stiffness based on the moduli in the three directions determined from strain rates in these directions as shown below:

$$E_R = \sqrt{E_X^2 + E_y^2 + E_Z^2} \tag{6.9}$$

Another option was be to assume that the material takes on one of the stiffnesses in either of the three global directions. To evaluate these assumptions, analyses were run to determine the best approach. Before this is reported, however, it is necessary to outline the procedure used in the CAPA-3D analyses.

6.4.3 CAPA-3D FEM analyses

As mentioned, the approach used to evaluate the SCB using CAPA-3D involved an iterative procedure. A load or force was applied to a node on the loading head at a constant displacement rate of 0.847 mm/s in time increments of 0.05 s. CAPA-3D allows prescribed displacements of nodes and calculates the nodal force given this displacement. Each time increment represented a time step. Within each time step, multiple runs were done to ensure that a stable stress/strain condition had been reached within the specimen. This procedure is best explained with reference to Figure 6.25.

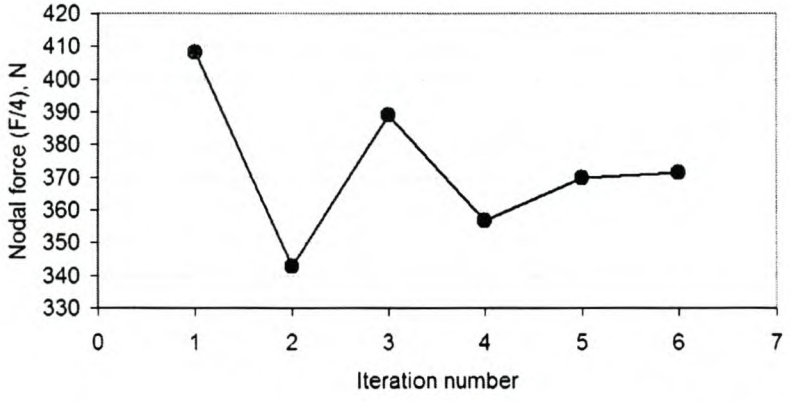

Figure 6.25: Convergence of applied load during CAPA-3D analyses

The figure shows how the nodal force converges with iteration. Consider a time step of 0.05 s. The displacement of the loading head after this time interval is 0.847*0.05=0.0423 mm. The nodal force required to ensure this displacement will depend on the moduli of the core elements, which in turn depend on the strain rates within the elements. From Figure 6.25 it can be seen that after the first run, the nodal force to achieve the imposed displacement was on the high side. It resulted in a rearrangement of the element moduli so that with next run a lower nodal force was

required and so on until the nodal force required converged after 6 runs. After convergence the next time step was imposed i.e. 0.1 s with a corresponding displacement of 0.847*0.1=0.0847 mm and the iterative procedure repeated. Instead of the nodal force, convergence could also habe been monitored by checking the change in moduli of the elements.

During each iteration run, possible tensile or compressive failure of the core elements was tested using the following equations that respectively present compressive (f_c) and tensile (f_t) strengths of asphalt materials as a function of strain rate and test temperature Erkens [2002]:

$$f_c = -108\left(1 - \frac{1}{1 + \left[\dot{\varepsilon} \cdot e^{\left(-86.3 + \frac{24260}{T}\right)}\right]^{0.32}}\right) \tag{6.10}$$

$$f_t = 5.5\left(1 - \frac{1}{\left(1 + \dot{\varepsilon}\left[e^{\left(-80.2 + \frac{25050}{T}\right)}\right]^{0.86}\right)}\right) \tag{6.11}$$

These equations were developed based on regression analyses of data from uniaxial compression and tensile tests on a variety of asphalt mixes although not on the same mix for which the master curves shown in Figures 6.22 and 6.23 for tension and compression stiffness were developed. No specific tensile or compressive strength relationships were available for this specific mix. It was assumed that the mix used in the analyses would have similar tension and compressive strength charactersitics compared to those from which Equations 6.10 and 6.11 were developed. There was no evidence to justify this assumption. However, given that the aim of the FEM analyses was towards a better characterisation of SCB response rather than the solution to the problem, the assumption was deemed feasible.

If the compressive or tensile stresses within an element exceeded the strengths calculated using the aforementioned equations, a very low modulus was assigned to the failed (damaged) element i.e. 1 MPa, simulating the initiation of "crack" growth.

With failure of the elements, a lower nodal force was required to achieve the imposed displacement. Damaged elements were assigned at the end of a time step i.e. after convergence, before the beginning of a subsequent time step.

The uncertainty of assigning moduli based on strain rates in any particular direction or using "resultant" moduli based on Equation 6.9 was evaluated as part of trial FEM analyses. It was found that if Equation 6.9 was used to assign element moduli the model would fail prematurely after only a single time step. This was not deemed realistic and for this reason seperate analyses were done by assigning element moduli based on strain rates in the horizontal and vertical directions respectively. Resulting force-displacement curves are shown in Figures 6.26 and 6.27 based on these analyses. Figure 6.26 represents the model response when assigning moduli based on horizontal strain rates and Figure 6.27 when moduli were assigned based on vertical strain rates.

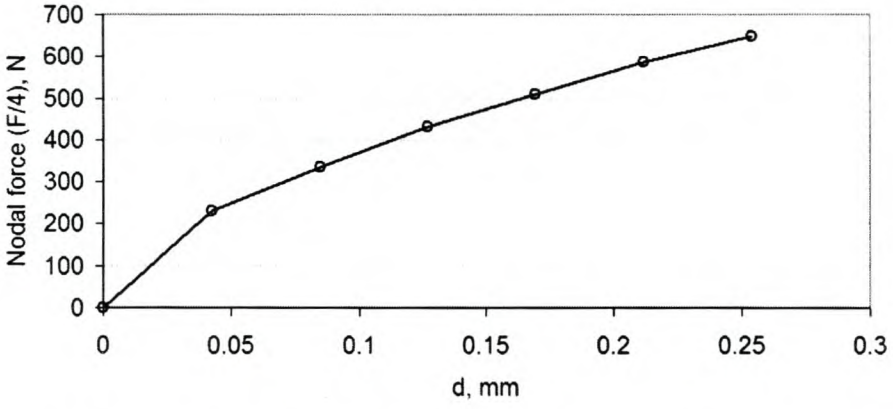

Figure 6.26: CAPA-3D SCB force-displacement response using moduli assigned based on horizontal strain rates

Damage in the SCB specimen after specific time steps are shown in Figure 6.28 through 6.33 (represented as grayed elements) when assigning moduli based on the horizontal strain rates and Figures 6.34 and 6.35 based on moduli determined from vertical strain rates.

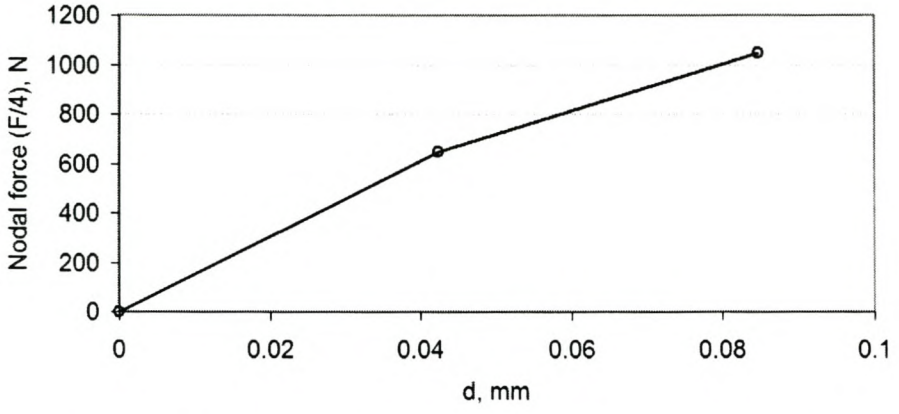

Figure 6.27: CAPA-3D SCB force-displacement response using moduli assigned based on vertical strain rates

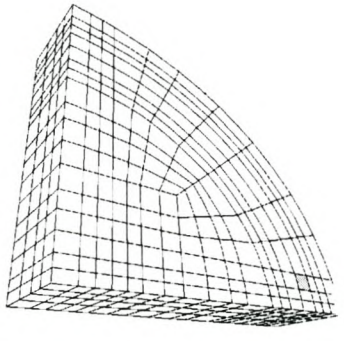

Figure 6.28: Damage after time step 2 using horizontal moduli

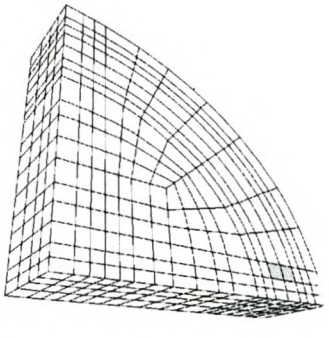

Figure 6.29: Damage after time step 3 using horizontal moduli

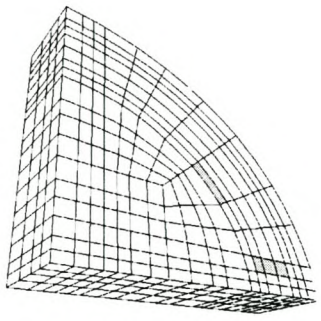

Figure 6.30: Damage after time step 4 using horizontal moduli

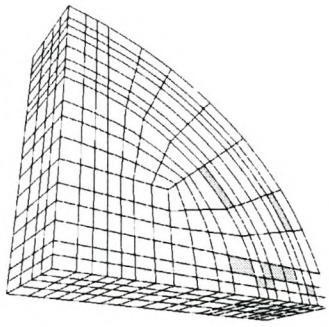

Figure 6.31: Damage after time step 5 using horizontal moduli

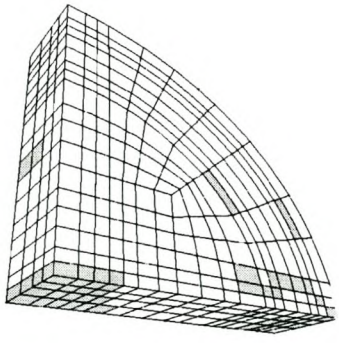

Figure 6.32: Damage after time step 6 using horizontal moduli

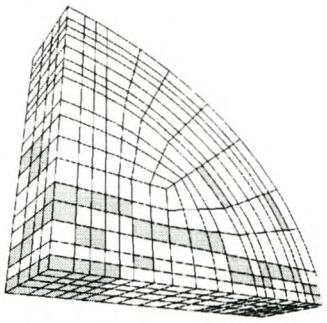

Figure 6.33: Damage after time step 7 using horizontal moduli

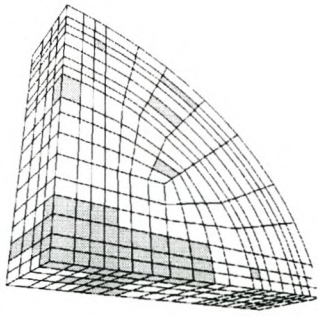

Figure 6.34: Damage after time step 1 using vertical moduli

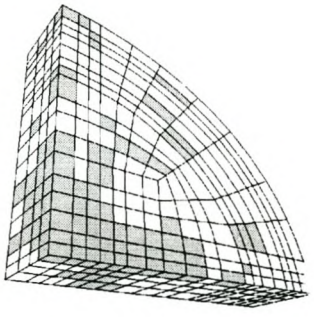

Figure 6.35: Damage after time step 2 using vertical moduli

6.4.4 Discussion of the CAPA-3D finite element analyses

From the force-displacement curves and the figures indicating damage it can be seen that the response of the model is vastly different depending on whether moduli are assigned based on horizontal or vertical strain rates. This is a shortcoming of the approach adopted and the material model assumed. Applying moduli based on horizontal strain rates generally resulted in lower moduli than those based on vertical strain rates. It is encouraging, however, to note that the force-displacement curves are non-linear, resulting from the application of different moduli depending on whether the elements were in tension or compression, but also accounting for the influence of damage.

The non-linear force-displacement curves shown in Figures 6.26 and 6.27 indicate response only up until a specific displacement and do not have a turning point characteristic of curves measured during actual SCB tests at ambient temperatures (as shown in Figure 6.13). The reason for this is that at these displacements too many elements comprising the model were damaged such that it could no longer sustain the applied load. This happened more rapidly when applying moduli based on vertical strain rates.

From the figures showing element damage it can be seen that applying moduli based on horizontal strain rates indicated that initial damage occurred in the vicinity of the support. It was only after the sixth time step that tensile damage was evident at the centre point of the specimen where cracking is usually evident in the SCB test. With the analyses of the model using moduli based on vertical strain rates, however, the damage at the centre of the specimen was evident even after the first time step.

The maximum force at "failure" for the two cases investigated are 2600 N and 4200 N respectively. These forces are considerable lower than typical failure loads encountered during SCB testing (see Figure 6.13). This indicates that the CAPA-3D

approaches adopted in the assessment of the SCB were particularly severe and that damage would not necessarily have occurred as assumed. Clearly both approaches investigated give unrealistic material responses and one cannot conclude that one is better than the other given the various assumptions imposed. It does not appear even that the response one would expect could be derived somewhere between that determined for the two approaches investigated, but then this was not the aim of the investigation.

The procedure adopted does, however, allow an assessment of the tensile strength of the asphalt mix evaluated. At the point of failure, the tensile strengths calculated using Equation 6.10 for the two approaches investigated were 2.8 MPa and 3.0 MPa respectively. Tensile strengths calculated using the failure loads and the original tensile strength Equation 6.3 based on linear analysis are 3.7 MPa and 6.0 MPa respectively. Based on these observations it must be concluded that the non-linear approach used to characterise the response of the SCB allowed a more realistic assessment of tensile strength compared to the linear elastic analysis.

Finally, it must be emphasised that the tensile strengths calculated using Equation 6.3 based on linear-elastic FEM analyses will give unrealistically high tensile strengths for materials tested using the SCB and the reader is discouraged from using this equation. This does not mean that the SCB cannot be used to evaluate the strength characteristics of HMA materials. Given that tensile strength is an intrinsic material property, strength tests may be done on a particular mix using tests such as the uniaxial tensile test that allow a more accurate assessment of tensile strength. Results of these tests may then be compared to results of SCB tests on the same mixes to derive equations for SCB strength determinations. This approach is somewhat empirical. The non-linear approaches adopted as part of the CAPA-3D analyses indicated an improvement over previous linear-elastic analyses even though broad assumptions were applied. The analyses further indicated that the stress/strain response in the

SCB under loading is particularly complex given the geometry of the structure. The approach used may be further refined to allow a more accurate assessment of SCB response. Smaller finite elements may be used to limit the influence of damage and a better approach for assigning element moduli could be adopted. One could even use different master curves to adjust the force-displacement curves such that they correspond to those of actual SCB tests. The problem remains, however, that it is unrealistic to model fracture response in the SCB using linear isotropic materials and further research along the lines adopted by Erkens et al. [2002] should be preferably be implemented. The benefits to be gained from using the SCB to evaluate the strength and fatigue properties of HMA materials warrant this research.

6.5 Summary

The chapter discusses the development of the SCB configuration. Special consideration should be given to the support structure to limit the development of horizontal stresses within SCB specimens under loading.

The advantages of the SCB over the ITS are discussed. Intense stress localisation within SCB specimens under loading as well as uniaxial states of stress may allow better characterisation of the tensile strength of HMA mixes compared to ITS tests.

Finite element methods using linear elastic approaches were used to develop analytical solutions for the three point loading stress/strain response on semi-cylindrical specimens. 3-D finite element models were used to determine the influence of specimen thickness and Poisson's ratio. It was found that the influence of specimen thickness on stress, strain and deflection response is limited although to reduce the influence of Poisson's ratio it is better to test specimens with thicknesses less than 30 mm.

Stiffness measurements using the SCB may best be done using strain gauges attached to specimens. FEM indicated a fairly uniform distribution of horizontal tensile

stress along the principal axis. This method of stiffness measurement for the SCB may be more practical than conventional methods since the magnitude of vertical deflection is limited and the translation and rotation of the bearing supports under loading must also be accounted for.

Based on linear elastic FEM analyses, the dissertation presents equations to calculate the tensile strengths and moduli of materials tested using the SCB. It must be emphasized that these equations do not provide a realistic assessment of the strengths or moduli of asphaltic materials. The strengths and moduli of HMA materials are influenced by strain rates within the materials that cannot be assessed using a simple linear approach. To address this, alternative non-linear FEM analyses using CAPA-3D were undertaken. An approach was adopted to account for the influence of tensile and compressive strain rates on modulus. The analyses made use of a quasi-isotropic material model and it was shown to better characterise the strengths of HMA materials using the SCB. It is recommended, however, that further research be done using non-linear material modelling to evaluate the very complex stress/strain conditions within an SCB specimen to better characterise fracture response.

6.6 References

ABAQUS. *ABAQUS Users manual.* Hibbit, Karlsson and Sorenson, Inc., Pawtucket, R.I., 1996.

W. Arand. Neue uberlegungen von anwendbarkeit des spaltversuches auf asphalte - new considerations regarding the suitability of the indirect tensile test for asphalt (german). *Die Asphaltstrasse*, Vol. 6/90, 1990.

F. Bonnaure, A. Gravois, and J. Udron. A new method for predicting the fatigue life of bituminous mixes. *Proceedings of the Association of Asphalt Paving Technologists*,

Vol. 49, 1980.

M. Butcher, H. van Loon, and T. Clark. Fracture testing of asphalt using the SCB test in South Australia. *AAPA Pavements Industry Conference, Surfers Paradise, Queensland, Australia*, 1998.

CSRA. *TRH8: Selection and design of hot-mix asphalt surfacing for highways.* Committee of State Road Authorities, Pretoria, South Africa, 1987.

S. M. J. G. Erkens. *Asphalt Concrete Response (ACRe) - Determination, Modelling and Prediction.* PhD thesis, Technical University of Delft, Delft, The Netherlands, 2002.

S. M. J. G. Erkens, X. Liu, A. Scarpas, A. A. A. Molenaar, and J. Blaauwendraad. Asphalt concrete response: Experimental determination of finite element implementation. *ISAP*, 2002.

L. Francken and C. Clauwaert. Characterization and structural assessment of bound materials for flexible road structures. *Proceedings Sixth International Conference on the Structural Design of Asphalt Pavements, Ann Arbor, Michigan*, 1987.

W. Heukelom. Observations on the rheology and fracture of bitumens and asphalt mixes. *Proceedings of the Association of Asphalt Paving Technologists*, Vol. 35, 1966.

F. Hugo, M. F. C. van de Ven, and A. D. F. Smit. N2 north coast contracts investigation: LAMBs. a limited comparative study between Hugo hammer and Superpave gyratory compactor. Prepared for Sabita, Institute for Transport Technology, University of Stellenbosch, 1996.

P. P. Khanal and M. S. Mamlouk. Program BIMODPAV for analysis of flexible pavements. *Journal of Transportation Engineering, American Society of Civil Engineering*, Vol. 123, No. 1, 1997.

R. L. Krans, F. Tolman, and M. van de Ven. Semi-circular bending test: a practical crack growth test using asphalt concrete cores. *Third International RILEM Conference on reflective cracking in pavements, Maastricht*, 1996.

I. L. Lim, I. W. Johnston ans S. K. Choi, and J. N. Boland. Fracture testing of a soft rock with semi-circular specimens under three-point bending. *International Journal of Rock Mechanics, Mineral Science and Geomechanics*, Vol. 31, 1994.

A. A. A. Molenaar. *Structural Performance and Design of Flexible Road Constructions and Asphalt Concrete Overlays.* PhD thesis, Technical University of Delft, Delft, The Netherlands, 1983.

A. A. A. Molenaar, A. Scarpas, X. Liu, and S. M. J. G. Erkens. Semi-circular bending test; simple but useful? *Presented at the Symposium of the Association of Asphalt Paving Technologists, Colorado Springs, Colorado*, 2002.

B. W. Porter and T. W. Kennedy. Comparison of fatigue test methods for asphaltic materials. CFHR 3-9-72-183-4, University of Texas at Austin, 1975.

SABITA. *LAMBs - The Design and Use of Large Aggregate Mixes for Bases.* Southern African Bitumen and Tar Association, Cape Town, 2 edition, 1997.

A. Scarpas. *CAPA-3D Finite Element System User's Manual, Parts I, II and III.* Department of Structural Mechanics, Faculty of Civil Engineering, Delft University of Technology, Delft, The Netherlands, 1992.

SHELL. *Shell pavement design manual and addendum.* SHELL International Petroleum Company Limited, Shell Ltd., London, 1985.

A. D. F. Smit, M. F. C. Van de Ven, and E. Fletcher. Towards the use of the semi-circular bending test as a performance related specification test. *South African Transport Conference, Johannesburg*, Transport Infrastructure 2, Vol. 3A, 1997.

A. D. F. Smit, M. F. C. van de Ven, and M. Henderson. The fatigue characteristics of a large aggregate asphalt base mixture. *South African Transport Conference, Pretoria*, Transport Infrastructure 2, Vol. 2D, 1998.

F. Tolman and A. Versluis. Ontwilleling SCB opstelling - Development of the SCB configuration (in Dutch). *Unpublished report, Road and Hydraulic Engineering Division, Ministry of Transport and Public Works, Delft, Netherlands*, 1996.

M. F. C. van de Ven and C. C. Montauban. Influence of creep on fatigue performance in the three point bending test, in Dutch. *Wegbouwkundige Werkdagen, CROW*, 1994.

M. F. C. van de Ven, A. D. F. Smit, and R. L. Krans. Possibilities of a semi-circular bending test. *Proceedings of the Eighth International Conference on Asphalt Pavements, Seattle*, Vol. 2, 1997.

Chapter 7

Conclusions and recommendations

The final product of the dissertation is PAVDAM, a model for the Probabilistic and Volumetric Design of Asphalt Mixes. The model addresses the volumetric design of HMA. A probabilistic approach is adopted to account for variabilities associated with the design of these mixes, particularly during the manufacturing stage. Central to the volumetric definition of HMA mixes was the development of a packing model incorporated within PAVDAM to estimate the VMA of these mixes based on gradation, porosities of the aggregate fractions making up the gradation and properties of the mix components. PAVDAM may be implemented as a subset of the volumetric optimisation stage forming part of existing mix design and analysis systems. It may serve as a tool to evaluate the reliability of candidate design mixes before performance analysis and optimisation.

The following objectives were established for the development of PAVDAM and the chapters in the dissertation in which these are addressed:

1. Understand the different philosophies underlying the design of asphalt mixes (Chapter 2).

2. Evaluate and develop accurate packing models to estimate the VMA of asphalt mixes (Chapter 3).

3. Identify the variabilities of factors influencing the mix design process (Chapter

4).

4. Develop procedures to account for the variabilities of these factors (Chapter 4).

5. Combine the packing model and probabilistic procedures to address variability within a single model, the Probabilistic and Volumetric Design of Asphalt Mixes or PAVDAM (Chapter 4).

6. Demonstrate the use of PAVDAM, including calibration thereof (Chapters 4 and 5).

7. Validate PAVDAM (Chapter 5).

Also included in the dissertation is a discussion on the development of the semi-circular bending (SCB) test. This test is proposed as a possible replacement to the indirect tensile test (ITS) for the performance evaluation and/or quality control of HMA. In the evaluation of the SCB, finite element analysis were done towards characterisation of the complex stress and strain conditions within this test during monotonic displacement controlled loading. In addition, accelerated pavement testing (APT) using the MMLS3 on selected sections at the NCAT test track are discussed for the purpose of validating PAVDAM.

7.1 Conclusions

7.1.1 HMA mix design

The dissertation presents a general overview of HMA mix design which serves as a literature review towards an understanding of the philosophies underlying the design of HMA. HMA mix design is a multi-stage process. Management of this process is required for optimisation. PAVDAM, as a tool, can assist in the management of aspects of this process, particularly during the volumetric optimisation stage. The effective

use of PAVDAM requires a knowledge base of material properties for definition of the variabilities influencing the volumetric properties of HMA.

To relate laboratory compaction to field densification, PAVDAM uses the Superpave N-design table. This allows volumetric definition of HMA at different design levels depending on the design traffic class. The Superpave N-design table is based on gyratory compaction effort. Underlying the table is the controversial assumption that laboratory compaction may be related to field densification given the obvious differences associated with the compaction of HMA in the laboratory compared to that in the field. Indications are that it is possible to establish these relationships or at least indices for continuous or open graded type mixes with sand-stone or stone-stone aggregate skeletons, in which the major component resisting compaction is the aggregate. One of the shortcomings of the N-design table, however, is that the compaction efforts associated for the different design traffic classes are the same regardless of mix type, aggregate structure or binder content. This was illustrated in the dissertation by comparing densification in the field of the different NCAT sections tested using the MMLS3 with compaction of the field mixes in the laboratory using the Superpave gyratory compactor. Results indicated extreme differences for mixes even with similar gradations.

There are two analytical approaches in asphalt mix design to determine the optimum binder content of a mix. The first considers the minimum VMA in the aggregate skeleton of a mix and the volume of binder or mastic required to fill it. The second approach considers the minimum film thickness required to coat the aggregate. PAVDAM was developed around the first approach. Both approaches aim to ensure the durability of HMA mixes i.e. to limit excessive ageing of the mix by limiting the volume of voids and binder. Volumetric mix design criteria regarding voids in the mix (VIM), voids in the mineral aggregate (VMA) and voids filled with binder (VFB) are

generally established to assist with the design of mixes based on the existing knowledge of which mixes work and which don't but also to establish specifications by which agencies may judge the quality of mixes. It was shown that these criteria may be restrictive. For example, it has been reported that coarse graded Superpave mixes (with gradations significantly below the restricted zone), if designed with the minimum VMA criteria based on nominal maximum aggregate size, could result in mixes with very thick binder film because these mixes have relatively lower surface area.

The significant influence of filler-binder interaction on the durability and workability of asphalt mixes must be addressed in mix design procedures. A critical parameter in mix design, the filler content, will define this interaction. Consideration of filler-binder interaction allows either the filler content or the binder content of a mix to be fixed. This interaction may be evaluated using viscosity measurements or softening point tests on mortars with varying percentages of bulk volume of filler.

7.1.2 Aggregate packing

PAVDAM includes a packing model for estimating the VMA of a mix based on its gradation. Having defined the VMA it is possible to establish binder contents for the mix to achieve desired voids in the mix at specific compaction levels. The dissertation discusses a number of packing models based on the successive combination of binary systems i.e. individual aggregate fractions of different sizes. The advantages and disadvantages of these are outlined.

A modified Aim and Toufar (MAT) packing model was selected for inclusion in PAVDAM. This model is used in the concrete industry for optimising the packing of aggregates from blends of stockpiles. The model is based on the theory of the packing of spheres. The Aim packing model is considered more accurate than the Toufar model for size ratios less than 0.22. At this size ratio, the fine fraction fits

within the interstices of the coarser fraction. These models were modified to make them more applicable for use in estimating the VMA of HMA mixes. A probabilistic approach used in the Belgian Road Research Centre's PRADO packing model was used in the MAT packing model to better characterise the influence of size ratio on packing estimates. Application of the model requires a mix gradation, porosities of individual fractions making up the gradation and voids in filler (Rigden voids). Porosities of the individual fractions may be determined by dry gyratory compaction. This compaction characteristic is used by PAVDAM to characterise to an extent the influence of compaction on particle porosity.

The VMA of a mix is difficult to estimate accurately since it is difficult to quantify the factors influencing VMA such as gradation, particle shape, angularity, texture and rugosity. Furthermore, the influence of binder content and compaction must be taken into account. The MAT packing model underestimates the VMA of mixes compared to measured values. For this reason it is necessary to calibrate the model to allow more accurate estimations.

7.1.3 PAVDAM

PAVDAM was developed to account for the variabilities associated with the manufacture of asphalt mixes during mix design. An understanding of this variability becomes increasing important with the industry trend towards the implementation of end result and performance related specifications.

PAVDAM input parameters required include the design traffic level, desired air voids and the associated compaction level. These criteria establish the range of acceptable binder contents. Additional parameters required include statistical properties (means and standard deviations) of the mix components i.e. gradation, porosities

of the individual fractions making up the gradation, bulk relative densities of the aggregate and binder, binder absorption and voids in the filler. Monte Carlo simulation is used to sample representative values for the various material properties assuming that these are normally distributed and defined by a mean and standard deviation. Binder contents are estimated to balance the spatial composition of the mix using volumetric algorithms. The statistical parameters required may be got through laboratory management programmes. For the case studies evaluated as part of the dissertation, parameters applied in product specifications were adopted. Given the nature of the random sampling routine applied as part of the Monte Carlo simulation algorithm, PAVDAM is only really applicable for the evaluation of continuously graded HMA mixes.

PAVDAM can only be effective if it is used in a mix design management system, which closely monitors variability and continually refines estimates based on actual measurements. The benefits of PAVDAM may be summarised as follows:

- The spatial composition of asphalt mixes may be defined.
- The influence of mix component variability may be addressed.
- Changes in the volumetric properties of asphalt mixes may be investigated.
- The influence of changes in mix properties may be evaluated.
- Reliability assessments of candidate gradations during volumetric optimisation are possible.

7.1.4 PAVDAM application, calibration and validation

The dissertation presents different examples to describe the application of PAVDAM. In one case study, PAVDAM was used to evaluate Marshall mix designs of two large

aggregate base mixes. In another, PAVDAM is used to evaluate mixes used on sections of the NCAT test track, which were tested with the MMLS3.

The dissertation outlines two procedures that may be used for calibration. The first makes use of a single calibration factor whereas the second is a more effective approach to better relate PAVDAM estimated and measured VMA. In the latter approach it is necessary to gyratory compact an asphalt mix (evaluated using PAVDAM) at a binder content estimated using PAVDAM without the use of calibration factors. Having done this, the PAVDAM estimated VMA is compared to the measured VMA at different compaction levels to establish appropriate calibration factors.

In order to validate the PAVDAM model, analyses were done to determine the reliability of each of the NCAT MMLS3 test section mixes in terms of densification in the field. PAVDAM estimated binder contents were determined for each of the section mixes to achieve 4 percent VIM at the design traffic level i.e. 10 million ESALs. Since PAVDAM estimates are based on the gyratory compaction characteristics of mixes, it was necessary to compare densification of the section mixes in the gyratory compactor and in the field to allow a more realistic evaluation of field densification. An analysis of field densification data allowed relationships to be established for each of the section mixes between gyratory compaction and applied ESALs. A comparison of PAVDAM estimated and field binder contents allowed a ranking of the reliabilities of the different section mixes to achieve 4 percent VIM at the design traffic level. This ranking compared favourably with that obtained from an analysis of actual densification trends monitored in the field under full-scale trafficking.

7.1.5 The semi-circular bending (SCB) test

The SCB test was developed as an alternative to the indirect tensile test (ITS) to determine the tensile strength properties of HMA mixes. The test is relatively simple

and can be done on cores or briquettes produced during a manufacturing or design process for quality control or performance evaluation.

Unlike the ITS, a uniaxial state of stress is apparent within a loaded SCB specimen at the point of maximum tensile stress. Specimens fail under tension due to significant localisation of (tensile) strains resulting in "intense localisation of cracking" along the diameter of the SCB specimen. Given this localisation effect, the SCB will probably result in more reliable indications of "tensile-type" failure than the ITS. In the ITS this effect is less pronounced and a lot of energy is spent in causing compressive failure in the loading area and support. In the SCB it appears that most of the energy is spent in splitting the specimen.

The dissertation discusses the SCB test configuration. Special attention must be given to support and roller assembly to minimise the development of horizontal stresses within SCB specimen during testing. The vertical distance from the point the support touches the specimen to the centre point of support rotation has a significant influence on the development of horizontal stresses.

Finite element analyses were done to characterise the tensile strength and moduli properties of HMA specimens tested using the SCB. This was necessary given that, unlike the ITS, there is no simple analytical solution for the three-point loading stress-strain response on semi-cylindrical specimens. 3-D finite element models were used to determine the influence of specimen thickness and Poisson's ratio. It was found that the influence of specimen thickness on stress, strain and deflection response is limited although to reduce the influence of Poisson's ratio it is better to test specimens with thicknesses less than 30 mm. Initial FEM analyses using linear elastic isotropic modelling allowed the development of equations to characterise the tensile strength and modulus characteristic of specimens tested using the SCB.

It was emphasized that these equations do not provide a realistic assessment of the strengths or moduli of asphaltic materials. The strengths and moduli of these

materials, particularly at higher test temperatures, are influenced by strain rates within the materials that cannot be assessed using a simple linear elastic approach. To address this, an alternative FEM analyses using CAPA-3D was undertaken. An approach was adopted to account for the influence of tensile and compressive strain rates on modulus. The analyses made use of a quasi-isotropic material model and it was shown to better characterise the tensile strengths of HMA materials using the SCB. The analyses also indicated that the tensile strengths determined using the equations initially developed based on a linear elastic approach result in strengths that are unrealistically high.

A good correlation was found between ITS and SCB test results. The SCB test was found to be more sensitive than the ITS to the tensile strength of the material being tested. The dissertation discusses SCB fatigue testing in relation to fatigue determined using ITS and four point bending and compares these to fatigue calculated using the SHELL fatigue equations. It was found that the SCB may overestimate the fatigue performance of mixes owing to the development of horizontal stresses within these specimens.

Stiffness measurements using the SCB may best be done using strain gauges attached to specimens. FEM indicated a fairly uniform distribution of horizontal tensile stress along the principal axis. This method of stiffness measurement for the SCB may be more practical than conventional methods since the magnitude of vertical deflection is limited and the translation and rotation of the bearing supports under loading must also be accounted for. Given the relatively low force required to split SCB specimens, strength tests may be done using conventional Marshall test equipment.

7.2 Recommendations

Based on the research undertaken, the following recommendations are made:

1. The PAVDAM model uses the Superpave N-design table to relate compaction level and design traffic. Further research is required to refine this table in terms of materials and conditions other than those for which it was developed. This table may also be further refined by evaluating the influence of mix type and binder content between mixes compacted in the laboratory and traffic densification in the field, particularly for fine mixes with relatively high binder contents.

2. Volumetric criteria used in mix design should preferably be established with consideration given to the interdependency between volumetric parameters, particularly in light of the trend towards performance-based specifications and implementation of warranty projects. Furthermore, current criteria used in mix design systems are generally established to ensure durability of the mix yet it is not often clear how these criteria relate to durability. Durability is a function not only of the VMA of a mix but other factors including VIM, binder content and the surface area of the aggregate. The use of criteria based on indices established from these properties may be a better measure of mix durability.

3. It is recommended that filler-binder interaction be evaluated as part of mix design analysis. This may be done using softening point tests on mortars. The softening point test is a simple test and the apparatus required is inexpensive and readily available. For this reason, as a preliminary measure it is recommended that an increase in softening point of 12 °C with the addition of filler be used as a first step in determining optimum filler:binder ratios for HMA. This will serve as a lower limit to ensure durability and improve workability of the mix. An upper limit of 16 °C for the increase in softening point temperature

is recommended to improve the stability of the mix.

4. The packing model used in PAVDAM is based on the successive combination of binary systems. More sophisticated models are required to more accurately estimate the VMA of mixes. It is recommended that the development of these be explored further. The influence of binder content and compaction on aggregate packing must also be investigated further.

5. PAVDAM was used in the dissertation to evaluate the reliability of asphalt mixes in terms of volumetric performance. It is recommended that PAVDAM be used to explore reliability in terms of performance, related to volumetric predictive equations (as outlined in Appendix C.

6. Calibration factors used in PAVDAM may be established based on gyratory compaction of mixes evaluated using PAVDAM at specific binder contents. It must still be validated whether these factors are valid at other binder contents other than that used for gyratory compaction of the mix.

7. Presently PAVDAM estimates binder contents to achieve a desired VIM. The option of estimating VIM at fixed binder contents could easily be programmed although it was not considered as part of the dissertation.

8. It is recommended that additional MMLS3 testing be done at the NCAT test track, not only for validation purposes but to better characterise the performance of the HMA mixes at the track.

9. It is recommended that further finite element research be done using non-linear material modelling to evaluate the very complex stress-strain conditions within an SCB specimen to better characterise fracture response. It is also recommended that the fatigue characterisation of HMA be explored based on strength tests using the SCB.

Appendix A

Dissertation software

This appendix includes the fortran source of the following models:

1. Francken and Verstraeten's PRADO packing model
2. Modified Aim and Toufer packing model
3. Probabilistic and Volumetric Design of Asphalt Mixes (PAVDAM)

Examples of output generated by the packing models is given in Appendix B.

A.1 PRADO packing model

This program calculates the VMA (or porosity) of a mix based on algorithms developed by Dr. Louis Francken of the Belgium Road Research Centre (BRRC) and is incorporated in the PRADO software package.

```
program brrc
character*12 fin, fout
character*4 mode
integer i, j, count, files
double precision e(12), k(12), kk(12), y(12), yy(12), r(12), c(10)
```

```
double precision s1(12), s2(12), ee(12)
double precision drj, fij, cij, rsj, ssj, ff, f, s, ss, smin, cmin
double precision smax, clim, ref, sc, s11, s22, c1, c2, sclim, cmax
write(*,*) 'BRRC - ''2000'
write(*,*)
write(*,*) 'BRRC is the BRRL packing model of Dr. Louis Franchen'
write(*,*) 'and calculates VMA from the gradation curve'
write(*,*)
write(*,*) '+ Welcome!'
write(*,*) '+ Input init'
files=iargc()
if (files<2) then
write(*,*) '+ Error: input and output files required'
write(*,*) '+ Usage: brrl input output'
write(*,*) '+ Terminating due to critical error'
do i=1,10
write(*,*)
end do
stop
end if
call getarg(1,fin)
call getarg(2,fout)
open(unit=1,file=fin,iostat=iochk)
open(unit=2,file=fout,iostat=iochk)
write(2,*) 'BRRC - ''2000'
write(2,*)
write(2,*) 'BRRC is the BRRL packing model of Dr. Louis Franchen'
```

```
write(2,*) 'and calculates VMA from the gradation curve'
write(2,*)
write(2,*) 'Input:'
write(2,fmt='(3a7)') 'Sieve ',' % Pass','% V'
count = 0
do while (iochk==0)
  count=count+1
  read(1,*,iostat=iochk) k(count), y(count), e(count)
end do
count=count-1
close(1)
do i=1,count
  write(2,fmt='(f6.3,1x,f6.2,1x,f6.1)') k(i), y(i), e(i) * 100
end do
write(2,*)
write(2,*) 'Converted grading:'
write(2,fmt='(3a7)') 'Sieve ',' % Pass','% V'
kk(1) = .0625
yy(1) = y(1)
ref = y(1)
do i=2,count
  kk(i) = kk(i - 1) * 2
  yy(i)=(((y(i))-(y(i-1)))/(log(k(i))-log(k(i-1)))*(log(kk(i)) &
 & -log(k(i-1)))+(y(i-1)))
end do
do i=1,count
  k(i) = kk(i)
```

```
  y(i) = yy(i)
  write(2,fmt='(f6.3,1x,f6.2,1x,f6.1)') k(i), y(i), e(i) * 100
end do
write(2,*)
r(1) = y(1)
do i=2,count
  r(i) = y(i) - y(i - 1)
end do
do i=2,count
  c(i) = r(i) / y(i)
  s2(i) = e(i) / (1 - e(i))
end do
write(*,fmt='(a4,5x,a6)') 'Step: ','VMA'
i = 1
write(*,fmt='(i4,5x,f6.3)')  i, e(1) * 100
s = e(1) / (1 - e(1))
s1(1) = s
write(2,*) 'Step: ', i
write(2,fmt='(a2,5x,a3,5x,a6,5x,a6,5x,a4,5x,a6)') &
& ' i','di','di+1','yi','f','V'
write(2,fmt='(i2,5x,f3.1,5x,f6.3,5x,f6.3,5x,a4,5x,f6.3)') &
& i, k(i-1), k(i), y(i), '----', e(i) * 100
write(2,*)
do i=2,count
  write(2,*)
  write(2,*) 'Step: ', i
  write(2,fmt='(a5,f6.3,a5,f6.3,a5,f6.3)') &
```

```
& ' Ci2= ', c(i), ' Si1= ', s1(i - 1), ' Si2= ', s2(i)
 write(2,*)
 write(2,fmt='(a2,5x,a2,5x,a3,5x,a6,5x,a5,5x,a7,5x,a4,5x,a4)') &
& 'i','j','drj','f(i,j)','rs(j)','fact(j)','Clim', 'Mode'
 ff = 0
 do j=1,i-1
   drj = k(j) / k(i)
   fij = (y(j) - y(j - 1)) / (y(i - 1) - 0)
   cij = (r(i) / y(i))
   if (j > 1) then
     s = ss
   end if
   smin = ((s / (1 + s)) * (s2(j + 1) / (1 + s2(j + 1))))
   cmax = (1 + s) / (1 + s + s2(j + 1))
   smax = (s + s2(j + 1)) / 2
   cmin = .5
   s11 = (smax - smin) / (cmin - cmax)
   sc = drj * s2(j + 1)
   s22 = (s - sc) / (-1)
   c1 = smax - s11 * .5
   clim = (s - c1) / (s11 - s22)
   if (cij < clim) then
     ssj = s - (s - s2(j + 1) * drj) * cij
     mode = 'Sub'
   else
     sclim = s - (s - s2(j + 1) * drj) * clim
     ssj = ((s2(j + 1) - sclim) / (1 - clim)) * (cij - clim) + &
```

```
      & sclim
      mode = 'Fill'
    end if
    rsj = ssj / s
    f = fij * rsj
    ff = ff + f
    if (j==1) then
     ss = s
    end if
    s = ssj
    write(2,fmt='(i2,5x,i2,5x,f4.2,5x,f4.2,5x,f6.3,5x,f6.3,5x, &
    & f7.3,5x,a5)') &
   & i, j, drj, fij, rsj, ff, clim, mode
  end do
  s1(i) = ff * s1(i - 1)
  ee(i) = s1(i) / (1 + s1(i))
  write(*,fmt='(i4,5x,f6.3)') i, ee(i) * 100
  s = s1(i)
  write(2,*)
  write(2,fmt='(a2,5x,a3,5x,a6,5x,a6,5x,a4,5x,a6)') &
 & ' i','di','di+1','yi','f','V'
  write(2,fmt='(i2,5x,f6.3,5x,f6.3,5x,f6.3,5x,f6.3,5x,f6.3)') &
 & i, k(i-1), k(i), y(i), ff, ee(i) * 100
  write(2,*)
end do
close(2)
write(*,*) '+ Calculation complete'
```

```
write(*,*) '+ Output to file: ', fout
write(*,*) '+ Bye!'
end program brrc
```

A.2 Modified Aim and Toufar (MAT) packing model

This program calculates the VMA (or porosity) of a mix based on the modified Aim and Toufar approach documented in Chapter 3. This model is incorporated in PAVDAM.

```
program mat
implicit none

character*80 fin,fout
character*4 mode, model
integer i,j,count,iochk,files
real (kind=2) k(20),y(20),e(20),r(20),c(20),s1(20),s2(20),kk(20), &
& ee(20),yy(20)
real (kind=2) drj,fij,cij,rsj,ssj,ff,f,s,ss
real (kind=2) phi,phi1,phi2
real (kind=2) kd,x,ks,ks1,ks2,pp,pmax,cmax,smin,pp2
real (kind=2) tol, pst, yst, srl
real (kind=2) k_a(20), y_a(20), e_a(20)
real (kind=2) f1,f2
real (kind=2) a
```

```
tol=0.0001
srl=0.22
f1=-0.44
f2=0.08

write(*,*) ' '
write(*,*) 'MAT - MODIFIED AIM & TOUFAR PACKING MODEL'
write(*,*) 'August ''2002'
write(*,*)
files=iargc()
if (files<2) then
write(*,*) '+ Error: input and output files required'
write(*,*) '+ Usage: MAT inputfile outputfile'
write(*,*) '+ eg: MAT grad.inp grad.out'
write(*,*) '+ Terminating due to critical error'
do i=1,10
write(*,*)
end do
stop
end if
call getarg(1,fin)
call getarg(2,fout)
open(unit=1,file=fin,iostat=iochk)
open(unit=2,file=fout,iostat=iochk)
write(2,*) 'MAT PACKING MODEL ''2002'
write(2,*)
write(2,*) 'Input:'
```

```
write(2,fmt='(3a7)') 'Sieve ',' % Pass','% V'
count = 0
do while (iochk==0)
  count=count+1
  read(1,*,iostat=iochk) k_a(count), y_a(count), e_a(count)
end do
count=count-1
close(1)

do i=1,count
  k(i)=k_a(i)
  y(i)=y_a(i)
  e(i)=e_a(i)
end do

do i=1,count
  write(2,fmt='(f6.3,1x,f6.2,1x,f6.1)') k(i), y(i), e(i) * 100
end do
write(2,*)
r(1) = y(1)
kk(1)=0.075/2.
yy(1)=0.
do i=2,count
  r(i) = y(i) - y(i - 1.)
  c(i) = r(i) / y(i)
  s2(i) = e(i) / (1. - e(i))
  yy(i)=y(i-1)
```

```
  kk(i)=k(i-1)
end do
write(*,*) '+ Estimating VMA from input gradation and porosities ...'
write(*,*) ' '
write(*,fmt='(a4,5x,a6)') 'Step: ','VMA'
i = 1
write(*,fmt='(i4,5x,f6.3)')  i, e(1) * 100
s = e(1) / (1 - e(1))
phi=1.-e(1)
s1(1) = s
write(2,*) 'Step: ', i
write(2,fmt='(a2,5x,a3,5x,a6,5x,a6,5x,a4,5x,a6)') ' i','di','di+1',&
& 'yi','f','V'
write(2,fmt='(i2,6x,f3.1,5x,f6.3,7x,f6.3,5x,a4,7x,f6.3)') i, k(i-1),&
& k(i), y(i), '----', e(i) * 100
write(2,*) '-----------------------------------------------------'

phi1=1.-e(i-1)

!Main loop
do i=2,count
!do i=2,3
  write(2,*)
  write(2,*) 'Step: ', i
  write(2,fmt='(a5,f6.3,a5,f6.3,a5,f6.3)') ' Ci2= ', c(i), ' Si1= ', &
  & s1(i - 1), ' Si2= ', s2(i)
  write(2,*)
```

```
  write(2,fmt='(a2,5x,a2,5x,a3,5x,a6,5x,a5,5x,a7,5x,a4,5x,a4,5x,a4,5x,&
  & a4)') &
  & 'i','j','drj','f(i,j)','rs(j)','fact(j)','cmax','smin','Model','Mode'
  ff = 0.


!Sub loop
  do j=1,i-1
    drj = k(j) / k(i)
    fij = (y(j) - yy(j)) / (y(i - 1) - 0)
    cij = (r(i) / y(i))
    if (j > 1) then
      s=ss
      phi=s/(1.+s)
      phi=1.-phi
    end if
    phi=s/(1.+s)  !:) Added this
    phi=1.-phi    !:) Added this
    phi2=1.-e(j)

    if (drj > srl)  then

!<-------+ Toufar model +-------->
      kd=(kk(i)-kk(j))/(kk(j)+kk(i))
      x=((1.-cij)/cij)*(phi2/phi)/(1.-phi2)
      ks1=(x/0.4753)*0.3881
      ks2=1.-(1.+4.*x)/((1.+x)**4.)
```

```
if (x < 0.4753) then
  ks=ks1
else
  ks=ks2
end if
phi=1./(((1.-cij)/phi)+(cij/phi2)-cij*(1./phi2-1.)*kd*ks)
cmax=tol
pmax=-999.
do while (cmax < 1.)
  x=((1.-cmax)/cmax)*(phi2/phi)/(1.-phi2)
  ks1=(x/0.4753)*0.3881
  ks2=1.-(1.+4.*x)/((1.+x)**4.)
  if (x < 0.4753) then
    ks=ks1
  else
    ks=ks2
  end if
  pp=1./(((1.-cmax)/phi)+(cmax/phi2)-cmax*(1./phi2-1.)*kd*ks)
  if (pp .gt. pmax) then
    pmax=pp
  else
    exit
  end if
  cmax=cmax+tol
end do
cmax=cmax-tol
pp=1./(((1.-cmax)/phi)+(cmax/phi2)-cmax*(1./phi2-1.)*kd*ks)
```

```
      model='TOUF'
    else
!<-------+ Aim model +-------->
      pst=(phi/phi2)-(1.+0.9*drj)*phi
      yst=pst/(1.+pst)
      if ((1.-cij) < yst ) then
        model='AIM1'
        phi=phi2/cij
      else
        model='AIM2'
        phi=1./((1.-cij)/phi + cij*(1.+0.9*drj))
      end if
      if (model=='AIM1') then
        pp=phi2/(1.-yst)
      else
        pp=1./((1.-yst)/phi + yst*(1.+0.9*drj))
      end if
      cmax=1.-yst
    end if
    smin=1.-pp    ! min porosity
    smin=smin/(1.-smin)
    if (cij .lt. cmax) mode='Sub'
    if (cij .gt. cmax) mode='Fill'
    ssj=1.-phi    ! porosity
    ssj=ssj/(1.-ssj)
    rsj = ssj / s
    f = fij * rsj
```

```
      ff = ff + f
      if (j==1) ss = s
      s = ssj
      write(2,fmt='(i2,5x,i2,5x,f4.2,4x,f4.2,6x,f6.3,4x,f6.3,5x,f7.3,&
      & 2x,f7.3,3x,a5,3x,a5)') &
      & i, j, drj, fij, rsj, ff, cmax, smin, model, mode
    end do
    s1(i) = ff * s1(i - 1)
    ee(i) = s1(i) / (1 + s1(i))
    write(*,fmt='(i4,5x,f6.3)') i, ee(i) * 100
    s = s1(i)
    write(2,*)
    write(2,fmt='(a2,5x,a3,5x,a6,5x,a6,5x,a4,5x,a6)') ' i','di','di+1',&
    & 'yi','f','V'
    write(2,fmt='(i2,5x,f6.3,3x,f6.3,6x,f7.3,4x,f6.3,6x,f6.3)') i, &
    & k(i-1), k(i), y(i), ff, ee(i) * 100
    write(2,*) '-------------------------------------------------'
  end do
  close(2)
  print*,'Final VMA: ',ee(count)*100.
  write(*,*) '+ Bye!'
  end program mat
```

A.3 Probabilistic and Volumetric Design of Asphalt Mixes (PAVDAM)

PAVDAM is described in Chapter 4.

```
program pavdam

integer clocks,seed(3),iseed
character*80 fin,fout
character*8 traft,compt
integer i,iochk,count,iter,traffic,compi
integer itercount,itern,niter
real (kind=2) k(20),y(20),e(20),meany(20),stdy(20),meane(20)
real (kind=2) rig,vim,vma,vbe,Gsb,Gb,Pb,Ps,Gmb,Gmm,slope,vmab
real (kind=2) mvma,svma,mPb,sPb,mGmm,sGmm,mGmb,sGmb,mvmap,svmap
real (kind=2) comp,nini,ndes,nmax,compa,compb,mvim,svim
real (kind=2) stdeve,mGsb,sGsb,mGb,sGb,fa,fb,mPba,sPba,Pba
real (kind=2) vmaest,tol,vbe1,vbe2,Ms,Mb,Gse,Vtb,Vse,Pbe,mPbe,sPbe
real ran,u(1000000)

common /random/ seed
common /adf/ u,ran

!!!!!!!!!!!!!!!!!!!!!!!!!!!!!!!!!!!!!!!!!!!!!!!!!!!!!!!!!!!!!!!!!!!
! Input
!!!!!!!!!!!!!!!!!!!!!!!!!!!!!!!!!!!!!!!!!!!!!!!!!!!!!!!!!!!!!!!!!!!
```

```
files=iargc()
if (files<2) then
write(*,*) '+ Error: input and output files required'
write(*,*) '+ Usage: dampav inputfile outputfile'
write(*,*) '+ eg: dampav data.inp data.out'
write(*,*) '+ Terminating due to critical error'
stop
end if
call getarg(1,fin)
call getarg(2,fout)
open(unit=1,file=fin,iostat=iochk)
open(unit=2,file=fout,iostat=iochk)
write(*,*)
write(*,*) 'PAVDAM'
write(*,*) 'Probabilistic And Volumetric Design of Asphalt Mixes'
write(*,*) 'May ''2002'
call paus
write(*,*) 'Inputs:'
!Read fudge factors
read(1,*) fa,fb
!Read Iterations, traffic level, compaction level, Mean vim and stdev vim
read(1,*) iter,traffic,compi,mvim,svim
select case (traffic)
  case(0)
    traft='User'
  case(1)
    nini=6.;ndes=50.;nmax=74.;traft='< 0.1'
```

```
  case(2)
    nini=7.;ndes=70.;nmax=107.;traft='0.1 - 1'
  case(3)
    nini=8.;ndes=100.;nmax=158.;traft='1 - 30'
  case(4)
    nini=9.;ndes=130.;nmax=212.;traft='> 30'
  case default
    write(*,*) 'Error in data file - check traffic'
    stop
end select
select case (compi)
  case(1) !nini
    comp=nini;compt='Nini'
  case(2) !ndes
    comp=ndes;compt='Ndes'
  case(3) !nmax
    comp=nmax;compt='Nmax'
  case default !User specified
    comp=compi;compt='User'
end select
!read Rigden voids and porosity stdev
read(1,*) rig,stdeve
!Read mean and stdev of Gsb
read(1,*) mGsb,sGsb
!Read mean and stdev of Gb
read(1,*) mGb,sGb
!Read mean and stdev of Pba
```

```
read(1,*) mPba,sPba
!Read aggregate porosity compaction parameters
read(1,*) compa,compb
count = 0
! Read gradation parameters
do while (iochk==0)
  count=count+1
  read(1,*,iostat=iochk) k(count), meany(count),stdy(count)
end do
count=count-1
close(1)
meane(1)=rig/100.
stdeve=stdeve/100.

! Determine porosities of fractions at specific compaction level
do i=2,count
  meane(i)=compa+compb*log(comp) ! Thesis derived
end do

!Output all inputs
write(*,'(a,2f6.3)') 'Fudge factors : ',fa,fb
write(*,'(a,i10)') 'Iterations : ',iter
write(*,'(2a)') 'Design traffic (million ESALs) : ',traft
if (compt=='User') then
  write(*,'(a,i3)') 'Compaction level : ',compi
else
  write(*,'(2a)') 'Compaction level : ',compt
```

```
end if
write(*,'(a,f6.1)') 'Mean VIM @ Compaction level : ',mvim
write(*,'(a,f6.1)') 'Stdev VIM @ Compaction level : ',svim
write(*,'(a,f6.1)') 'Rigden voids (%) : ',rig
write(*,'(a,f6.1)') 'Aggregate porosity (%) : ',meane(2)*100.
write(*,'(a,f6.3)') 'Fraction porosity stdev (%) : ',stdeve*100.
write(*,'(a,2f6.3)') 'Gsb mean and stdev : ',mGsb,sGsb
write(*,'(a,2f6.3)') 'Gb mean and stdev : ',mGb,sGb
write(*,'(a,2f6.3)') 'Pba mean and stdev : ',mPba,sPba
write(*,'(a,2f10.4)') 'Porosity compaction parameters : ',compa,compb
write(*,'(a)') 'Sieve size, Percentage passing mean and stdev :'
do i=1,count
  write(*,fmt='(f6.3,1x,f6.2,1x,f6.1)') k(i), meany(i), stdy(i)
end do
call paus


!!!!!!!!!!!!!!!!!!!!!!!!!!!!!!!!!!!!!!!!!!!!!!!!!!!!!!!!!!!!!!!!!!!!!!!
! Main Loop
!!!!!!!!!!!!!!!!!!!!!!!!!!!!!!!!!!!!!!!!!!!!!!!!!!!!!!!!!!!!!!!!!!!!!!!
!Randomize
call system_clock(clocks)
iseed=max(1+mod(clocks,1000)/10, 1+mod(clocks,100))
seed(1)=iseed
print*,'Charging random buffer ...'
call randit(u,1000000) ! Generate 1000000 random numbers
```

```
itercount=0
itern=1000
niter=1
ran=1
mvma=0.;svma=0.;mGmm=0.;sGmm=0.;mGmb=0.;sGmb=0.;mvmap=0.;svmap=0.
mPb=0.;sPb=0.
mPbe=0.;sPbe=0.
tol=0.001
!Gsb=mGsb
!Gb=mGb

do i=1,iter
  if (itercount==niter*itern) then  ! Count off iterations
    write(*,'(i10,a,i10)') itercount,' / ',iter
    niter=niter+1
  end if
! Simulate gradation
  call normal(meany(1),stdy(1),y(1))
  do j=2,count-1
    y(j)=y(j-1)-1.            ! Force the loop
    do while (y(j)<y(j-1).or.y(j)>meany(j+1)+stdy(j+1))
      call normal(meany(j),stdy(j),y(j))
    end do
  end do
  y(count)=100.
! Simulate aggregate porosities
  do j=1,count
```

```
    e(j)=-1.  ! Force the loop
    do while (e(j)<0.3.or.e(j)>0.55)
      call normal(meane(j),stdeve, e(j))
    end do
  end do
! Call Aim and Toufar packing model to calc vma of combined aggregate
  call atm(count,k,y,e,vma)
  vma=vma*fa-fb
  vma=vma*100.
  vmaest=vma
! Calc vim
  call normal(mvim,svim,vim)
  vbe=vma-vim
! Calc Gsb
  call normal(mGsb,sGsb,Gsb)
! Calc Gb
  call normal(mGb,sGb,Gb)
! Calc Pba  ! Absorbed binder
  call normal(mPba,sPba,Pba)
! Calc Gse
  Gse=-100.*Gb*Gsb/(Pba*Gsb-100.*Gb)
! Calc Vsb = Volume of bulk aggregate
  Vsb=(100.-vbe-vim)/100.
! Calc Mass aggregate Ms
  Ms=Vsb*Gsb
! Calc volume of effective aggregate Vse
  Vse=Ms/Gse
```

```
! Calc volume of absorbed binder Vba
  Vba=Vsb-Vse
! Calc total binder volume Vtb
  Vtb=vbe/100.+Vba
  Mb=Vtb*Gb
! Calc Gmm
  Gmm=(Ms+Mb)/(Vbe/100.+Vsb)
!  slope=(Gb-Gsb)              !======= Experimental =======
!  Gmm=slope*(vbe/100.)+Gsb    !============================
! Calc Gmb
  Gmb=Gmm*(100.-vim)/100.
! Calc Pb
  Ps=(100.-vbe)*(Gsb/Gmm)
  Pb=100.-Ps
  Pbe=Pb-(Pba*Ps/100.)
! Calc means and stdev
  mvmap=mvmap+vma
  svmap=svmap+vma**2.
  mvma=mvma+vmaest
  svma=svma+vmaest**2.
  mPb=mPb+Pb
  sPb=sPb+Pb**2.
  mGmm=mGmm+Gmm
  sGmm=sGmm+Gmm**2.
  mGmb=mGmb+Gmb
  sGmb=sGmb+Gmb**2.
  mPbe=mPbe+Pbe
```

```
  sPbe=sPbe+Pbe**2.
  itercount=itercount+1
  write(2,*) Pb
end do
!!!!!!!!!!!!!!!!!!!!!!!!!!!!!!!!!!!!!!!!!!!!!!!!!!!!!!!!!!!!!!!!!!!!!!!
! Output results
!!!!!!!!!!!!!!!!!!!!!!!!!!!!!!!!!!!!!!!!!!!!!!!!!!!!!!!!!!!!!!!!!!!!!!!
write(*,'(i6,a,i6)') itercount,' / ',iter
mvmap=mvmap/real(iter)
svmap=sqrt((1./(real(iter)-1.))*(svmap-real(iter)*mvmap**2.))
mvma=mvma/real(iter)
svma=sqrt((1./(real(iter)-1.))*(svma-real(iter)*mvma**2.))
mPb=mPb/real(iter)
sPb=sqrt((1./(real(iter)-1.))*(sPb-real(iter)*mPb**2.))
mGmm=mGmm/real(iter)
sGmm=sqrt((1./(real(iter)-1.))*(sGmm-real(iter)*mGmm**2.))
mGmb=mGmb/real(iter)
sGmb=sqrt((1./(real(iter)-1.))*(sGmb-real(iter)*mGmb**2.))
mPbe=mPbe/real(iter)
sPbe=sqrt((1./(real(iter)-1.))*(sPbe-real(iter)*mPbe**2.))

write(*,'(a,f6.2)') 'Design Mean VIM (%) : ', mvim
write(*,'(a,f6.2)') 'Number of gyrations : ', comp
write(*,'(a,f6.2)') 'Mean VMA (estimated) (%) : ', mvmap
write(*,'(a,f6.2)') 'Stdev VMA (estimated) (%) : ', svmap
write(*,'(a,f6.2)') 'Mean Pb (%) : ', mPb
write(*,'(a,f6.2)') 'Stdev Pb (%) : ', sPb
```

```
write(*,'(a,f6.3)') 'Mean Gmm : ', mGmm
write(*,'(a,f6.3)') 'Stdev Gmm : ', sGmm
write(*,'(a,f6.3)') 'Mean Gmb : ', mGmb
write(*,'(a,f6.3)') 'Stdev Gmb : ', sGmb
write(*,'(a,f6.2)') 'Mean Pbe (%) : ', mPbe
write(*,'(a,f6.2)') 'Stdev Pbe (%) : ', sPbe
close(2)
write(*,*) '+ Bye!'
stop
end program pavdama

subroutine atm(count,k,y,e,vma)
implicit none
integer i,j,count
real (kind=2) k(20),y(20),e(20),r(20),c(20),s1(20),s2(20)
real (kind=2) kk(20),ee(20),yy(20)
real (kind=2) drj,fij,cij,rsj,ssj,ff,f,s,ss
real (kind=2) phi,phi1,phi2
real (kind=2) kd,x,ks,ks1,ks2
real (kind=2) pst, yst, srl, vma
srl=0.22
r(1) = y(1)
kk(1)=0.075/2.
yy(1)=0.
do i=2,count
  r(i) = y(i) - y(i - 1.)
  c(i) = r(i) / y(i)
```

```
  s2(i) = e(i) / (1. - e(i))
  yy(i)=y(i-1)
  kk(i)=k(i-1)
end do
i = 1
s = e(1) / (1 - e(1))
phi=1.-e(1)
s1(1) = s
phi1=1.-e(i-1)
!Main loop
do i=2,count
  ff = 0.
!Sub loop
  do j=1,i-1
    drj = k(j) / k(i)
    fij = (y(j) - yy(j)) / (y(i - 1) - 0)
    cij = (r(i) / y(i))
    if (j > 1) then
      s=ss
      phi=s/(1.+s)
      phi=1.-phi
    end if
    phi=s/(1.+s)
    phi=1.-phi
    phi2=1.-e(j)
    if (drj > srl)  then
      kd=(kk(i)-kk(j))/(kk(j)+kk(i))
```

```
      x=((1.-cij)/cij)*(phi2/phi)/(1.-phi2)
      ks1=(x/0.4753)*0.3881
      ks2=1.-(1.+4.*x)/((1.+x)**4.)
      if (x < 0.4753) then
        ks=ks1
      else
        ks=ks2
      end if
      phi=1./(((1.-cij)/phi)+(cij/phi2)-cij*(1./phi2-1.)*kd*ks)
    else
      pst=(phi/phi2)-(1.+0.9*drj)*phi
      yst=pst/(1.+pst)
      if ((1.-cij) < yst ) then
        phi=phi2/cij
      else
        phi=1./((1.-cij)/phi + cij*(1.+0.9*drj))
      end if
    end if
    ssj=1.-phi
    ssj=ssj/(1.-ssj)
    rsj = ssj / s
    f = fij * rsj
    ff = ff + f
    if (j==1) ss = s
    s = ssj
  end do
  s1(i) = ff * s1(i - 1)
```

```
  ee(i) = s1(i) / (1 + s1(i))
  s = s1(i)
end do
vma=ee(count)
return
end subroutine atm

block data
  integer seed(3)
  common /random/ seed
  data seed(1),seed(2),seed(3) /1,10000,3000/
end block data

subroutine randit(u,n)
  integer n,x,y,z
  real u(n),v
  common /random/ x,y,z
  if (n.le.0) return
  do i=1,n
    x=171*mod(x,177)-2*(x/177)
    if(x.lt.0) x=x+30269
    y=172*mod(y,176)-35*(y/176)
    if(y.lt.0) y=y+30307
    z=170*mod(z,178)-63*(z/178)
    IF(z.lt.0) z=z+30323
    v=x/30269.0 + y/30308.0 + z/30323.0
    u(i)=v-int(v)
```

```
  end do
  return
end subroutine randit

subroutine normal(meanx, sdx, x)
real (kind=2) meanx, sdx
real (kind=2) x, gauss
real (kind=2) fac, r, v1, v2
integer seed(3),ran
real u(1000000)
common /random/ seed
common /adf/ u,ran
r=2.
do while (r>1.)
  if (ran>1000000) then
    print*,'Charging random buffer ...'
    call randit(u,1000000) ! Generate another 1000000 random numbers
    ran=1
  end if
  v1=2.*u(ran)-1.
  ran=ran+1
  if (ran>1000000) then
    print*,'Charging random buffer ...'
    call randit(u,1000000) ! Generate another 1000000 random numbers
    ran=1
  end if
  v2=2.*u(ran)-1.
```

```
  r=v1**2.+v2**2.
end do
fac=sqrt((-2.)*log(r)/r)
gauss=v2*fac
x=gauss*sdx+meanx
ran=ran+1
return
end subroutine normal

subroutine paus
character*1 ans
integer iochk
write(*,*)
write(*,fmt='(a,$)') 'Press <ENTER> to continue...'
write(*,*)
read(*,'(a)',iostat=iochk) ans
return
end subroutine paus
```

PAVDAM generates an output file containing the estimated binder contents for each iteration. Given the vast number of data generated this output will not be shown although Figure 4.4 shows an example of the output in the form of a histogram.

The structure of an input file for PAVDAM is shown in Table A.1. The different input parameters listed in Table A.1 are as follows:

a = Calibration factor a (See Equation 5.12)

b = Calibration factor b (See Equation 5.12)

Table A.1: PAVDAM input parameters

(a)	1.	(b)	0.						
(c)	100000	(d)	3	(e)	2	(f)	4.	(g)	0.5
(h)	40.	(i)	0.5						
(j)	2.682	(k)	0.010						
(l)	1.026	(m)	0.0008						
(n)	0.2	(o)	0.001						
(p)	0.472	(q)	-0.0181						
(r)	0.075	(s)	5.700	(t)	1.				
(r)	0.150	(s)	9.000	(t)	2.				
(r)	0.300	(s)	14.00	(t)	3.				
(r)	0.600	(s)	20.00	(t)	4.				
(r)	1.180	(s)	27.00	(t)	4.				
(r)	2.360	(s)	36.00	(t)	4.				
(r)	4.750	(s)	53.00	(t)	4.				
(r)	9.500	(s)	82.00	(t)	5.				
(r)	19.000	(s)	100.0	(t)	0.				

c = Number of iterations

d = Traffic level (see Note. 1 below)

e = Compaction level (see Note. 2 below)

f = Desired voids in the mix, percentage (mean)

g = Desired voids in the mix, percentage (standard deviation))

h = Rigden's voids, percentage

i = Fraction porosity standard deviation, percentage

j = Aggregate bulk relative density (mean)

k = Aggregate bulk relative density (standard deviation)

l = Bitumen bulk relative density (mean)

m = Bitumen bulk relative density (standard deviation)

n = Binder absorption (percentage by mass of aggregate (mean)

o = Binder absorption (percentage by mass of aggregate (standard deviation)

p = Aggregate fraction compaction characteristic intercept (See Equation 3.33)

q = Aggregate fraction compaction characteristic slope (See Equation 3.33)

r = Gradation sieve size, mm

s = Gradation passing (p), percentage (mean)

t = Gradation passing (p), percentage (standard deviation)

Notes:

1. Traffic level is defined by an integer between 0 and 4 such that:

   0 = User defined (Compaction level may be defined by user)

   1 = < 0.1 million ESALs

   2 = 0.1 - 1 million ESALs

   3 = 1 - 30 million ESALs

   4 = > 30 million ESALs

2. Compaction level is defined by an integer such that:

   1 = N_{ini}

   2 = N_{des}

   3 = N_{max}

   > 3 = User defined number of gyrations

As a guide the following Superpave compaction levels are used for the different traffic levels (refer to Table 2.1).

< 0.1 million ESALs = N_{ini}=6, N_{des}=50, N_{max}=74

0.1 - 1 million ESALs $= N_{ini}=7,\ N_{des}=70,\ N_{max}=107$

1 - 30 million ESALs $= N_{ini}=8,\ N_{des}=100,\ N_{max}=158$

$>$ 30 million ESALs $= N_{ini}=9,\ N_{des}=130,\ N_{max}=212$

Appendix B

Packing model outputs

B.1 BRRL PRADO packing model

```
Input:
Sieve  % Pass   % V
0.075   6.1  0.4
0.150   8.3  0.4
0.300  11.4  0.4
0.600  15.6  0.4
1.180   21.1  0.4
2.360  28.8  0.4
4.750  39.5  0.4
9.500  53.9  0.4
19.000  73.6  0.4
37.500  100.0    0.4

Output:
Converted grading:
Sieve  % Pass    % V
```

```
 0.063    6.10   40.0
 0.125    7.72   40.0
 0.250   10.58   40.0
 0.500   14.50   40.0
 1.000   19.75   40.0
 2.000   26.96   40.0
 4.000   36.87   40.0
 8.000   50.33   40.0
16.000   68.72   40.0
32.000   93.84   40.0

 Step:  1
 i  di   di+1    yi      f     V
 1  ***  0.063  6.100  ----  40.000
 ------------------------------------------------
 Step:  2
 Ci2= 0.210 Si1= 0.667 Si2= 0.667
 i  j  drj   f(i,j) rs(j)  fact(j) Clim   Mode
 2  1  0.50  1.00   0.895  0.895   0.574  Sub
 i   di    di+1    yi     f       V
 2  0.063  0.125  7.721  0.895  37.370
 ------------------------------------------------
 Step:  3
 Ci2= 0.271 Si1= 0.597 Si2= 0.667
 i  j  drj   f(i,j) rs(j)  fact(j) Clim   Mode
 3  1  0.25  0.79   0.805  0.636   0.618  Sub
 3  2  0.50  0.21   0.881  0.821   0.573  Sub
```

```
i   di    di+1    yi     f       V
3  0.125  0.250  10.585  0.821   32.878
-----------------------------------------------
Step:  4
Ci2= 0.270 Si1= 0.490 Si2= 0.667
i  j  drj   f(i,j) rs(j)  fact(j) Clim   Mode
4  1  0.13  0.58   0.776  0.447   0.640  Sub
4  2  0.25  0.15   0.822  0.573   0.615  Sub
4  3  0.50  0.27   0.914  0.820   0.571  Sub
i   di    di+1    yi     f       V
4  0.250  0.500  14.495  0.820  28.665
-----------------------------------------------
Step:  5
Ci2= 0.266 Si1= 0.402 Si2= 0.667
i  j  drj   f(i,j) rs(j)  fact(j) Clim   Mode
5  1  0.06  0.42   0.761  0.320   0.647  Sub
5  2  0.13  0.11   0.789  0.409   0.635  Sub
5  3  0.25  0.20   0.844  0.575   0.611  Sub
5  4  0.50  0.27   0.955  0.833   0.569  Sub
i   di    di+1    yi     f       V
5  0.500  1.000  19.754  0.833  25.078
-----------------------------------------------
Step:  6
Ci2= 0.267 Si1= 0.335 Si2= 0.667
i  j  drj   f(i,j) rs(j)  fact(j) Clim   Mode
6  1  0.03  0.31   0.749  0.231   0.648  Sub
6  2  0.06  0.08   0.766  0.294   0.642  Sub
```

```
6  3  0.13  0.14   0.799  0.410   0.630  Sub
6  4  0.25  0.20   0.866  0.581   0.607  Sub
6  5  0.50  0.27   0.999  0.847   0.567  Sub
i   di    di+1    yi     f       V
6  1.000  2.000 26.961  0.847  22.097
-----------------------------------------------
Step:  7
Ci2= 0.269 Si1= 0.284 Si2= 0.667
i  j  drj   f(i,j) rs(j)  fact(j) Clim   Mode
7  1  0.02  0.23   0.741  0.168   0.646  Sub
7  2  0.03  0.06   0.751  0.213   0.643  Sub
7  3  0.06  0.11   0.771  0.295   0.637  Sub
7  4  0.13  0.15   0.810  0.412   0.625  Sub
7  5  0.25  0.20   0.889  0.586   0.604  Sub
7  6  0.50  0.27   1.047  0.866   0.565  Sub
i   di    di+1    yi     f       V
7  2.000  4.000 36.871  0.866   19.711
-----------------------------------------------
Step:  8
Ci2= 0.267 Si1= 0.246 Si2= 0.667
i  j  drj   f(i,j) rs(j)  fact(j) Clim   Mode
8  1  0.01  0.17   0.738  0.122   0.643  Sub
8  2  0.02  0.04   0.744  0.155   0.641  Sub
8  3  0.03  0.08   0.755  0.214   0.638  Sub
8  4  0.06  0.11   0.778  0.296   0.633  Sub
8  5  0.13  0.14   0.823  0.413   0.622  Sub
8  6  0.25  0.20   0.914  0.592   0.601  Sub
```

```
8  7  0.50  0.27   1.096  0.887   0.563  Sub
i   di    di+1    yi     f       V
8  4.000  8.000  50.330  0.887  17.876
-----------------------------------------------
Step:  9
Ci2= 0.268 Si1= 0.218 Si2= 0.667
i  j  drj   f(i,j) rs(j)  fact(j) Clim   Mode
9  1  0.00  0.12   0.736  0.089   0.640  Sub
9  2  0.01  0.03   0.739  0.113   0.639  Sub
9  3  0.02  0.06   0.745  0.155   0.637  Sub
9  4  0.03  0.08   0.758  0.214   0.635  Sub
9  5  0.06  0.10   0.784  0.296   0.629  Sub
9  6  0.13  0.14   0.835  0.416   0.619  Sub
9  7  0.25  0.20   0.937  0.600   0.598  Sub
9  8  0.50  0.27   1.142  0.906   0.562  Sub
i   di    di+1    yi     f       V
9  8.000 16.000  68.716  0.906  16.467
-----------------------------------------------
Step:  10
Ci2= 0.268 Si1= 0.197 Si2= 0.667
i  j  drj   f(i,j) rs(j)  fact(j) Clim   Mode
10 1  0.00  0.09   0.734  0.065   0.637  Sub
10 2  0.00  0.02   0.736  0.083   0.637  Sub
10 3  0.01  0.04   0.739  0.113   0.636  Sub
10 4  0.02  0.06   0.746  0.156   0.635  Sub
10 5  0.03  0.08   0.761  0.214   0.632  Sub
10 6  0.06  0.10   0.789  0.297   0.627  Sub
```

```
10 7  0.13  0.14   0.845  0.419   0.616  Sub
10 8  0.25  0.20   0.959  0.606   0.596  Sub
10 9  0.50  0.27   1.185  0.923   0.560  Sub
i   di     di+1    yi     f       V
10 16.000 32.000  93.842 0.923  15.402
-----------------------------------------------
```

B.2 Modified Aim and Toufar packing model

```
Input:
Sieve  % Pass   % V
0.075   6.1  0.4
0.150   8.3  0.4
0.300  11.4  0.4
0.600  15.6  0.4
1.180  21.1  0.4
2.360  28.8  0.4
4.750  39.5  0.4
9.500  53.9  0.4
19.000 73.6  0.4
37.500 100.0    0.4


Output:
```

```
Step:  1
i       di        di+1          yi         f          V
1       ***       0.075        6.100      ----        40.000
-------------------------------------------------------
Step:  2
Ci2= 0.265 Si1= 0.667 Si2= 0.667
i  j  drj   f(i,j)  rs(j)  fact(j)  cmax   smin   Model  Mode
2  1  0.50  1.00    0.868  0.868    0.584  0.464  TOUF   Sub
i       di        di+1          yi         f          V
2 0.075     0.150         8.300      0.868       36.667
-------------------------------------------------------
Step:  3
Ci2= 0.272 Si1= 0.579 Si2= 0.667
i  j  drj   f(i,j)  rs(j)  fact(j)  cmax   smin   Model  Mode
3  1  0.25  0.73    0.808  0.594    0.543  0.339  TOUF   Sub
3  2  0.50  0.27    0.886  0.829    0.533  0.437  TOUF   Sub
i       di        di+1          yi         f          V
3       0.150     0.300        11.400      0.829       32.431
-------------------------------------------------------
Step:  4
Ci2= 0.269 Si1= 0.480 Si2= 0.667
i  j  drj   f(i,j)  rs(j)  fact(j)  cmax   smin   Model  Mode
4  1  0.13  0.54    0.794  0.425    0.728  0.308  AIM2   Sub
4  2  0.25  0.19    0.827  0.584    0.496  0.307  TOUF   Sub
4  3  0.50  0.27    0.920  0.835    0.458  0.403  TOUF   Sub
i       di        di+1          yi         f          V
4       0.300     0.600        15.600      0.835       28.599
```

Step: 5

Ci2= 0.261 Si1= 0.401 Si2= 0.667

i	j	drj	f(i,j)	rs(j)	fact(j)	cmax	smin	Model	Mode
5	1	0.06	0.39	0.777	0.304	0.697	0.234	AIM2	Sub
5	2	0.13	0.14	0.814	0.418	0.717	0.266	AIM2	Sub
5	3	0.25	0.20	0.851	0.588	0.452	0.280	TOUF	Sub
5	4	0.51	0.27	0.959	0.846	0.365	0.370	TOUF	Sub

i	di	di+1	yi	f	V
5	0.600	1.180	21.100	0.846	25.302

Step: 6

Ci2= 0.267 Si1= 0.339 Si2= 0.667

i	j	drj	f(i,j)	rs(j)	fact(j)	cmax	smin	Model	Mode
6	1	0.03	0.29	0.755	0.218	0.677	0.182	AIM2	Sub
6	2	0.06	0.10	0.778	0.299	0.687	0.199	AIM2	Sub
6	3	0.13	0.15	0.823	0.420	0.708	0.231	AIM2	Sub
6	4	0.25	0.20	0.871	0.594	0.406	0.256	TOUF	Sub
6	5	0.50	0.26	1.004	0.855	0.107	0.340	TOUF	Fill

i	di	di+1	yi	f	V
6	1.180	2.360	28.800	0.855	22.465

Step: 7

Ci2= 0.271 Si1= 0.290 Si2= 0.667

i	j	drj	f(i,j)	rs(j)	fact(j)	cmax	smin	Model	Mode
7	1	0.02	0.21	0.742	0.157	0.664	0.148	AIM2	Sub
7	2	0.03	0.08	0.756	0.215	0.669	0.156	AIM2	Sub

7	3	0.06	0.11	0.782	0.299	0.679	0.172	AIM2	Sub
7	4	0.13	0.15	0.835	0.421	0.700	0.204	AIM2	Sub
7	5	0.25	0.19	0.894	0.592	0.363	0.234	TOUF	Sub
7	6	0.50	0.27	1.045	0.871	0.000	0.303	TOUF	Fill

i	di	di+1	yi	f	V
7	2.360	4.750	39.500	0.871	20.156

Step: 8

Ci2= 0.267 Si1= 0.252 Si2= 0.667

i	j	drj	f(i,j)	rs(j)	fact(j)	cmax	smin	Model	Mode
8	1	0.01	0.15	0.740	0.114	0.655	0.125	AIM2	Sub
8	2	0.02	0.06	0.748	0.156	0.657	0.129	AIM2	Sub
8	3	0.03	0.08	0.763	0.216	0.662	0.137	AIM2	Sub
8	4	0.06	0.11	0.793	0.300	0.673	0.153	AIM2	Sub
8	5	0.12	0.14	0.851	0.419	0.693	0.183	AIM2	Sub
8	6	0.25	0.19	0.916	0.597	0.327	0.215	TOUF	Sub
8	7	0.50	0.27	1.089	0.892	0.000	0.275	TOUF	Fill

i	di	di+1	yi	f	V
8	4.750	9.500	53.900	0.892	18.383

Step: 9

Ci2= 0.268 Si1= 0.225 Si2= 0.667

i	j	drj	f(i,j)	rs(j)	fact(j)	cmax	smin	Model	Mode
9	1	0.00	0.11	0.737	0.083	0.649	0.109	AIM2	Sub
9	2	0.01	0.04	0.741	0.114	0.650	0.111	AIM2	Sub
9	3	0.02	0.06	0.749	0.157	0.653	0.115	AIM2	Sub
9	4	0.03	0.08	0.766	0.216	0.657	0.123	AIM2	Sub

9	5	0.06	0.10	0.799	0.298	0.667	0.139	AIM2	Sub
9	6	0.12	0.14	0.865	0.421	0.688	0.169	AIM2	Sub
9	7	0.25	0.20	0.939	0.608	0.290	0.201	TOUF	Sub
9	8	0.50	0.27	1.135	0.911	0.000	0.256	TOUF	Fill

i	di	di+1	yi	f	V
9	9.500	19.000	73.600	0.911	17.025

Step: 10

Ci2= 0.264 Si1= 0.205 Si2= 0.667

i	j	drj	f(i,j)	rs(j)	fact(j)	cmax	smin	Model	Mode
10	1	0.00	0.08	0.738	0.061	0.644	0.098	AIM2	Sub
10	2	0.00	0.03	0.741	0.083	0.645	0.099	AIM2	Sub
10	3	0.01	0.04	0.745	0.115	0.646	0.101	AIM2	Sub
10	4	0.02	0.06	0.755	0.158	0.649	0.106	AIM2	Sub
10	5	0.03	0.07	0.772	0.216	0.654	0.113	AIM2	Sub
10	6	0.06	0.10	0.809	0.300	0.664	0.129	AIM2	Sub
10	7	0.13	0.15	0.883	0.428	0.686	0.160	AIM2	Sub
10	8	0.25	0.20	0.961	0.616	0.255	0.191	TOUF	Fill
10	9	0.51	0.27	1.172	0.930	0.000	0.240	TOUF	Fill

i	di	di+1	yi	f	V
10	19.000	37.500	100.000	0.930	16.025

Appendix C

Performance prediction based on HMA volumetric properties

Various models have been developed to estimate the performance of HMA based on the volumetric properties of the mix. What follows is a review of popular prediction models for two engineering properties i.e. stiffness and fatigue. The author considered reporting prediction models for permanent deformation but these models were too condition specific and often required results from sophisticated testing. For examples of these models, readers are referred to [May and Witczak, 1992; Baladi, 1989; Francken, 1977b]. The stiffness and fatigue models are provided to present a general knowledge base of volumetric predictive equations but the reader is strongly encouraged to review the references for the conditions under which the models may be applied and the context in which they were established.

A large part of the work reported here was taken from unpublished lecture notes originally presented by Dr Loius Francken.

C.1 Stiffness

The Shell method allows the stiffness modulus of an asphalt mix to be calculated from the stiffness modulus of the bitumen. The term "stiffness modulus" is used by Shell in lieu of dynamic modulus. Van der Poel [1954] developed a nomograph

that enables the estimation of S_{bit} from binder charactersitics (penetration index and softening point) and test conditions (temperature and loading time). This nomograph was revised slightly by Heukelom [1966]. Equations have been developed to estimate S_{bit} based on the nomograph [Shahin, 1977]:

If $10^{-8} < S_{bit} < 1$ MPa, then:

$$\log S_{bit} = -1.35927 - 0.06743T - 0.90251 \log t + 0.00038T^2 - 0.00138T \log t + 0.00661PI \times T \quad \text{(C.1)}$$

where

S_{bit} = Bitumen stiffness, 0.1 MPa

T = Test temperature - softening point temperature, °C

t = Loading time, seconds

PI = Penetration Index

The ranges for which this equation have been derived are:

-2 < PI < +2

-100 °C < T < 50 °C

-10^2 < t < 10^5 sec

If $1 < S_{bit} < 2000$ MPa, then:

$$\log S_{bit} = -1.90072 - 0.11485T - 0.38423PI - 0.94259 \log t - 0.00879T \log t - 0.05643PI \log t - 0.02915 (\log t)^2 - 0.51873 \times 10^{-3}T^2 + 0.00113PI^3 \times T - 0.01403 (PI \times T)^3 \times 10^{-5} \quad \text{(C.2)}$$

The ranges for which this equation have been derived are:

-1.5 < PI < +2

-100 °C < T < 50 °C

$-10^2 < t < 10^5$ sec

Having determined the stiffness of the bitumen (S_{bit}) it may be used to estimate mix stiffness if the percentage volume of bitumen and the percentage volume of aggregate in the mix is known. The stiffness modulus of HMA based on the Shell approach is related to the aggregate concentration in the mix, C_v, defined as:

$$C_v = \frac{V_s}{V_s + V_b} \tag{C.3}$$

where

V_s = Volume of aggregate, %

V_b = Volume of binder, %

In 1964, Heukelom and Klomp [1964] suggested the following formula to estimate the stiffness modulus of a mix based on the binder stiffness and volumetric composition:

$$S_{mix} = S_{bit}\left(1 + \frac{2.5}{n}\frac{C_v}{1 - C_v}\right)^n \tag{C.4}$$

$$n = 0.83 \log \frac{4 \times 10^{10}}{S_{bit}} \tag{C.5}$$

where

S_{mix}= Stiffness modulus of the mix, Pa

S_{bit} = Stiffness modulus of the bitumen, Pa

This equation was developed using results from mixes containing about 3 percent air voids. The stiffness of HMA is significantly influenced by air voids. To allow the

estimation of stiffness at higher air void contents, the correction to C_v suggested by Draat and Sommer [1965] may be applied:

$$C_v' = \frac{100C_v}{100 + V_a - 3} \tag{C.6}$$

In 1977, Francken [1977a] developed a relationship to estimate the maximum stiffness of a mix under extreme conditions of low temperature and high frequencies. Under these conditions, the material is purely elastic with an asymptotic value of the modulus, $E\infty$ (MPa):

$$E\infty = 3.56 \times 10^4 \frac{(V_a + V_b)}{V_b} e^{-0.1V_a} \tag{C.7}$$

where

V_a = Volume of air voids, %

V_b = Volume of binder, %

The ranges for which this equation have been derived are:

$1.5\ \% < V_a < 32\ \%$

$3 < V_s/V_b < 12$

$0.3\ \text{MPa} < S_{bit} < 3000\ \text{MPa}$

This equation holds for the pure elastic case. At higher temperatures and longer loading times the bitumen behaves more visco-elastic and this will influence the mix stiffness. Sabha et al. [1995], based on a comparison of methods available to predict the stiffness of HMA from the binder stiffness, recommended this equation because it was valid for a wide range of binder stiffness.

From the analysis of a large amount of experimental data on the relation between mix stiffness and binder complex modulus, Francken and Vanelstraete [1996],

presented the following equation:

$$E\infty = C(\frac{V_s}{V_b})^{0.55e^{-0.0584V_a}} \tag{C.8}$$

where

C = a parameter equal to 14360 MPa for pure bitumen

This equation was developed from data for conventional, aged and polymer-modified bitumens, covering a range of bitumen stiffnesses from 0.3 MPa to 3000 MPa. The ranges for which this equation have been derived are:

$1.5\ \% < V_a < 32\ \%$

$0.16 < V_s/V_b < 12$

The application of the Francken equations is not immediately apparent since these allow prediction of the maximum stiffness of HMA mixes and not the stiffness under normal working conditions. To apply these equations it is necessary to consider the relationship proposed by Huet [1967]. According to Huet, the stiffness modulus of an asphalt mix may be written as follows:

$$\mathrm{S_{mix}}(T, f) = E\infty \times R^*_{mix}(T, f) \tag{C.9}$$

In this equation, the stiffness modulus is a function of the product of the maximum modulus defined previously and a reduced or normalised modulus, R^*. The reduced modulus is a function of temperature and frequency varying between 0 and 1 with an asymptotical upper limit. The reduced modulus gives the form of the temperature frequency dependence of the stiffness modulus. An empirical relationship between the reduced modulus of the mix (R^*_{mix}) and the reduced modulus of the binder (R_bit^*) was established by Francken and Vanelstraete [1996]:

$$\log(R^*_{mix}) = \log(R^*_{bit}) \left[1 - 1.35 \left(1 - e^{-0.13\frac{V_a}{V_b}}\right) (1 + 0.11 \log(R^*_{bit}))\right] \tag{C.10}$$

where

R^*_{bit} = Reduced modulus of binder = $G^*/G\infty$

$G\infty$ = 1000 MPa

G^* = $S_{bit}/2(1+\upsilon)$

υ = Poisson's ratio

Sayegh [1967] described the relationship between frequency and Poisson's ratio for bitumen at different temperatures. He found that for low frequencies and high temperatures a value of 0.5 is valid. Thus S_{bit} is equal to $3G^*$.

In 1977, Bonnaure et al. [1977] established the following relationships to determine the stiffness modulus of an asphalt mix from the bitumen stiffness and volumetric properties. These were determined based on a comprehensive study involving a wide variety of mixes from which complex moduli were determined using two point bending tests on trapezoidal specimens under sinusoidal loading:

$$\beta_1 = \log(E\infty) = 10.82 - 1.342\frac{(100 - V_s)}{(V_s + V_b)} \tag{C.11}$$

$$\beta_2 = 8.0 + 0.00568V_s + 0.0002135V_s^2 \tag{C.12}$$

$$\beta_3 = 0.6\log\left(\frac{1.37V_b^2 - 1}{1.33V_b - 1}\right) \tag{C.13}$$

$$\beta_4 = 0.7582(\beta_1 - \beta_2) \tag{C.14}$$

For $5 \times 10^6 N/m^2 < S_{bit} < 10^9$ N/m^2 :

$$\log S_{mix} = \frac{\beta_3 + \beta_4}{2}(\log S_{bit} - 8) + \frac{\beta_4 - \beta_3}{2}|\log S_{bit} - 8| + \beta_2 \tag{C.15}$$

For $10^9 N/m^2 < S_{bit} < 3 \times 10^9$ N/m^2 :

$$\log S_{mix} = \beta_2 + \beta_3 + 2.0959(\beta_1 - \beta_2 - \beta_4)(\log S_{bit} - 9) \tag{C.16}$$

In Equation C.11, β_1 is an estimate of the maximum stiffness of the mix in Pa. Bonnaure et al. [1977] also derived a formula for predicting the phase angle of an asphalt mix as a function of the binder stiffness modulus (MPa) and percent air voids (V_a). For a binder stiffness between 5 and 2000 MPa:

$$\varphi_{mix} = 16.36 V_b^{0.352} \times \exp\left[0.974 \times \frac{\log\left(\frac{S_{bit}}{5}\right)}{\log\left(\frac{S_{bit}}{2000}\right)} \times V_a^{-0.172}\right] \tag{C.17}$$

For S_{bit} higher than 2000 MPa, the phase angle is assumed to be zero.

Hardening of the binder occurs with ageing under in situ conditions. This leads to reduced penetration and an increase in the softening point of the bitumen. Shahin [1977] have developed empirical equations to account for the ageing of bitumen:

$$\begin{aligned} \text{Pen(t)} = -48.258 - 2.561\sqrt{t} + 0.1438\text{Pen}(0) - 8.466 V_a X_t \\ +1.363\text{TFOT} + 0.9225\text{Pen}(0) X_t \end{aligned} \tag{C.18}$$

$$T_{RB}(t) = 7.826 + 1.757\sqrt{t} + 1.585 T_{RB}(0) - 0.516\text{TFOT} \tag{C.19}$$

where

t = Time the binder has been in the pavement, months

Pen(t) = Penetration at 25 °C of the aged bitumen, 0.1 mm

Pen(0) = Penetration at 25 °C of the original bitumen, 0.1 mm

$T_{RB}(t)$ = Softening point of aged binder, °C

$T_{RB}(0)$ = Softening point of original binder, °C

V_a = Volume of voids in the mix, %

TFOT = Thin Film Oven Test, % of original penetration

$$X_t = \frac{1}{\sqrt{t}+1} \tag{C.20}$$

Dauzats and Rampal [1988] report modifications to the above equations based on a study of binders recovered from pavements in France over a ten year period. These modified equations are not a function of the thin film oven test.

$$\text{Pen(t)} = 11.9925 - 1.2578\sqrt{t} + 0.3322\text{Pen}(0) - 2.9965V_v X(t) + 0.765\text{Pen}(0)X(t) \quad \text{(C.21)}$$

$$T_{RB} = 64.448 + 1.5755\sqrt{(t)} - 0.2531\text{Pen}(0) + 0.5518V_a \quad \text{(C.22)}$$

Pell [1987] presented the following relationship between mix stiffness, binder stiffness and VMA in the elastic region, derived from earlier work done by Heukelom. The n in the equation is the same as that defined in Equation C.5:

$$\text{S}_{\text{mix}} + \text{S}_{\text{bit}} \left[1 + \frac{257.5 - 2.5\text{VMA}}{n\,(\text{VMA} - 3)}\right]^n \quad \text{(C.23)}$$

In developing the DAMA computer program for the Asphalt Institute, Hwang and Witczak [1979] applied the following formulas to determine the dynamic modulus of HMA:

$$|E^*| = 100000 \times 10^{\beta_1} \quad \text{(C.24)}$$

$$\beta_1 = \beta_3 + 0.000005\beta_2 - 0.00189\beta_2 \times f^{-1.1} \quad \text{(C.25)}$$

$$\beta_2 = \beta_4^{0.5} \times T^{\beta_5} \quad \text{(C.26)}$$

$$\beta_3 = 0.553833 + 0.028829P_{200} \times f^{-0.1703} - 0.03476V_a + 0.070377\lambda + 0.931757f^{-0.02774} \quad \text{(C.27)}$$

$$\beta_4 = 0.483V_b \quad \text{(C.28)}$$

$$\beta_5 = 1.3 + 0.49825 \log f \quad \text{(C.29)}$$

where

f = Load frequency, Hz

T = Temperature, fahrenheit

P_{200} = Percentage by weight of aggregate passing 0.075 mm sieve

λ = Binder viscosity at 70 fahreheit in 10^6 poise

If insufficient viscosity data are available to estimate λ at 70 fahreheit, the following equation may be used:

$$\lambda = 29508.2\,(\text{Pen})^{-2.1939} \tag{C.30}$$

where

λ = Binder viscosity at 70 fahreheit in 10^6 poise

Pen = Penetration at 25 °C

Fonseca and Witczak [1996] have developed an empirical model for estimating the dynamic modulus of HMA, shown below:

$$\begin{aligned}\log E = {} & -0.261 + 0.008225P_{200} - 0.00000101P_{200}^2 + 0.00196P_4 \\ & -0.03157V_a - 0.415\frac{V_b}{V_b + V_a} + \frac{1.87 + 0.002808P_4 + 0.0000404P_{3/8}}{1 + e^{(-0.716\log f - 0.7425\log \eta)}} \\ & - \frac{0.0001786P_{3/8}^2 - 0.0164P_{3/4}}{1 + e^{(-0.716\log f - 0.7425\log \eta)}}\end{aligned} \tag{C.31}$$

where

E = Asphalt mix dynamic modulus, 10^5 psi

η = Bitumen viscosity, 10^6 poise

f = Load frequency, Hz

$P_{3/4}$ = Percent retained on the 3/4 inch sieve by total aggregate weight

$P_{3/8}$ = Percent retained on the 3/8 inch sieve by total aggregate weight

P_4 = Percent retained on the No. 4 sieve by total aggregate weight

P_{200} = Percent retained on the No. 200 sieve by total aggregate weight

C.2 Fatigue

Fatigue models for HMA based on tensile strain and stiffness generally need to be calibrated by applying shift factors. These factors account for healing, crack propagation and traffic wandering in the field. Therefore fatigue damage is represented by two distinct stages that includes crack initiation followed by crack propagation. The formulations that follow are specific to crack initiation.

Based on 146 fatigue lines covering a wide range of mixes, bitumens, and testing conditions, Shell [Bonnaure et al., 1980] developed separate equations for constant stress and constant strain tests.

For constant stress tests:

$$\varepsilon_t = (36.43PI - 1.82PI \times V_b + 9.71V_b - 24.04) \times 10^6 \left(\frac{\mathrm{S_{mix}}}{5 \times 10^9}\right)^{-0.28} \left(\frac{N_f}{10^6}\right)^{-0.2} \tag{C.32}$$

For constant strain tests:

$$\varepsilon_t = (36.43PI - 1.82PI \times V_b + 9.71V_b - 24.04) \times 10^6 \left(\frac{\mathrm{S_{mix}}}{5 \times 10^10}\right)^{-0.36} \left(\frac{N_f}{10^6}\right)^{-0.2} \tag{C.33}$$

where

ε_t = Tensile strain

PI = Penetration Index

V_b = Volume of binder, %

$\mathrm{S_{mix}}$ = Stiffness modulus of the mix, Pa

N_f = Number of repetitions to failure

The laboratory fatigue equations developed by the Asphalt Institute [AI, 1982] are based on the constant stress criterion. The number of constant strain applications to failure (20 percent fatigue cracking over the entire pavement area) is determined as follows:

$$N_f = 0.00432 \times C \times \varepsilon_t^{-3.291} |E^*|^{-0.854} \tag{C.34}$$

in which C is the correction factor expressed as $C = 10^M$ and

$$M = 4.84 \left(\frac{V_b}{V_b + V_v} - 0.69 \right) \tag{C.35}$$

where

N_f = Number of load applications to failure

V_b = Volume of binder, %

V_a = Volume of air voids, %

E^* = Dynamic modulus, lbf/in^2

A fatigue life shift factor of 18.4 is typically used to account for the differences between laboratory and field conditions.

Cooper and Pell [1974] developed a procedure for predicting the laboratory fatigue behaviour of bitumen bound materials. Fatigue testing on a wide range of mixes was conducted in the laboratory under controlled stress conditions. Analysis of the data collected showed that the fatigue relationships for the mixes considered intersect at a common point, or focus. For the tests conducted, they observed that the focus occurred at a strain level of $6.3x10^4$ in/in and at a life, N, equal to 40 applications. From this result, a simple procedure for predicting the laboratory fatigue behavior

of bituminous mixes was developed. Essentially the procedure involves the establishment of a mean fatigue life N_1 at a particular value of strain ε_1 and the connection of this point to the focus. On the basis of the fatigue test results, a regression equation for predicting the number of allowable applications for a strain level of 1 x $10^{-}4$ in/in was developed. The regression analysis showed that the fatigue life at this particular strain level is related to the binder volume (V_b) and the ring and ball softening point by the equation:

$$\log N_f \left(\varepsilon = 10^{-4}\right) = 4.13 \log V_b + 6.95 \log T_{RB} - 11.13 \qquad \text{(C.36)}$$

where

N_f = Number of cycles to failure

V_b = Volume of binder, %

T_{RB} = Ring and ball softening point, °C

ε = Strain , in/in

This relationship was used to develop the performance model for predicting fatigue cracking in the British design procedure. However, to account for differences between laboratory and field conditions, the fatigue life at any strain level is increased by a factor 100, which results from a factor 5 that accounts for the effect of rest periods and from a factor of 20 that accounts for differences in crack propagation times between laboratory and field conditions.

Pell and Cooper [1975] have also shown that the effect of binder content and void content on fatigue performance can be determined using a correction factor proportional to:

$$\frac{V_b}{V_b + V_a} \qquad \text{(C.37)}$$

where

V_b = Binder volume, percent

V_a = Air void volume, percent

Based on SHRP research [SHRP, 1994], the following strain-dependent fatigue model was used for surrogate analysis:

$$N_f = 0.3592 \exp(0.077 \cdot \text{VFB}) \cdot \varepsilon_i^{-3.624} \cdot (E_0^{**})^{-2.72} \tag{C.38}$$

where

N_f = Fatigue life

ε_i = Initial strain

E_0^{**} = Initial loss modulus, MPa

VFB = Voids filled with binder, %

This model is being further revised.

C.3 References

AI. Research and development of the asphalt institute's thickness design manual (MS-1). Technical Report Research Report 82-2, Asphalt Institute, 1982.

G. Baladi. Fatigue life and permanent deformation characteristics of asphalt concrete mixes. Technical Report Transportation Research Record 1227, Transportation Research Board, Washington, D.C., 1989.

F. Bonnaure, G. Gest, A. Gravois, and P. Uge. A new method of predicting the stiffness of asphalt paving mixtures. *Proceedings of the Association of Asphalt Paving Technologists*, Vol. 46, 1977.

F. Bonnaure, A. Gravois, and J. Udron. A new method for predicting the fatigue life of bituminous mixes. *Proceedings of the Association of Asphalt Paving Technologists*, Vol. 49, 1980.

K. E. Cooper and P. S. Pell. The effect of mix variables on the fatigue strength of bituminous materials. Technical Report TRRL Report 633, Transportation and Road Research Laboratory, 1974.

M. Dauzats and A. Rampal. Mécanisme de fissuration de surface des couches de roulement (in french). *Bulletin de Liaison des Laboratoires des Ponts et Chaussées*, 1988.

W. E. Fijn Van Draat and P. Sommer. Ein gerat zur bestimmung der dynamischen elastizitatsmoduln von asphalt (in german). *Strasse und Autobahn*, Vol. 6, 1965.

O. A. Fonseca and W.M. Witczak. Prediction methodology for the dynamic modulus of in-place aged asphalt mixtures. *Proceedings of the Association of Asphalt Paving Technologists*, Vol. 65, 1996.

L. Francken. Module complexe des mélanges bitumineux (in french). Technical report, Bulletin de Liaison des Laboratoires des Ponts et Chaussées, spécial V, Paris, 1977a.

L. Francken. Permanent deformation law of bituminous road mixes in repeated triaxial compression. *Proceedings of the Fourth International Conference on the Structural Design of Asphalt Pavements, Ann Arbor, Michigan*, 1977b.

L. Francken and A. Vanelstraete. Complex moduli of bituminous binders and mixtures. interpretation and evaluation. *Eurasphalt and Eurobitume Congress, Strasbourg*, 1996.

W. Heukelom. Observations on the rheology and fracture of bitumens and asphalt mixes. *Proceedings of the Association of Asphalt Paving Technologists*, Vol. 35, 1966.

W. Heukelom and J. G. Klomp. Road design and dynamic loading. *Poceedings Association of Asphalt Paving Technologists*, Vol. 33, 1964.

C. Huet. Représentation des modules et complaisances complexes dans les plans complexes arithmétique et logarithmique (in french). *Cahiers du groupe français de rhéologie, Tome I N5*, 1967.

D. Hwang and M. W. Witczak. *Program DAMA (Chevron), User's Manual.* Department of Civil Engineering, University of Maryland, 1979.

R. W. May and M. W. Witczak. An automated asphalt concrete mix analysis system. *Association of Asphalt Paving Technologists*, Vol. 61, 1992.

P. S. Pell. Pavement materials. *Proceedings of the Sixth International Conference on the Structural Design of Asphalt Pavements, Ann Arbor, Michigan*, 1987.

P. S. Pell and K. E. Cooper. The effect of testing and mix variables on the fatigue performance of bituminous materials. *Proceedings of the Association of Asphalt Paving Technologists*, Vol. 44, 1975.

H. Sabha, J. Groenendijk, and A. A. A. Moolenaar. Estimation of crack growth parameters and fatigue characteristics of asphalt mixes using simple tests. Technical report, Delft University of Technology, Faculty of Civil Engineering, Road and Railway Research Laboratory, 1995.

G. Sayegh. Viscoelastic properties of bituminous mixtures. *Proceedings of the Second International Conference on the Structural Design of Asphalt Pavements, Ann Arbor, Michigan*, 1967.

M. Y. Shahin. Design system for minimising asphalt concrete thermal cracking. *Proceedings of the Fourth International Conference on the Structural Design of Asphalt Pavements, Ann Arbor, Michigan*, 1977.

SHRP. Fatigue response of asphalt-aggregate mixtures. Technical Report SHRP-A-404, Strategic Highway Research Program, Washington, D.C., 1994.

C. van der Poel. A general system describing the visco-elastic properties of bitumens and its relation to routine test data. *Journal of Applied Chemistry*, Vol. 4, 1954.

Appendix D

Marshall mix designs

This appendix contains reference information referred to in Section 5.2, which addresses the validation of the PAVDAM model.

The following Marshall mix designs were received from Much Asphalt Ltd., an asphalt contractor in the Western Cape, South Africa and were used for the validation of PAVDAM.

MUCH ASPHALT (Pty).Ltd - CONTERMANSKLOOF

ASPHALT MIX DESIGN

MUCH

REF NUMBER : CK4
Date : February 2000
MIX NAME : B T B
MIX TYPE : 26mm Bitumen Treated Basecourse : Continuously Graded (CSRA)

AGGREGATES		
Number	Nominal Size	**Description and source**
1	26mm Stone	Malmesbury Hornfels, ex Alpha Stone - Peninsula Quarry
2	13mm Stone	Malmesbury Hornfels, ex Alpha Stone - Peninsula Quarry
3	6mm Stone	Malmesbury Hornfels, ex Alpha Stone - Peninsula Quarry
4	Crusher Dust	Malmesbury Hornfels, ex Alpha Stone - Peninsula Quarry
FILLERS		
	Type	**Description and source**
5		

	Sieve analysis and % passing								
	AGGREGATES					FILLERS		Combined	
Number	1	2	3	4				Grading	Specification
% In Mix	16%	22%	12%	50%				100%	
37.5	100	100	100	100				**100**	100 - 100
26.5	100	100	100	100				**100**	100 - 100
19.0	13	100	100	100				**86**	85 - 95
13.2	2	99	100	100				**84**	71 - 86
9.5	1	34	100	100				**70**	62 - 78
6.7		4	94	100				**62**	52 - 69
4.75		2	31	99				**54**	42 - 60
2.36		1	3	75				**38**	30 - 48
1.18			1	49				**25**	22 - 38
0.600				34				**17**	16 - 28
0.300				26				**13**	12 - 20
0.150				20				**10**	8 - 15
0.075				15.2				**7.6**	5 - 10
Bulk Relative Density	2.701	2.717	2.703	2.709				**2.717**	
Surface Area								**5.97**	
Sand Equivalent									
Flakiness Index	16.7	21.1	32.6						

REF NUMBER : CK4
Date : February 2000
MIX TYPE : 26mm Bitumen Treated Basecourse : Continuously Graded (CSRA)

BINDER			
Grade\Type	60/70 PEN	Bulk Relative Density	1.025
Penetration	65	Mixing Temperature	150 deg.C
Source	CalRef	Compaction Temp.	140 deg.C

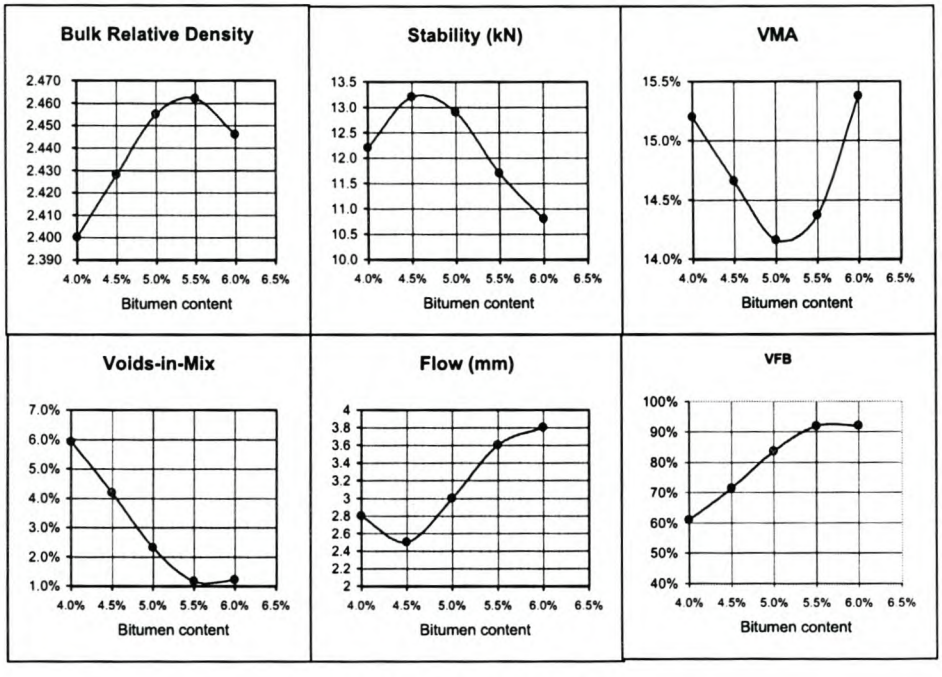

PRODUCT ENGINEERING DATA

							PROPOSAL
Binder Content	4.0%	4.5%	5.0%	5.5%	6.0%		
Bulk Relative Density	2.400	2.428	2.455	2.462	2.446		
Max. Theor. Density	2.551	2.534	2.513	2.491	2.476		
% Voids-In-Mix	5.9%	4.2%	2.3%	1.2%	1.2%		
% V.M.A.	15.2%	14.7%	14.2%	14.4%	15.4%		
% V.F.B.	61.1%	71.5%	83.7%	91.9%	92.1%		
Stability (kN)	12.2	13.2	12.9	11.7	10.8		
Flow (mm)	2.8	2.5	3.0	3.6	3.8		
Dynamic ITS (kPa)	890	1100	1235	1360	1400		
Dynamic Creep (mPa)	18	22	30	24	23		
Air Permeability	impermeable	impermeable	impermeable	impermeable	impermeable		
Film Thickness (µm)	6.1	6.9	7.8	8.8	9.6		
% Binder Absorbtion	0.2%	0.2%	0.2%	0.1%	0.1%		
Immersion Index (%)	90.0%	92.5%	95.5%	96.1%	97.1%		
Effective Density							

MUCH ASPHALT (Pty).Ltd - CONTERMANSKLOOF

ASPHALT MIX DESIGN

MUCH

REF NUMBER : CK6
Date : February 2000
MIX NAME : Lambs
MIX TYPE : 37mm Lamb's : Continuously Graded (Colto)

AGGREGATES		
Number	Nominal Size	**Description and source**
1	37mm RoC	Malmesbury Hornfels, ex Alpha Stone - Peninsula Quarry
2	Crusher Dust	Malmesbury Hornfels, ex Alpha Stone - Peninsula Quarry
FILLERS		
	Type	**Description and source**

	Sieve analysis and % passing								
	AGGREGATES					FILLERS		Combined	
Number	1	2	3	4				Grading	Specification
% In Mix	75%	25%						100%	
37.5	100	100						**100**	100 - 100
26.5	83	100						**87**	100 - 100
19.0	67	100						**75**	85 - 95
13.2	57	100						**68**	71 - 86
9.5	47	100						**60**	62 - 78
6.7	36	100						**52**	52 - 69
4.75	29	99						**47**	42 - 60
2.36	19	75						**33**	30 - 48
1.18	13	51						**23**	22 - 38
0.600	9	34						**15**	16 - 28
0.300	7	26						**12**	12 - 20
0.150	6	20						**10**	8 - 15
0.075	5.2	13.4						**7.3**	5 - 10
Bulk Relative Density	2.685	2.699				2.595		**2.689**	
Surface Area								**5.94**	
Sand Equivalent		58							
Flakiness Index	21.8								

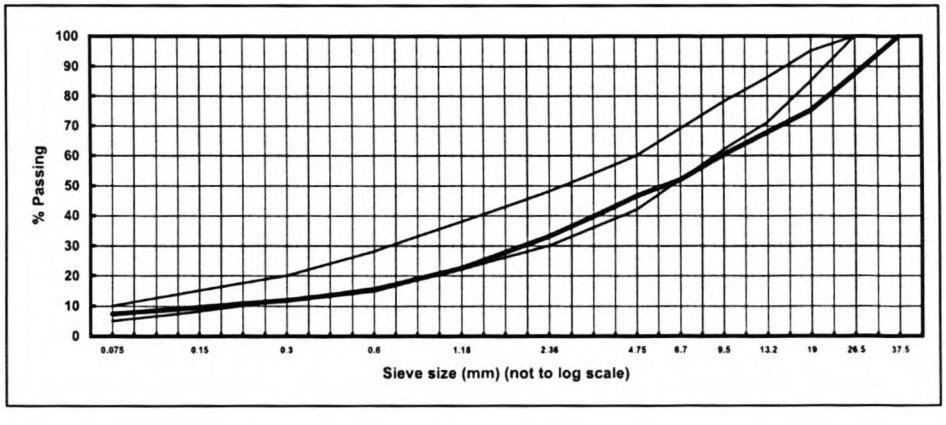

REF NUMBER : CK6
Date : February 2000
MIX TYPE : 37mm Lamb's : Continuously Graded (Colto)

BINDER			
Grade\Type	60/70PEN	Bulk Relative Density	1.025
Penetration	65	Mixing Temperature	150 deg.C
Source	CalRef	Compaction Temp.	140 deg.C

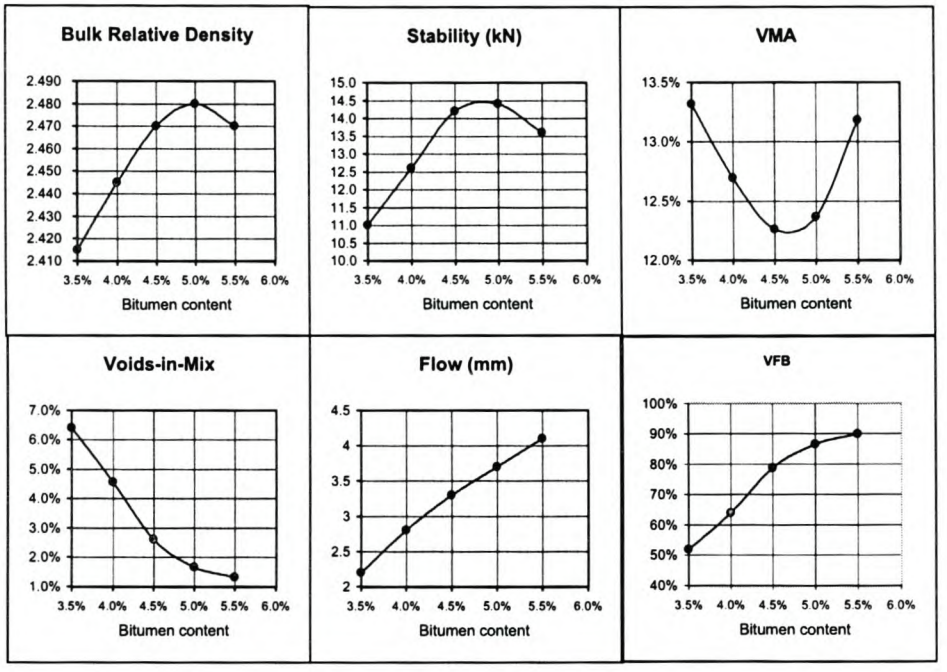

PRODUCT ENGINEERING DATA

							PROPOSAL
Binder Content	3.5%	4.0%	4.5%	5.0%	5.5%		
Bulk Relative Density	2.415	2.445	2.470	2.480	2.470		
Max. Theor. Density	2.580	2.562	2.536	2.522	2.503		
% Voids-In-Mix	6.4%	4.6%	2.6%	1.7%	1.3%		
% V.M.A.	13.3%	12.7%	12.3%	12.4%	13.2%		
% V.F.B.	52.0%	64.0%	78.8%	86.5%	90.0%		
Stability (kN)	11.0	12.6	14.2	14.4	13.6		
Flow (mm)	2.2	2.8	3.3	3.7	4.1		
ITS (kPa)	1250	1333	1389	1400	1410		
Dynamic Creep (mPa)	22	25	22	20	20		
Air Permeability	impermeable	impermeable	impermeable	impermeable	impermeable		
Film Thickness (µm)	0.9	1.7	2.6	3.5	4.3		
% Binder Absorbtion	3.0%	3.0%	3.0%	3.0%	3.0%		
Immersion Index (%)	82.9%	85.8%	90.0%	90.0%	89.0%		
Effective Density							

Appendix E

NCAT MMLS3 section construction data

Section S9

Laboratory Diary

General Description of Mix and Materials

Design Method:	Superpave
Compactive Effort:	100 gyrations
Binder Performance Grade:	67-22
Modifier Type:	NA
Aggregate Type:	Granite
Gradation Type:	BRZ

Avg. Lab Properties of Plant Produced Mix

Sieve Size:	% Passing:
1"	100
3/4"	100
1/2"	93
3/8"	82
No. 4	53
No. 8	36
No. 16	27
No. 30	20
No. 50	14
No. 100	9
No. 200	5.7

Asphalt Binder Content:	4.7%
Compacted Pill Bulk Gravity:	2.419
Theoretical Maximum Gravity:	2.510
Computed Air Voids:	3.6%

Construction Diary

Relevant Conditions for Construction

Completion Date:	Monday, July 10, 2000
24 Hour High Temperature (F):	101
24 Hour Low Temperature (F):	75
24 Hour Rainfall (in):	0.00
Lift Type:	dual
Design Thickness of Test Mix (in):	3.0

Plant Configuration and Placement Details

Component:		% Setting:
Liquid Binder Setting		4.8%
Granite	67	15.0%
Granite	78M	47.0%
Granite	Dry Screenings	20.0%
Granite	Washed Screenings	18.0%

Approximate Length (ft):	206
Surveyed Thickness of Section (in):	3.0
Std Dev of Section Thickness (in):	0.1
Type of Tack Coat Utilized:	CQS-1h
Target Tack Application Rate:	0.03 gal / sy
Avg Mat Temperature Behind Paver (F):	331
Average Section Compaction:	93.4%

General Notes:

1) Mixes are listed chronologically in order of completion date (i.e., construction began with E2 and ended with E1).
2) Sections are referenced by quadrant and sequence number, where "E2" refers to section 2 of the east quadrant.
3) "dual " lift type indicates that the lower and upper lifts were constructed with the same experimental mix.
4) The total thickness of all experimental sections is 4 inches by design, with the exception of S8, S9, S10, S11.
5) ARZ, TRZ, and BRZ refer to gradations intended to pass above, through, and below the restricted zone.
6) SMA and OGFC refer to stone matrix asphalt and open-graded friction course, respectively.

Section S10

Laboratory Diary

General Description of Mix and Materials

Design Method:	Superpave
Compactive Effort:	100 gyrations
Binder Performance Grade:	67-22
Modifier Type:	NA
Aggregate Type:	Granite
Gradation Type:	ARZ

Avg. Lab Properties of Plant Produced Mix

Sieve Size:	% Passing:
1"	100
3/4"	100
1/2"	95
3/8"	88
No. 4	69
No. 8	52
No. 16	38
No. 30	27
No. 50	19
No. 100	11
No. 200	6.6

Asphalt Binder Content:	5.2%
Compacted Pill Bulk Gravity:	2.407
Theoretical Maximum Gravity:	2.488
Computed Air Voids:	3.2%

Construction Diary

Relevant Conditions for Construction

Completion Date:	Tuesday, July 11, 2000
24 Hour High Temperature (F):	98
24 Hour Low Temperature (F):	78
24 Hour Rainfall (in):	0.00
Lift Type:	dual
Design Thickness of Test Mix (in):	3.0

Plant Configuration and Placement Details

Component:		% Setting:
Liquid Binder Setting		5.3%
Granite	67	11.0%
Granite	78M	25.0%
Granite	Dry Screenings	32.0%
Granite	Washed Screenings	32.0%

Approximate Length (ft):	195
Surveyed Thickness of Section (in):	3.1
Std Dev of Section Thickness (in):	0.1
Type of Tack Coat Utilized:	CQS-1h
Target Tack Application Rate:	0.03 gal / sy
Avg Mat Temperature Behind Paver (F):	300
Average Section Compaction:	93.7%

General Notes:

1) Mixes are listed chronologically in order of completion date (i.e., construction began with E2 and ended with E1).
2) Sections are referenced by quadrant and sequence number, where "E2" refers to section 2 of the east quadrant.
3) "dual " lift type indicates that the lower and upper lifts were constructed with the same experimental mix.
4) The total thickness of all experimental sections is 4 inches by design, with the exception of S8, S9, S10, S11.
5) ARZ, TRZ, and BRZ refer to gradations intended to pass above, through, and below the restricted zone.
6) SMA and OGFC refer to stone matrix asphalt and open-graded friction course, respectively.

Section E2

Laboratory Diary

General Description of Mix and Materials

Design Method:	Superpave
Compactive Effort:	100 gyrations
Binder Performance Grade:	67-22
Modifier Type:	NA
Aggregate Type:	Granite
Gradation Type:	BRZ

Avg. Lab Properties of Plant Produced Mix

Sieve Size:	% Passing:
1"	100
3/4"	100
1/2"	96
3/8"	74
No. 4	41
No. 8	29
No. 16	22
No. 30	18
No. 50	12
No. 100	7
No. 200	4.1

Asphalt Binder Content:	4.7%
Compacted Pill Bulk Gravity:	2.434
Theoretical Maximum Gravity:	2.505
Computed Air Voids:	2.8%

Construction Diary

Relevant Conditions for Construction

Completion Date:	Tuesday, April 11, 2000
24 Hour High Temperature (F):	76
24 Hour Low Temperature (F):	50
24 Hour Rainfall (in):	0.00
Lift Type:	dual
Design Thickness of Test Mix (in):	4.0

Plant Configuration and Placement Details

Component:		% Setting:
Liquid Binder Setting		4.8%
Granite	7	48.0%
Granite	89	17.0%
Granite	M10	20.0%
Granite	W10	15.0%

Approximate Length (ft):	213
Surveyed Thickness of Section (in):	4.2
Std Dev of Section Thickness (in):	0.2
Type of Tack Coat Utilized:	CQS-1h
Target Tack Application Rate:	0.03 gal / sy
Avg Mat Temperature Behind Paver (F):	297
Average Section Compaction:	94.7%

General Notes:

1) Mixes are listed chronologically in order of completion date (i.e., construction began with E2 and ended with E1).
2) Sections are referenced by quadrant and sequence number, where "E2" refers to section 2 of the east quadrant.
3) "dual " lift type indicates that the lower and upper lifts were constructed with the same experimental mix.
4) The total thickness of all experimental sections is 4 inches by design, with the exception of S8, S9, S10, S11.
5) ARZ, TRZ, and BRZ refer to gradations intended to pass above, through, and below the restricted zone.
6) SMA and OGFC refer to stone matrix asphalt and open-graded friction course, respectively.

Section E6

Laboratory Diary

General Description of Mix and Materials

Design Method:	Superpave
Compactive Effort:	100 gyrations
Binder Performance Grade:	67-22
Modifier Type:	NA
Aggregate Type:	Granite
Gradation Type:	TRZ

Avg. Lab Properties of Plant Produced Mix

Sieve Size:	% Passing:
1"	100
3/4"	100
1/2"	96
3/8"	81
No. 4	52
No. 8	37
No. 16	28
No. 30	22
No. 50	15
No. 100	8
No. 200	4.3

Asphalt Binder Content:	5.0%
Compacted Pill Bulk Gravity:	2.411
Theoretical Maximum Gravity:	2.510
Computed Air Voids:	3.9%

Construction Diary

Relevant Conditions for Construction

Completion Date:	Thursday, April 13, 2000
24 Hour High Temperature (F):	75
24 Hour Low Temperature (F):	51
24 Hour Rainfall (in):	0.00
Lift Type:	dual
Design Thickness of Test Mix (in):	4.0

Plant Configuration and Placement Details

Component:		% Setting:
Liquid Binder Setting		5.0%
Granite	7	33.0%
Granite	89	23.0%
Granite	M10	24.0%
Granite	W10	20.0%

Approximate Length (ft):	211
Surveyed Thickness of Section (in):	4.2
Std Dev of Section Thickness (in):	0.1
Type of Tack Coat Utilized:	CQS-1h
Target Tack Application Rate:	0.03 gal / sy
Avg Mat Temperature Behind Paver (F):	299
Average Section Compaction:	92.9%

General Notes:

1) Mixes are listed chronologically in order of completion date (i.e., construction began with E2 and ended with E1).
2) Sections are referenced by quadrant and sequence number, where "E2" refers to section 2 of the east quadrant.
3) "dual " lift type indicates that the lower and upper lifts were constructed with the same experimental mix.
4) The total thickness of all experimental sections is 4 inches by design, with the exception of S8, S9, S10, S11.
5) ARZ, TRZ, and BRZ refer to gradations intended to pass above, through, and below the restricted zone.
6) SMA and OGFC refer to stone matrix asphalt and open-graded friction course, respectively.

Section E8

Laboratory Diary

General Description of Mix and Materials

Design Method:	Superpave
Compactive Effort:	100 gyrations
Binder Performance Grade:	67-22
Modifier Type:	NA
Aggregate Type:	Granite
Gradation Type:	ARZ

Avg. Lab Properties of Plant Produced Mix

Sieve Size:	% Passing:
1"	100
3/4"	100
1/2"	98
3/8"	86
No. 4	66
No. 8	51
No. 16	38
No. 30	28
No. 50	18
No. 100	10
No. 200	5.2

Asphalt Binder Content:	5.6%
Compacted Pill Bulk Gravity:	2.372
Theoretical Maximum Gravity:	2.477
Computed Air Voids:	4.2%

Construction Diary

Relevant Conditions for Construction

Completion Date:	Tuesday, April 18, 2000
24 Hour High Temperature (F):	85
24 Hour Low Temperature (F):	50
24 Hour Rainfall (in):	0.00
Lift Type:	dual
Design Thickness of Test Mix (in):	4.0

Plant Configuration and Placement Details

Component:		% Setting:
Liquid Binder Setting		5.7%
Granite	7	30.0%
Granite	89	10.0%
Granite	M10	24.0%
Granite	W10	36.0%

Approximate Length (ft):	208
Surveyed Thickness of Section (in):	4.2
Std Dev of Section Thickness (in):	0.1
Type of Tack Coat Utilized:	CQS-1h
Target Tack Application Rate:	0.03 gal / sy
Avg Mat Temperature Behind Paver (F):	290
Average Section Compaction:	92.7%

General Notes:

1) Mixes are listed chronologically in order of completion date (i.e., construction began with E2 and ended with E1).
2) Sections are referenced by quadrant and sequence number, where "E2" refers to section 2 of the east quadrant.
3) "dual " lift type indicates that the lower and upper lifts were constructed with the same experimental mix.
4) The total thickness of all experimental sections is 4 inches by design, with the exception of S8, S9, S10, S11.
5) ARZ, TRZ, and BRZ refer to gradations intended to pass above, through, and below the restricted zone.
6) SMA and OGFC refer to stone matrix asphalt and open-graded friction course, respectively.

Appendix F

NCAT MMLS3 section performance data

SECTION S9

Laboratory Performance

General Description of Mix and Materials

Design Method:	Superpave
Compactive Effort:	100 gyrations
Binder Performance Grade:	67-22
Modifier Type:	NA
Laboratory Determined Asphalt Content:	4.7%
General Aggregate Type:	Granite
Approximate Gradation Type:	BRZ

Avg. Lab Properties of Plant Produced Mix

SST Repeated Load Perm. Strain (microns):	NA
Unconfined Creep Perm. Strain:	NA
Confined Creep Perm. Strain:	NA
Unconfined Dynamic Perm. Strain:	NA
Confined Dynamic Perm. Strain:	NA
Dynamic Modulus:	NA
COE Gyratory Shear Index:	NA
SGC Shear Ratio:	NA
Asphalt Pavement Analyzer (mm):	2.15
Hamburg Loaded Wheel Tester (mm):	3.65
Rotary Loaded Wheel Tester (mm):	2.46
Purwheel Loaded Wheel Tester (mm):	NA

Roadway Performance (9/18/02)

Relevant Field Conditions

Total Traffic Applied (ESAL's):	8,599,781
Avg 7 Day High Air Temp (F):	NA
Avg Surface Temp in Past Week:	NA
Avg Surface Temp in 2001:	NA
Highest Surface Temp in 2001:	NA

Roadway Performance Properties

Rutting via ARAN 3 Point Approx. (in):	0.19
Rutting via Transverse Profile (in):	NA
Approximate Fn:	0.369
Average IRI (inches/mile):	21.5
MTD in inches:	0.030

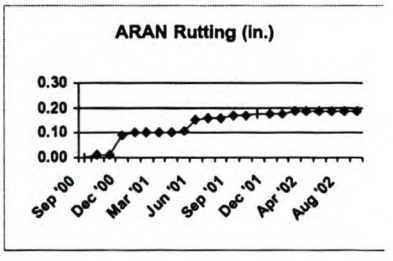

General Notes:

1) Test specimens were compacted to 7 +/- 1% air voids for tensile strength ratio (TSR) testing.
2) Test specimens were compacted to avg QC +/- 1% air voids for SST, creep, APA, and assorted LWT testing.
3) The vast majority of pills used as research test specimens were compacted during construction.
4) When an insufficient quantity of construction-compacted pills met target air voids, reheated mix was used.
5) All suitable pills were randomly assigned to test protocols in a manner to achieve equal avg and std dev in VTM.
6) All test protocols utilized sample sets consisting of 3 replicates per test (e.g., APA result is avg of 3 pills).
7) Loaded wheel testing consisted of 8000 cycles in the dry state with samples conditioned at 147.2 F long enough to insure a uniform temperature throughout the specimen but in no case longer than 24 hours.
8) APA testing utilized 1 inch OD hose, 120 psi pressure, 120 lb load, cylindrical specimens, manual depths.
9) Gyratory shear testing was conducted at mat compaction temperatures based upon construction measurements.

SECTION S10

Laboratory Performance

General Description of Mix and Materials

Design Method:	Superpave
Compactive Effort:	100 gyrations
Binder Performance Grade:	67-22
Modifier Type:	NA
Laboratory Determined Asphalt Content:	5.2%
General Aggregate Type:	Granite
Approximate Gradation Type:	ARZ

Avg. Lab Properties of Plant Produced Mix

SST Repeated Load Perm. Strain (microns):	NA
Unconfined Creep Perm. Strain:	NA
Confined Creep Perm. Strain:	NA
Unconfined Dynamic Perm. Strain:	NA
Confined Dynamic Perm. Strain:	NA
Dynamic Modulus:	NA
COE Gyratory Shear Index:	NA
SGC Shear Ratio:	NA
Asphalt Pavement Analyzer (mm):	2.55
Hamburg Loaded Wheel Tester (mm):	3.51
Rotary Loaded Wheel Tester (mm):	2.68
Purwheel Loaded Wheel Tester (mm):	NA

Roadway Performance (9/18/02)

Relevant Field Conditions

Total Traffic Applied (ESAL's):	8,599,781
Avg 7 Day High Air Temp (F):	NA
Avg Surface Temp in Past Week:	NA
Avg Surface Temp in 2001:	NA
Highest Surface Temp in 2001:	NA

Roadway Performance Properties

Rutting via ARAN 3 Point Approx. (in):	0.18
Rutting via Transverse Profile (in):	NA
Approximate Fn:	0.404
Average IRI (inches/mile):	29.2
MTD in inches:	0.020

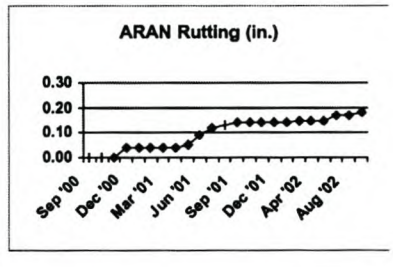

General Notes:

1) Test specimens were compacted to 7 +/- 1% air voids for tensile strength ratio (TSR) testing.
2) Test specimens were compacted to avg QC +/- 1% air voids for SST, creep, APA, and assorted LWT testing.
3) The vast majority of pills used as research test specimens were compacted during construction.
4) When an insufficient quantity of construction-compacted pills met target air voids, reheated mix was used.
5) All suitable pills were randomly assigned to test protocols in a manner to achieve equal avg and std dev in VTM.
6) All test protocols utilized sample sets consisting of 3 replicates per test (e.g., APA result is avg of 3 pills).
7) Loaded wheel testing consisted of 8000 cycles in the dry state with samples conditioned at 147.2 F long enough to insure a uniform temperature throughout the specimen but in no case longer than 24 hours.
8) APA testing utilized 1 inch OD hose, 120 psi pressure, 120 lb load, cylindrical specimens, manual depths.
9) Gyratory shear testing was conducted at mat compaction temperatures based upon construction measurements.

SECTION E2

Laboratory Performance

General Description of Mix and Materials

Design Method:	Superpave
Compactive Effort:	100 gyrations
Binder Performance Grade:	67-22
Modifier Type:	NA
Laboratory Determined Asphalt Content:	4.7%
General Aggregate Type:	Granite
Approximate Gradation Type:	BRZ

Avg. Lab Properties of Plant Produced Mix

SST Repeated Load Perm. Strain (microns):	NA
Unconfined Creep Perm. Strain:	NA
Confined Creep Perm. Strain:	NA
Unconfined Dynamic Perm. Strain:	NA
Confined Dynamic Perm. Strain:	NA
Dynamic Modulus:	NA
COE Gyratory Shear Index:	NA
SGC Shear Ratio:	NA
Asphalt Pavement Analyzer (mm):	2.26
Hamburg Loaded Wheel Tester (mm):	2.80
Rotary Loaded Wheel Tester (mm):	1.29
Purwheel Loaded Wheel Tester (mm):	NA

Roadway Performance (9/18/02)

Relevant Field Conditions

Total Traffic Applied (ESAL's):	8,599,781
Avg 7 Day High Air Temp (F):	NA
Avg Surface Temp in Past Week:	NA
Avg Surface Temp in 2001:	NA
Highest Surface Temp in 2001:	NA

Roadway Performance Properties

Rutting via ARAN 3 Point Approx. (in):	0.08
Rutting via Transverse Profile (in):	NA
Approximate Fn:	0.361
Average IRI (inches/mile):	22.0
MTD in inches:	0.020

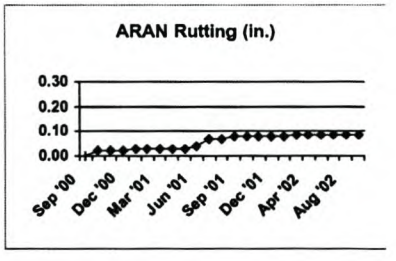

General Notes:

1) Test specimens were compacted to 7 +/- 1% air voids for tensile strength ratio (TSR) testing.
2) Test specimens were compacted to avg QC +/- 1% air voids for SST, creep, APA, and assorted LWT testing.
3) The vast majority of pills used as research test specimens were compacted during construction.
4) When an insufficient quantity of construction-compacted pills met target air voids, reheated mix was used.
5) All suitable pills were randomly assigned to test protocols in a manner to achieve equal avg and std dev in VTM.
6) All test protocols utilized sample sets consisting of 3 replicates per test (e.g., APA result is avg of 3 pills).
7) Loaded wheel testing consisted of 8000 cycles in the dry state with samples conditioned at 147.2 F long enough to insure a uniform temperature throughout the specimen but in no case longer than 24 hours.
8) APA testing utilized 1 inch OD hose, 120 psi pressure, 120 lb load, cylindrical specimens, manual depths.
9) Gyratory shear testing was conducted at mat compaction temperatures based upon construction measurements.

SECTION E6

Laboratory Performance

General Description of Mix and Materials

Design Method:	Superpave
Compactive Effort:	100 gyrations
Binder Performance Grade:	67-22
Modifier Type:	NA
Laboratory Determined Asphalt Content:	5.0%
General Aggregate Type:	Granite
Approximate Gradation Type:	TRZ

Avg. Lab Properties of Plant Produced Mix

SST Repeated Load Perm. Strain (microns):	NA
Unconfined Creep Perm. Strain:	NA
Confined Creep Perm. Strain:	NA
Unconfined Dynamic Perm. Strain:	NA
Confined Dynamic Perm. Strain:	NA
Dynamic Modulus:	NA
COE Gyratory Shear Index:	NA
SGC Shear Ratio:	NA
Asphalt Pavement Analyzer (mm):	2.25
Hamburg Loaded Wheel Tester (mm):	2.67
Rotary Loaded Wheel Tester (mm):	1.31
Purwheel Loaded Wheel Tester (mm):	NA

Roadway Performance (9/18/02)

Relevant Field Conditions

Total Traffic Applied (ESAL's):	8,599,781
Avg 7 Day High Air Temp (F):	NA
Avg Surface Temp in Past Week:	NA
Avg Surface Temp in 2001:	NA
Highest Surface Temp in 2001:	NA

Roadway Performance Properties

Rutting via ARAN 3 Point Approx. (in):	0.08
Rutting via Transverse Profile (in):	NA
Approximate Fn:	0.359
Average IRI (inches/mile):	34.5
MTD in inches:	0.020

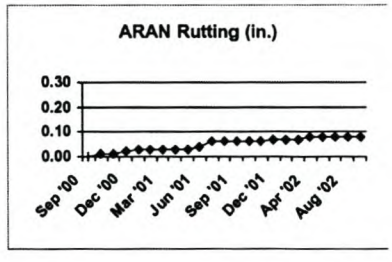

General Notes:

1) Test specimens were compacted to 7 +/- 1% air voids for tensile strength ratio (TSR) testing.
2) Test specimens were compacted to avg QC +/- 1% air voids for SST, creep, APA, and assorted LWT testing.
3) The vast majority of pills used as research test specimens were compacted during construction.
4) When an insufficient quantity of construction-compacted pills met target air voids, reheated mix was used.
5) All suitable pills were randomly assigned to test protocols in a manner to achieve equal avg and std dev in VTM.
6) All test protocols utilized sample sets consisting of 3 replicates per test (e.g., APA result is avg of 3 pills).
7) Loaded wheel testing consisted of 8000 cycles in the dry state with samples conditioned at 147.2 F long enough to insure a uniform temperature throughout the specimen but in no case longer than 24 hours.
8) APA testing utilized 1 inch OD hose, 120 psi pressure, 120 lb load, cylindrical specimens, manual depths.
9) Gyratory shear testing was conducted at mat compaction temperatures based upon construction measurements.

SECTION E8

Laboratory Performance

General Description of Mix and Materials

Design Method:	Superpave
Compactive Effort:	100 gyrations
Binder Performance Grade:	67-22
Modifier Type:	NA
Laboratory Determined Asphalt Content:	5.6%
General Aggregate Type:	Granite
Approximate Gradation Type:	ARZ

Avg. Lab Properties of Plant Produced Mix

SST Repeated Load Perm. Strain (microns):	NA
Unconfined Creep Perm. Strain:	NA
Confined Creep Perm. Strain:	NA
Unconfined Dynamic Perm. Strain:	NA
Confined Dynamic Perm. Strain:	NA
Dynamic Modulus:	NA
COE Gyratory Shear Index:	NA
SGC Shear Ratio:	NA
Asphalt Pavement Analyzer (mm):	4.56
Hamburg Loaded Wheel Tester (mm):	3.02
Rotary Loaded Wheel Tester (mm):	3.90
Purwheel Loaded Wheel Tester (mm):	NA

Roadway Performance (9/18/02)

Relevant Field Conditions

Total Traffic Applied (ESAL's):	8,599,781
Avg 7 Day High Air Temp (F):	NA
Avg Surface Temp in Past Week:	NA
Avg Surface Temp in 2001:	NA
Highest Surface Temp in 2001:	NA

Roadway Performance Properties

Rutting via ARAN 3 Point Approx. (in):	0.08
Rutting via Transverse Profile (in):	NA
Approximate Fn:	0.374
Average IRI (inches/mile):	20.8
MTD in inches:	0.020

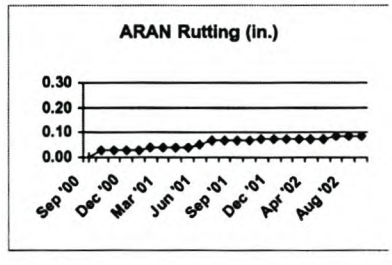

General Notes:

1) Test specimens were compacted to 7 +/- 1% air voids for tensile strength ratio (TSR) testing.
2) Test specimens were compacted to avg QC +/- 1% air voids for SST, creep, APA, and assorted LWT testing.
3) The vast majority of pills used as research test specimens were compacted during construction.
4) When an insufficient quantity of construction-compacted pills met target air voids, reheated mix was used.
5) All suitable pills were randomly assigned to test protocols in a manner to achieve equal avg and std dev in VTM.
6) All test protocols utilized sample sets consisting of 3 replicates per test (e.g., APA result is avg of 3 pills).
7) Loaded wheel testing consisted of 8000 cycles in the dry state with samples conditioned at 147.2 F long enough to insure a uniform temperature throughout the specimen but in no case longer than 24 hours.
8) APA testing utilized 1 inch OD hose, 120 psi pressure, 120 lb load, cylindrical specimens, manual depths.
9) Gyratory shear testing was conducted at mat compaction temperatures based upon construction measurements.

Appendix G

NCAT MMLS3 sections Superpave gyratory compaction data

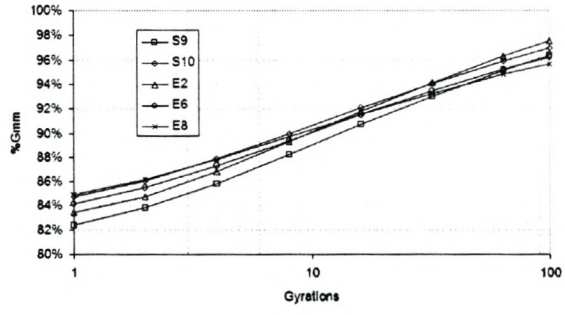

Figure G.1: Mean gyratory $\%G_{mm}$ of MMLS3 section mixes

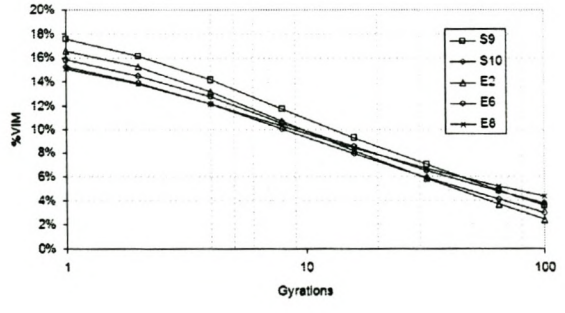

Figure G.2: Mean gyratory VIM of MMLS3 section mixes

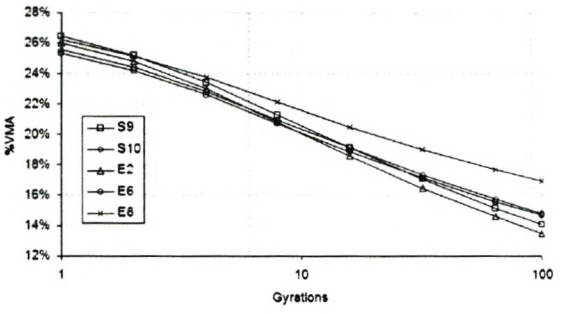

Figure G.3: Mean gyratory VMA of MMLS3 section mixes

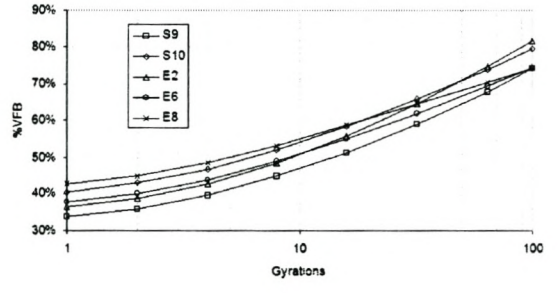

Figure G.4: Mean gyratory VFB of MMLS3 section mixes

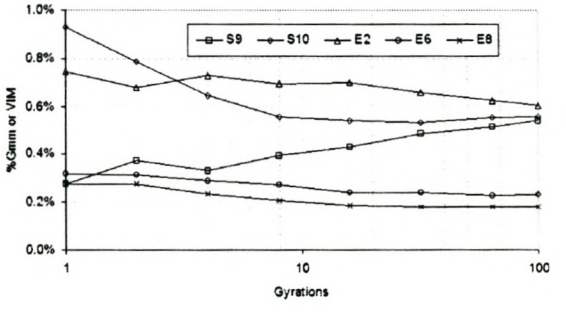

Figure G.5: Standard deviation gyratory $\%G_{mm}$ or VIM of MMLS3 section mixes

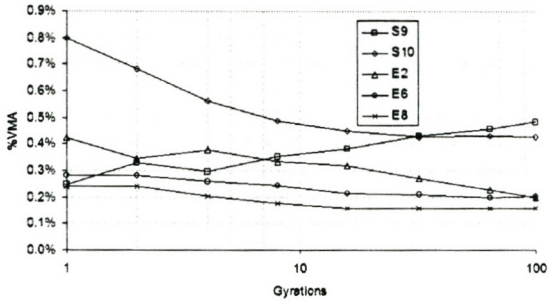

Figure G.6: Standard deviation gyratory VMA of MMLS3 section mixes

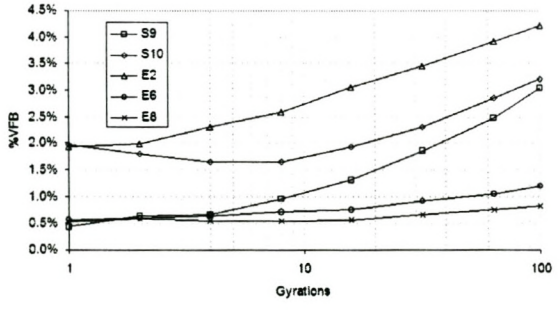

Figure G.7: Standard deviation gyratory VFB of MMLS3 section mixes

Appendix H

NCAT MMLS3 rutting performance

H.1 NCAT MMLS3 transverse rutting profiles

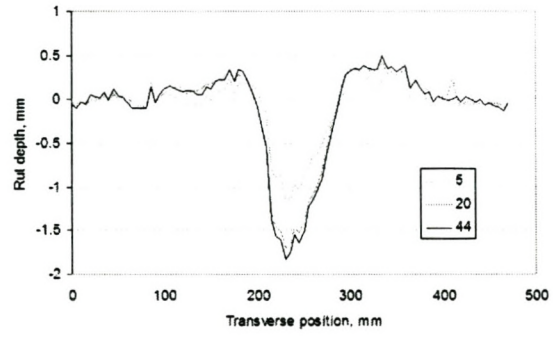

Figure H.1: MMLS3 test 1: Section S9 (Dry), 250 mm transverse profiles

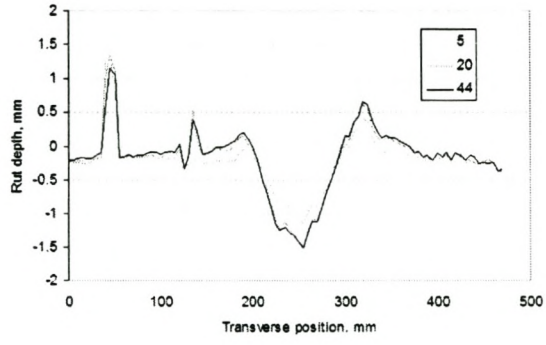

Figure H.2: MMLS3 test 1: Section S9 (Dry), 500 mm transverse profiles

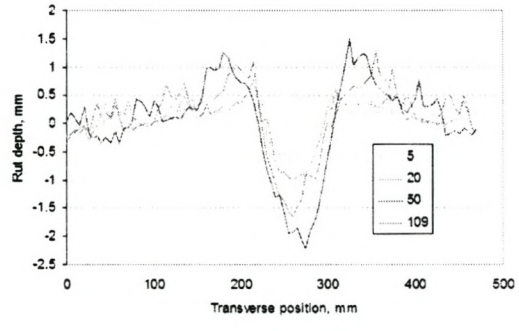

Figure H.3: MMLS3 test 2: Section S10 (Dry), 250 mm transverse profiles

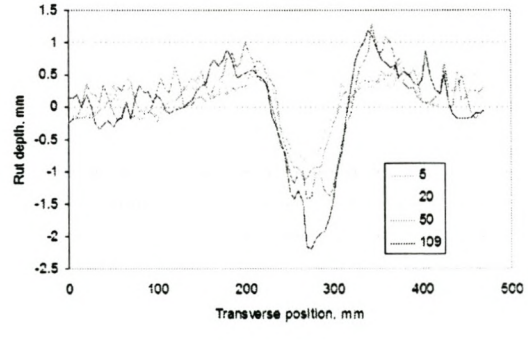

Figure H.4: MMLS3 test 2: Section S10 (Dry), 500 mm transverse profiles

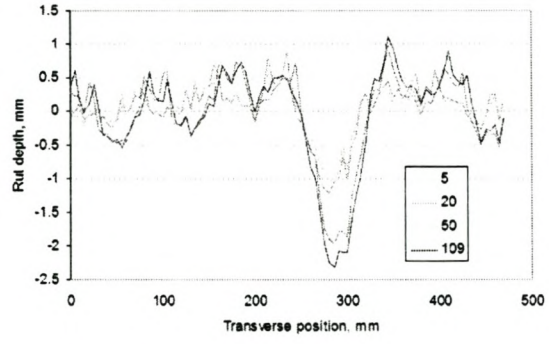

Figure H.5: MMLS3 test 2: Section S10 (Dry), 750 mm transverse profiles

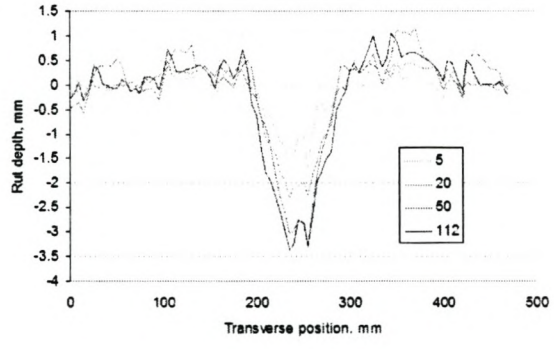

Figure H.6: MMLS3 test 3: Section E2 (Dry), 250 mm transverse profiles

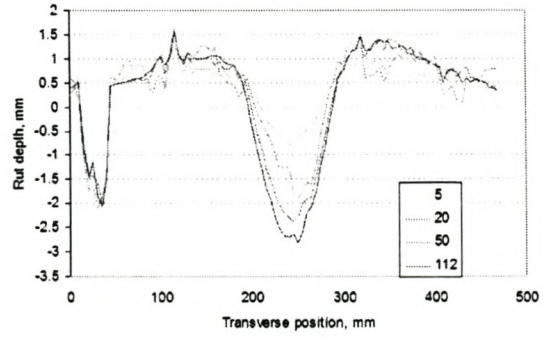

Figure H.7: MMLS3 test 3: Section E2 (Dry), 500 mm transverse profiles

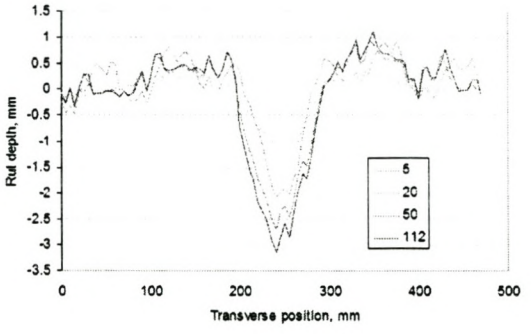

Figure H.8: MMLS3 test 3: Section E2 (Dry), 750 mm transverse profiles

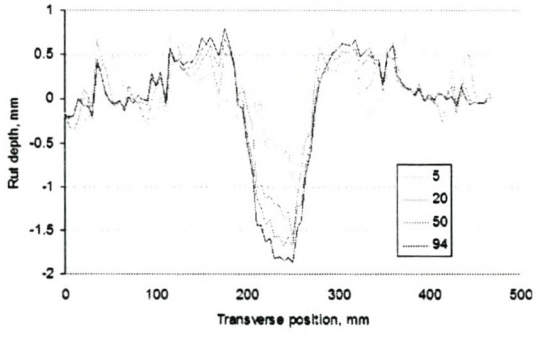

Figure H.9: MMLS3 test 4: Section S9 (Dry), 250 mm transverse profiles

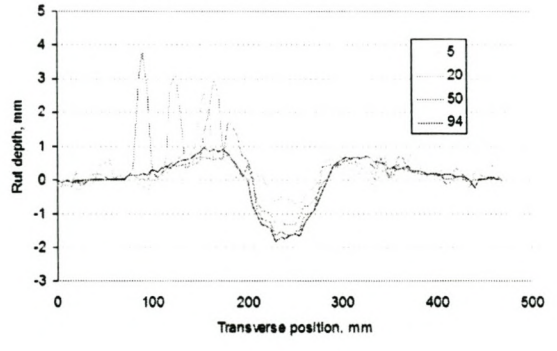

Figure H.10: MMLS3 test 4: Section S9 (Dry), 500 mm transverse profiles

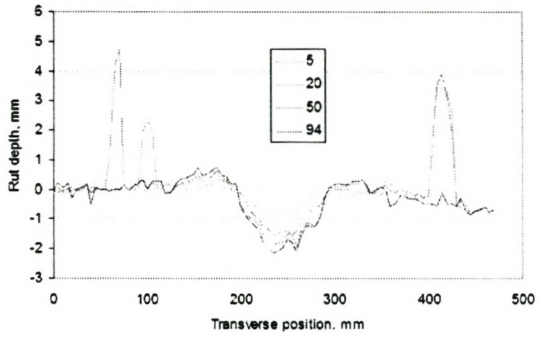

Figure H.11: MMLS3 test 4: Section S9 (Dry), 750 mm transverse profiles

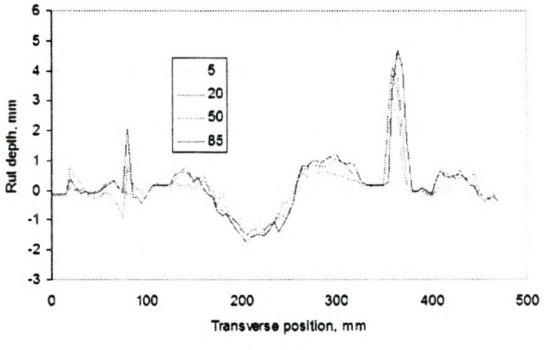

Figure H.12: MMLS3 test 5: Section E6 (Wet), 250 mm transverse profiles

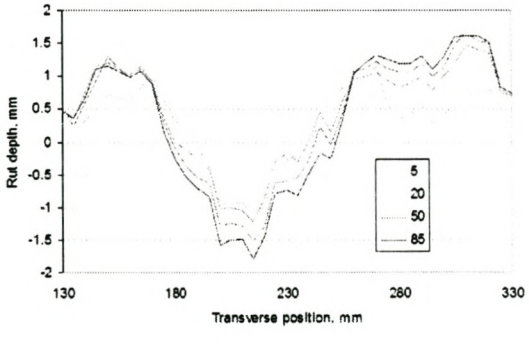

Figure H.13: MMLS3 test 5: Section E6 (Wet), 500 mm transverse profiles

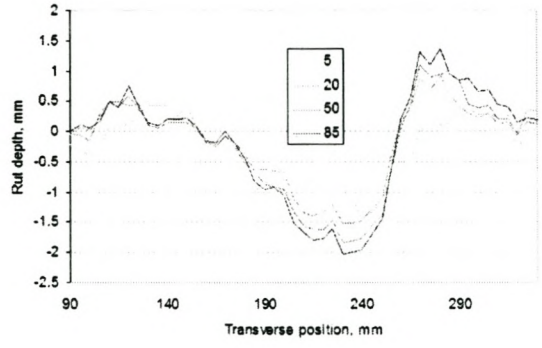

Figure H.14: MMLS3 test 5: Section E6 (Wet), 750 mm transverse profiles

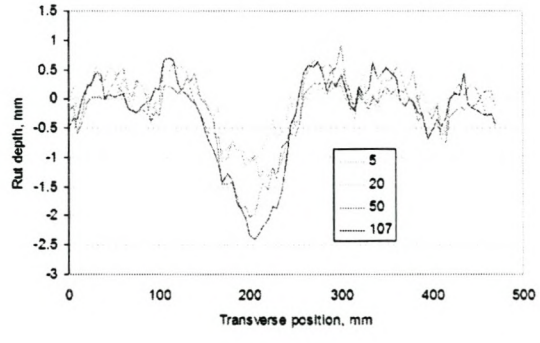

Figure H.15: MMLS3 test 6: Section E2 (Dry), 250 mm transverse profiles

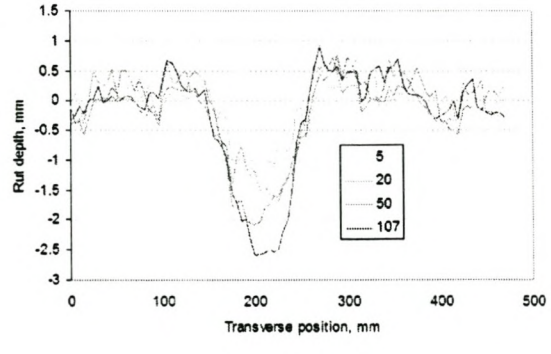

Figure H.16: MMLS3 test 6: Section E2 (Dry), 500 mm transverse profiles

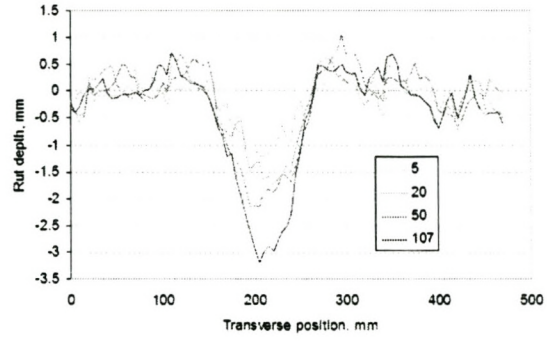

Figure H.17: MMLS3 test 6: Section E2 (Dry), 750 mm transverse profiles

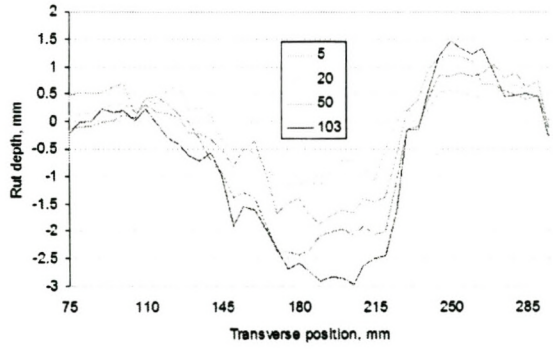

Figure H.18: MMLS3 test 7: Section E2 (Wet), 250 mm transverse profiles

Figure H.19: MMLS3 test 7: Section E2 (Wet), 500 mm transverse profiles

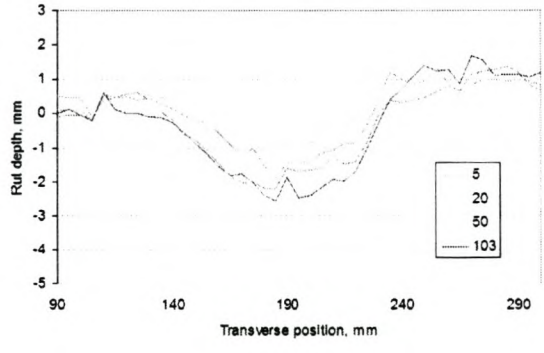

Figure H.20: MMLS3 test 7: Section E2 (Wet), 750 mm transverse profiles

H.2 NCAT MMLS3 cumulative rutting

H.2.1 MMLS3 Test 1: Section S9

This was the first of two dry MMLS3 tests on section S9. Average cumulative rutting is shown in Figure H.27 and detailed in Table H.1 for both total and down rut (as defined in Figure 5.13). This particular test was done when temperatures at the track were low and more time than usual was required to heat the pavement to the required test temperature. In the time available, a total of 44,000 MMLS3 axle loads could be

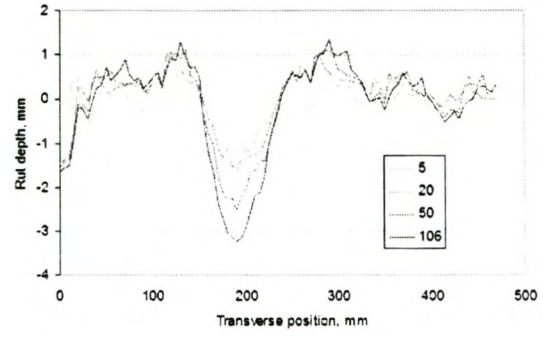

Figure H.21: MMLS3 test 6: Section E8 (Dry), 250 mm transverse profiles

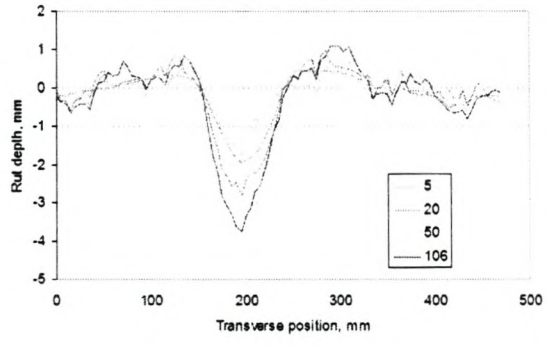

Figure H.22: MMLS3 test 6: Section E8 (Dry), 500 mm transverse profiles

applied. After the application of 44,000 load applications, swelling of the pavement alongside the MMLS3 wheelpath (difference between the total and down rut) is less than 1 mm.

H.2.2 MMLS3 Test 2: Section S10

The second test was also a dry test. A total of 109,000 MMLS3 loads were applied. Average cumulative rutting is shown in Figure H.28 and detailed in Table H.2.

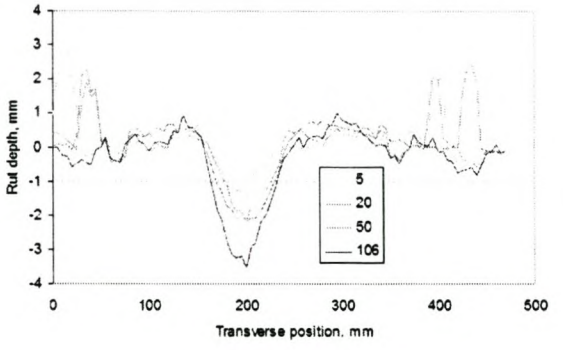

Figure H.23: MMLS3 test 6: Section E8 (Dry), 750 mm transverse profiles

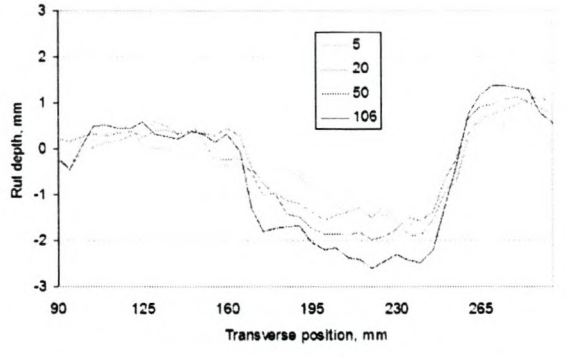

Figure H.24: MMLS3 test 7: Section E8 (Wet), 250 mm transverse profiles

H.2.3 MMLS3 Test 3: Section E2

Another dry test, the first of two on section E2. A total of 112,000 MMLS3 loads were applied. Average cumulative rutting is shown in Figure H.29 and detailed in Table H.3.

H.2.4 MMLS3 Test 4: Section S9

This was the second dry test on section S9. A total of 94,000 MMLS3 loads were applied. The testing of this section was repeated to investigate the possible influence of the increase in temperatures at the track. As will be shown later, the rutting trends

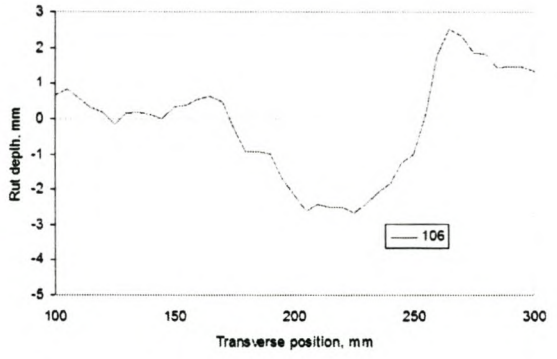

Figure H.25: MMLS3 test 7: Section E8 (Wet), 500 mm transverse profiles

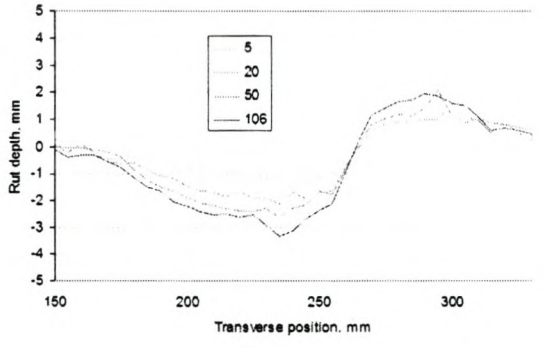

Figure H.26: MMLS3 test 7: Section E8 (Wet), 750 mm transverse profiles

for the two tests on this section were similar (see Figure 5.17). Average cumulative rutting is shown in Figure H.30 and detailed in Table H.4. For the second dry test on section S9 use was made of an environmental chamber to prevent heat loss during testing.

H.2.5 MMLS3 Test 5: Section E6

This was the first wet MMLS3 test at the NCAT test track and the first field trial using the wet heating pavement testing system. A total of 85,000 MMLS3 axles loads were applied. Average cumulative rutting is shown in Figure H.31 and detailed in

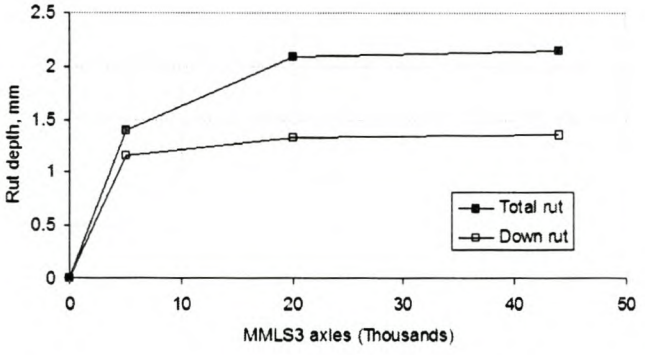

Figure H.27: MMLS3 test 1: Section S9 (Dry) average cumulative rutting

Table H.1: MMLS3 test 1: Section S9 (Dry) rutting results

Statistic	Rut	**0k**	**5k**	**20k**	**44k**
Avg	Total rut	0	1.39	2.09	2.15
	Down rut	0	1.17	1.33	1.35
Stdev	Total rut	0	0.06	0.01	0.15
	Down rut	0	0.01	0.22	0.25

Table H.5.

H.2.6 MMLS3 Test 6: Section E2

This was the second dry test on section E2. A total of 107,000 MMLS3 loads were applied. Average cumulative rutting is shown in Figure H.32 and detailed in Table H.6.

H.2.7 MMLS3 Test 7: Section E2

This was a wet test on section E2. A total of 103,000 MMLS3 loads were applied. As will be shown later (see Figure 5.18), the difference in rutting between the wet and dry tests was minimal. Average cumulative rutting is shown in Figure H.33 and detailed in Table H.33.

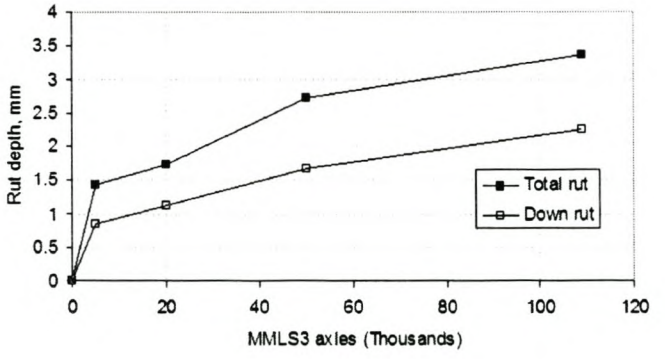

Figure H.28: MMLS3 test 2: Section S10 (Dry) average cumulative rutting

Table H.2: MMLS3 test 2: Section S10 (Dry) rutting results

Statistic	Rut	**0k**	**5k**	**20k**	**50k**	**109k**
Avg	Total rut	0	1.43	1.73	2.73	3.36
	Down rut	0	0.84	1.11	1.68	2.24
Stdev	Total rut	0	0.24	0.17	0.14	0.20
	Down rut	0	0.23	0.12	0.28	0.07

H.2.8 MMLS3 Test 8: Section E8

A dry test on section E8. A total of 106,000 MMLS3 loads were applied. Average cumulative rutting is shown in Figure H.34 and detailed in Table H.8.

H.2.9 MMLS3 Test 9: Section E8

A wet test on section E8. A total of 106,000 MMLS3 loads were applied. Average cumulative rutting is shown in Figure H.35 and detailed in Table H.9.

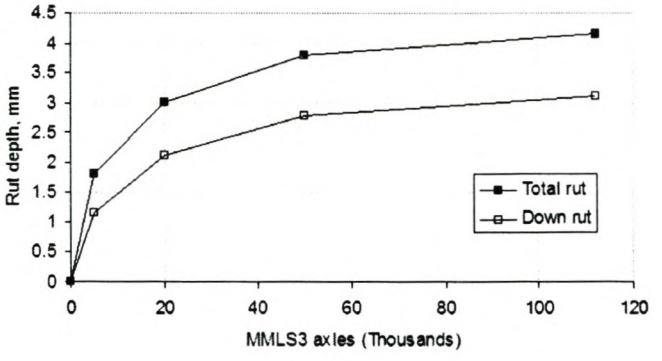

Figure H.29: MMLS3 test 3: Section E2 (Dry) average cumulative rutting

Table H.3: MMLS3 test 3: Section E2 (Dry) rutting results

Statistic	Rut	**0k**	**5k**	**20k**	**50k**	**112k**
Avg	Total rut	0	1.81	3.01	3.80	4.14
	Down rut	0	1.17	2.10	2.78	3.11
Stdev	Total rut	0	0.38	0.24	0.40	0.08
	Down rut	0	0.46	0.22	0.45	0.27

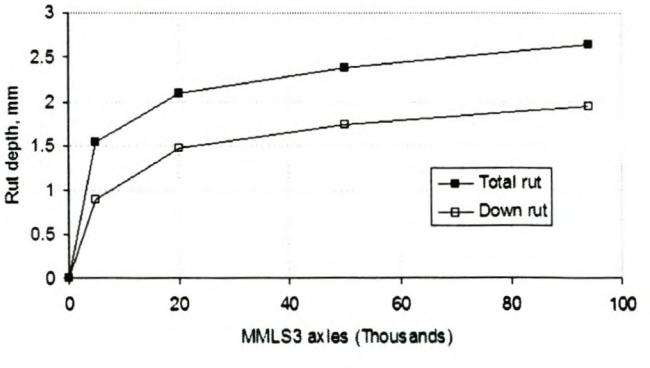

Figure H.30: MMLS3 test 4: Section S9 (Dry) average cumulative rutting

Table H.4: MMLS3 test 4: Section S9 (Dry) rutting results

Statistic	Rut	**0k**	**5k**	**20k**	**50k**	**94k**
Avg	Total rut	0	1.55	2.11	2.38	2.65
	Down rut	0	0.90	1.49	1.74	1.95
Stdev	Total rut	0	0.28	0.19	0.09	0.05
	Down rut	0	0.12	0.15	0.15	0.18

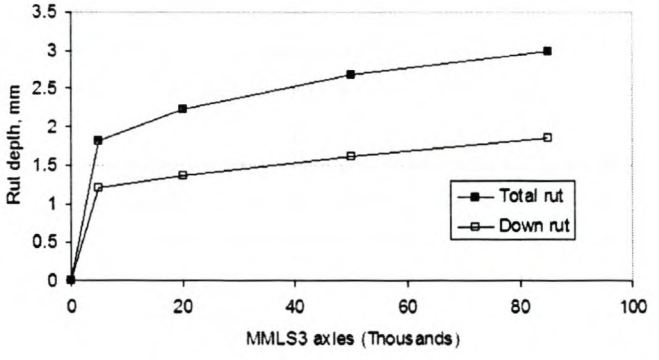

Figure H.31: MMLS3 test 5: Section E6 (Wet) average cumulative rutting

Table H.5: MMLS3 test 5: Section E6 (Dry) rutting results

Statistic	Rut	**0k**	**5k**	**20k**	**50k**	**85k**
Avg	Total rut	0	1.83	2.24	2.69	2.99
	Down rut	0	1.21	1.38	1.62	1.85
Stdev	Total rut	0	0.36	0.32	0.29	0.25
	Down rut	0	0.20	0.14	0.19	0.16

Table H.6: MMLS3 test 6: Section E2 (Dry) rutting results

Statistic	Rut	**0k**	**5k**	**20k**	**50k**	**107k**
Avg	Total rut	0	1.51	2.14	2.81	3.39
	Down rut	0	1.15	1.56	2.09	2.74
Stdev	Total rut	0	0.11	0.23	0.17	0.46
	Down rut	0	0.06	0.20	0.07	0.42

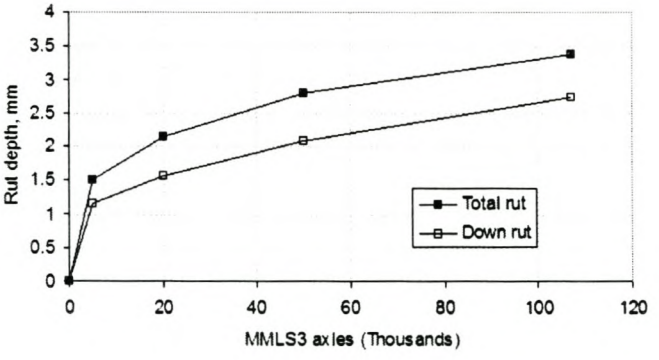

Figure H.32: MMLS3 test 6: Section E2 (Dry) average cumulative rutting

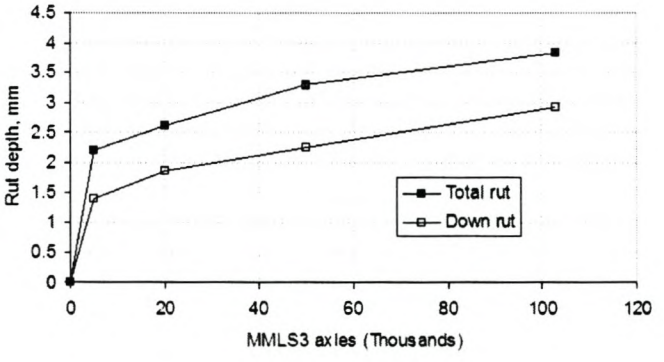

Figure H.33: MMLS3 test 7: Section E2 (Wet) average cumulative rutting

Table H.7: MMLS3 test 7: Section E2 (Wet) rutting results

Statistic	Rut	**0k**	**5k**	**20k**	**50k**	**103k**
Avg	Total rut	0	2.21	2.62	3.30	3.84
	Down rut	0	1.39	1.85	2.25	2.92
Stdev	Total rut	0	0.31	0.22	0.18	0.40
	Down rut	0	0.18	0.08	0.16	0.32

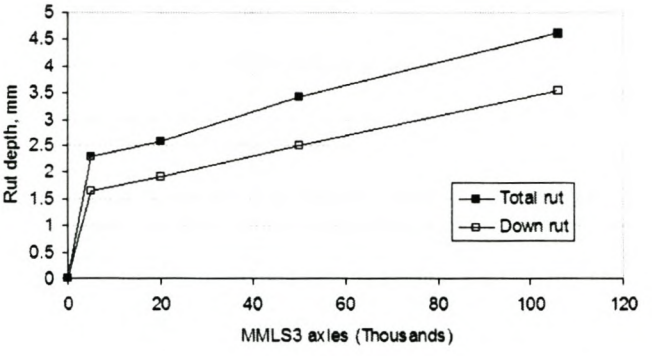

Figure H.34: MMLS3 test 8: Section E8 (Dry) average cumulative rutting

Table H.8: MMLS3 test 8: Section E8 (Dry) rutting results

Statistic	Rut	**0k**	**5k**	**20k**	**50k**	**106k**
Avg	Total rut	0	2.30	2.59	3.43	4.61
	Down rut	0	1.64	1.90	2.51	3.52
Stdev	Total rut	0	0.08	0.16	0.46	0.11
	Down rut	0	0.10	0.32	0.32	0.25

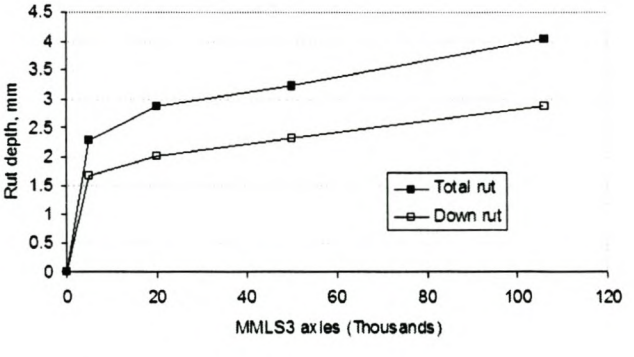

Figure H.35: MMLS3 test 9: Section E8 (Wet) average cumulative rutting

Table H.9: MMLS3 test 9: Section E8 (Wet) rutting results

Statistic	Rut	**0k**	**5k**	**20k**	**50k**	**106k**
Avg	Total rut	0	2.30	2.88	3.22	4.04
	Down rut	0	1.67	2.01	2.32	2.87
Stdev	Total rut	0	0.03	0.16	0.65	0.38
	Down rut	0	0.03	0.17	0.47	0.40

Appendix I

Results of the FEM analyses

I.1 SCB 2-D FEM analyses

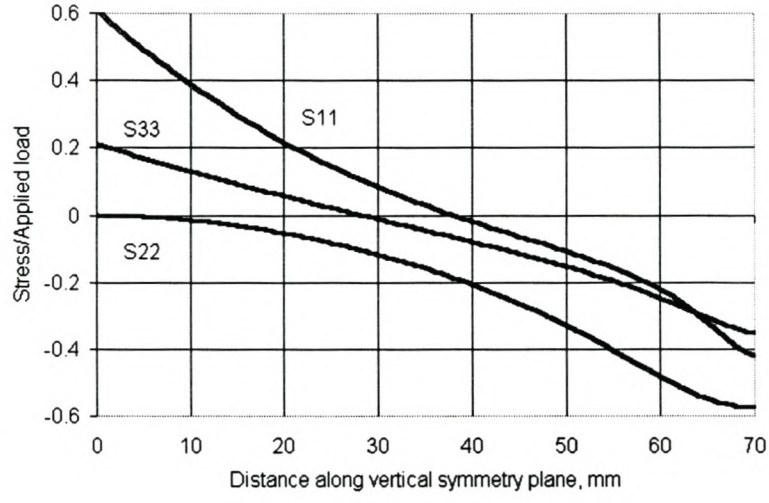

Figure I.1: 2-D FEM solution of SCB stress distribution in vertical plane

I.2 SCB 3-D FEM analyses

Tables I.1 through I.3 give the results of the 3-D FEM analyses. The maximum horizontal tensile stress (S11) and vertical deflection (U2) with variation in asphalt

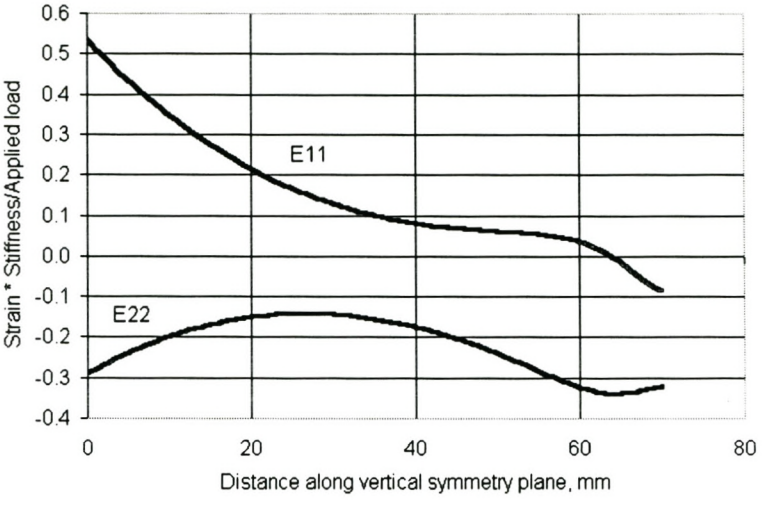

Figure I.2: 2-D FEM solution of SCB strain distribution in vertical plane

stiffness, thickness and Poisson's ratio are tabulated.

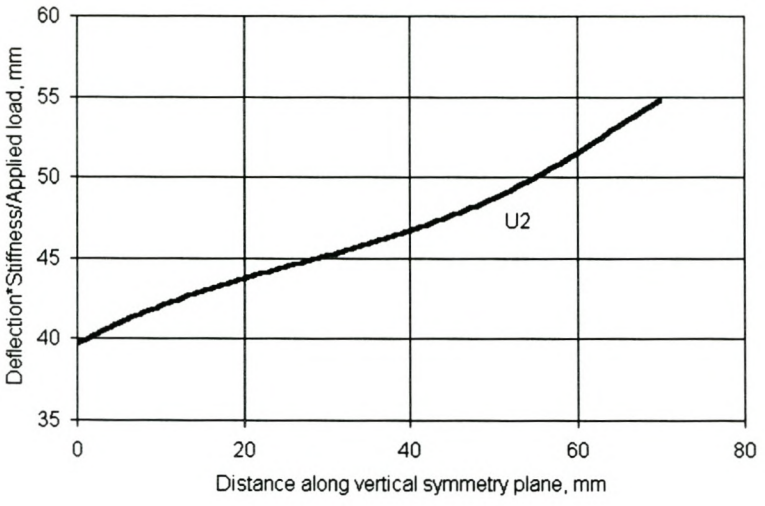

Figure I.3: 2-D FEM solution of SCB deflection distribution in vertical plane

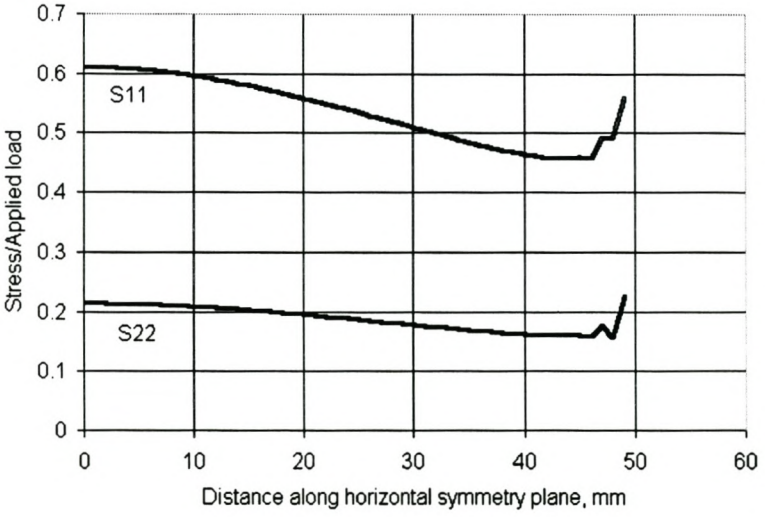

Figure I.4: 2-D FEM solution of SCB stress distribution in horizontal plane

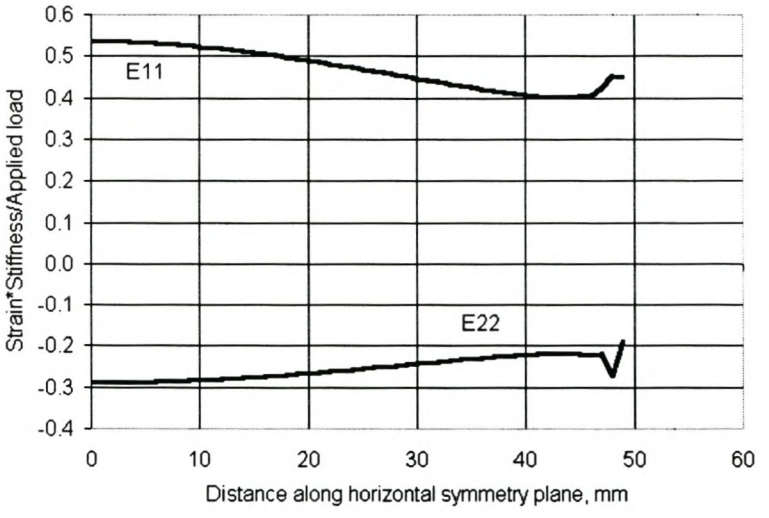

Figure I.5: 2-D FEM solution of SCB strain distribution in horizontal plane

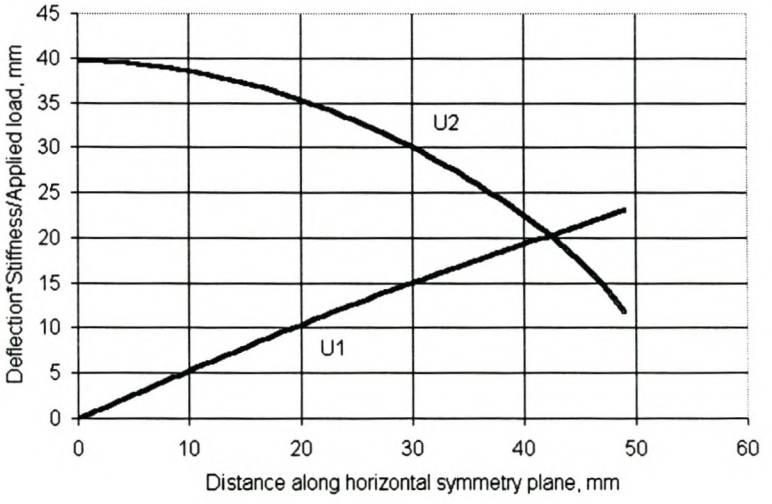

Figure I.6: 2-D FEM solution of SCB deflection distribution in horizontal plane

Table I.1: FEM 3-D analysis with 10 mm specimen thickness

Thickness mm	Poisson's ratio	Stiffness MPa	S11 MPa	U2 mm
10	0.2	1000	0.570058	0.044201
10	0.35	1000	0.573794	0.0441818
10	0.45	1000	0.578819	0.0438567
10	0.2	2000	0.570119	0.0223112
10	0.35	2000	0.573823	0.0223041
10	0.45	2000	0.57885	0.0221472
10	0.2	4000	0.57025	0.0113655
10	0.35	4000	0.573899	0.0113645
10	0.45	4000	0.578934	0.0112913
10	0.2	8000	0.570541	0.058915
10	0.35	8000	0.574103	0.0589332
10	0.45	8000	0.579166	0.0586126

Table I.2: FEM 3-D analysis with 25 mm specimen thickness

Thickness mm	Poisson's ratio	Stiffness MPa	S11 MPa	U2 mm
25	0.2	1000	0.570842	0.0440489
25	0.35	1000	0.575001	0.0438282
25	0.45	1000	0.581185	0.0433027
25	0.2	2000	0.570938	0.0222341
25	0.35	2000	0.575104	0.0221284
25	0.45	2000	0.581313	0.0218731
25	0.2	4000	0.57112	0.0113257
25	0.35	4000	0.575289	0.011277
25	0.45	4000	0.581543	0.0111562
25	0.2	8000	0.571466	0.0586991
25	0.35	8000	0.575626	0.0584909
25	0.45	8000	0.58196	0.057944

Table I.3: FEM 3-D analysis with 50 mm specimen thickness

Thickness mm	**Poisson's ratio**	**Stiffness MPa**	**S11 MPa**	**U2 mm**
50	0.2	1000	0.575057	0.0436555
50	0.35	1000	0.582864	0.0429872
50	0.45	1000	0.592322	0.0420793
50	0.2	2000	0.57516	0.0220366
50	0.35	2000	0.58298	0.0217092
50	0.45	2000	0.592463	0.0212644
50	0.2	4000	0.575353	0.0112255
50	0.35	4000	0.583192	0.0110673
50	0.45	4000	0.59274	0.0108531
50	0.2	8000	0.575738	0.058183
50	0.35	8000	0.58362	0.0574375
50	0.45	8000	0.593308	0.0564357

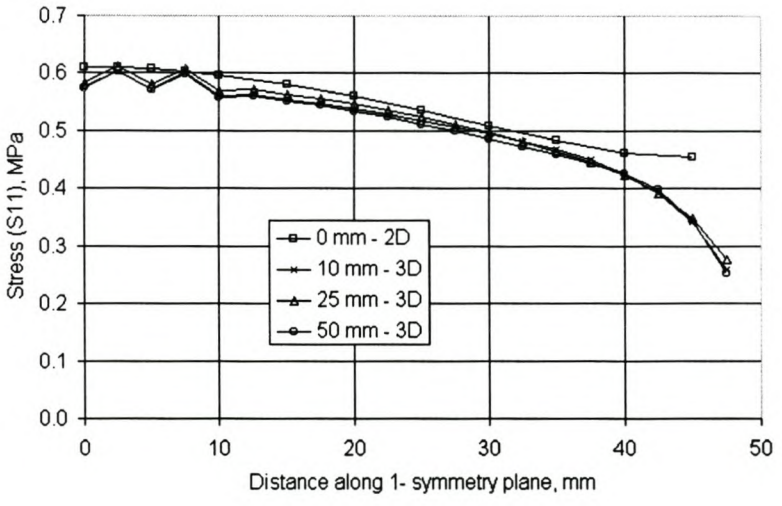

Figure I.7: 3-D FEM solution of SCB S11 stress distribution in 1- symmetry plane

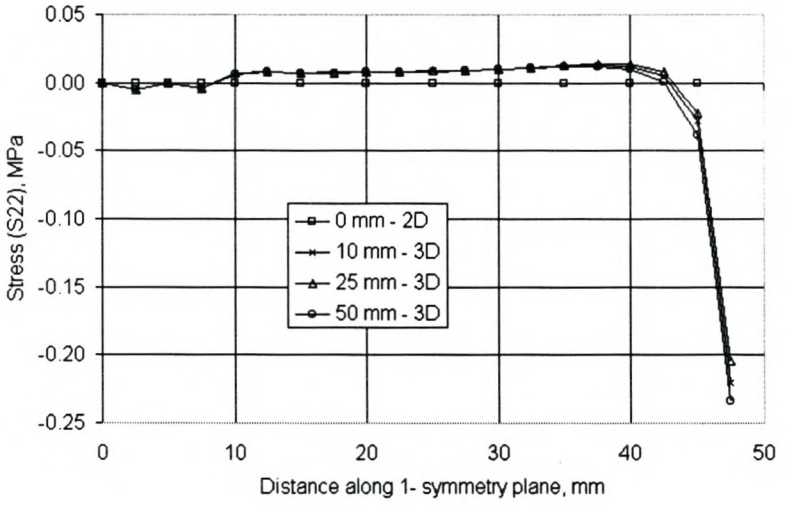

Figure I.8: 3-D FEM solution of SCB S22 stress distribution in 1- symmetry plane

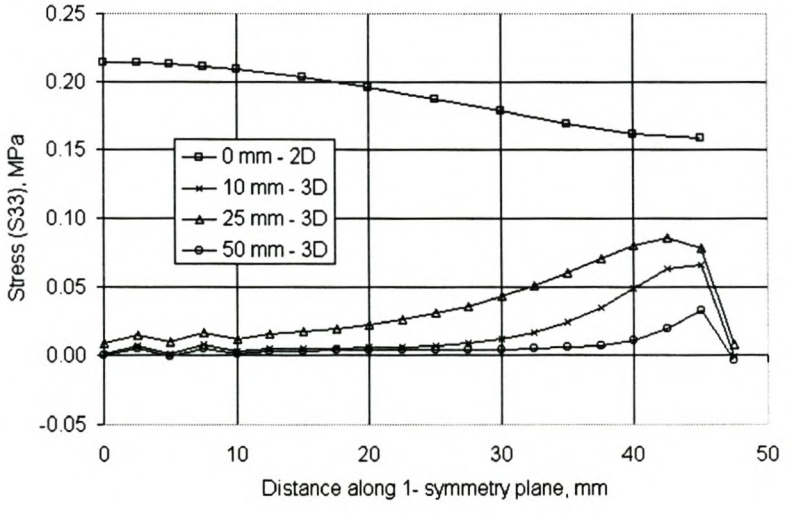

Figure I.9: 3-D FEM solution of SCB S33 stress distribution in 1- symmetry plane

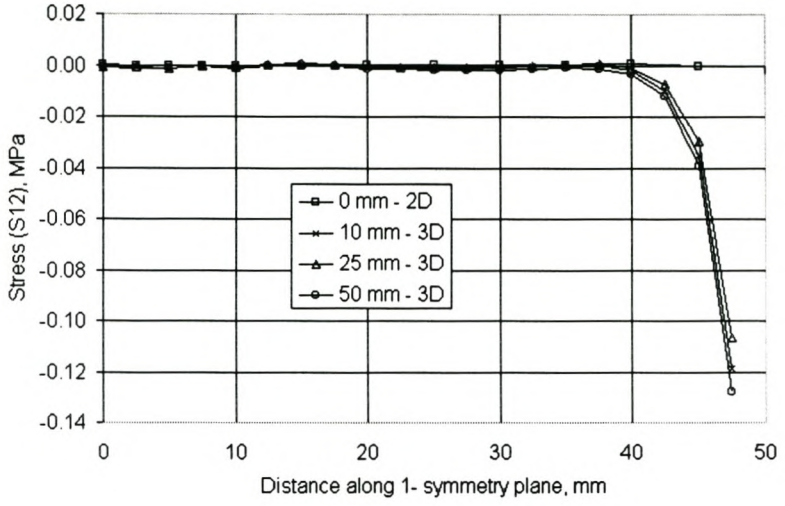

Figure I.10: 3-D FEM solution of SCB S12 stress distribution in 1- symmetry plane

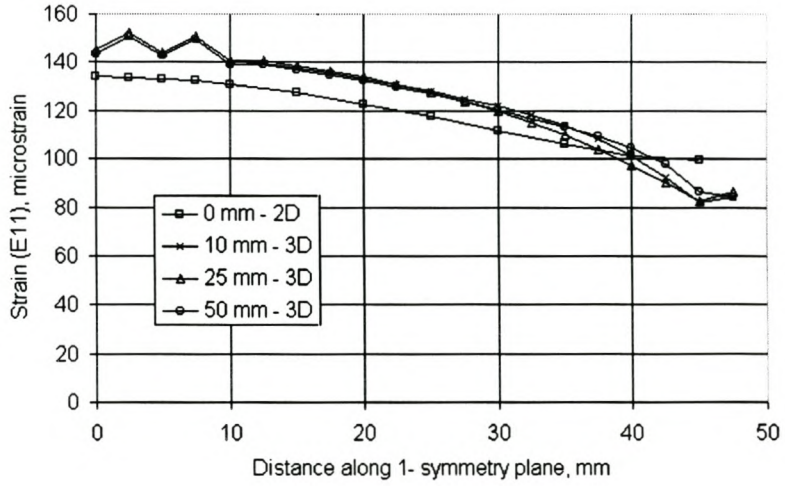

Figure I.11: 3-D FEM solution of SCB E11 strain distribution in 1- symmetry plane

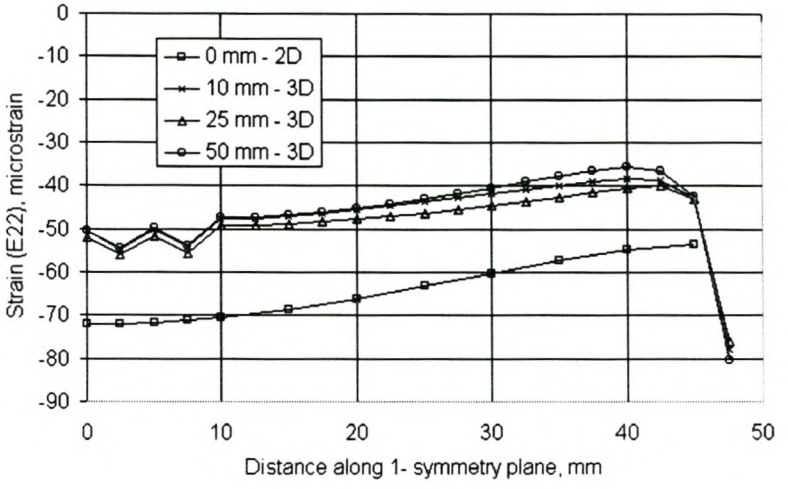

Figure I.12: 3-D FEM solution of SCB E22 strain distribution in 1- symmetry plane

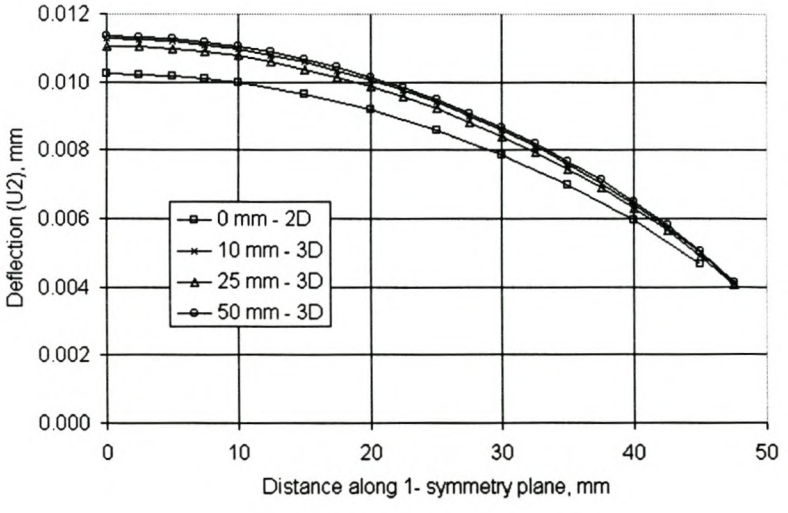

Figure I.13: 3-D FEM solution of SCB U2 deflection distribution in 1- symmetry plane

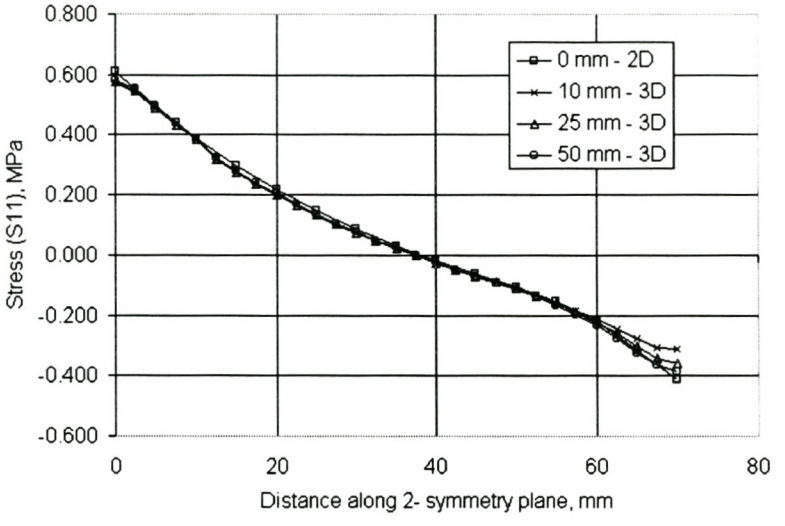

Figure I.14: 3-D FEM solution of SCB S11 stress distribution in 2- symmetry plane

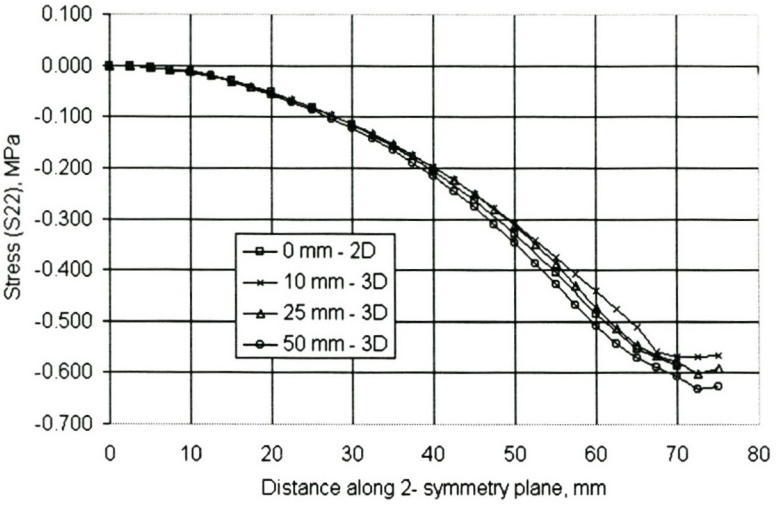

Figure I.15: 3-D FEM solution of SCB S22 stress distribution in 2- symmetry plane

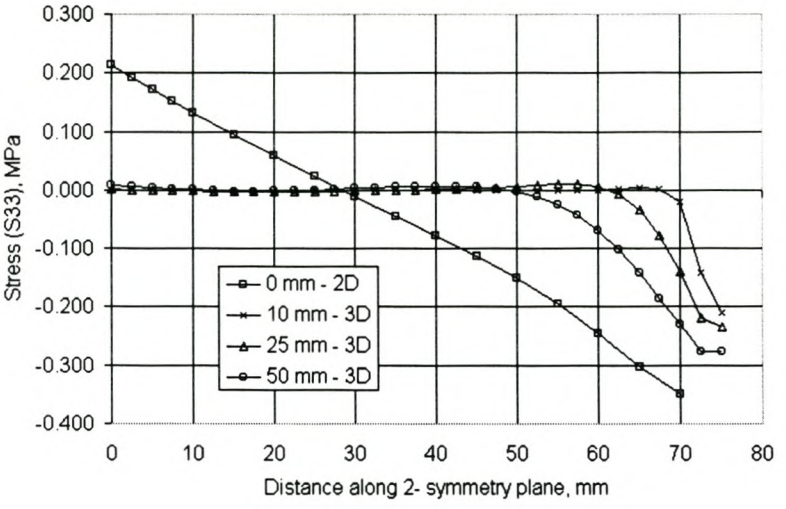

Figure I.16: 3-D FEM solution of SCB S33 stress distribution in 2- symmetry plane

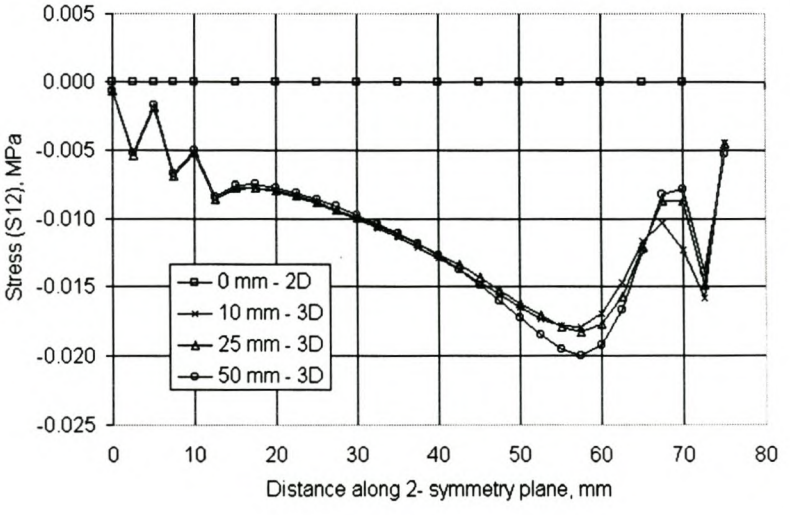

Figure I.17: 3-D FEM solution of SCB S12 stress distribution in 2- symmetry plane

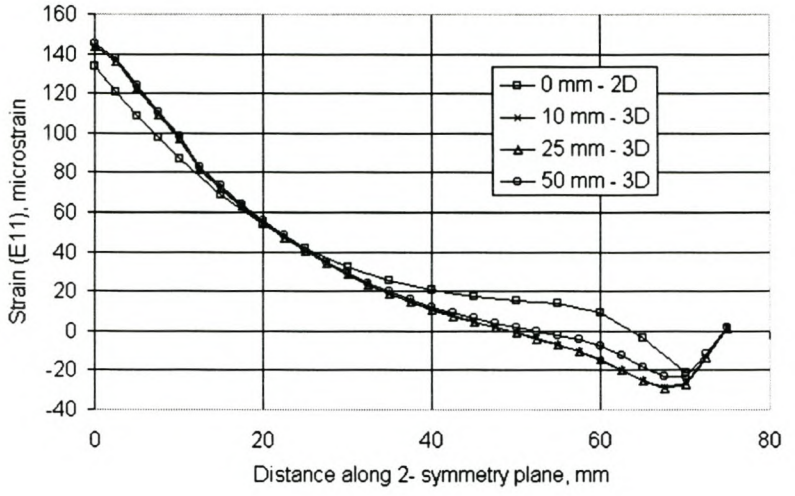

Figure I.18: 3-D FEM solution of SCB E11 strain distribution in 2- symmetry plane

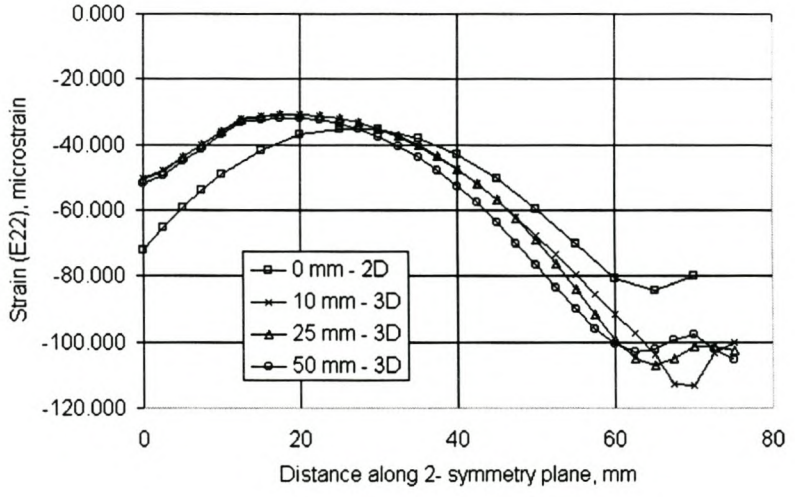

Figure I.19: 3-D FEM solution of SCB E22 strain distribution in 2- symmetry plane

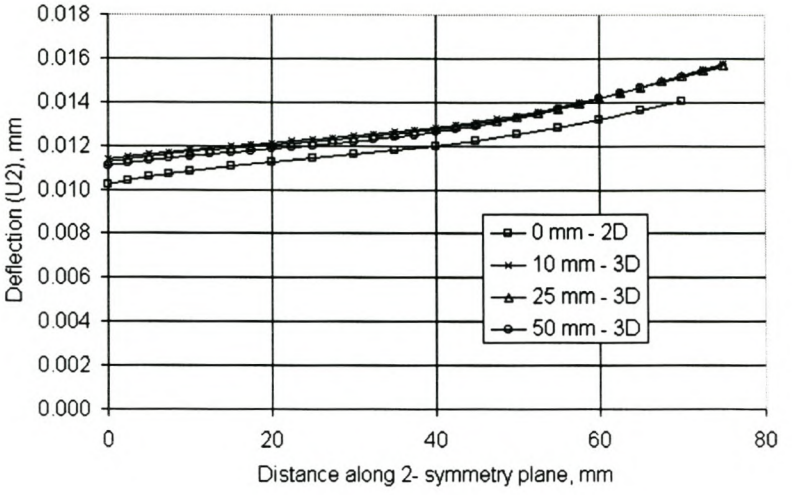

Figure I.20: 3-D FEM solution of SCB U2 deflection distribution in 2- symmetry plane

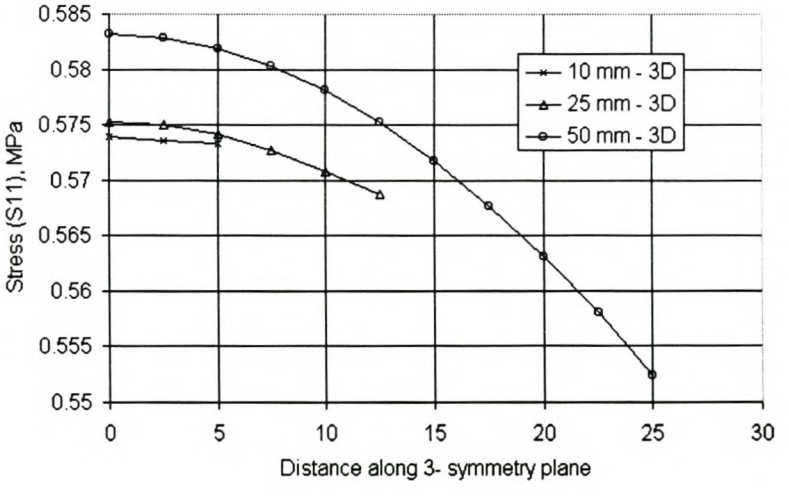

Figure I.21: 3-D FEM solution of SCB S11 stress distribution in 3- symmetry plane

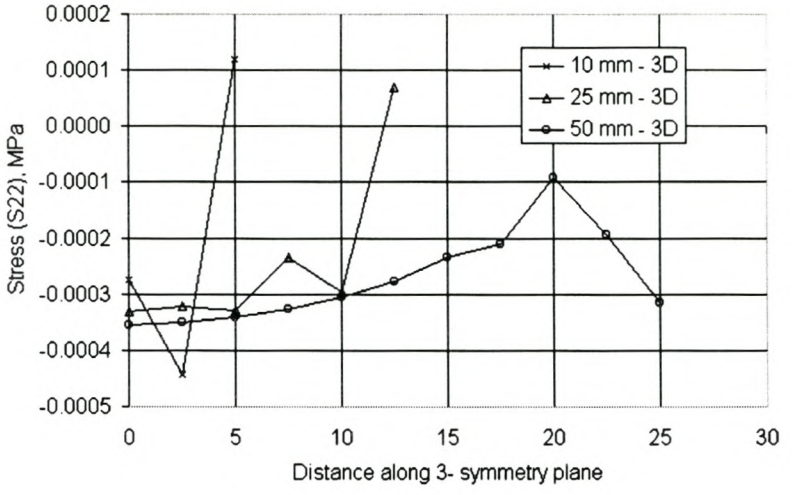

Figure I.22: 3-D FEM solution of SCB S22 stress distribution in 3- symmetry plane

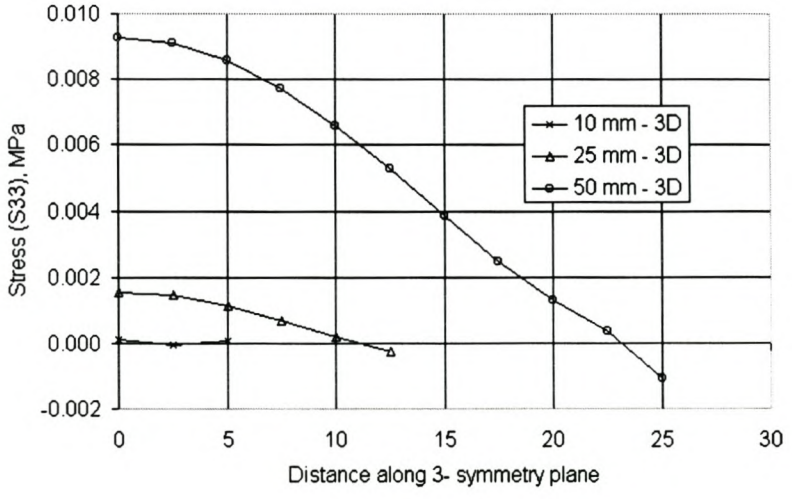

Figure I.23: 3-D FEM solution of SCB S33 stress distribution in 3- symmetry plane

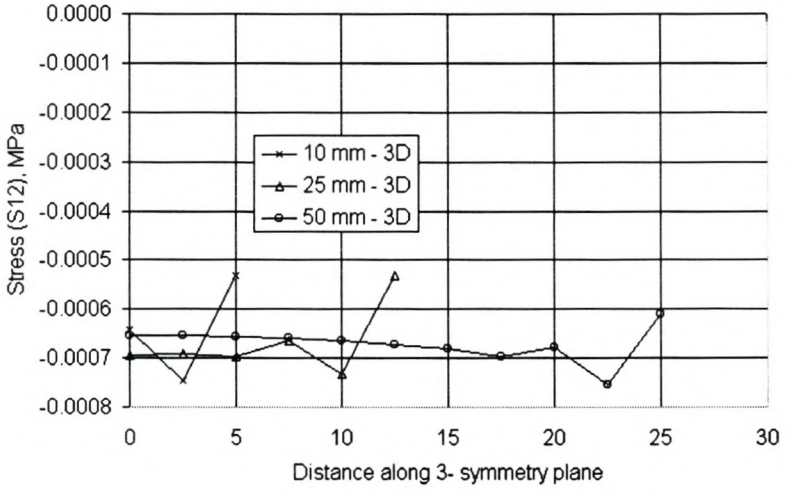

Figure I.24: 3-D FEM solution of SCB S12 stress distribution in 3- symmetry plane

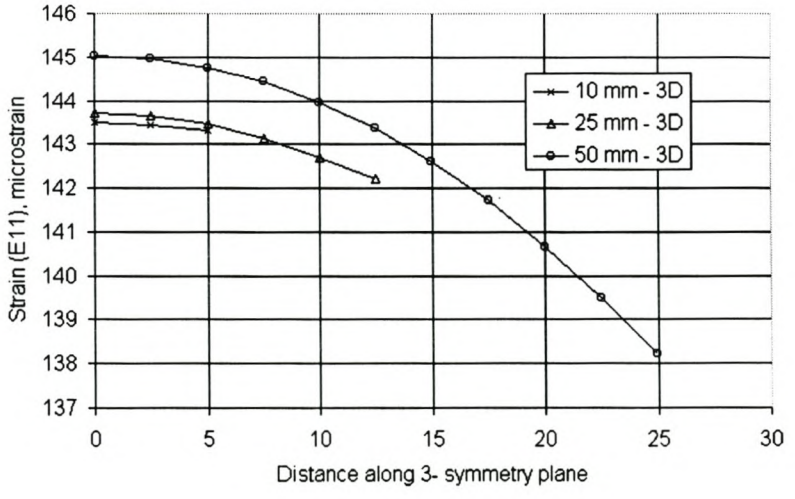

Figure I.25: 3-D FEM solution of SCB E11 strain distribution in 3- symmetry plane

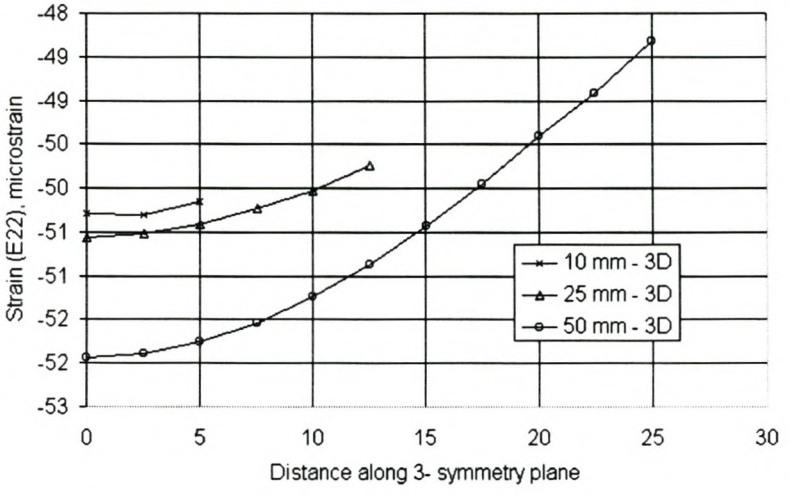

Figure I.26: 3-D FEM solution of SCB E22 strain distribution in 3- symmetry plane

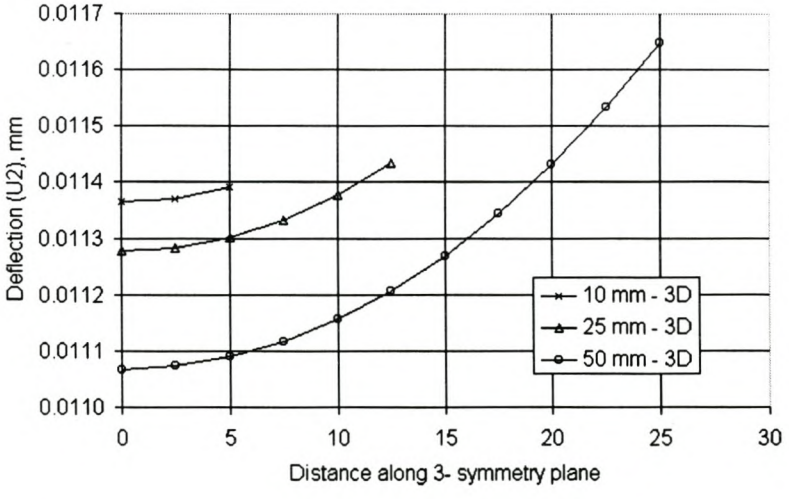

Figure I.27: 3-D FEM solution of SCB U2 deflection distribution in 3- symmetry plane